Measurement of Transverse Spin Effects at the COMPASS Experiment

Der Naturwissenschaftlichen Fakultät
der Friedrich-Alexander-Universität Erlangen-Nürnberg
zur
Erlangung des Doktorgrades

vorgelegt von
Andreas Michael Julius Richter
aus Erlangen

Als Dissertation genehmigt von der Naturwissenschaftlichen
Fakultät der Universität Erlangen-Nürnberg

Tag der mündlichen Prüfung:	23.06.2010
Vorsitzender der Promotionskommission:	Prof. Dr. E. Bänsch
Erstberichterstatter:	Prof. Dr. W. Eyrich
Zweitberichterstatter:	Prof. Dr. K. Rith

Meiner viel zu früh verstorbenen Mutter, Christiane von Bernus,
der ich so viel zu verdanken habe.

Abstract

In spite of the progress made so far the spin structure of the nucleon is still a matter of ongoing research interest. Particularly the so-called *"spin crisis"* or *"spin puzzle"*, i.e., how is the composition of the nucleon spin from its constituents, the quarks and gluons, is not yet solved.

For a full description of the nucleon spin structure at quark level at leading twist ignoring transverse momentum it is necessary to know three quark distribution functions, namely the unpolarized distribution function (momentum distribution) $q(x)$, which describes the probability of finding a quark with momentum fraction x of the nucleon momentum, the helicity distribution function $\Delta q(x) = q^+(x) + \bar{q}^+(x) - q^-(x) - \bar{q}^-(x)$, which decribes the difference of the probability to find a quark with momentum fraction x with spin parallel and antiparallel to the nucleon spin inside a longitudinally polarized nucleon (w.r.t. the direction of motion) and the transverse distribution function $\Delta_T q(x) = q^{\uparrow}(x) + \bar{q}^{\uparrow}(x) - q^{\downarrow}(x) - \bar{q}^{\downarrow}(x)$, the so-called "Transversity", which describes the difference of the probability to find a quark with momentum fraction x with spin parallel and antiparallel to the nucleon spin inside a transversely polarized nucleon (w.r.t. the direction of motion).

The distribution functions $q(x)$ and $\Delta q(x)$ are well known, $\Delta_T q(x)$ on the other hand is still the object of current investigations.

While for a long time transversity and transverse spin effects were believed to be neglectible, today their significance is clearly confirmed.

One possibility to extract the transversity distribution is the measurement of the Collins effect in semi-inclusive deep inelastic scattering of leptons on a transversely polarized nucleon target. This effect describes the fragmentation of transversely polarized quarks into spinless hadrons and results in an azimuthal modulation in the distribution of the produced hadrons. This left-right asymmetry is due to the combination of two chiral-odd functions, the transversity distribution function $\Delta_T q(x)$ and the transverse fragmentation function (FF) $H_1^{\perp}$.

Furthermore with the Sivers effect a different mechanism was studied to explain the spin asymmetries in the cross-section of SIDIS of leptons on a transversely polarized nucleon target was studied. This effect describes the fragmentation of an unpolarized (unknown spin state) quark inside a transversely polarized target nucleon. Assumed is here the existence of a correlation between the transverse momentum $\vec{k}_T$ of an unpolarized quark in a transversely polarized nucleon and the nucleon spin vector.

The measurements described in this work were done at the COMPASS experiment at CERN's second large accelerator ring, the Super-Proton-Synchrotron (SPS), using a 160 GeV/c polarized μ^+ beam. In the years 2002-2004 COMPASS has collected data with a

transversely polarized deuteron (^{6}LiD) target. In 2007, COMPASS has used for the first time a proton (NH_3) target.
In this work the extraction of the Collins and Sivers asymmetries for the fragmentation into K^0 for the COMPASS measurements on deuteron and proton targets as well as the one for the production of charged hadrons without and with particle identification for the COMPASS measurements on a proton target is described. An interpretation of the results, particularly for the extraction of the transversity distribution function $\Delta_T q(x)$ and the transverse momentum dependent Sivers distribution function $\Delta_T^0 q(x, {k_T}^2)$, concludes the work.

Abstract (Deutsch)

Trotz der bislang erreichten Fortschritte ist die Spinstruktur des Nukleons noch immer ein hochaktuelles Forschungsgebiet. Insbesondere ist die so genannte *„Spin-Krise"* bzw. das *„Spinrätsel"*, d.h., wie setzt sich der Spin des Nukleons aus dem Spin seiner Bestandteile, der Quarks und Gluonen, zusammen, noch immer nicht gelöst.
Für eine vollständige Beschreibung der Spinstruktur des Nukleons auf Quark-Ebene in führender Ordnung unter Vernachlässigung des transversalen Impulses sind drei Quark-Verteilungsfunktionen notwendig: Die unpolarisierte Verteilungsfunktion (Impulsverteilung) $q(x)$, welche die Wahrscheinlichkeit, ein Quark mit Impulsanteil x am Nukleonenspin zu finden, beschreibt, die Helizitätsverteilungsfunktion $\Delta q(x) = q^+(x)+\bar{q}^+(x)-q^-(x)-\bar{q}^-(x)$, welche die Differenz der Wahrscheinlichkeiten, ein Quark mit Impulsanteil x am Nukleonenspin mit Spin parallel bzw. antiparallel zum Nukleonenspin in einem longitudinal polarisierten Nukleon (in Richtung der Bewegungsrichtung) zu finden, beschreibt und die transversale Verteilungsfunktion $\Delta_T q(x) = q^\uparrow(x) + \bar{q}^\uparrow(x) - q^\downarrow(x) - \bar{q}^\downarrow(x)$, die so genannte „Transversity", welche die Differenz der Wahrscheinlichkeiten, ein Quark mit Impulsanteil x mit Spin parallel bzw. antiparallel zum Nukleonenspin in einem transversal polarisierten Nukleon (in Richtung der Bewegungsrichtung) zu finden, beschreibt.
Während die Verteilungsfunktionen $q(x)$ und $\Delta q(x)$ gut bekannt sind, ist $\Delta_T q(x)$ Gegenstand aktueller Untersuchungen.
Lange Zeit wurden Transversity und transversale Spin-Effekte für vernachlässigbar gehalten, heute jedoch ist ihre Bedeutung klar erwiesen.
Eine Möglichkeit zur Extraktion der Transversity-Verteilung ist die Messung des Collins-Effekts in semi-inklusiver tiefinelastischer Streuung (SIDIS) von Leptonen an einem transversal polarisierten Nukleonentarget. Dieser Effekt beschreibt die Fragmentation von transversal polarisierten Quarks in spinlose Hadronen und bewirkt eine azimuthale Modulation in der Verteilung der erzeugten Hadronen. Diese Links-Rechts-Asymmetrie kommt durch die Kombination von zwei chiral-ungeraden Funktionen, der Transversity-Verteilungsfunktion $\Delta_T q(x)$ und der transversalen Fragmentationsfunktion (FF) $H_1^\perp$, zustande.
Desweiteren wurde mit dem Sivers-Effekt ein anderer Mechanismus zur Erklärung der Spin-Asymmetrien im Wirkungsquerschnitt der SIDIS von Leptonen an einem transversal polarisierten Nukleonen-Target untersucht. Durch diesen Effekt wird die Fragmentation eines unpolarisierten (unbekannter Spin-Zustand) Quarks in einem transversal polarisierten Target-Nukleon beschrieben. Angenommen wird hier das Vorliegen einer Korrelation zwischen dem transversalen Impuls $\vec{k}_T$ eines unpolarisierten Quarks in einem transversal polarisierten Nukleon und dem Spin-Vektor des Nukleons. Die in dieser Arbeit beschriebenen Messungen wurden am COMPASS-Experiment am zweitgrößten Beschleunigerring

des CERN, dem Super-Proton-Synchrotron (SPS), unter Verwendung eines polarisierten μ^+-Strahls der Energie 160 GeV/c durchgeführt. In den Jahren 2002-04 wurden Daten an einem transversal polarisierten Deuterium-Target (^{6}LiD) genommen. 2007 verwendete COMPASS erstmals ein Protonen-Target (NH_3).
In dieser Arbeit wird die Extraktion der Collins- und Sivers-Asymmetrien zum einen für die Fragmentation in K^0-Mesonen für die COMPASS-Messungen am Deuterium- und am Protonen-Target, zum anderen für geladene Hadronen mit und ohne Identifikation für die Messungen am Protonen-Target beschrieben. Eine Interpretation der gewonnenen Resultate, insbesondere in Bezug auf die Extraktion der Transversity-Verteilungsfunktion und der Sivers-Verteilungsfunktion, schließt die Arbeit ab.

Contents

Chapter 1

Introduction

> Der wissenschaftliche Mensch ist die Weiterentwicklung des künstlerischen.
>
> The scientific man is the further evolution of the artistic.
>
> F. W. Nietzsche (1844-1900),
> German philosopher and philologist

The question of what matter and therefore our world consists of might be as old as mankind itself. The idea that the natural world is composed of elementary particles goes back to the ancient Greek philosophers in the 6th century BC like Leucippus and his student Democritus and later Epicurus, who called those particles "$\alpha\tau o\mu o\varsigma$" meaning "uncuttable". The theory was developed further by the roman philosopher Lucretius. Also ancient Indian philosophers as Kanada, Dignāga and Dharmakirti were follower of the idea of elementary constituents of matter.

During the medieval, while the western world was dominated by fanatism and superstition, the idea of elementary particles was still present in the Islamic philosophy associated e.g. with the names of Alhazen, Avicenna and Algazel.

Early modern physicists like Isaak Newton or Robert Boyle later picked up the atomic theory. While all those early atomists were motivated by philosophical reasoning rather than experimental observation, it was John Dalton in 1808, who concluded from his stoichiometric work that each chemical element consists of certain atoms.

As we know now those atoms are not the fundamental constituents of matter, but consist themself of a central nucleus of protons and neutrons surrounded by an electron cloud.

Our present understanding of particles and their interactions is the Standard Model of particle physics, which describes the elementary particles and three of the four fundamental interactions (electromagnetism, weak and strong interaction, not including gravitation) intermediated by the exchange of gauge bosons. In this model three generations of particles exist. Of these particles those carrying a color charge and thus interacting via the strong interaction described by the Quantum Chromodynamics (QCD) are called quarks, the other ones leptons. The quarks are forming composite particles like e.g. the nucleons. In the constituent quark model the nucleon consists of three constituent quarks, in the case of the proton two up quarks with an electric charge of $+\frac{2}{3}\,e$ and one down quark with a charge of $-\frac{1}{3}\,e$ and in the case of the neutron two down and one up quark. Two quarks have a spin of $\frac{1}{2}\,\hbar$ and one has a spin of $-\frac{1}{2}\,\hbar$ adding up to the spin of the nucleon of $\frac{1}{2}\,\hbar$. With this model it is possible to explain many properties of the nucleon.

In the more detailed view of the extended Quark Parton Model those three valence quarks are inside a “sea” of quark-antiquark pairs created and annihilated by the exchange of gluons, the gauge bosons of the strong interaction.

In the end of the 1980s measurements of the EMC[1] experiment at CERN[2] in Geneva had detected that not more than one third of the nucleon spin is covered by quark spin [1, 2]. This very surprising phenomenum was called *“spin crisis”* or *“spin puzzle”* and triggered intense theoretical and experimental efforts to explain the spin structur of the nucleon.

In a measurement, where a beam of leptons is scattered on a longitudinally polarized target, the total spin of the nucleon S_z is given by:

$$S_z = \frac{1}{2} = \frac{1}{2}\Delta\Sigma + \Delta G + \langle L_z^q \rangle + \langle L_z^g \rangle \tag{1.1}$$

where $\Delta\Sigma = \sum_i \Delta q_i + \Delta\bar{q}_i$ is the spin contribution from the quarks and antiquarks (sum over flavors i), ΔG is the contribution of the gluons and $\langle L_z^q \rangle$ and $\langle L_z^g \rangle$ the orbital angular momentum of the quarks and gluons, respectively.

While it is not possible in current experiments to measure precisely the orbital angular momenta, measurements of ΔG are an object of high interest in COMPASS[3] as well as in other experiments.

For a complete description of the nucleon structur at leading order, however, there are three quark distribution functions necessary: the momentum distribution $q(x)$, which describes the probability of finding a quark with momentum fraction x of the nucleon momentum, the helicity distribution $\Delta q(x) = q^+(x) + \bar{q}^+(x) - q^-(x) - \bar{q}^-(x)$, which decribes the difference of the probability to find a quark with momentum fraction x with spin parallel and antiparallel to the nucleon spin inside a longitudinally polarized nucleon (w.r.t. the direction of motion) and the transversity distribution $\Delta_T q(x) = q^\uparrow(x) + \bar{q}^\uparrow(x) - q^\downarrow(x) - \bar{q}^\downarrow(x)$, which describes the difference of the probability to find a quark with momentum fraction x with spin parallel and antiparallel to the nucleon spin inside a transversely polarized nucleon (w.r.t. the direction of motion).

One may think that the helicity and the transversity distribution can be transformed into each other by a simple rotation in space, but this is only possible for non-relativistic partons. In the experiments, which investigate the nucleon spin structure one has to take into account the relativistic nature, which destroys the rotation invariance.

While today the significance of transversity and parton transverse momenta is evident, for a long time transverse spin effects were believed for a long time to be neglectible.

[1] **E**uropean **M**uon **C**ollaboration

[2] **C**onseil **E**uropéen pour la **R**echerche **N**ucléaire, European Nuclear Research Center

[3] **CO**mmon **M**uon **P**roton **A**pparatus for **S**tructure and **S**pectroscopy

As the gluon spin in the transverse case does not contribute to the nucleon spin (see chapter 2.2.4), the Bakker Leader Trueman sum rule found for a transversely polarized nucleon [3] gives an independent access to the contribution of the orbital angular momentum of quarks, antiquarks and gluons to the nucleon spin:

$$S_z = \frac{1}{2} = \frac{1}{2}\sum_i \int_0^1 \left(\Delta_T q_i(x) + \Delta_T \bar{q}_i(x)\right) dx + \sum_i \langle L_T^{q_i} \rangle + \sum_i \langle L_T^{\bar{q}_i} \rangle + \sum_g \langle L_T^{g} \rangle \tag{1.2}$$

$$= \frac{1}{2}\sum_i \left(\Delta_T q_i + \Delta_T \bar{q}_i\right) + \sum_{q,\bar{q},g} \langle L_T \rangle$$

A property, which makes the measurement of the transversity distribution very challenging, is its chiral-odd nature. This effects that it is not possible to measure transversity in inclusive deep inelastic scattering (DIS) (for the definition of inclusive scattering etc. see section 2.1), because to have a measurable process, which as a whole has to be chiral-even, a combination with another chiral-odd function is needed.
A possibility of measuring transversity is the semi-inclusive DIS (SIDIS), in which beside the scattered lepton at least one particle of the hadronic end-product is detected. For this Collins et al. [4] have predicted a mechanism, which describes the fragmentation of a transversely polarized quark in a transversely polarized target nucleon into spinless ("unpolarized") hadrons. This mechanism results in an azimuthal asymmetry in the distribution of the produced hadrons, which is proportional to the combination of two chiral-odd functions, the transversity distribution $\Delta_T q(x)$ and the transverse fragmentation function $H_1^{\perp}$ (so-called Collins fragmentation function).
This Collins effect in SIDIS was measured at HERMES at DESY and at COMPASS, where also further measurements are ongoing. Independent information about the Collins fragmentation function in e^+e^- annihilation is provided by the Belle collaboration at KEK in Japan, which allows in combination with the SIDIS results an extraction of the transversity distribution.
A different mechanism to explain other spin asymmetries in SIDIS on a transversely polarized nucleon target was suggested by Sivers [5]. The Sivers effect describes the fragmentation of an unpolarized (unknown spin state) quark inside a transversely polarized target nucleon. It is based on the correlation between the transverse momentum $\vec{k}_T$ of an unpolarized quark in a transversely polarized nucleon and the nucleon spin vector.
The work described in this thesis is devoted to the extraction of Collins and Sivers asymmetries in SIDIS with COMPASS data on a deuteron target (2002-04) and on a proton target (2007).
The structur of the thesis is the following:
In chapter 2 the theoretical background is described giving an introduction to the theory of the inner structur of the nucleon. Chapter 3 gives a description of the COMPASS apparatus and its detection technique. In chapter 4 the data analysis and the extraction of the Collins and Sivers asymmetries for K^0 on a transversely polarized deuteron target at COMPASS is presented. The analysis of the data on a transversely polarized proton target

and the extraction of asymmetries in the production of charged hadrons without identification as well as for the neutral K^0 and charged hadrons with identification is given in chapter 5. An interpretation of the COMPASS results for Collins and Sivers asymmetries as well as a comparison with the results of the HERMES experiment at DESY and with theoretical models and the results of the first extraction of the transversity distribution function and the Sivers distribution function are given in chapter 6. A conclusion and outlook can be found in chapter 7.

Chapter 2

Theoretical Background

La matematica è l'alfabeto nel quale
Dio ha scritto l'universo.

Mathematics is the language with
which God has written the universe.

G. Galilei (1564-1642),
Italian physicist

2.1 Deep Inelastic Scattering (DIS)

A very important tool to get information about the structur of nucleons is the scattering of charged leptons on nucleons. Leptons are an ideal probe, because they are point-like particles with no substructure and they are not strongly interacting in our present understanding [6].

Kinematics of Deep Inelastic Scattering

The inelastic scattering of an incoming, polarized beam lepton l with four-momentum $k = (E, \vec{p})$ and spin vector $\vec{s}$ on a polarized target nucleon N at rest in the laboratory frame with mass M, four-momentum $P \stackrel{lab}{=} (M, 0, 0, 0)$ and spin vector $\vec{S}$ can be described by the equation:

$$l(k, \vec{s}) + N(P, \vec{S}) \rightarrow l'(k', \vec{s'}) + X \tag{2.1}$$

with the scattered lepton l' with reduced four-momentum k' and energy E' and X as the hadronic end-product (see fig. 2.1).
In the following we will assume that the lepton is longitudinally polarized and the nucleon is either longitudinally or transversely polarized as it is the experimental case.
If only the scattered lepton is detected, the scattering process is called inclusive. In contrary, if the complete end-product is detected, we speak about exclusive scattering. In

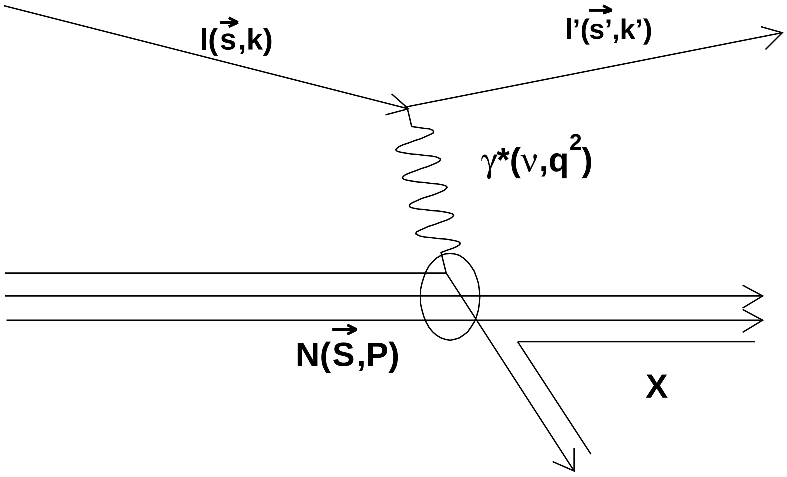

Figure 2.1: *View of the deep inelastic scattering of a lepton l with spin $\vec{s}$ and four-momentum k via the exchange of a virtual photon γ^* with energy ν and four-momentum q^2 on a nucleon N with spin $\vec{S}$ and four-momentum P. The hadronic end-product X is a priori unknown. Figure taken from [36].*

the case of a partially detection of the (hadronic) end-product the process is called semi-inclusive.
For describing the scattering the following Lorentz invariables are important [7, 8]:

$$Q^2 := -q^2 = -(k-k')^2 \stackrel{lab}{=} -2\,(m_l^2 - EE' + pp' \cdot \cos\Theta) \approx 4\,EE' \cdot \sin^2\frac{\Theta}{2} \tag{2.2}$$

with Θ as the scattering angle of the lepton. The lepton mass is neglected in comparison to its momentum.

$$P \cdot k \stackrel{lab}{=} M \cdot E \tag{2.3}$$

$$P \cdot q \stackrel{lab}{=} M(E-E') := M\nu \tag{2.4}$$

where ν is the energy of the virtual photon exchanged in the scattering process.
The scattering is deep inelastic, if the invariant mass W of the hadronic end-product X is above the energy range of nuclear resonances. This condition is fulfilled for $Q^2 > 1$ (GeV/c)^2). At COMPASS the range of Q^2 is approximately 1 (GeV/c)$^2 \leqq Q^2 \leqq$ 100(GeV/c)^2.
One can now define two further Lorentz invariables, the Bjørken scaling variable x_{bj} and the fractional energy transfer via the exchanged photon y, which are both dimensionless [9, 7]:

$$x_{bj} := \frac{Q^2}{2P \cdot q} \stackrel{lab}{=} \frac{Q^2}{2M \cdot \nu}; \qquad 0 \leq x \leq 1 \tag{2.5}$$

$$y := \frac{P \cdot q}{P \cdot k} \stackrel{lab}{=} \frac{\nu}{E}; \qquad 0 \leq y \leq 1 \tag{2.6}$$

x_{bj} is a measure of the elasticity of a process. $x_{bj} = 0$ means totally inelastic scattering, while $x_{bj} = 1$ means an elastic process. Moreover in the Quark Parton Model x_{bj} represents the fraction of the nucleon momentum carried by the struck quark (hit quark) in the scattering (see section 2.2.1).
Relevant variables are also the centre-of-mass energy $\sqrt{s}$ given by:

$$s = (P + k)^2 \stackrel{lab}{=} M^2 + 2ME \tag{2.7}$$

and the mass W of the hadronic end-product calculated by:

$$W^2 = (P + q)^2 \stackrel{lab}{=} M^2 + 2M\nu - Q^2 \tag{2.8}$$

The Deep Inelastic Cross-Section

The processes in the nucleon are describable by the Quantum Chromodynamics (QCD). In this theory the "confinement" of the quarks in the nucleon is assumed, i.e. the larger the distance between the quarks, the larger the interacting force between them. The quarks are therefore asymptotically free, the interaction between them becomes arbitrarily weak in the limit of ever small distances.
In scattering experiments the energy transfer to the quarks is so high that a description within the "confinement" is not possible anymore, so that on quark level approximative methods like e.g. lattice QCD are used.
The part of the scattering, which is described by perturbative QCD, is called the "hard" process, while the part, which is only accessible by lattice QCD, holds the name "soft" process. The latter one is described by a hadronic tensor, for which an evolution in terms of $1/Q$ is possible. The first term of this evolution holds the information about the quark distribution functions and is named "leading twist" or "twist-two", while the so-called "higher twist" terms comprise the interaction of quarks and gluons among themselves and are suppressed with $1/Q$ [10, 11].
The differential inclusive DIS cross-section for a solid angle $d\Omega$ in an energy range $[E', E' + dE']$ can be expressed as the product of the leptonic tensor $L_{\mu\nu}$ and the hadronic tensor $W_{\mu\nu}$ [12, 13]:

$$\frac{d^2\sigma}{d\Omega dE'} = \frac{\alpha^2}{2Mq^4} \frac{E'}{E} L_{\mu\nu} W^{\mu\nu} \tag{2.9}$$

where α is the fine structure constant.
In the following considerations we will restrict us to the approximation for the one photon exchange and we will take the sum over all spin states of the final lepton.
For both, the leptonic and the hadronic tensor, a splitting in a not spin-depending, symmetric part (S) and a spin-depending, asymmetric part (A), is possible:

$$L_{\mu\nu}(k, \vec{s}; k') = 2[L_{\mu\nu}^{(S)}(k; k') + iL_{\mu\nu}^{(A)}(k, \vec{s}); k'] \tag{2.10}$$

$$W_{\mu\nu}(q;P,\vec{S}) = W^{(S)}_{\mu\nu}(q;P) + iW^{(A)}_{\mu\nu}(q;P,\vec{S}) \tag{2.11}$$

Inserting (2.10) and (2.11) in (2.12) gives for the cross-section:

$$\frac{d^2\sigma}{d\Omega dE'} = \frac{\alpha^2}{2Mq^4}\frac{E'}{E}[L^S_{\mu\nu}W^{\mu\nu(S)} - L^{(A)}_{\mu\nu}W^{\mu\nu(A)}] \tag{2.12}$$

The leptonic tensor describes the emission of the virtual photon from the lepton in the scattering and can be calculated in Quantum Electrodynamics (QED). In contrary a calculation of the hadronic tensor is not possible due to the complex inner structure of the nucleon. One can only parameterize the tensor in terms of the four scalar inelastic form factors $W_1(Q^2,\nu)$, $W_2(Q^2,\nu)$, $G_1(Q^2,\nu)$ and $G_2(Q^2,\nu)$. The spin-independent form factors W_1 and W_2 and the spin-dependent form factors G_1 and G_2 can be formulated in terms of the following dimensionless scaling functions. For the symmetric part of the hadronic tensor we have for those:

$$F_1(x_{bj},Q^2) = MW_1(Q^2,\nu) \tag{2.13}$$

$$F_2(x_{bj},Q^2) = \nu W_2(Q^2,\nu) \tag{2.14}$$

and for the asymmetric part:

$$g_1(x_{bj},Q^2) = M^2\nu G_1(Q^2,\nu) \tag{2.15}$$

$$g_2(x_{bj},Q^2) = M\nu^2 G_2(Q^2,\nu) \tag{2.16}$$

As one can see for the example of F_2 in fig. 2.2, the structure functions F_1, F_2, g_1 and g_2 are approximately independent of Q^2 and depend nearly only on x_{bj}. This can be interpreted as the consequence of scattering of spin-1/2 beam particles on point-like particles, which means that the nucleon has a substructure of point-like constituents [6].
F_1 and F_2 are connected via the Callan-Gross relation [21]:

$$2x_{bj}F_1(x_{bj}) = F_2(x_{bj}) \tag{2.17}$$

which has been proven experimentally [6].

Measurement of g_1 and g_2

In the following we will note with $\leftarrow$ and $\rightarrow$ the longitudinal polarization of the lepton beam and with $\Leftarrow$ and $\Rightarrow$ the longitudinal polarization of the target nucleon. We then have for the unpolarized cross section:

$$\frac{d^2\sigma^{\leftarrow\Leftarrow}}{d\Omega dE'} + \frac{d^2\sigma^{\leftarrow\Rightarrow}}{d\Omega dE'} = \frac{\alpha^2}{4E^2\sin^4\frac{\theta}{2}}\left[2\sin^2\frac{\theta}{2}F_1 + \frac{M}{\nu}\cos^2\frac{\theta}{2}F_2\right] \tag{2.18}$$

and for the polarized part in the case of longitudinally polarized target nucleons:

$$\frac{d^2\sigma^{\leftarrow\Leftarrow}}{d\Omega dE'} - \frac{d^2\sigma^{\leftarrow\Rightarrow}}{d\Omega dE'} = \frac{4\alpha^2}{M\nu}\frac{E'}{Q^2E}\left[(E+E'\cos\theta)\,g_1 - 2x_{bj}Mg_2\right] \tag{2.19}$$

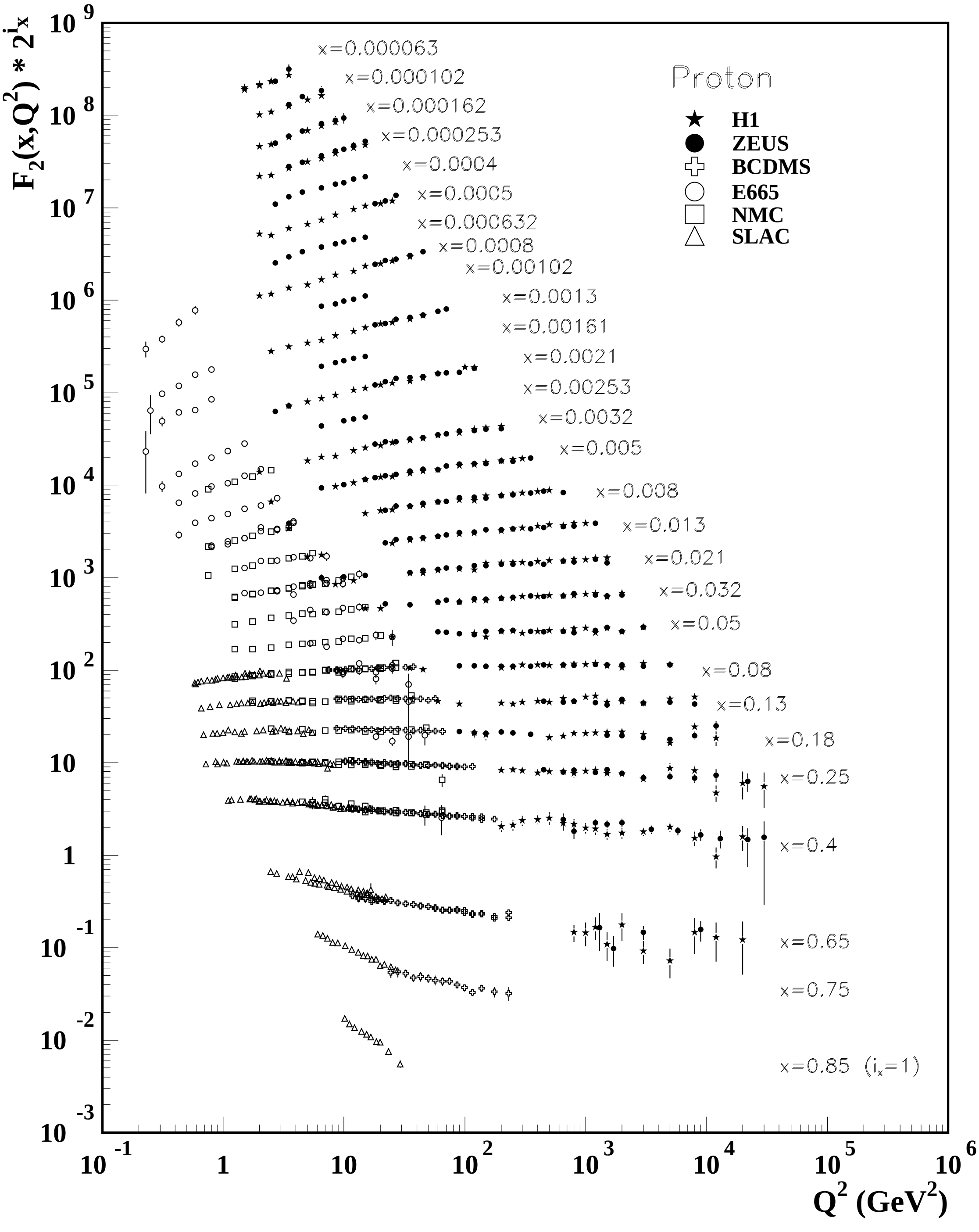

Figure 2.2: *The proton structure function F_2^p as function of Q^2 in bins of $x_{bj}(= x)$. The measurements were in electromagnetic scattering of positrons on protons for $x > 0.00006$ in the Zeus[14] and H1[15] experiments at HERA as well as for electrons (SLAC[16]) and muons (BCDMS[17], E665[18], NMC[19]) on a fixed target. Statistical and systematic errors in quadrature are shown. F_2^p was multiplied by 2^{i_x} with i_x as the number of x bin in the range $i_x = 1(x = 0.85)$ to $i_x = 28(x = 0.000063)$. Figure taken from [20].*

while we get for transversely polarized target nucleons:

$$\frac{d^2\sigma^{\leftarrow\Uparrow}}{d\Omega dE'} - \frac{d^2\sigma^{\leftarrow\Downarrow}}{d\Omega dE'} = \frac{4\alpha^2}{M\nu}\frac{E'^2}{Q^2E}\sin\theta\left[g_1 - \frac{2E}{\nu}g_2\right] \tag{2.20}$$

In the performed experiments, which used a longitudinally polarized lepton beam and a longitudinally polarized target, the following longitudinal spin-spin asymmetry was measured:

$$A_{\parallel} = \frac{d\sigma^{\leftarrow\Rightarrow} - d\sigma^{\leftarrow\Leftarrow}}{d\sigma^{\leftarrow\Rightarrow} + d\sigma^{\leftarrow\Leftarrow}} \tag{2.21}$$

with $d\sigma$ shortly for $\frac{d^2\sigma}{d\Omega dE'}$.

In principal from the measurement of $A_{\parallel}$ we get information about the combination of g_1 and g_2 and not about g_1 or g_2 alone. But, because in eq. (2.19) the coefficient of g_2 is much smaller relative to the one of g_1, g_2 is kinematically suppressed and $A_{\parallel}$ gives us effectively a direct measurement of the structure function g_1. Experimental results from corresponding measurements of $x \cdot g_1(x)$ are shown in fig. 2.3.

For a transversely polarized target one measures the asymmetry:

$$A_{\perp} = \frac{d\sigma^{\leftarrow\Uparrow} - d\sigma^{\leftarrow\Downarrow}}{d\sigma^{\leftarrow\Uparrow} + d\sigma^{\leftarrow\Downarrow}} \tag{2.22}$$

here, for transversely polarized target nucleons (eq. (2.20)), g_2 is not suppressed. Therefore it is possible to get information about g_2 from $A_{\perp}$ in combination with the results from $A_{\parallel}$. For this structure function the E155 collaboration [30, 31] and the E143 collaboration have published results [23].

2.2 The Quark Parton Model

2.2.1 The Naïve Quark Parton Model and its Distribution Functions

As already mentioned in section 2.1 the structure functions F_1, F_2, g_1 and g_2 vary in good approximation only on x_{bj} and very weakly on Q^2, as a function of $\ln Q^2$. This scaling behavior was the reason for Feynman to develop the parton model of the nucleon in the late 1960s. In this model the nucleon consists of point-like constituents [32], which Feynmann called partons. Those were indentified fast with the quarks[1] independently postulated by Gell-Mann and Zweig some years before [33, 34]. In their theory the quarks are particles with a charge of one-third integer and a spin of one half.

In the Quark Parton Model (QPM) it is assumed that the momentum transfer Q^2 of the virtual photon is sufficiently large so that the individual photons can be resolved and

[1]The word quark is taken from the roman “Finnegans Wake” from James Joyce in the phrase: “Three quarks for Muster Mark”. James Joyce has lived many years in Trieste.

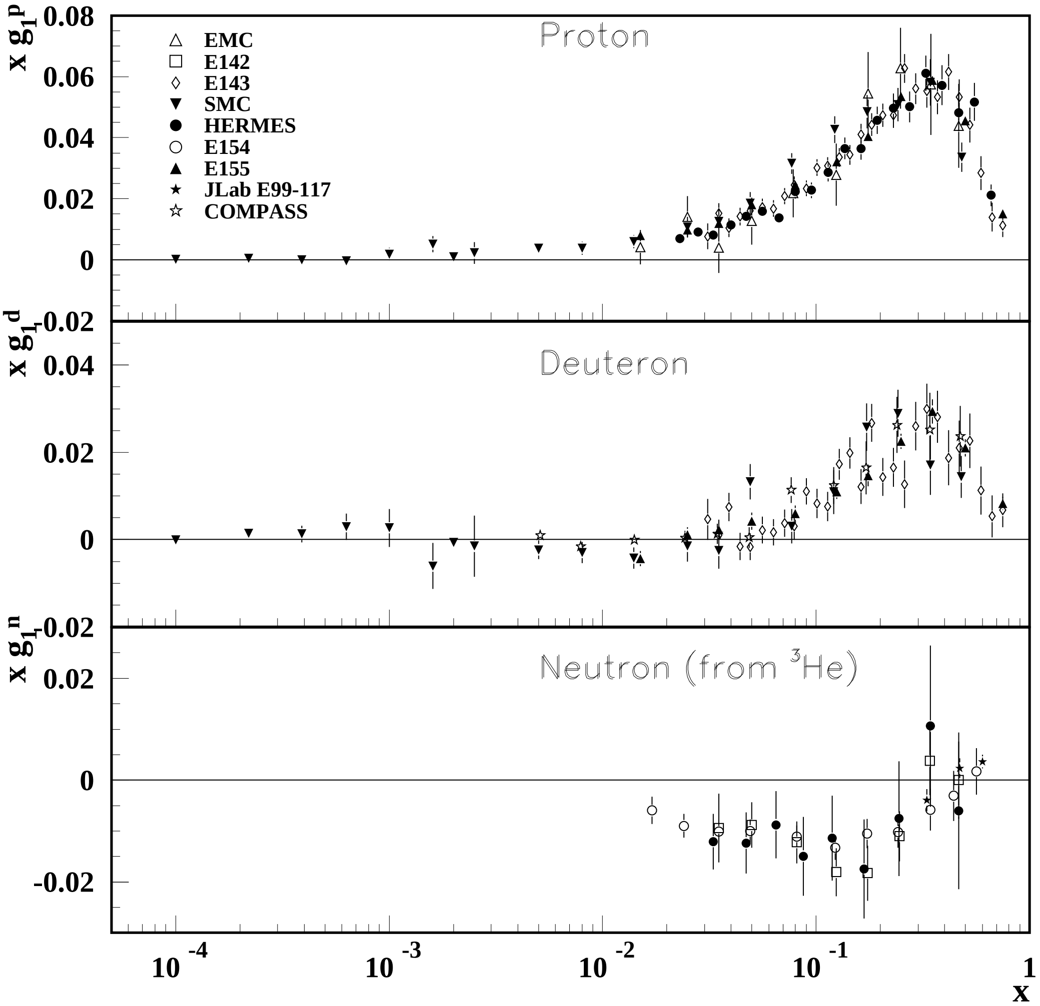

Figure 2.3: *The spin-dependent structure function* $xg_1(x)$ *of the proton (top), deuteron (middle) and neutron (bottom) measured in deep-inelastic scattering of polarized electrons, respectively positrons in E142[22] (*$Q^2 \approx 0.3-10(\mathrm{GeV})^2$*), E143[23] (*$Q^2 \approx 0.3-10(\mathrm{GeV})^2$*), E154[24] (*$Q^2 \approx 1-17(\mathrm{GeV})^2$*), E155[25] (*$Q^2 \approx 1-40(\mathrm{GeV})^2$*), JLab E99-117[26] (*$Q^2 \approx 2.71-4.83(\mathrm{GeV})^2$*), HERMES[27] (*$Q^2 \approx 0.8-20(\mathrm{GeV})^2$*) as well as muons in EMC[2] (*$Q^2 \approx 1-100(\mathrm{GeV})^2$*), SMC[28] (*$Q^2 \approx 0.1-100(\mathrm{GeV})^2$*) and COMPASS[29] (*$Q^2 \approx 1-100(\mathrm{GeV})^2$*). All data shown at the measured* Q^2*, except for EMC shown at* $Q^2 = 10.7(\mathrm{GeV})^2$ *and E155 shown at* $Q^2 = 5(\mathrm{GeV})^2$*. Statistical and systematic errors added in quadrature. Figure taken from [20].*

that the duration of the interaction is so short that the partons cannot interact among themselves. Then a deep inelastic scattering event can be regarded as the superposition of elastic scattering on the single partons.
The QPM is defined in the infinite momentum frame, in which the nucleon moves very fast along a direction. The nucleon is then considered as a beam of massless partons moving parallel to the nucleon, meaning that the transverse momentum of the partons is being neglected. We assume that the hit parton (struck quark) carries a fraction ξ of the nucleon's four-momentum P: $p_q = \xi P$. For the invariant mass W of the hadronic end-product we get:

$$(p_q + q)^2 = W^2 \tag{2.23}$$

For the case of the assumed elastic lepton-parton collisions we have:

$$W^2 = (\xi M)^2 \tag{2.24}$$

With this we can deduce:

$$\xi^2 P^2 + 2\xi Pq + q^2 = \xi^2 M^2 \tag{2.25}$$

With $q^2 = -Q^2$ and $P = M$ this leads to (see eq. (2.5)):

$$\xi = \frac{Q^2}{2pq} = x_{bj} \tag{2.26}$$

So x_{bj} (in the following mostly simple written as x) can be interpreted as the momentum fraction of the nucleon carried by the parton before the scattering.
In our assumed case the hadronic tensor $W^{\mu\nu}$ can be calculated and we get for the parton structure functions:

$$F_1^{parton}(x) = \frac{1}{2} e_p^2 \delta(\xi - x); \quad F_2^{parton}(x) = e_p^2 \xi \delta(\xi - x) \tag{2.27}$$

$$g_1^{parton}(x) = \lambda \frac{1}{2} e_p^2 \delta(\xi - x); \quad g_2^{parton}(x) = 0 \tag{2.28}$$

where e_p denominates the parton's charge and $\lambda = \pm 1$ gives the spin direction of the parton in relation to the one of the nucleon.
Because a parton spin transverse to the spin of the nucleon does not exist in the naïve QPM, the structure function g_2 has there no interpretation.
If the partons in the QPM are ascertained as quarks, the nucleon structure functions can be calculated by summing the parton structure functions over all spin and charge states of the quarks:

$$\mathcal{F}(x) = \sum_{i,\lambda} \int_0^1 q_i^\lambda(\xi); \mathcal{F}^{parton}(x, \xi,) d\xi, \quad \mathcal{F} \in F_1.F_2.g_1, g_2 \tag{2.29}$$

$q_i^\lambda(\xi)$ are the parton distribution functions (PDFs), which give the probability to find a quark with a certain flavor i in a momentum intervall $d\xi$. In an unpolarized nucleon one gets the quark distribution function $q_i(x)$ through the sum of quarks and antiquarks of the flavor i with spin parallel or anti-parallel to the nucleon's spin. Connected to an unpolarized nucleon are the unpolarized structure functions F_1 an F_2, which are:

$$F_1(x) = \frac{1}{2}\sum_i e_i^2 \left(q_i^+(x) + \bar{q}_i^+(x) + q_i^-(x) + \bar{q}_i^-(x)\right) := \frac{1}{2}\sum_i e_i^2 q_i(x) \tag{2.30}$$

$$F_2(x) = x\sum_i e_i^2 \left(q_i^+(x) + \bar{q}_i^+(x) + q_i^-(x) + \bar{q}_i^-(x)\right) := x\sum_i e_i^2 q_i(x) \tag{2.31}$$

For a polarized nucleon the situation is divided in two cases. The first is that the spin of the nucleon is longitudinal to the spin of the incoming lepton. There the corresponding structure functions are:

$$g_1(x) = \frac{1}{2}\sum_i e_i^2 \left(q_i^+(x) + \bar{q}_i^+(x) - q_i^-(x) - \bar{q}_i^-(x)\right) := \frac{1}{2}\sum_i e_i^2 \Delta q_i(x) \tag{2.32}$$

$$g_2(x) = 0 \tag{2.33}$$

The second case is that the polarization of the nucleon is transverse to the spin of the beam lepton. The direction of the quark spin we denote here with $\uparrow$, if it is parallel to the spin of the nucleon and with $\downarrow$, if it is anti-parallel. Analog to g_1 we define a structure function h_1:

$$h_1(x) = \frac{1}{2}\sum_i e_i^2 \left(q_i^{\uparrow}(x) + \bar{q}_i^{\uparrow}(x) - q_i^{\downarrow}(x) - \bar{q}_i^{\downarrow}(x)\right) := \frac{1}{2}\sum_i e_i^2 \Delta_T q_i(x) \tag{2.34}$$

where $\Delta_T q_i(x)$ is the distribution function of transversely polarized quarks, also called *"transversity"*.

2.2.2 Sum Rules and the Spin Crisis

In several models there are existing sum rules to describe the nucleon structure. For this we need the first moment $\Gamma_1^{p,n}$ of g_1 (with proton p and neutron n), which we get by integrating over the whole range of x:

$$\Gamma_1^{p,n} = \int_0^1 g_1^{p,n}(x)dx \tag{2.35}$$

The integrated polarized quark distribution functions we will write as:

$$\Delta q_i = \int_0^1 \Delta q_i(x)dx \tag{2.36}$$

By convention the distribution functions are refering usually to the quark distribution in the proton, but connected via isospin symmetry to the corresponding ones of the neutron:

$$\Delta u_p = \Delta d_n := \Delta u \tag{2.37}$$

$$\Delta d_p = \Delta u_n := \Delta d \tag{2.38}$$

With this notation we obtain for the first moment of g_1 by inserting (2.32) in (2.35) for the proton (valence quarks: uud) and the neutron (udd), respectively:

$$\Gamma_1^p = \frac{1}{2}\left(\frac{4}{9}\Delta u + \frac{1}{9}\Delta d + \frac{1}{9}\Delta s\right) \tag{2.39}$$

$$\Gamma_1^n = \frac{1}{2}\left(\frac{1}{9}\Delta u + \frac{4}{9}\Delta d + \frac{1}{9}\Delta s\right) \tag{2.40}$$

Δs stands hereby for the contribution of the strange sea quarks, heavier quarks in the sea are neglected.
Those relations can also be expressed in terms of the proton matrix elements of the axial vextor current a_k:

$$\Gamma_1^{p,n} = \pm\frac{1}{12}\underbrace{(\Delta u - \Delta d)}_{a_3} + \frac{1}{36}\underbrace{(\Delta u + \Delta d - 2\Delta s)}_{\sqrt{3}a_8} + \frac{1}{9}\underbrace{(\Delta u + \Delta d + \Delta s)}_{a_0} \tag{2.41}$$

The matrix elements a_3 and a_8 can be gained from hyperon β-decay and are therefore connected to the weak decay constants F and D via [12]:

$$a_3 = F + D \tag{2.42}$$

$$\sqrt{3}a_8 = 3F - D \tag{2.43}$$

Measurements from hyperon decay gave here [35]:

$$F = 0.46 \pm 0.01; \qquad D = 0.79 \pm 0.01 \tag{2.44}$$

The Bjørken sum rule we get now by the difference between the first moments of the proton (eq. (2.39)) and the neutron (2.40):

$$\Gamma_1^p - \Gamma_1^n = \frac{1}{6}a_3 \tag{2.45}$$

A check of this sum rule was realized for the first time with the measurements of Γ_1^p by the EMC collaboration [1] and Γ_1^n by the SMC collaboration [28]. The resulting value for the Bjørken sum rule was found to be consistent with the expectation from the known value of a_3.
By assuming $\Delta s = \Delta\bar{s} = 0$ we can deduce $a_0 = \sqrt{3}a_8$ and by this we obtain from (2.41) the Ellis-Jaffe sum rule:

$$\Gamma_1^{p,n} = \frac{1}{12}a_3\left(\pm 1 + \frac{5}{\sqrt{3}}\cdot\frac{a_8}{a_3}\right) \tag{2.46}$$

The result of the EMC collaboration for Γ_1^p brought a large violation of the Ellis-Jaffe sum rule, meaning that the assumption $\Delta s = \Delta\bar{s} = 0$ had to be abandoned. Γ_1^p was then used to extract a_0, Δu, Δd and Δs.
In (2.41) a_0 corresponds to

$$a_0 = \Delta u + \Delta d + \Delta s := \Delta\Sigma \tag{2.47}$$

and is therefore equivalent to the quark helicity distribution or axial charge $\Delta\Sigma$, which calculates the sum of the spin contributions of the quarks and antiquarks of all flavors and should in the QPM therefore give the total nucleon spin[2]:

$$S_z = \frac{1}{2}\sum_i \Delta q_i = \frac{1}{2}\Delta\Sigma \tag{2.48}$$

As the spin of the nucleon is 1/2, a_0 should consequently have a value near 1. Surprisingly the EMC result was unexpectedly small and compatible with zero [12]:

$$a_0 = 0.06 \pm 0.12 \pm 0.17 \tag{2.49}$$

where the first error is the statistical and the second the systematic one.
Later experiments confirmed this measurement at least qualitatively. The actual values of $\Gamma_1^p(Q^2)$ for $Q^2 = 10(GeV/c)^2$ measured by many experiments lie in the range:

$$0.130 \leqq \Gamma_1^p(Q^2 = 10(GeV/c)^2) \leqq 0.142 \tag{2.50}$$

resulting for a_0 in

$$0.22 \leqq a_0(Q^2 = 10(GeV/c)^2) \leqq 0.34 \tag{2.51}$$

meaning that not more than nearly one third of the nucleon spin is covered by the quarks. This not understanded observation was called the *"spin crisis"*. It clearly means that the naïve Quark Parton Model is not a sufficient description of the nucleon structure.

2.2.3 The QCD-extended Parton Model

The missing part of the nucleon spin was an indication that there some constituents are missing, which were identified with the gluons. Those don't have a direct interaction with the exchanged virtual photon, but they mediate the strong interaction as the exchanged gauge bosons in the field theory of Quantum Chromodynamics (QCD) and yield therefore to corrections to the Quark Parton Model. With the QCD we have a more-or-less complete description of the nucleon corresponding to our current knowledge.
The PDFs then depend in a way on Q^2, which is calculable in QCD. Consequently the formalism of the QPM remains in principle unchanged, apart from replacing $q(x)$ by $q(x, Q^2)$.

The interpretation for this Q^2 dependance can be found in the interaction between quarks and gluons. The gluons as gauge bosons are radiated by the quarks and can be re-absorbed by the quarks, but can also produce quark-antiquark pairs by themselves or radiate further gluons. This dynamics creates a "cloud" of gluons and virtual $q\bar{q}$ pairs, the so-called "sea"[3]. How the outside world observes a quark therefore depends on the resolution power of the virtual photon depending on $1/\sqrt{Q^2}$. With a larger Q^2 the photon starts to see the sea in

[2]The polarization is assumed to be in the z-direction.
[3]Accordingly the quarks and antiquarks in the sea are called "sea quarks".

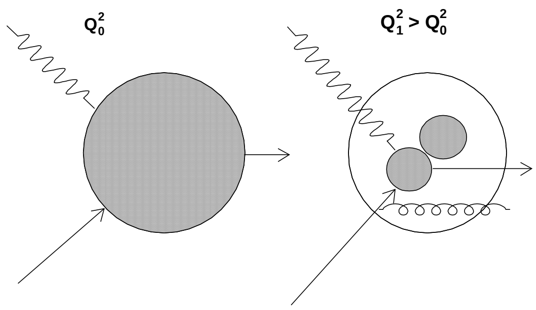

Figure 2.4: *Resolution power of the virtual photon. Left: At a small momentum transfer Q_0^2 the photon resolves only large structures. Right: With increasing momentum transfer $Q_1^2 > Q_0^2$ smaller structures become visible and the number of resolved partons increases. Therefore the averaged momentum fraction x of the partons sinks accordingly. This is known as scaling violation. Figure taken from [36].*

more detail and the number of the resolved partons increases (see fig. 2.4).
Thus the number of partons with a smaller momentum fraction x grows with Q^2, while the number of those with a large one falls. This causes the phenomenom of scaling violation for the nucleon structure functions. As said in section 2.1 those functions are only approximatively independent of Q^2. Various experiments had verified that in consistency with the expectation from the QCD-extended QPM the structure functions grow for small values of x with Q^2 and sink for large ones and the scaling behavior is therefore violated (see fig. 2.5).
The Q^2 evolution of the PDFs can be calculated by the Dokshitzer-Gribov-Lipatov-Altarelli-Parisi (DGLAP) equations [37, 38, 39]. Those describe the fact that a quark with momentum fraction x can come from a parent quark with a larger momentum, which had radiated a gluon before or from a parent gluon, which had created a $q\bar{q}$ pair. If the PDFs are known at a certain scale of Q^2, they can so be calculated at any other scale.

Total Nucleon Spin in the Longitudinal Case

In the QCD-extended Quark Parton Model we then have in the case of a measurement on a longitudinal polarized target for the total nucleon spin from eq. (2.48) by including in addition to $\Delta\Sigma$ the possible contributions from the gluon spin ΔG, the orbital angular momenta of the quarks and gluons, $\langle L_z^q \rangle$ and $\langle L_z^g \rangle$, respectively:

$$S_z = \frac{1}{2} = \frac{1}{2}\Delta\Sigma + \Delta G + \langle L_z^q \rangle + \langle L_z^g \rangle \tag{2.52}$$

The direct measurement of ΔG is one of the most important goals at COMPASS as well as other polarized SIDIS experiments as HERMES at DESY and high energy polarized pp scattering experiments at RHIC at the Brookhaven National Laboratory.

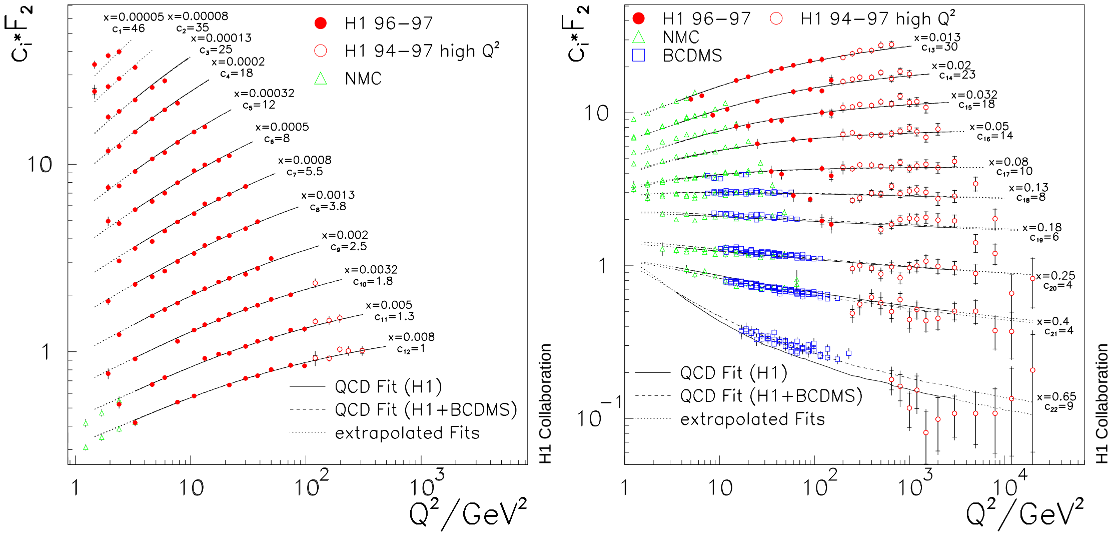

Figure 2.5: *Scaling violation of the structure function F_2 (figure from the H1 collaboration [15]. Left: For small x the F_2 function increases with growing Q^2. Right: From $x \approx 0.25$ on the structure function falls with growing Q^2.*

2.2.4 The Transverse Quark Distribution Function (Transversity)

For a complete description of the spin structure of the nucleon at leading twist we need all three quark distribution function mentioned in section 2.2.1: The spin independent quark distribution function $q(x)$, the longitudinal quark distribution function (helicity distribution function) $\Delta q(x)$ and the transverse quark distribution function (transversity) $\Delta_T q(x)$. Because transverse spin effects are suppressed kinematically in many cases [40] and thus can be neglected in leading order under this circumstances, the investigation of transverse spin effects was for a long time theoretically and experimentally disregarded.
In contrast in other situations the significance of transverse spin effects has become evident in recent years. Particulary the quark transversity is in no way suppressed and gives the largest contributions for some hadronic processes.
The optical theorem connects the hadronic tensor to the imaginary part of the forward virtual Compton scattering amplitude [13]. The distribution functions, which occur in the tensor parametrisation at leading twist, can therefore be written in terms of the imaginary part of the quark-nucleon forward amplitudes. Descriptively this can be understood as a process in which a nucleon radiates a quark, which interacts with the incoming virtual photon and is afterwards re-absorbed by the nucleon. This procedure is represented by a "handbag" diagram in fig. 2.6.
Generally there are 16 possible scattering amplitudes of the form $A_{\Lambda\lambda,\Lambda'\lambda'}$ with Λ, Λ' and λ, λ' as the nucleon and quark helicities, respectively. Because of time-reversal ($A_{\Lambda\lambda,\Lambda'\lambda'} = A_{\Lambda'\lambda',\Lambda\lambda}$) and parity invariance ($A_{\Lambda\lambda,\Lambda'\lambda'} = A_{-\Lambda'-\lambda',-\Lambda-\lambda}$) as well as helicity[4]

[4]The helicity of a particle is given by the projection of its spin $\vec{s}$ onto its momentum $\vec{p}$: $h = \frac{\vec{s}\cdot\vec{p}}{|\vec{s}|\cdot|\vec{p}|}$.

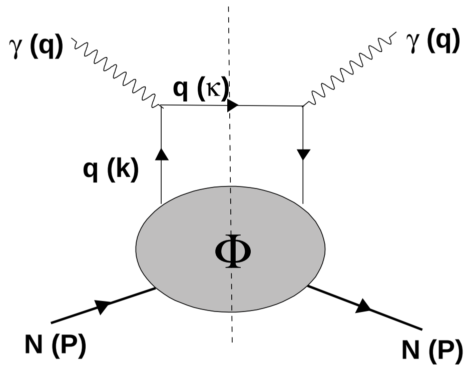

Figure 2.6: *Handbag diagram for emission and reabsorption of a quark, taken from [41].*

conservation ($\Lambda + \lambda = \Lambda' + \lambda'$), only three of them remain:

$$A_{++,++}, A_{+-,+-}, A_{+-,-+}$$

illustrated as handbag diagrams in fig. 2.7.

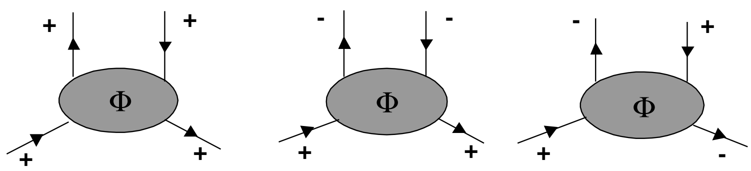

Figure 2.7: *Handbag diagrams of the three quark-nucleon helicity amplitudes, taken from [41].*

As for $A_{++,++}, A_{+-,+-}$ the quark does not flip its helicity, those amplitudes are diagonal in the helicity basis. $A_{++,++}$ hereby corresponds to the quark distribution $q^+(x)$ from section 2.2.1 and $A_{+-,+-}$ accordingly to $q^-(x)$. So we get the following relations:

$$q(x) = q^+(x) + q^-(x) \propto \Im(A_{++,++} + A_{+-,+-}) \tag{2.53}$$

$$\Delta q(x) = q^+(x) - q^-(x) \propto \Im(A_{++,++} - A_{+-,+-}) \tag{2.54}$$

For the third amplitude $A_{+-,-+}$ we have a helicity flip, thus this amplitude is off-diagonal in the helicity basis and has there no probabilistic interpretation. But if we consider the transversity basis:

$$|\uparrow>=\frac{1}{\sqrt{2}}[|+>+i|->], \quad |\downarrow>=\frac{1}{\sqrt{2}}[|+>-i|->] \tag{2.55}$$

with $\uparrow$ parallel to the transverse spin of the nucleon, we can relate the amplitude $A_{+-,-+}$ to the transversity distribution function:

$$\Delta_T q(x) = q^{\uparrow} - q^{\downarrow} \propto \Im(A_{\uparrow\uparrow,\uparrow\uparrow} - A_{\uparrow\downarrow,\uparrow\downarrow}) \tag{2.56}$$

The transverse distribution function has partly a very different behavior than the unpolarized or the longitudinal distribution functions. Unlike as for the latter ones, there is no gluonic contribution for transversity. A hypothetical $\Delta_T G(x)$ would require a gluon-nucleon amplitude with a helicity flip, which cannot be realized due to helicity conservation. Gluons have a helicity of ± 1, therefore we need a helicity change of the nucleon of ± 2, which is impossible.
Consequently the transverse structure function $h_1(x)$ connected to the transversity $\Delta_T q(x)$ has no scaling violation as the unpolarized and the longitudinal polarized structure functions do (see section 2.2.3).
Transversity is chiral-odd[5], meaning in this context that the helicity of the quark has to be flipped. As the helicity is conserved, the process as a whole has to be chiral-even, so we need another chiral-odd function from a second hadron, which we do not have in inclusive DIS. $\Delta_T q(x)$ is therefore not accessible by inclusive DIS, but the measurement can be done e.g. in polarized semi-inclusive lepton-nucleon DIS (SIDIS), where we have another hadron in the final state [4], or in the Drell-Yan process, where the second hadron is in the initial state [4].

Soffer Inequality

From the definition of $q(x)$ and $\Delta q(x)$ we can deduce two bounds for the leading twist distribution functions:

$$|\Delta q(x)| \leqq q(x) \tag{2.57}$$

$$|\Delta_T q(x)| \leqq q(x) \tag{2.58}$$

Another inequality comprising simultaneously $q(x)$, $\Delta q(x)$ and $\Delta q_T(x)$ was developed by Soffer ("Soffer bound") [43]:

$$q(x) + \Delta q(x) \geqq 2|\Delta_T q(x)| \tag{2.59}$$

[5]The chirality gives the "handedness" of a particle in the spinor solutions of the Dirac equation. In the relativistic limit $m/E \to 0$ chirality is identical with helicity [42].

Tensor Charge

Analog to the axial charge in the longitudinal case we can define the tensor charge Σ_T or g_T as a fundamental parameter for the properties of the nucleon:

$$\Sigma_T\ (= g_T) = \sum_i \int_0^1 (\Delta_T q_i(x) - \Delta_T \bar{q}_i(x))\, dx = \sum_i \int_0^1 \Delta_T u(x) + \Delta_T d(x) + \Delta_T s(x) dx \tag{2.60}$$

Thus Σ_T gives the net number of transverse polarized valence quark in a transversely polarized nucleon. The difference to the axial charge $\Delta\Sigma$ is related to the relativistic nature of the nucleon [13].

Total Nucleon Spin in the Transverse Case: Bakker Leader Trueman sum rule

In the case of a measurement on a transversely polarized nucleon the Bakker Leader Trueman sum rule is valid [3]:

$$S_z = \frac{1}{2} = \frac{1}{2}\sum_i \int_0^1 (\Delta_T q_i(x) + \Delta_T \bar{q}_i(x))\, dx + \sum_i \langle L_T^{q_i} \rangle + \sum_i \langle L_T^{\bar{q}_i} \rangle + \sum_g \langle L_T^{g} \rangle \tag{2.61}$$

$$= \frac{1}{2}\sum_i (\Delta_T q_i + \Delta_T \bar{q}_i) + \sum_{q,\bar{q},g} \langle L_T \rangle$$

As emphasized before there is no gluon contribution to the transverse polarization of the nucleon, so the measurement in this case offers an independent access to the contribution of the orbital angular momentum of quarks, antiquarks and gluons to the nucleon spin.

2.3 Extension to Semi-Inclusive DIS (SIDIS)

Like already mentioned in section 2.2.4 in semi-inclusive DIS of a lepton on a nucleon, at least a part of the hadronic final state is detected:

$$l(k, \vec{s}) + N(P, \vec{S}) \rightarrow l'(k', \vec{s'}) + h(P_h) + X \tag{2.62}$$

where h is the observed hadronic end-product with four-momentum P_h and energy E_h. The corresponding hand-bag-diagram can be seen in fig. 2.8. The Φ term illustrated there is the same as in DIS (hand-bag diagram fig. 2.6), the Δ term gives the evolution of the struck quark into the hadronic final state. These terms are representing the "soft" part of the scattering process, while the actual scattering of the virtual photon is described with the "hard" part.
In addition to the Lorentz variables for DIS, for SIDIS we can define two further Lorentz variables:

$$P \cdot P_h \stackrel{lab}{=} M E_h \tag{2.63}$$

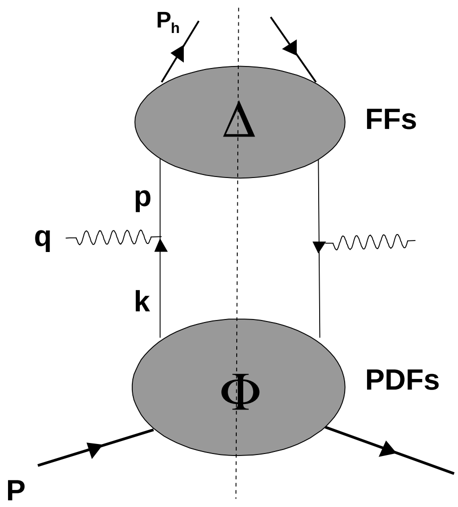

Figure 2.8: *Handbag diagram in the SIDIS case. The Φ term is the same like in DIS, the Δ term describes the hadronization. Taken from [41].*

$$q \cdot P_h \overset{lab}{=} \nu E_h - \vec{q} \cdot \vec{P_h} \tag{2.64}$$

Beside x_{bj} and y we define also a third scaling variable z, which gives the proportion of the energy of the virtual photon carried by the hadron:

$$z := \frac{P \cdot P_h}{P \cdot q} \overset{lab}{=} \frac{E_h}{\nu}; \qquad 0 \leq z \leq 1 \tag{2.65}$$

2.3.1 Fragmentation Functions

To extend the QPM to semi-inclusive processes we need a closer consideration of the production process of the hadrons from the quark struck by the virtual photon, which is called the fragmentation. If we regard the struck quark as a source of a beam of hadrons by neglecting their transverse momentum, the fraction of the quark momentum, which is carried by a hadron produced in the fragmentation, can be expressed by:

$$P_h = \eta p_q = \eta(xP + q) \tag{2.66}$$

The fragmentation functions $D_{h/q}(\eta)$ are then defined in that way that $D_{h/q}(\eta)d\eta$ gives the number of hadrons of a type h with their momentum in the interval $d\eta$ produced in the fragmentation of a quark of type q.
For eq. (2.66) we get by multiplying by the initial nucleon momentum P:

$$P \cdot P_h = \eta P(xP + q) = \eta(xP^2 + P \cdot q) \approx \eta P \cdot q \tag{2.67}$$

then we obtain by neglecting the nucleon mass given by $M = P$ in the laboratory frame to the second power:

$$\eta = \frac{P \cdot P_h}{P \cdot q} \tag{2.68}$$

which we can identify with z defined in eq. (2.65).
The fragmentation functions depend strongly on the flavor of the initial quark in comparison to the flavor of the quarks, which build the produced hadron.
More precisely we distinguish two types of fragmentation functions: the *favored* fragmentation functions, where the fragmenting quark has the same flavor as one of the valence quarks of the produced hadron and the *unfavored* fragmentation functions, where the fragmenting quark is not a valence quark of the hadronic product.
Because of isospin symmetry and charge conjugation the number of different fragmentation functions connected to π^+ and π^- e.g. is reduced to two:

$$D_{\pi^+/u} = D_{\pi^+/\bar{d}} = D_{\pi^-/\bar{u}} = D_{\pi^-/d} \qquad \textit{favored} \tag{2.69}$$

$$D_{\pi^+/\bar{u}} = D_{\pi^+/d} = D_{\pi^-/u} = D_{\pi^-/\bar{d}} \qquad \textit{unfavored} \tag{2.70}$$

From measurements we know that $D_{fav} > D_{unfav}$.

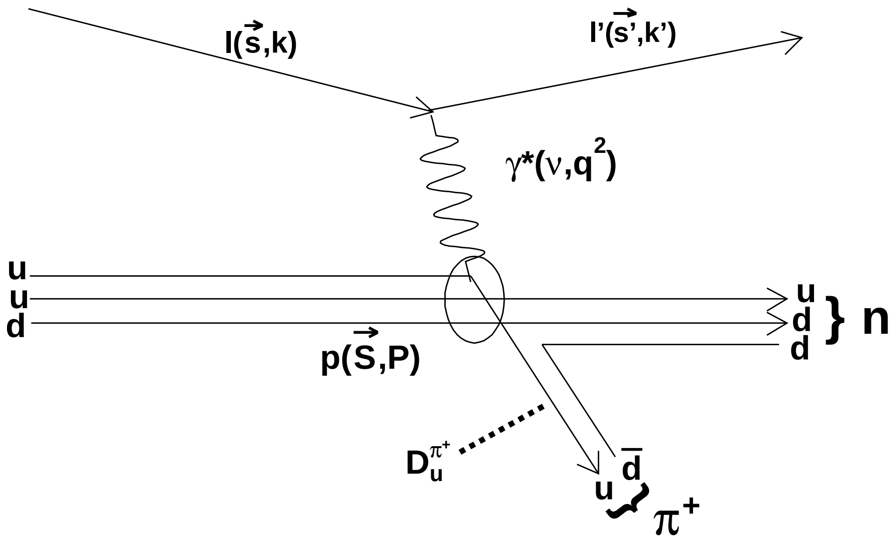

Figure 2.9: *View of a semi-inclusive DIS process. Here the virtual photon interacts with an u quark in a proton resulting in the production of a $d\bar{d}$ quark-antiquark pair and the fragmentation of the proton in a π^+ and a neutron, which can fragment anew. In this case the probability of the fragmentation of a u quark into a positive pion is given by the favored fragmentation function $D_{\pi^+/u}$. Figure taken from [36].*

As in the case of the quark distribution functions we distinguish between unpolarized, longitudinally polarized and transversely polarized quarks. Declaring the probability that a quark q is fragmenting in a hadron h with momentum fraction z by $\mathcal{N}_{h/q}(z)$, the spin direction of a longitudinally polarized quark by $\pm$ and the one of a transversely polarized quark by $\uparrow\downarrow$, we have the following fragmentation functions:

$$D_{h/q}(z) = \mathcal{N}_{h/q}(z) \qquad \textit{unpolarized} \tag{2.71}$$

$$\Delta D_{h/q}(z) = \mathcal{N}_{h/q^+}(z) - \mathcal{N}_{h/q^-}(z) \qquad \textit{longitudinally polarized} \tag{2.72}$$

$$\Delta_T D_{h/q}(z) = \mathcal{N}_{h/q^\uparrow}(z) - \mathcal{N}_{h/q^\downarrow}(z) \qquad \textit{transversely polarized} \tag{2.73}$$

The hadronic structure functions for semi-inclusive production we get by adjoining the according fragmentation functions to the DIS structure functions:

$$F_1^h(x,z) = \frac{1}{2}\sum_q e_q^2 q_q(x) D_{h/q}(z) \tag{2.74}$$

$$F_2^h(x,z) = x\sum_q e_q^2 q_q(x) D_{h/q}(z) \tag{2.75}$$

$$g_1^h(x,z) = \frac{1}{2}\sum_q e_q^2 \Delta q_q(x) \Delta D_{h/q}(z) \tag{2.76}$$

$$h_1^h(x,z) = \frac{1}{2}\sum_q e_q^2 \Delta_T q_q(x) \Delta_T D_{h/q}(z) \tag{2.77}$$

2.3.2 SIDIS Cross-Section

The dependance of the parton distributions of the transverse momentum is neglected in the standard parametrization for the collinear case. In contrary to this we will describe here the semi-inclusive DIS cross-section in terms of transverse momentum dependent (TMD) parton distribution functions and fragmentation functions, which explicitly depend on the transverse momentum of the parton $\vec{k_T}$ with respect to the direction of the virtual photon and on the transverse momentum $\vec{p}_T^h$ of the produced hadron with respect to the direction of the fragmenting quark.

As coordinate system we will use the "gamma-nucleon-system" (GNS), where the virtual photon direction defines the z axis and the lepton scattering plane, which is given by the initial and final lepton momenta, defines the xz plane (see fig. 2.10). In this system the SIDIS cross-section depends on the azimuthal angle ϕ_h of the produced hadron with respect to the scattering plane and on the azimuthal angle of the spin of the target nucleon ϕ_S.

If we assume single photon exchange and spin-0 ("unpolarized") final state hadrons we get

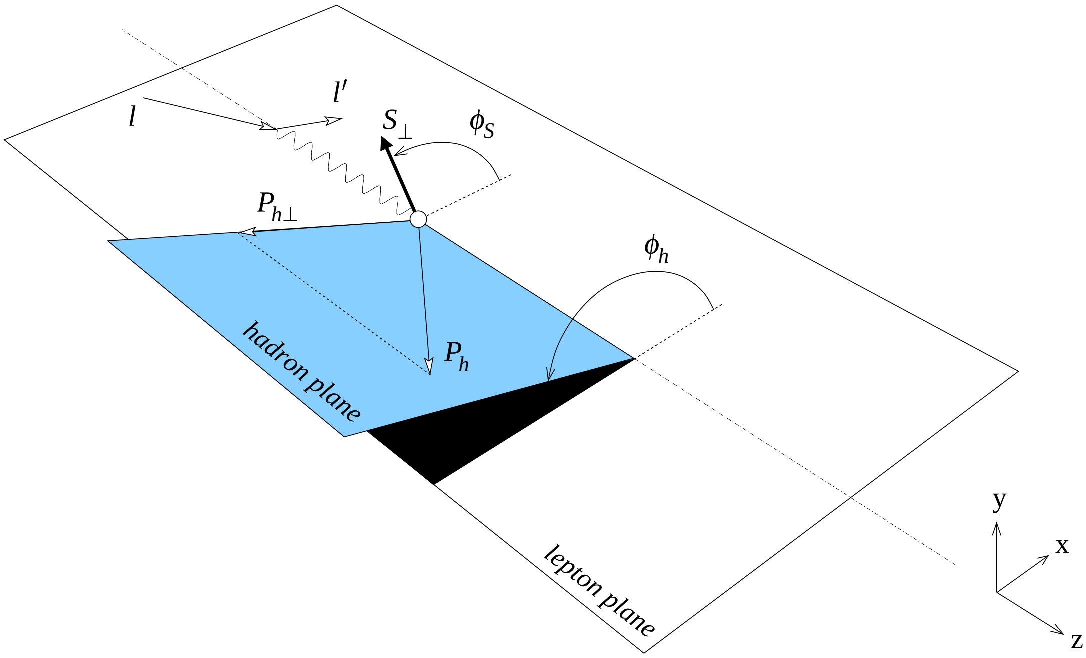

Figure 2.10: *Definition of the "gamma-nucleon-system" (GNS): The z axis is defined by the direction of the virtual photon and the xz plane is the lepton scattering plane. Figure taken from [44].*

for the SIDIS cross-section [45]:

$$
\begin{aligned}
&\frac{d\sigma}{dx dy d\phi_S dz d\phi_h dP_T^{h2}} = \\
&\quad \frac{\alpha^2}{xyQ^2}\frac{y^2}{2(1-\varepsilon)}\left(1+\frac{\gamma^2}{2x}\right)\Big\{F_{UU,T} + \varepsilon F_{UU,L} + \sqrt{2\varepsilon(1+\varepsilon)}\cos\phi_h F_{UU}^{\cos\phi_h} \\
&\quad + \varepsilon\cos(2\phi_h) F_{UU}^{\cos(2\phi_h)} + \lambda_\varepsilon\sqrt{2\varepsilon(1-\varepsilon)}\sin\phi_h F_{LU}^{\sin\phi_h} \\
&\quad + S_{||}\left[\sqrt{2\varepsilon(1+\varepsilon)}\sin\phi_h F_{UL}^{\sin\phi_h} + \varepsilon\sin(2\phi_h) F_{UL}^{\sin(2\phi_h)}\right] \\
&\quad + S_{||}\lambda\varepsilon\left[\sqrt{1-\varepsilon^2} F_{LL} + \sqrt{2\varepsilon(1-\varepsilon)}\cos\phi_h F_{LL}^{\cos\phi_h}\right] \\
&\quad + S_\perp\Big[\sin(\phi_h-\phi_S)\left(F_{UT,T}^{\sin(\phi_h-\phi_S)} + \varepsilon F_{UT,L}^{\sin(\phi_h-\phi_S)}\right) \\
&\quad + \varepsilon\sin(\phi_h+\phi_S) F_{UT}^{\sin(\phi_h+\phi_S)} + \varepsilon\sin(3\phi_h-\phi_S) F_{UT}^{\sin(3\phi_h-\phi_S)} \\
&\quad + \sqrt{2\varepsilon(1+\varepsilon)}\sin\phi_S F_{UT}^{\sin\phi_S} + \sqrt{2\varepsilon(1+\varepsilon)}\sin(2\phi_h-\phi_S) F_{UT}^{\sin(2\phi_h-\phi_S)}\Big] \\
&\quad + S_\perp\lambda_\varepsilon\Big[\sqrt{1-\varepsilon^2}\cos(\phi_h-\phi_S) F_{LT}^{\cos(\phi_h-\phi_S)} + \sqrt{2\varepsilon(1-\varepsilon)}\cos(\phi_S) F_{LT}^{\cos(\phi_S)} \\
&\quad + \sqrt{2\varepsilon(1-\varepsilon)}\cos(2\phi_h-\phi_S) F_{LT}^{\cos(2\phi_h-\phi_S)}\Big]\Big\}
\end{aligned}
\tag{2.78}
$$

where λ_ε is the helicity of the beam lepton and $S_{||}$ and $S_\perp$ give the projection of the target spin in the plane longitudinal or transverse with respect to the direction of the virtual photon, respectively. ε is the ratio of the longitudinal and the transverse photon flux:

$$\varepsilon = \frac{1 - y - \frac{1}{4}\gamma^2 y^2}{1 - y + \frac{1}{2}y^2 + \frac{1}{4}\gamma^2 y^2} \tag{2.79}$$

Because of $\gamma = \frac{2Mx}{Q} \approx 0$, we will neglect it in the following. As we can see the structure functions F depend on the variables x, Q^2, z and P_T^h[6]. The notation of the structure functions (e.g. $F_{UT}^{\sin(\phi_h+\phi_S)}$ or $F_{UT,T}^{\sin(\phi_h-\phi_S)}$) is the following: The first two subscripts represant the polarization of the beam and the target, respectively (U = unpolarized, L = longitudinally polarized, T = transversely polarized), the third subscript indicates the polarization of the virtual photon, while the superscript indicates the corresponding azimuthal modulation in ϕ_h and ϕ_S.
Alltogether there are eighteen structure functions, eight of them depend on the transverse polarization of the target with a different azimuthal modulation for each term. Due to this it is possible to build cross-section asymmetries and extract each term from data.

2.3.3 Structure Functions, Notation, Terminology

The basis for the calculation of the structure functions in eq. (2.78) is the factorization of the cross-section into the photon-quark scattering process as the "hard" part, and into TMD parton distribution and fragmentation functions as the "soft" part. For the explicit expression of those structure functions see [45].
The eight leading twist transverse momentum dependent parton distribution functions in the cross-section are listed in table 2.1. The notation follows [45]: f, g and h denote respectively the unpolarized, longitudinally and transversely polarized polarization of the quark, the subscript 1 signifies that the corresponding function is a leading twist contribution, the subscripts L and T mark the polarization of the target nucleon (L = longitudinally, T = transversely polarized) and the superscript $\perp$ tags the presence of a transverse momentum effect.
One gets the structure functions in eq. (2.78) from the TMD PDFs by a convolution of the type:

$$\mathcal{C}[wfD] = x \sum_a e_a^2 \int d^2\vec{k}_T d^2\vec{p}_T^h \delta^{(2)}\left(\vec{k}_T - \vec{p}_T^h - \vec{P}_T^h/z\right) w(\vec{p}_T^h, \vec{k}_T) f_a(x, k_T^2) D_a(z, {p_T^h}^2) \tag{2.80}$$

where f and D are generic parton distribution and fragmentation functions, respectively and $w(\vec{p}_T^h, \vec{k}_T)$ is a function of the transverse momenta and the summation is over all quarks and antiquarks, while the δ-function guarantees the transverse momentum conservation.

[6] P_T^h stands for the transverse momentum of the produced hadron with respect to the photon direction, while p_T^h gives the transverse momentum of the produced hadron with respect to the direction of the fragmenting quark.

Distribution function (DF)	meaning
$f_1(x, k_T^2)$	unpolarized distribution
$g_{1L}(x, k_T^2)$	helicity distribution
$g_{1T}(x, k_T^2)$	distribution of longitudinally polarized quarks in a transversely polarized nucleon
$f_{1T}^{\perp}(x, k_T^2)$	Sivers distribution
$h_{1T}(x, k_T^2)$	distribution of transversely polarized quarks in a transversely polarized nucleon
$h_{1L}^{\perp}(x, k_T^2)$	distribution of transversely polarized quarks along their intrinsic transverse momentum in a longitudinally polarized nucleon
$h_{1T}^{\perp}(x, k_T^2)$	distribution of transversely polarized quarks along their intrinsic transverse momentum in a transversely polarized nucleon
$h_1^{\perp}(x, k_T^2)$	distribution of transversely quarks polarized along the normal to the plane defined by the quark intrinsic transverse momentum and the nucleon momentum in an unpolarized nucleon

Table 2.1: *The eight leading twist TMD parton distribution functions.*

Four of those eight TMD structure functions given in eq. (2.78) can be expressed by leading twist parton distribution functions:

$$F_{UT}^{\sin(\phi_h+\phi_S)} = \mathcal{C}\left[-\frac{\hat{h}\cdot\vec{p}_T^{\,h}}{M_h} h_1 H_1^{\perp}\right] \tag{2.81}$$

$$F_{UT,T}^{\sin(\phi_h-\phi_S)} = \mathcal{C}\left[-\frac{\hat{h}\cdot\vec{k}_T}{M} f_{1T}^{\perp} D\right] \tag{2.82}$$

$$F_{UT}^{3\sin(\phi_h-\phi_S)} = \mathcal{C}\left[\frac{2(\hat{h}\cdot\vec{k}_T)(\vec{k}_T\cdot\vec{p}_T^{\,h}) + k_T^2(\hat{h}\cdot\vec{p}_T^{\,h}) - 4(\hat{h}\cdot\vec{k}_T)^2(\hat{h}\cdot\vec{p}_T^{\,h})}{2M^2 M_h} h_{1T}^{\perp} H_1^{\perp}\right] \tag{2.83}$$

$$F_{LT}^{\cos(\phi_h-\phi_S)} = \mathcal{C}\left[\frac{\hat{h}\cdot\vec{k}_T}{M} g_{1T} D\right] \tag{2.84}$$

with M as the nucleon mass, M_h as the mass of the produced hadron and $\hat{h} = \vec{P}_T^h/|\vec{P}_T^h|$. Analog to the TMD structure functions one gets the unpolarized structure function by:

$$F_{UU,T} = \mathcal{C}\left[f_1 D\right] \tag{2.85}$$

with the unpolarized PDF $f_1 = q$ and the unpolarized fragmentation function D.
Eq. (2.81) which contains the transversity $h_1(x, k_T^2)$ in the transverse momentum dependent form is connected to the Collins effect (see the following section for the description). The TMD transversity is defined as:

$$h_1(x, k_T^2) = h_{1T}(x, k_T^2) - \frac{k_T^2}{2M^2} h_{1T}^{\perp}(x, k_T^2) \tag{2.86}$$

We get the transversity distribution introduced in section 2.2.1 from the TMD transversity by integration over the transverse momentum $\vec{k}_T$:

$$\Delta_T q(x) = h_1(x) = \int d^2\vec{k}_T h_1(x, k_T^2) \tag{2.87}$$

The fragmentation function $H_1^{\perp}$ in eq. (2.81) is the so-called Collins fragmentation function, which describes the spin-dependent part of the fragmentation of a transversely polarized quark into a spinless ("unpolarized") hadron.
Eq. (2.82) is related to the Sivers effect (description in section 2.5). Here the Sivers (distribution) function $f_{1T}^{\perp}$ is convoluted with the unpolarized fragmentation function D.
The Collins and Sivers contributions are the ones, which until now attract the most experimentally and theoretically attention.
The structure functions in the other two eq. (2.83) and (2.84) contain the parton distribution functions $h_{1T}^{\perp}$ convoluted with $H_1^{\perp}$ and g_{1T} convoluted with D, respectively.
The four structure functions in eq. (2.78) beside those four twist-2-functions are twist-3-contributions and do not have a simple interpretation in the parton model.

2.4 The Collins Mechanism

The Collins mechanism in SIDIS describes the fragmentation of an transversely polarized quark in a transversely polarized target nucleon into spinless ("unpolarized") hadrons. It results in an azimuthal modulation in the distribution of the produced hadrons. This left-right asymmetry is due to the combination of two chiral-odd functions, the transversity $\Delta_T q(x)$ and the transverse fragmentation function (FF) $H_1^{\perp}$. At leading twist such a naïvely T-odd FF[7] caused by final state interactions was predicted by Collins [4] and is now called the Collins FF.
We can define $H_1^{\perp}$ by considering the distribution of hadrons produced from quarks with opposite polarization [13]:

$$\mathcal{N}_{h/q^{\uparrow}}(z, \vec{p}_T^{\,h}) - \mathcal{N}_{h/q^{\downarrow}}(z, \vec{p}_T^{\,h}) = \frac{|\vec{p}_T^{\,h}|}{M_h} \sin(\phi_h - \phi_s') H_1^{\perp}(z, {p_T^h}^2) \tag{2.88}$$

where ϕ_h is the azimuthal angle of the moment of the produced hadron and ϕ_s' is the azimuthal angle of the spin vector of the fragmenting quark. For a schematic view of the

[7] T-even (T-odd) means that a function is invariant (not invariant) under time-reversal.

angles see fig. 2.11. The Collins angle is defined as $\Phi_{Coll} = \phi_h - \phi_s'$. From QED it can be shown that the directions of the final and the initial spin of the quark ϕ_s' and ϕ_s are related by $\phi_s' = \pi - \phi_s$ resulting with $\phi_s = \phi_S$ in the following expression for the Collins angle:

$$\Phi_{Coll} = \phi_h - \phi_s' = \phi_h + \phi_S - \pi \tag{2.89}$$

with ϕ_S as the azimuthal angle of the transverse target nucleon spin.

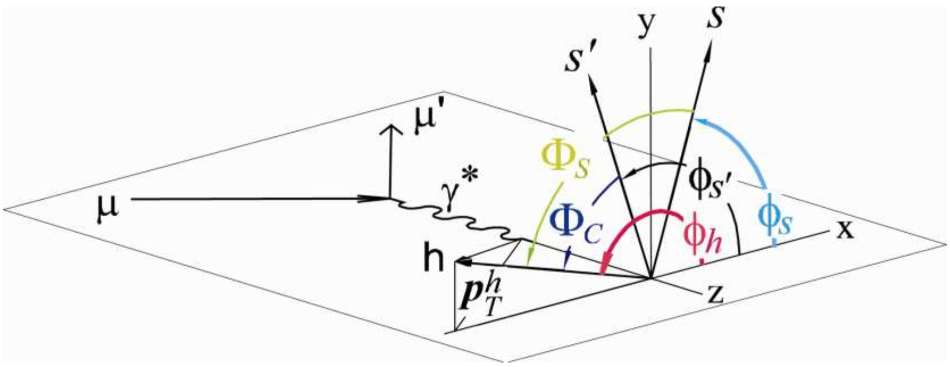

Figure 2.11: *Schematic view of the angles ϕ_h and ϕ_S in the "gamma-nucleon-system" (GNS).*

We then define:

$$\Delta_T^0 D(z, {p_T^h}^2) = -\frac{|\vec{p}_T^h|}{M_h} H_1^\perp(z, {p_T^h}^2) \tag{2.90}$$

and with the unpolarized and the Collins term of eq. (2.78) and using eq. (2.85) and eq. (2.81) we get for the cross-section:

$$\begin{aligned}\frac{d\sigma}{dx dy d\phi_S dz d\phi_h d{P_T^h}^2} = \frac{\alpha^2}{xyQ^2} \sum_q e_q^2 \cdot \Big\{ \frac{1}{2}\left[1 + (1-y)^2\right] \cdot x \cdot q(x) \cdot D_q^h(z, {P_T^h}^2) \\ +(1-y) S_\perp \sin \Phi_{Coll} \cdot x \cdot \Delta_T q(x) \cdot \Delta_T^0 D_q^h(z, {P_T^h}^2) \Big\}\end{aligned} \tag{2.91}$$

We then receive the transverse single spin asymmetries by comparing the cross-sections on oppositely polarized target nucleons:

$$A_C^h = \frac{d\sigma(\vec{S}_\perp) - d\sigma(-\vec{S}_\perp)}{d\sigma(\vec{S}_\perp) + d\sigma(-\vec{S}_\perp)} = S_\perp \cdot D_{NN} \cdot A_{Coll} \cdot \sin \Phi_{Coll} \tag{2.92}$$

where the Collins asymmetry A_{Coll} is given by:

$$A_{Coll} = \frac{\sum_q e_q^2 \cdot \Delta_T q(x) \cdot \Delta_T^0 D_q^h(z, {P_T^h}^2)}{\sum_q e_q^2 \cdot q(x) \cdot D_q^h(z, {P_T^h}^2)} \tag{2.93}$$

and D_{NN}, the depolarization factor, which describes the proportion of the lepton spin transfered to the virtual photon, by:

$$D_{NN} = \frac{1-y}{1-y+y^2/2} \tag{2.94}$$

As one can see in eq. (2.93) we have via the Collins asymmetry access to the transversity distribution $\Delta_T q(x)$. By identifying the different final state hadrons and the use of different targets it is possible to extract also different quark distributions.

2.5 The Sivers Mechanism

A different mechanism to explain the spin asymmetries in the cross-section of SIDIS of leptons on a transversely polarized nucleon target was suggested by Sivers [5]. This effect describes the fragmentation of an unpolarized (unknown spin state) quark inside a transversely polarized target nucleon. The assumption is here the existence of a correlation between the transverse momentum $\vec{k}_T$ of an unpolarized quark in a transversely polarized nucleon and the nucleon spin vector.
If we consider the number density of unpolarized quarks in opposite transversely polarized nucleons, we can define the T-odd Sivers distribution function $f_{1T}^{\perp}(x, {k_T}^2)$ already introduced in section 2.3.3 as follows:

$$\begin{aligned} \mathcal{P}_{q/N^{\uparrow}}(x,\vec{k}_T) - \mathcal{P}_{q/N^{\downarrow}}(x,\vec{k}_T) &= \mathcal{P}_{q/N^{\uparrow}}(x,\vec{k}_T) - \mathcal{P}_{q/N^{\uparrow}}(x,-\vec{k}_T) \\ &= -\frac{|\vec{k}_T|}{M} S_{\perp} \sin(\phi_q - \phi_S) f_{1T}^{\perp}(x,{k_T}^2) \end{aligned} \tag{2.95}$$

defining the Sivers angle $\Phi_{Siv} = \phi_q - \phi_S$, corresponding to the relative azimuthal angle between the target spin $S_{\perp}$ and the transverse quark momentum $\vec{k}_T$.
Following the notation in [49] we notice:

$$\Delta_T^0 q(x,{k_T}^2) = -\frac{|\vec{k}_T|}{M} f_{1T}^{\perp}(x,{k_T}^2) \tag{2.96}$$

We assume that the hadron produced in the fragmentation and the fragmenting quark are collinear. This means that the transverse momentum of the hadron has its origin completely in the intrinsic transverse momentum of the quark in the target nucleon ($\vec{p}_T^{\,h} = z\vec{k}_T$). For the Sivers angle follows:

$$\Phi_{Siv} = \phi_h - \phi_S \tag{2.97}$$

With eq. (2.96) in combination with the unpolarized and the Sivers term formulated in eq. (2.85) and eq. (2.82), respectively, we obtain for the cross-section in leading order QCD for Sivers:

$$\begin{aligned} \frac{d\sigma}{dx dy d\phi_S dz d\phi_h d{P_T^h}^2} &= \frac{\alpha^2}{xyQ^2} \sum_q e_q^2 \cdot \frac{1}{2}\left[1+(1-y)^2\right] \cdot x \\ &\cdot \left[q(x,{P_T^h}^2/z^2) + S_{\perp} \sin\Phi_{Siv} \cdot \Delta_0^T q(x,{P_T^h}^2/z^2)\right] D_q^h(z) \end{aligned} \tag{2.98}$$

Analog to the Collins case we receive for the transverse single spin asymmetry by comparing the cross-sections of opposite transversely polarized target nucleons for Sivers:

$$A_S^h = \frac{d\sigma(\vec{S}_\perp) - d\sigma(-\vec{S}_\perp)}{d\sigma(\vec{S}_\perp) + d\sigma(-\vec{S}_\perp)} = S_\perp \cdot D_{NN} \cdot A_{Siv} \cdot \sin\Phi_{Siv} \tag{2.99}$$

with the Sivers asymmetry A_{Siv}:

$$A_{Siv} = \frac{\sum_q e_q^2 \cdot \Delta_0^T q(x, P_T^{h^2}/z^2) \cdot D_q^h(z)}{\sum_q e_q^2 \cdot q(x, P_T^{h^2}/z^2) \cdot D_q^h(z)} \tag{2.100}$$

to find as $\sin\Phi_{Siv}$ modulation in the number of produced hadrons.
In the Sivers effect the photon couples to an unpolarized quark in a transversely polarized nucleon, for which the kinematical factor is $1 - y + y^2/2$ and therefore identical to the factor in unpolarized scattering. So we get for D_{NN}:

$$D_{NN} = \frac{1 - y + y^2/2}{1 - y + y^2/2} = 1 \tag{2.101}$$

Because the angles A_{Coll} and A_{Siv}, from which the Collins and the Sivers term in the cross-section depend, are independent, we can disentangle the Collins and the Sivers effect in SIDIS on a transversely polarized target and so extraxt the two asymmetries separately.

2.6 Experimental Overview

Since the end of the 90s the HERMES collaboration at DESY in Hamburg and later the COMPASS collaboration at CERN in Geneva did a series of measurements of azimuthal asymmetries in SIDIS of leptons on transversely polarized targets. The HERMES results for the Collins and Sivers asymmetries from a proton target with all available statistics (2002-2005 data) were presented at the DIS 07 conference [46]. For the Sivers effect the results are published in [47].
The first publication of COMPASS refers to the data from the 2002 deuteron run [48], while the complete data sample on the deuteron from 2002 to 2004 for unidentified hadrons was published in [49] and the one with hadron identification in [50].
On the proton target the HERMES experiment measured a non-zero single spin asymmetry for both, Collins and Sivers. The kinematical region covered by HERMES is: $Q^2 > 1$ (GeV/c)^2), $W^2 > 10$ GeV^2, $0.023 < x_{bj} < 0.4$, $0.1 < y < 0.85$ and $0.2 < z < 0.7$.
The Collins proton result of HERMES (see fig. 2.12) is positive for π^+ and negative and comparable in strength for π^-. For K^+ the Collins asymmetry is comparable with the one for π^+, while for K^- it has the same magnitude, but opposite sign to π^-. In the Sivers case HERMES obtained a positive signal for π^+ and a result consistent with zero for π^- (see fig. 2.13). The corresponding kaon asymmetries are larger for K^+ and also compatible with zero for K^-. For the neutral π^0 HERMES had a positive Collins asymmetry of similar

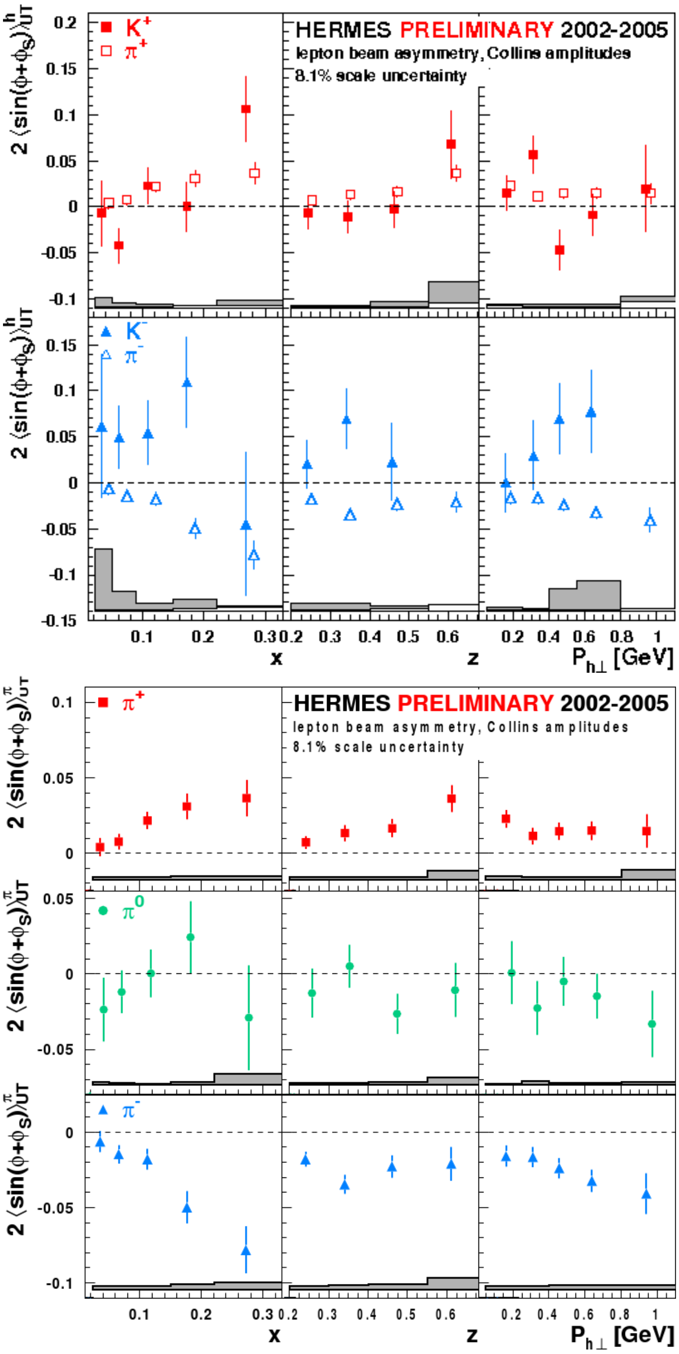

Figure 2.12: *Left: The Collins asymmetries for charged pions (open symbols) and charged kaons (closed symbols) as function of x, z and P_T^h from a proton target at the HERMES experiment. Right: The Collins asymmetries for charged and neutral pions as function of x, z and P_T^h from a proton target at the HERMES experiment. Both from [46].*

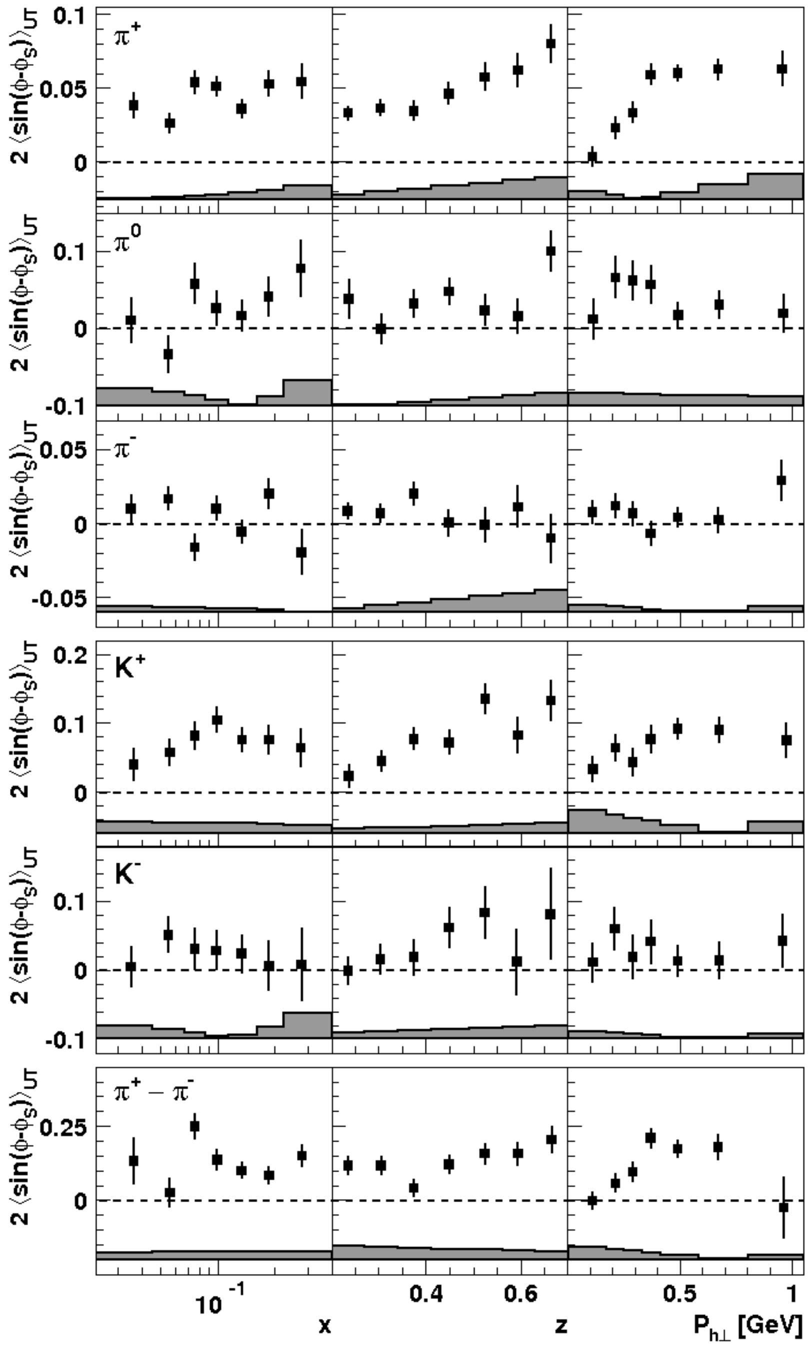

Figure 2.13: *The Sivers asymmetries for (from top to bottom) π^+, π^0 and π^- as well as for K^+, K^- and the difference $\pi^+ - \pi^-$ as function of x, z and P_T^h from a proton target at the HERMES experiment [47].*

strength as for the positive pions, while the Sivers asymmetry is compatible with zero for the π^0.
The COMPASS collaboration has measured the Collins and the Sivers asymmetry also on a transversely polarized deuteron target. At this experiment the kinematical region covered is: $Q^2 > 1$ (GeV/c)^2), $W^2 > 25$ GeV^2, $0.003 < x_{bj} < 0.3$, $0.1 < y < 0.9$, $z > 0.2$ and $P_T^h > 0.1\text{GeV}/c$. For the results of the whole data collected in 2002-04 on the deuteron target for unidentified produced hadrons see fig. 2.14. For the asymmetries of identified charged hadrons (π^+, π^-, K^+, K^-) in the data from 2003 and 2004 see fig. 2.15. As one can see all asymmetries on deuteron are small and compatible with zero. For all these results only statistical errors are shown, systematic errors are considerably smaller [48].

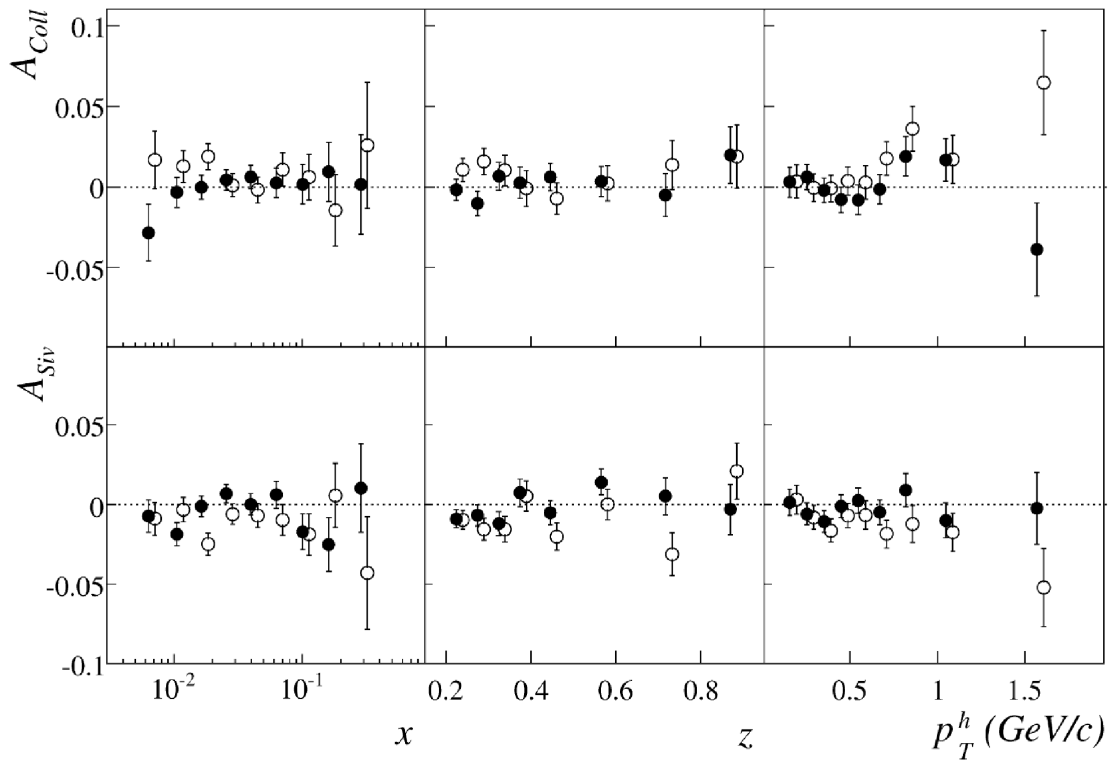

Figure 2.14: *The Collins (top) and Sivers (bottom) asymmetries for unidentified charged hadrons (full circles: positive, open circles: negative) as function of x, z and P_T^h from a deuteron target at the COMPASS experiment published in [49]. Only statistical errors are shown.*

This result could already be seen in the publication of the 2002 data and was confirmed with more precision by the whole statistics. This fact was theoretically explained as a cancelation of the u and d quark contributions on an isoscalar target like the deuteron.
Independent information about the Collins fragmentation function came by the measurements of azimuthal hadron asymmetries in e^+e^- annihilation done by the Belle collaboration at KEK in Japan [51]. Together with the measurement of HERMES on the u dominated proton and of the Collins fragmentation function at Belle it was possible for

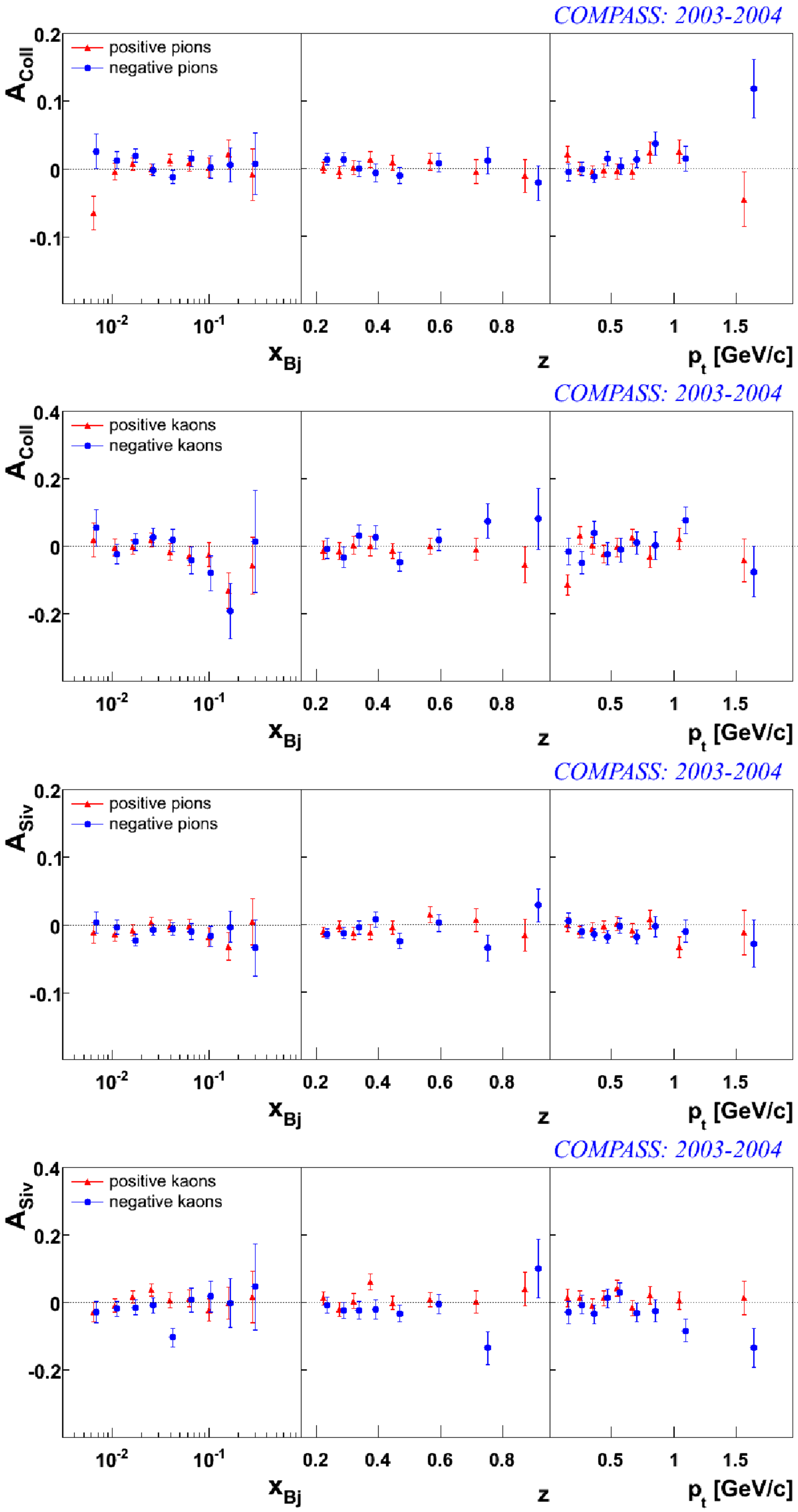

Figure 2.15: *The Collins (top) and Sivers (bottom) asymmetries for charged pions and kaons (red: positive, blue: negative) as function of x, z and P_T^h from a deuteron target at the COMPASS experiment. Only statistical errors are shown.*

the first time to extract the transversity distributions for the u and d quarks (see chapter 6).
In 2007 the COMPASS collaboration did also a measurement on a transversely polarized proton target.
In this work the analysis of the asymmetries on the deuteron target for K^0 published also in [50] and the analysis of the proton data for unidentified hadrons as well as for π^+, π^-, K^+, K^- and K^0 identified will be presented.
At JLab Hall A in 2008/09 transverse spin effects were measured on a transversely polarized neutron (^{3}He) target [52].
It should further be mentioned that there are also ongoing efforts at RHIC at the Brookhaven National Laboratory (BNL) and the proposal for FAIR at the Gesellschaft für Schwerionenforschung (GSI) as well as plans at COMPASS and J-Park for measuring transverse spin effects via the Drell-Yan process with pp or $p\bar{p}$ collisions in the reaction:

$$q\bar{q} \rightarrow l^+l^- \tag{2.102}$$

Chapter 3

The COMPASS Experiment

> Research is four things: brains with which to think, eyes with which to see, machines with which to measure and, fourth, money.
>
> A. Szent-Györgyi (1893-1986),
> American-hungarian biochemist,
> Nobel Prize 1937

COMPASS is a fixed target experiment at the M2 beamline of the Super-Proton-Synchrotron (SPS) at CERN[1] in Geneva. The physics program of COMPASS consists of two parts, the detailed study of the nucleon spin structure using a high energy muon beam and hadron spectroscopy using a hadron beam [53]. From 2002 to 2007, apart from a short pilot run with a hadron beam in 2004, only the muon beam was used. The years 2008 and 2009 then were dedicated to the hadron program of COMPASS.
The data for the analysis of the transverse spin asymmetries presented here were collected with a ^{6}LiD (effective deuteron) target in 2002-04 and a NH_3 (effective proton) target in 2007.
After the year 2004 there were two larger upgrades: One improvement was the installation of a new target solenoid magnet with increased geometrical acceptance and the implementation of a three cell setup for the target material instead of the two cell setup used before. The second one was the improvement of the RICH[2] detector for the particle identification (see section 3.4.1) with a new photodetection system for the central and new frontend electronics for the outer part.
In the following a description of the apparatus and the detection technique is given, restricted to the parts regarding the muon beam setup. For a complete and elaborate illustration of the COMPASS spectrometer see: [53].

[1] **C**onseil **E**uropéen pour la **R**echerche **N**ucléaire, European Nuclear Research Center
[2] **R**ing **I**maging **CH**erenkov

3.1 The Polarized Muon Beam

The muon beam for COMPASS is derived from a primary proton beam coming from the second large accelerator ring at CERN, the Super Proton Synchrotron (SPS) (see fig. 3.1). This proton beam is injected from the smaller Proton Synchrotron (PS), where it has an energy of 26 GeV and a rate of $3.4 \cdot 10^{13}$ particles per cycle. In the SPS the beam is accelerated to an energy of 400 GeV and then directed onto the T6 production target. One SPS acceleration cycle takes 16.8 s including an extraction time, the so-called "spill", of 4.8 s.

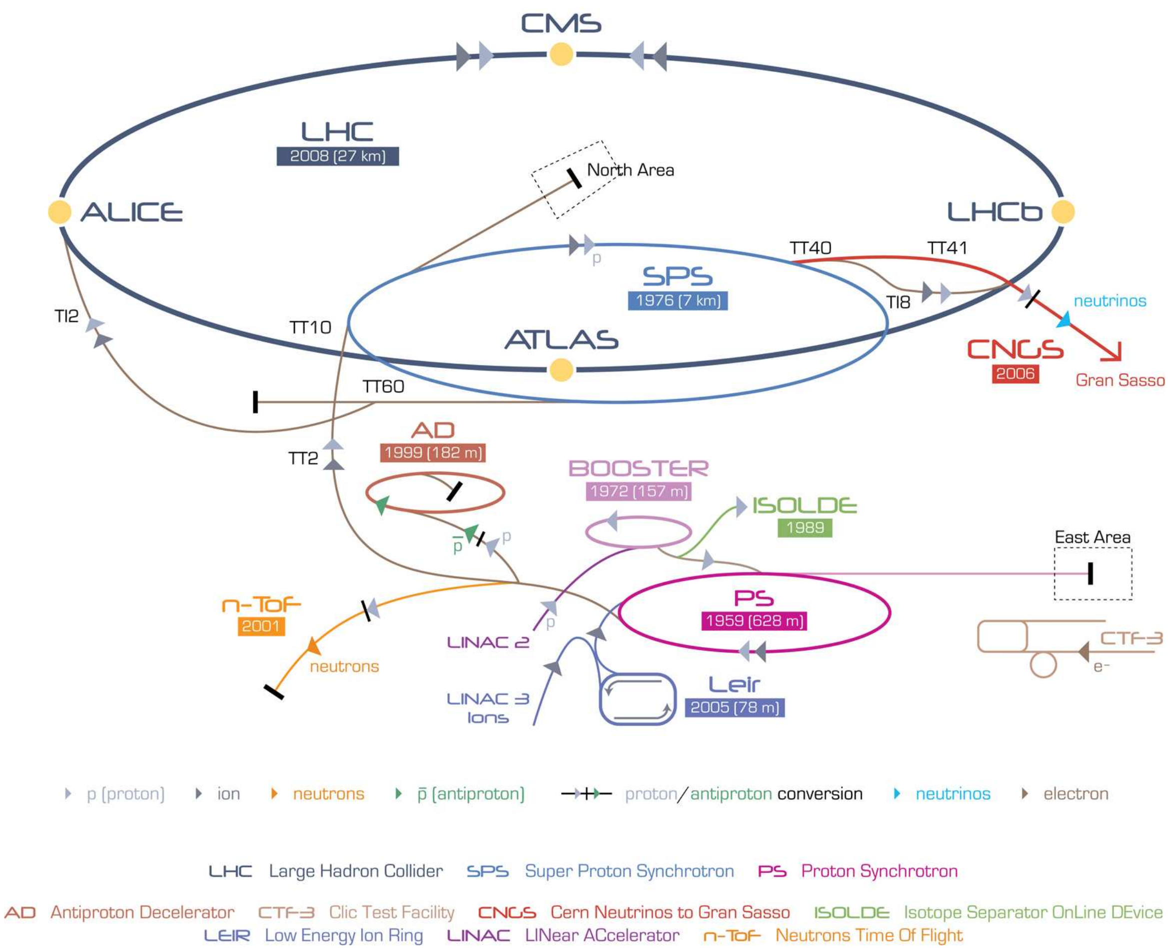

Figure 3.1: *The CERN accelerator complex. COMPASS is situated in the North Area, at the second large accelerator ring, the SPS. Figure taken from [54].*

On the T6 Beryllium target, which has a length of 500 mm [55] for the full muon intensity, the secondary beam mostly consisting of pions with a contamination of kaons, is produced. In the M2 beamline the secondary beam particles are selected for momentum by dipole magnets and along their 500 m long way a fraction of the pions decays into muons and neutrinos (e.g. $\pi^+ \rightarrow \mu^+ + \nu_\mu$).

Because of the parity violating nature of the pion decay the resulting muon beam is naturally polarized [56, 57, 6]. The fraction of the polarized muons depends in the laboratory system on the selected p_π and p_μ – in the case of COMPASS the polarization is about 80%. When the beam is arriving at the end of the decay tunnel, the hadronic component is stopped by a hadron absorber. The muon beam is then momentum selected by magnets and directed to the surface level at the COMPASS experimental hall in the North Area of the CERN site at Prévessin (France).
Before entering the COMPASS hall the muon momentum with a nominal value of 160 GeV/c and a spread of about 5% of this is measured by the Beam Momentum Station (BMS) consisting of a bending magnet and six hodoscopes. Four of those hodoscopes, two located downstream and two upstream of this dipole magnet are plastic-scintillator detectors consisting of horizontal strips adapted in size to handle the varying flux around the beam axis, the other two ones are scintillating fibre detectors. The time resolution of the BMS is about 0.3 ns.
After the BMS the incoming beam with a flux of $2 \cdot 10^8$ muons per SPS cycle is focused on the target.

3.2 The Polarized Target

The COMPASS physics program using the muon beam consists mainly of measuring spin asymmetries using a target polarized either longitudinally or transversely. Until 2006 COMPASS has taken data with an isoscalar ^{6}LiD target, while in 2007 an ammonium (NH_3) target was used. The ^{6}Li nucleus can be described in good approximation as a spin-0 ^{4}He nucleus combined with a deuteron, so that ^{6}LiD effectively consists of two spin-1 deuterons and an unpolarized (spin-0) He core. This corresponds to a fraction of polarizable nucleon (dilution factor) of $f = \frac{4}{8} = 0.5$. In praxis the liquid He present in the target region to maintain low temperature necessary to get polarization has to be taken into account and the dilution factor becomes $f \approx 0.38$. The polarization reached by the polarizable material is $P_T \approx 0.5$.
For the NH_3 (effective proton) target the dilution factor is lower, $f \approx 0.17$, but on the other hand the polarization is higher: about 0.8 - 0.9.
One of the upgrades in 2005 already mentioned was the substitution of the superconducting target solenoid with a geometrical acceptance of ± 75 mrad by a new one with an acceptance of ± 180 mrad and the changing of the target configuration from a two cell to a three cell setup. The cells in the two cell setup had a diameter of 3 cm and a lenght of 60 cm, while the cells in the new installation separated by 10 cm had a diameter of 3 cm in 2006 and 4 cm in 2007 and are 30, 60 and 30 cm long. For an illustration of the target see fig. 3.2. In both setups the neighbouring cells are polarized oppositely and their polarization is reversed in a certain time interval to prevent false asymmetries e.g. created by different acceptances. In the longitudinal mode this was done from 2006 on every 24 hours, while in the years before the reversal was every 8 hours.
The old as well as the new superconducting solenoid provide a homogeneous magnetic field

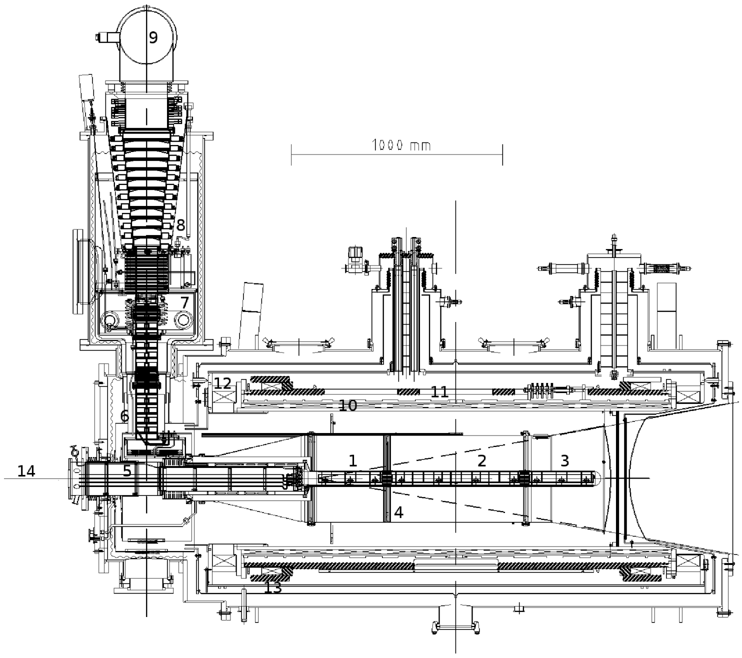

Figure 3.2: *Side view of the COMPASS polarized target from the year 2006 on (three cell system): 1: upstream, 2: central and 3: downstream target cell, 4: microwave cavity, 5: target holder, 6-9:* ^{3}He-^{4}He *refrigerator, 10: solenoid coil, 11-12: compensation coil, 13: dipole coil, 14: muon beam entrance (from the left-hand side).*

of 2.5 T longitudinal along the beam direction. The polarization is given by Curie's law:

$$P_T = \tanh \frac{\mu B}{k_B T} \tag{3.1}$$

with the magnetic moment μ of the polarizable target particles and the Boltzmann constant k_B. This implies aside of a strong magnetic field a low temperature of about 200 mK. To polarize the target the technique of the Dynamic Nucleon Polarization (DNP) [58] is used. The cooling is performed by a ^{3}He-^{4}He dilution refrigerator.
For the transverse mode a dipole field of 0.42 T transverse to the beam direction is switched on, which as a by-product results in a bend of all charged particles. Therefore performing the field rotation like for the longitudinal data taking would introduce differences in the acceptance for the two opposite spin configurations. For this reason the spin reversal in the transverse mode is only done after five to seven days of data taking.

3.3 Tracking Detectors

The COMPASS spectrometer (see fig. 3.3[3] and 3.4) is a two-stage forward spectrometer consisting of a Large Angle Spectrometer (LAS) and a Small Angle Spectrometer (SAT).

[3]In this figure and in the following the COMPASS coordinate system is used, in which the z axis is in beam direction, and the x and y axes are horizontal and vertical transverse to z, respectively. At

The first stage detects particles with large scattering angles, while the second stage those with larger momentum and smaller scattering angles [53]. Each stage is equipped with detectors for track reconstruction and possesses a spectrometer magnet, SM1 (first stage) and SM2 (second stage), respectively. These magnets are necessary for momentum measurement and have integrated field-strengths of $\int Bdl$ of 1.0 Tm (SM1) and 4.4 Tm (SM2), respectively.
According to the different angular ranges the detectors can be divided in three groups:

- Very Small Area Trackers (VSAT): These detectors are situated directly in the beam region for the detection of particles deflected at very small angles. Due to the high rates they have to withstand, the VSAT require a very good time-resolution and a short dead-time. Because the VSAT are installed in the area around the target, they need also a good spatial resolution of about 50 μm to reconstruct interaction vertices with high precision. For this purpose eight stations of scintillating-fibre detectors with an excellent time-resolution to correlate hits belonging to the same particle and three stations of double-sided silicon micro-strip detectors with a high space-resolution are installed.

- Small Area Trackers (SAT): For particles scattered at slightly larger angles the detectors must also have a high spatial resolution, but the requirement for the time-resolution is lower. At COMPASS the gas-filled Micromega (Micromesh Gaseous Structure) detectors and GEMs (Gas Electron Multipliers) are used in this area. Both detector types have a central dead zone with a diameter of 5 cm.

- Large Area Trackers (LAT): The aim of the detectors of this last category is the verification of particles deflected at larger angles and distances from the beam. Those detectors must cover the large area defined by the acceptance of the experimental setup and nevertheless guarantee a good spatial resolution. For this drift chambers (DCs, W45), multi-wire proportional chambers (MWPCs) and straw drift tubes are installed at COMPASS.

For a detailed description of the various detector types see: [53]. In the following only a description of the scintillating-fibre hodoscopes (SciFis), which are constructed by the Nagoya group (Japan, stations 1 to 4) and by the groups of the HISKP Bonn (J. Bisplinghoff et al.) and Erlangen (W. Eyrich et al.) (stations 5 to 8), is given. In the last years the groups of Bonn and Erlangen were also responsible for monitoring and maintenance of the Japanese SciFis.

3.3.1 Scintillating-Fibre Hodoscopes (SciFis)

The most important detectors for the reconstruction of particle tracks in the beam region at COMPASS are the scintillating-fibre detectors. Those hodoscopes must handle the difficult

COMPASS also the terms "Jura" and "Salève" for the left and right sides of the hall in beam direction are used. Those names are derived from the mountains in the nearby region of Geneva, which lie in the corresponding directions.

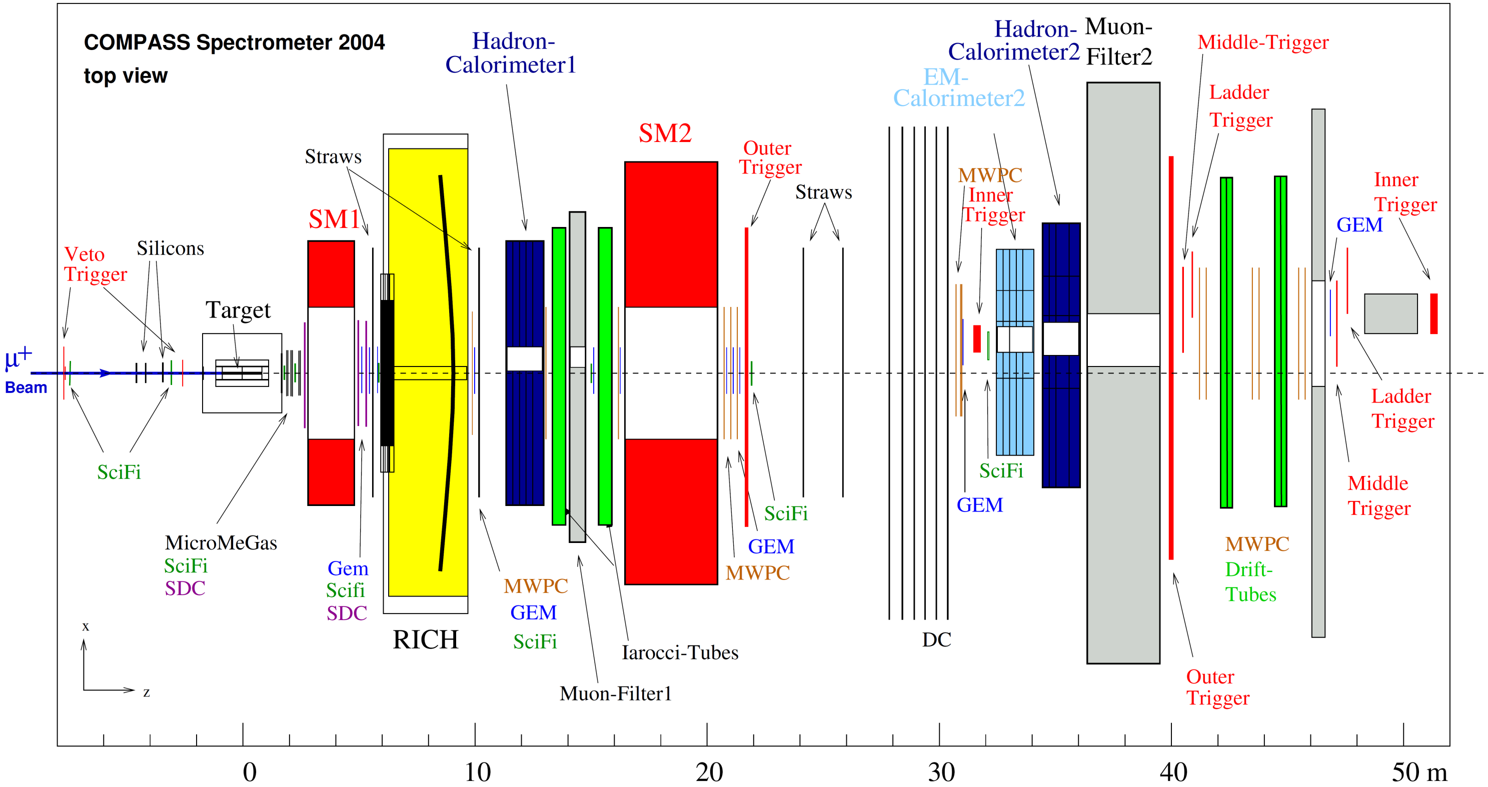

Figure 3.3: *The COMPASS spectrometer (muon setup, 2004 run) in top view.*

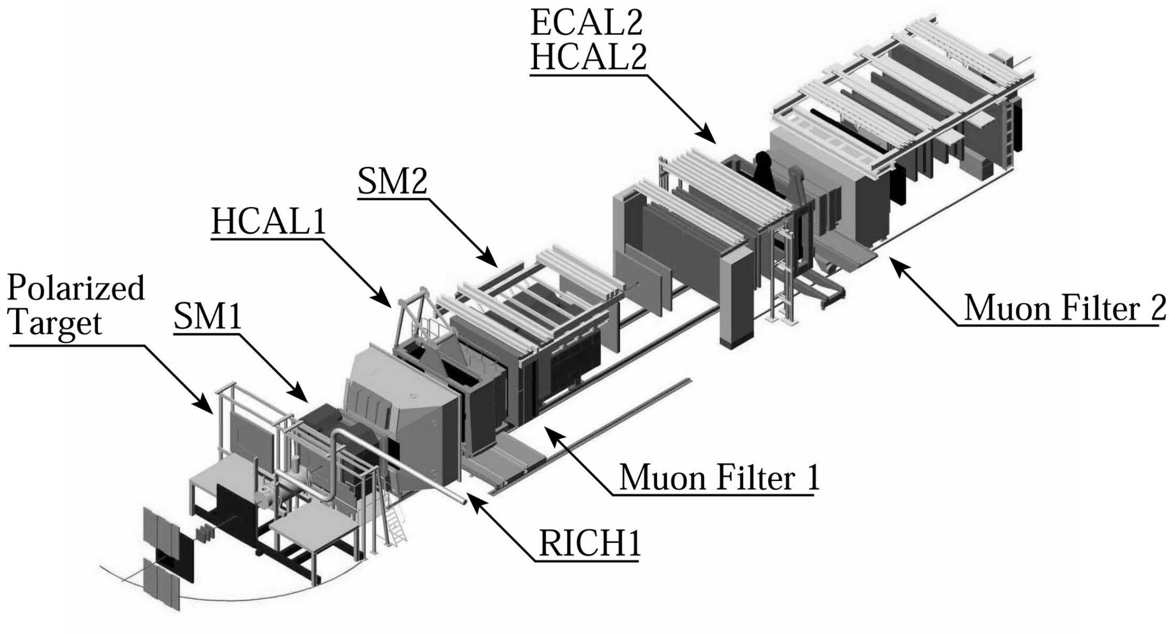

Figure 3.4: *The COMPASS spectrometer (muon setup) in artistic view.*

conditions in this part of the spectrometer. This means among other requirements that the SciFis must withstand a radiation dose of 31 kGy for a run time of about 100 days per year and they must have a high time-resolution of < 1ns, a high reconstruction efficiency combined with a low mass occupation.
Each of the eight stations comprises at least two planes, a horizontally (X) and a vertically (Y) sensitive one, three stations have in addition a plane inclined at around 45° named U or V. The active area of those planes is between 3.9×3.9 and 12.3×12.3 m^2 depending of the station. To obtain a sufficient amount of photoelectrons several layers of fibres (four to seven) with a diameter between 0.5 and 1 mm are stacked together for each plane (see fig. 3.5). One detector channel consists therefore of several fibres in a row.
For the hodoscopes the fibres Kuraray SCSF-78MJ [59] were chosen and the read-out is done by 16-channel Multi-Anode Photomultipliers (MAPMT, type Hamamatsu H6568 [60]), to which the scintillation light is transported via clear (non-scintillating) fibres of a length between 0.5 and 3 m.

3.4 Particle Identification Detectors

To be able to distinguish particles of different types beside the track information also knowledge of the energy or the velocity of the particles is needed. For this purpose the COMPASS spectrometer provides several particle identification detectors introduced in the following.

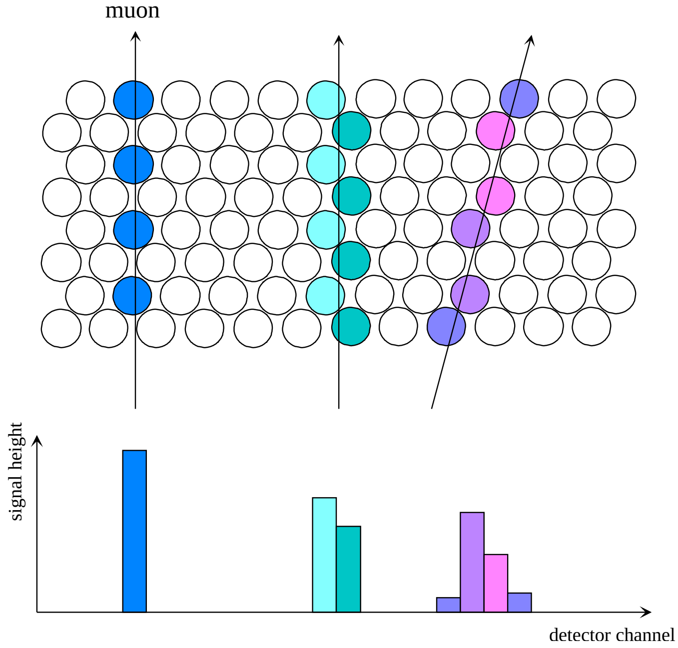

Figure 3.5: *Cross-section through a SciFi detector plane. One detector channel consists of several fibres arranged one after the other to get a higher light output. Figure taken from [61].*

3.4.1 The Ring Imaging Cherenkov (RICH) Detector

To determine the mass and therefore the type of the particles from the momentum measurement by the spectrometer magnets it is necessary to have informations about the velocity, too. At COMPASS this is done using the RICH[4] detector. Its working principle takes advantage of the Čerenkov effect [6]: A particle, which moves through a medium with a velocity larger than the velocity of light in this medium, emittes photons in a cone symmetric to its direction. The angle of this Čerenkov light, the Čerenkov angle, is given by:

$$\theta_{\check{C}} = \cos^{-1}\left(\frac{1}{n\beta}\right) \tag{3.2}$$

where n is the refraction index of the medium (at COMPASS: C_4F_{10} with $n = 1.00153$) and $\beta = v/c$ is the velocity of the particle divided by the speed of light *in vacuo*. The emitted photons are reflected by two spherical mirrors systems and focussed onto photon detectors positioned in the focal plane resulting in a ring image (see fig. 3.6). From the radius of this ring the Čerenkov angle and the corresponding velocity are extracted.

In the years 2001-2004 multi-wire proportional chambers (MWPCs) equipped with CsI photocathodes were used as photon detectors. As already mentioned there was a major upgrade after 2004. In the central region of the RICH the use of Multi-Anode Photomultipliers (MAPMT) replaced both, the detection and the read-out system, leading to a sup-

[4] **R**ing **I**maging **CH**erenkov

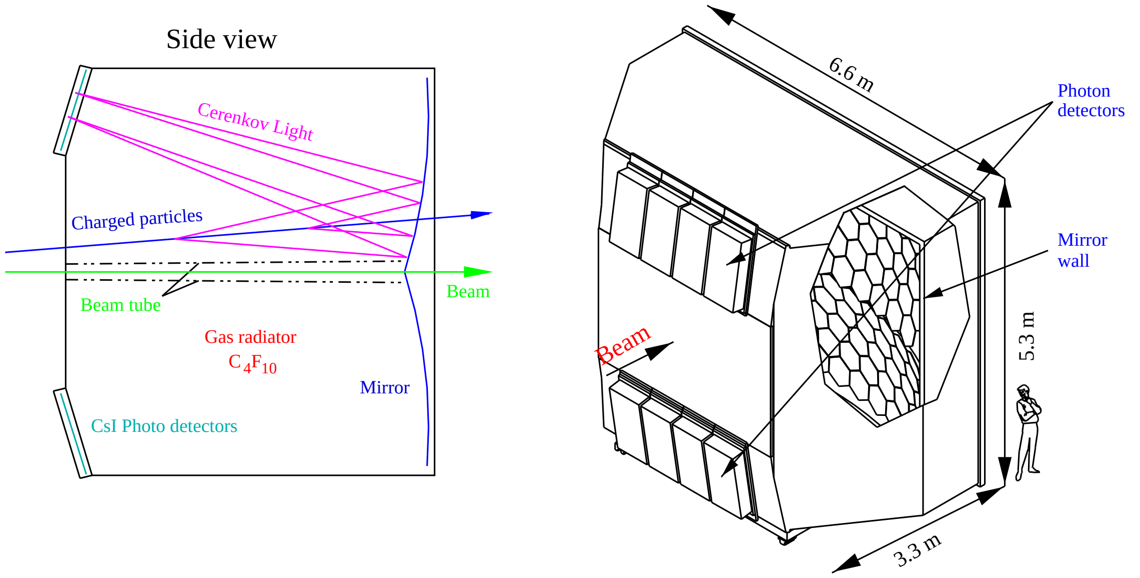

Figure 3.6: *The COMPASS RICH: principle (left-hand side) and artistic view (right-hand side).*

pression of the uncorrelated background signals due to the high time-resolution (< 1 ns) of the MAPMTs. The work-intensive quality testing of the 576 MAPMTs of the type R7600-03-M16 of the company Hamamatsu [60] used in the RICH upgrade was performed in Erlangen and coordinated by the Erlangen group.
In the external part of the RICH the existing read-out of the MWPCs was replaced by APV chips leading also to an improved time-resolution.

3.4.2 Calorimeters

Both hadronic calorimeters of COMPASS (HCAL1 and 2) are situated at the end of each spectrometer stage in front of the muon filters. Apart from measuring the energy of the produced hadrons the hadronic calorimeters participate also in triggering on semi-inclusive scattering events. HCAL1 and 2 are sampling calorimeters consisting of alternating layers of iron and scintillating material, where incoming hadrons generate a cascade of hadronic secondary particles in the iron layers, which are absorbed completely in the calorimeter. The integrated energy of the following light signals in all scintillator plates is proportional to the energy of the incoming hadron [6].
To detect photons from the decay of hadrons an electromagnetic calorimeter (ECAL2) consisting of lead glass modules is placed downstream of HCAL2. Since the COMPASS run 2006 downstream of HCAL1 another electromagnetic calorimeter (ECAL1) also consisting of lead glass modules was installed, which allows the detection of low-energy photons and/or neutral pions decaying to photons.

3.4.3 Muon Identification

The scattered muons are detected by two muon detectors (Muon Walls, MW1 and MW2), one in each spectrometer stage, using the low interaction probability and consequentially large penetration depth of muons. Those stations are built of a set of tracking detectors and a hadron absorber made of iron (MW1) and of concrete (MW2), respectively, followed by further tracking detectors. All particles, which penetrate the absorber are regarded as muons.

3.4.4 Rich Wall

After 2004 the Rich Wall, a new tracking station, was installed downstream of the RICH, directly in front of ECAL1 to obtain a better reconstruction of particle trajectories in the RICH and in addition to improve the spatial resolution of ECAL1.

3.5 The Trigger System

To form a physics event from all the information provided by the individual detectors mentioned before a trigger signal must be distributed to the read-out of all detectors. This command causes the processing of all data collected within a specified time-window.
The COMPASS trigger system consists of four stations of fast scintillation detectors covering different kinematic regions ("inner" (I), "middle" (M), "ladder" (L), "outer" (O)) and two veto counters upstream the target (see fig. 3.7). In addition information from the hadronic calorimeters is used.
To get maximum flexibility for the broad physics program in the COMPASS muon run different triggers are used. Events in or near the region of deep inelastic scattering ($Q^2 \gtrapprox 0.5$ (GeV/c)^2)) are mainly triggered by measuring the muon scattering angle in the non-bending plane and checking its compatibility with the target position. Halo muons are suppressed by the veto system.
For the quasi-real photon regime (low Q^2) this technique to check the compatibility with the target position is not possible due to the very small scattering angles. Thus the trigger for low Q^2 is built in another way, as a combination of measuring the energy loss with two scintillator hodoscopes using the deflection of the muon track by the spectrometer magnets and a calorimeter trigger signal above a threshold.
To cover regions of high Q^2, which cannot be covered by the OT, a standalone calorimeter trigger is used together with hodoscope triggers. A trigger signal is created, if a minimum energy is deposit in the calorimeter.

3.6 Read-Out and Data Acquisition (DAQ)

The Data Acquisition system (DAQ) of COMPASS has to handle the read-out of approximately 1400 single detector elements and 250000 detector channels at a trigger rate for the

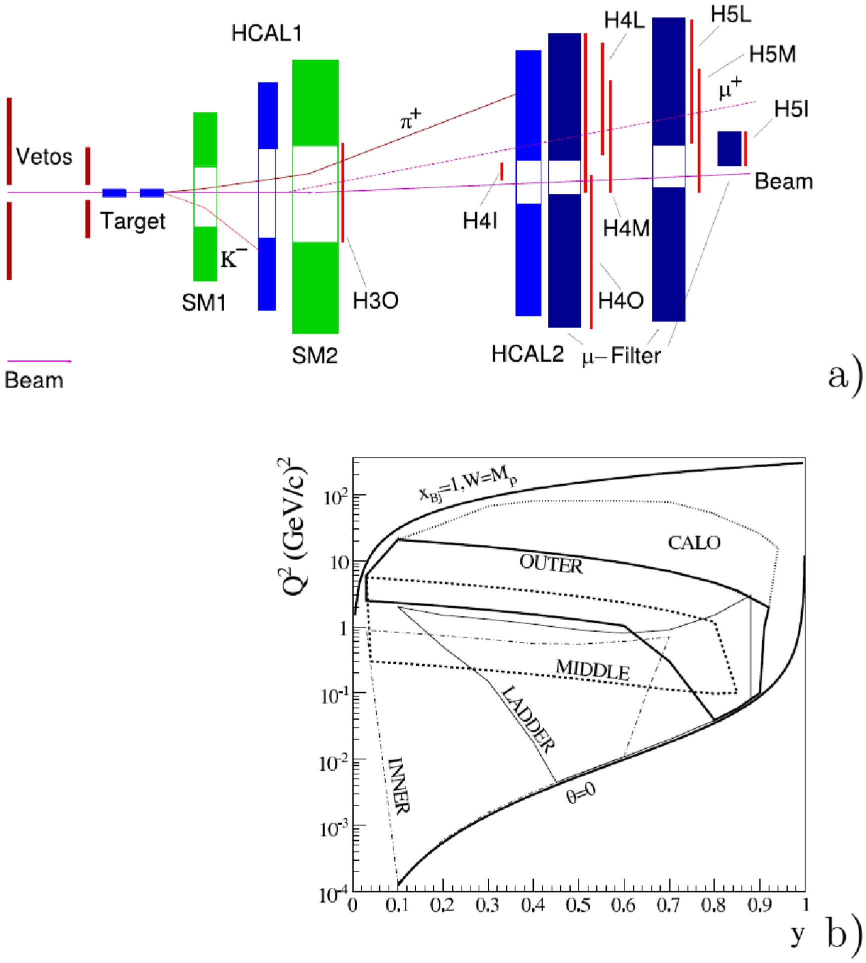

Figure 3.7: a) *Schematic view of the location of the trigger components at the COMAPSS setup.* b) *The kinematic range in y and Q^2 for the four hodoscope trigger sub-systems and the standalone calorimeter trigger.*

muon beam of about 10kHz and an event size of typically 35kByte. To fulfill these demands a pipelined and nearly dead-time free read-out scheme was designed (for a schematic view see fig. 3.8).
Due to this all signals are digitalized as soon as possible by so-called Front-End (FE) boards and then read-out by modules called CATCH[5] and (only for GEM and Silicon detectors and the RICH) GeSiCA[6]. In case a trigger signal is given, the data-bits are combined directly at the CATCH to a "local" event (so-called sub-event building).
Afterwards the data are transferred for a temporary storage to ROB[7] PCs, where enough memory capacity is available for the data of several spills. The sub-events, which do not contain the data from all the detectors, are then distributed from the ROBs to the event-

[5](**C**OMPASS **A**ccumulate, **T**ransfer and **C**ontrol **H**ardware)
[6]**Ge**m and **Si**licon **C**ontrol and **A**cquisition)
[7]**R**ead **O**ut **B**uffer

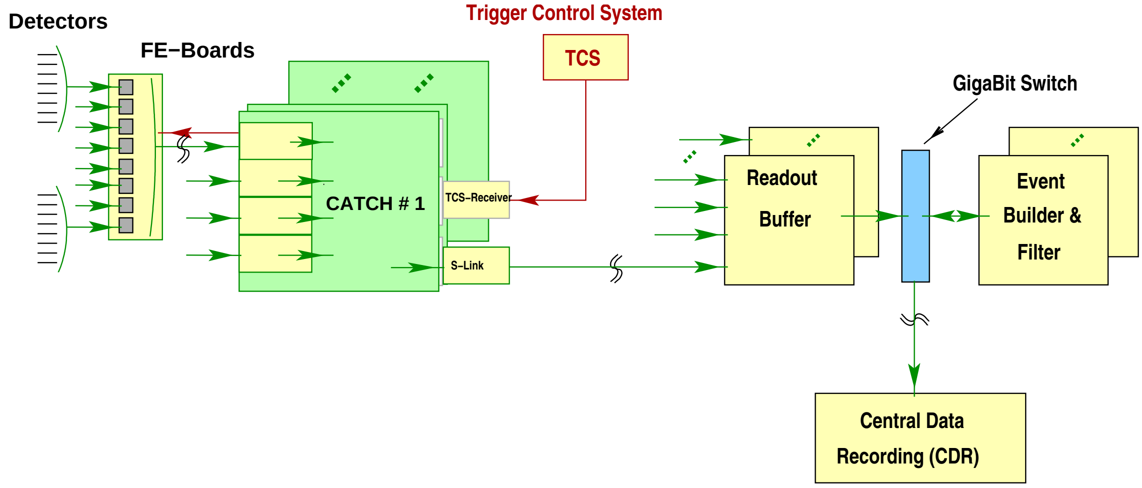

Figure 3.8: *View of the DAQ system at COMPASS, taken from [62]. The data are transferred from the detectors via the CATCH modules to the ROB PCs and the EBs and finally to the CERN computer center.*

builder PCs (EBs), where they are combined to complete events. Usually 100 or 200 spills are combined to a run; those are split into files of 1GByte (so-called chunks) and finally written onto tapes of the CASTOR[8] system at CERN.
For an online monitoring of the data quality during the data taking, i.e. to detect technical problems and announce corresponding error messages, the program MurphyTV was developed. Furthermore any information and parameters important for further quality checks and the data analysis like e.g. the field-strength of the magnets or the target polarization are written in an online logbook.

3.7 Data-Analysis at the COMPASS Experiment

Ahhh, what an awful dream. Ones and zeroes everywhere... and I thought I saw a two.

Bender Bending Rodríguez,
character in the animated television series Futurama

For further processing, the raw data on CASTOR actually needed are copied on hard disk. To start the physics analysis it is necessary to extract the physical objects like vertices, tracks, charges etc. from the raw data. This so-called "data production" is done with the program CORAL[9] based on C++. These by a factor of about 100 reduced data are stored

[8]CERN **A**dvanced **STOR**orage
[9]**CO**MPASS **R**econstruction and **A**na**L**ysis, see: [63]

in the compressed mDST[10] format.
The most important working tool for the COMPASS physics data analysis is the program PHAST[11], especially developed for this purpose. This program, which provides classes and functions for the C++ based CERN software package ROOT[65], reads the information of the mDST files, processes them and writes the output as a ROOT tree.
More details concerning the analysis are discussed in the following chapters.

[10] mini **D**ata **S**ummary **T**ape
[11] **PH**ysics **A**nalysis **S**oftware and **T**ools, see: [64]

Chapter 4

Collins and Sivers Asymmetries for K^0 from a Deuteron Target

> All models are wrong, but some are useful.
>
> G. E. P. Box (1919-), British statistician

In this chapter the analysis of the data from a transversely polarized deuteron target taken in 2002-04 at COMPASS is described. Beside a general description of the data analysis valid for all measured Collins and Sivers asymmetries this chapter is restricted to the Collins and Sivers asymmetries in K^0 production.

4.1 Transverse Data 2002-04 from the Deuteron Target

4.1.1 Data Sample

In the years 2002-04 the COMPASS collaboration has spent about 20% of its run-time for measurements with a transverse target spin, corresponding to 11 days in 2002, 9 days in 2003 and 14 days in 2004. The transverse data were taken in time intervals of several days with opposite spin polarization for the two target cells. This would in principle allow to calculate the asymmetries from the difference of the counting rates in the two cells. Because this method is susceptible for systematic effects due to a difference in the acceptance of the two target cells, the polarization of the cells is reversed between two intervals treated as two sub-periods to avoid this. The counting rate asymmetries are then calculated by combining the events of both cells in the two sub-periods with opposite target spin configurations (see section 4.3). According to the spin configuration the sub-periods are called *down-up* or *up-down*, respectively (see fig. 4.1).
In the year 2002 there were three time intervals of transverse data taking: P2B, P2C and P2H with a polarization reversal between P2B and P2C as well as in the middle

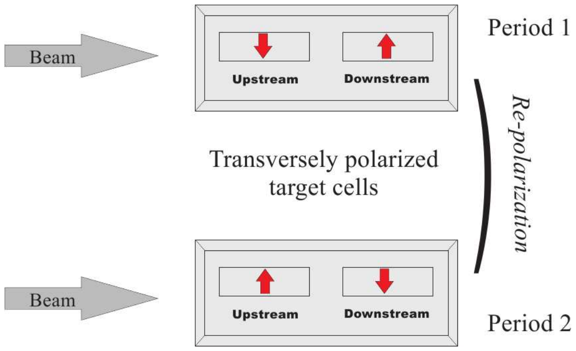

Figure 4.1: *Schematic illustration of the target cells and their polarization in transverse mode with longitudinally polarized muon beam. The two cells have always an opposite polarization, which is reversed between two sub-periods. Figure taken from [66].*

Year	Sub-period	Polarization upstream	Polarization downstream
2002	P2B	$\Downarrow$	$\Uparrow$
2002	P2C	$\Uparrow$	$\Downarrow$
2002	P2H.1	$\Downarrow$	$\Uparrow$
2002	P2H.2	$\Uparrow$	$\Downarrow$
2003	P1G	$\Downarrow$	$\Uparrow$
2003	P1H	$\Uparrow$	$\Downarrow$
2004	W33	$\Uparrow$	$\Downarrow$
2004	W34	$\Downarrow$	$\Uparrow$
2004	W35	$\Uparrow$	$\Downarrow$
2004	W36	$\Downarrow$	$\Uparrow$

Table 4.1: *The transversity data taking (sub-)periods for the 2002-04 deuteron runs and their spin configurations.*

of P2H, which therefore consists of two parts, P2H1 and P2H2, treated as sub-periods with opposite spin configuration. The COMPASS transverse run in 2003 consists of two sub-periods: P1G and P1H, while in 2004 there were four: W33, W34, W35, W36 with polarization reversals between P1G and P1H, between W33 and W34 and between W35 and W36. For an overview of the (sub-)periods of the transverse deuteron data see table 4.1.

Data Production

For all the sub-periods the whole production chain described in sections 3.6 and 3.7 was performed. The accuracy of the data reconstruction can be influenced by changes in the spectrometer, which can occur during the data acquisition. To prevent this for each sub-

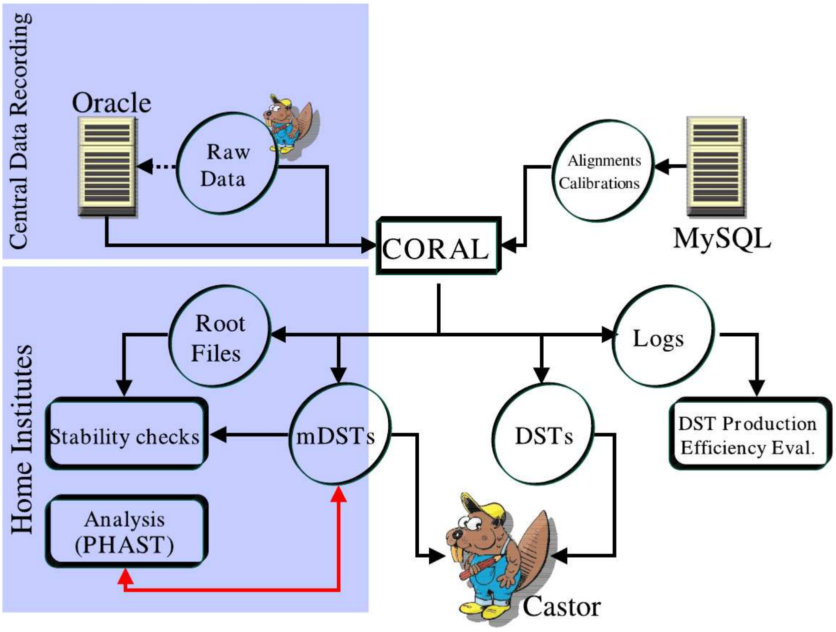

Figure 4.2: *Illustration of the production and analysis system.*

period special calibration and alignment[1] runs are taken and the data production is done separately for each sub-period.
One physics run has usually 70 gigabytes of disk space. The runs are divided in several chunks during storage, each of them occupies typically 1 Gbyte corresponding to about 25000 events. A schematic view of the production and analysis system is given in fig. 4.2.
Before producing the data they are pre-selected due to criteria registered in the online-logbook like e.g. beam stability, larger problems in several detectors, target polarization and the magnetic fields of SM1 and SM2.
In the production the size of the data is reduced to about 1% of the raw data. The analysis of the data in the mDST format is then performed with the program PHAST (see section 3.7). The overall amount of data in the years 2002-04 is larger than 1 PByte/; $(1 \cdot 10^{12})$ corresponding to about $12 \cdot 10^5$ spills with about $30 \cdot 10^9$ events.

4.1.2 Data Selection and Quality

The measured raw transverse asymmetries are very small effects of the order of a fraction of 10^{-4}. Therefore it is mandatory to control the stability of the data taking conditions inside each sub-period as well as between both consecutive sub-periods, which then are combined. In a complex apparatus like the COMPASS spectrometer there are several sources of possible instabilities in the data, which cannot always be identified during data

[1]In an alignment file all detector coordinates with respect to a defined reference system are stored. This information is necessary to get the relative positions of the single detectors and to compute correctly quantities like e.g. track parameters. Every time a detector is moved in the COMPASS hall, a new alignment file is needed.

taking. So it is necessary to analyze the stability versus time and reject bad runs or spills from the physics analysis, which could introduce false asymmetries. In the first step those runs or groups of runswere excluded, from which serious problems are reported in the COMPASS electronic logbook.
For the remaining runs the following quality checks were performed:

- Stability of detector profiles: The profiles of 316 detector planes were checked.
- Reconstruction stability: The stability of quantities like the number of vertices or tracks per event was controlled.
- K^0 stability test: The stability of the K^0 reconstruction was checked.
- Kinematic stability: The stability of kinematical variables like Q^2, x_{bj} or y was controlled.

In those tests 79 runs from a total number of 1379 were rejected corresponding to a fraction of 5.7%. For more information about the tests see: [67]. For the quality checks of the proton data a more detailed description is given in section 5.1.1.

4.2 Event Reconstruction and Selection

For the calculation of the transverse target spin asymmetries deep-inelastic scattering (DIS) events are needed, where at least one hadron is produced. In the case of the asymmetries for the neutral K^0 regarded here, it is necessary to reconstruct indirectly the neutral particles. All cuts used in the event selection are discussed in the following.

4.2.1 General DIS Cuts

As stressed before a deep-inelastic data sample, which is selected by $Q^2 > 1$ (GeV/c)^2, is needed. Another cut in the selection of DIS events is on the relative energy transfer y, for which very small and very large values are excluded. Events with $y < 0.1$ are in the region of elastic scattering and therefore discarded. By this cut also events with poorly reconstructed scattered muons or beam halo muons, falsely identified as scattered muons, are removed. The upper cut $y > 0.9$ removes events with a low momentum of the scattered muon (μ') and discards events, for which large radiative corrections are expected. To eliminate elastic scattering events even better, there is a cut on the mass of the final hadronic state $W > 5$ GeV/c^2, which excludes the region of nucleon resonances in the selection of DIS events.
The final distributions of the kinematical variables Q^2, y and x_{bj} after all cuts described in this section are shown in fig. 4.3 and the distribution of W after the corresponding cut in fig. 4.4.

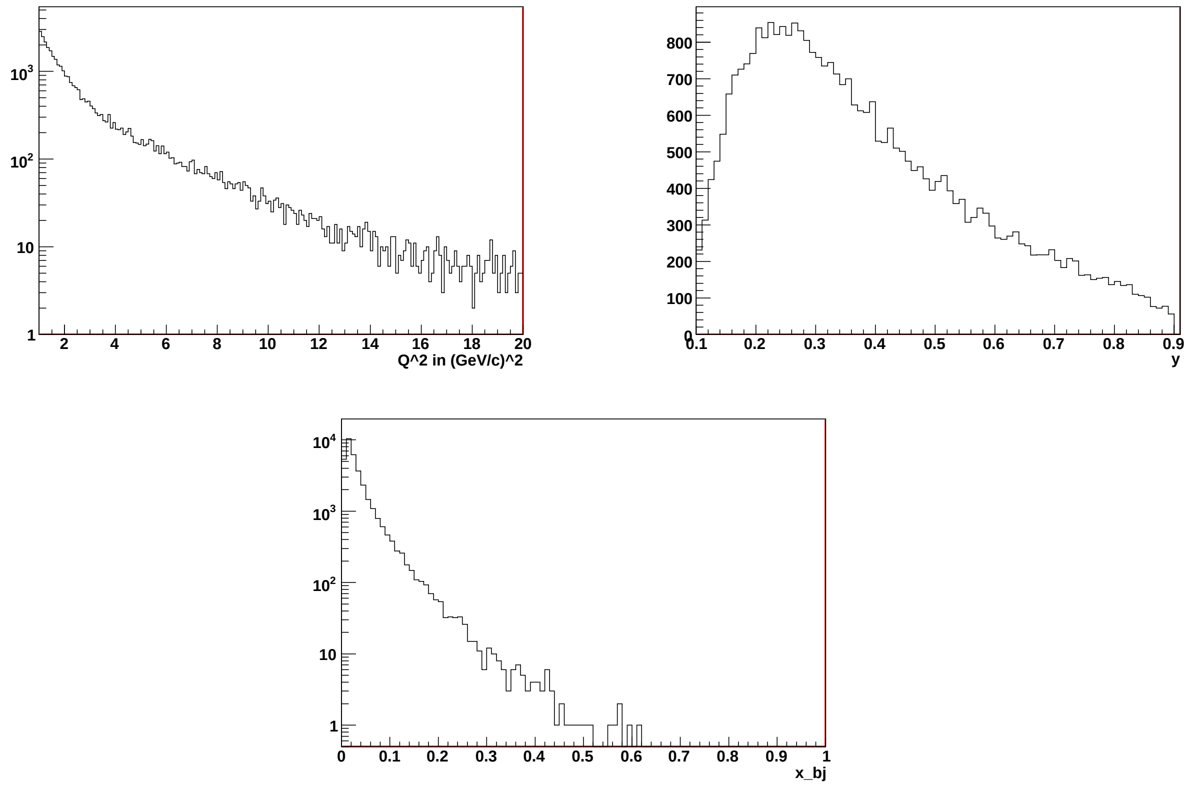

Figure 4.3: *From upper left to down: final distributions of* Q^2*,* y *and* x_{bj} *after all cuts.*

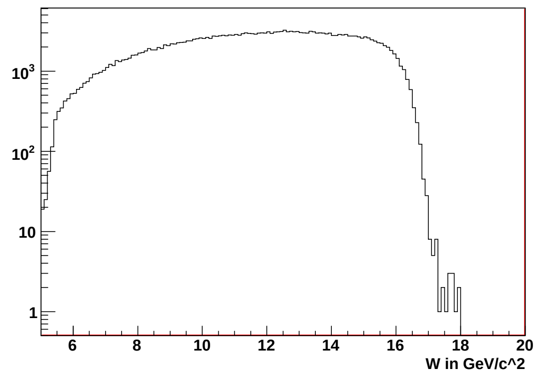

Figure 4.4: *Distribution of the mass of the hadronic final state* W *after the cut* $W > 5\ \mathrm{GeV}/c^2$.

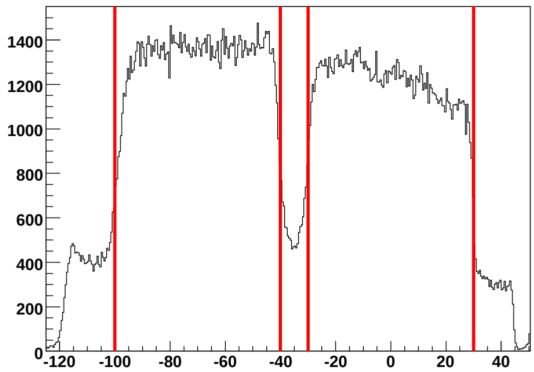

Figure 4.5: *Distribution of the z coordinate of the primary vertex. The marked region corresponds to the vertices well inside the target cells.*

4.2.2 Muon and Primary Vertex Cuts

The condition of a primary vertex is to have an incoming as well as a scattered muon. Because it is possible that there is more than one primary vertex in the reconstruction, the COMPASS analysis software PHAST provides a “best primary vertex” function. This function selects the primary vertex with the most outgoing particle tracks. For the case that two or more vertices with the same numbers exist, the one with the best χ^2 values in the reconstruction of the particle tracks is taken as “best primary vertex”.
The distribution of the primary vertex z coordinate before cutting can be seen in fig. 4.5. It is controlled that the found primary vertex lies well inside one of the target cells (z coordinates between -100 cm and -40 cm (upstream cell) and between -30 cm and 30 cm (downstream cell)).
In comparison to the longitudinal case the target cells are displaced in the transverse running because of the additional dipole field. The position of the target is determined by examing the distribution of the primary vertices in the xy plane (see fig. 4.6). The displacement in x and y can then be extracted by locating the position of the target cylinder with the radius of 1.5 cm. This dislocation is evaluated for every year. The applied cut is a radial cut of $r < 1.3$ cm. For having the same muon flux in both target cells it is tested in addition that the beam muon would cross the target cell, meaning that the projection of the muon track to the most upstream and the most downstream end of the target lies inside this cut.

Muon Cuts

The incoming particle connected to the primary vertex identified as the best one is taken as the beam muon. The momentum of the beam muon has to be below 200 GeV/c. In the production of the mDSTs a total χ^2 fit expressing the summed probability, that each hit

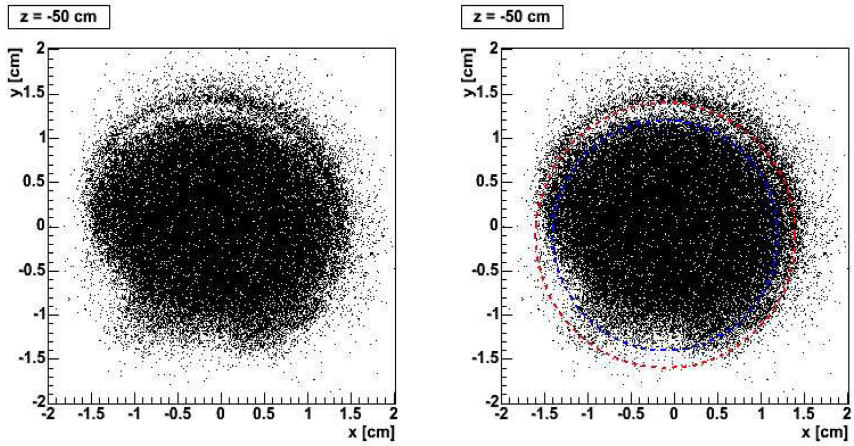

Figure 4.6: *Left: Distribution of the primary vertices at the most upstream part of the target. The target cylinder is easily to identify. Right: The same distribution with a red circle marking the shape of the cylinder. The blue circle indicates the region accepted by the radial cut of* $r < 1.3$ cm.

assigned to the track, does belong to it, is calculated. Now the reduced χ^2 is calculated by

$$\chi^2_{red} = \frac{\chi^2_{tot}}{N_{hits} - 5} \tag{4.1}$$

N_{hits} means here the number of hits along the track. The number of degrees of freedom is reduced by five due to the five parameters extracted from the track: the coordinates x, y (z is determined by the first hit of the track downstream of the target), the directions $\frac{dx}{dz}$, $\frac{dy}{dz}$ and the track momentum. The event is discarded for a χ^2_{red} of the beam or the scattered muons larger than 10.

For the scattered muon also a certain radiation length is demanded. This quantity indicates the fraction of energy loss of a particle traversing through material. nX/X_0 corresponds to the ratio of the amount nX of detector material passed to the particle-specific radiation length X_0 in this material. A particle with $nX/X_0 = x$ would have a fraction of $1/2^x$ of its original energy at the end of the track. If the particle has a large radiation length, thus losing a small fraction of its energy, it is probabily a muon. For this analysis this leads to the condition that only a particle, which has a radiation length of $nX/X_0 > 30$ is accepted as scattered muon.

The COMPASS trigger hodoscopes do not cover the whole kinematic range in the large-angle spectrometer. To recover lost muons scattered at large angles the information of the Muon Wall detector 1 in front of and behind the absorber is used. The conditions are four or more hits in front of the hadron absorber and six or more hits behind it. This iron absorber with a thickness of 60 cm should be transversed only by muons. The recovered muons also have to satisfy the conditions of $\chi^2_{red} < 10$ and $nX/X_0 > 30$. The latter one should be fulfilled anyway for particles, which have penetrated the absorber.

If in this way a “normal” scattered muon as well as a muon “regained” in the LAS is detected or if more than one of those "regained" muons is found, the event is discarded, because for a reaction with more than one muon the scattered and other, produced muons are not distinguashible. The same is done, if more than one "normal" flagged scattered muon is found.

4.2.3 Hadron Identification

All particles connected to the best primary vertex, which are not recognized as beam or scattered muons, are considered as hadrons. In the following the data sample is divided in two and analysed separately. One sample, where all hadrons produced in one event are considered and one, which contains only the most energetic hadron ("leading hadron", the one with the largest z value) in this event, because the investigated asymmetries containing the physical information of interest are expected to be larger for the more energetic hadrons in some models [68].
For the leading hadron analysis for K^0 it is not only necessary to examine all neutral particles from the primary vertex, but also the charged ones, to find the most energetic hadron. Furthermore the reconstruction of all hadrons from the primary vertex, charged and neutral ones, is in principle necessary for both analysis to calculate the sum of z, which should not excceed 1 beside a region of tolerance (see definition of z in eq. (2.65)).
For the selection of the charged hadrons from the primary vertex in the leading hadron analysis the following cuts are used:

- $\chi^2_{red} < 10$ as for the beam and the scattered muon.
- The radiation length nX/X_0 has to be below 10.
- Tracks only reconstructed in the fringe field of SM1 have to be discarded. For this the tracks must have at least one hit after SM1. This is guaranteed by a cut on the z coordinate of the last measured hit associated with the track: $Z_{last} > 350$ cm.
- A cluster in the hadronic calorimeters HCAL1 and HCAL2 associated with the hadron must have a minimum energy deposition to clean further the hadron sample from muonic contamination. For 2002 and 2003 $E^{HCAL1} > 5$ GeV and $E^{HCAL2} > 8$ GeV is required, for 2004 the conditions are $E^{HCAL1} > 4$ GeV and $E^{HCAL2} > 4$ GeV. If more than one cluster is found, at least one of them must have an energy over the corresponding thresholds, the other clusters are then assumed to be from muons. If no cluster at all is found, the particle is also accepted to sort out not to much hadrons.

As described in [69] there appears a peak in the y distribution at high y for positive hadrons of high energy (last z bin $(0.8 < z < 1)$), which is also visible in the distribution of the momentum of the scattered muons. The origin of this peak lies in the misidentification of scattered muons as positive hadrons. Because the corresponding muons go through a hole in the muon absorber, the amount of radiation length associated with their tracks is too small to identify these particles as muons. Then a positive muon from the primary vertex is

reconstructed and wrongly considered as the scattered muon. Those wrong reconstructed events were rejected by cuts on the extrapolated x and y coordinates of the tracks after the iron absorber following the proposal in [69]. For negative hadrons none of these peak problems is visible.
In this analysis the identification of the K^0 is done by reconstructing V^0 vertices from the decays of neutral particles. These V^0 are vertices with no incoming charged particle and exactly two outcoming opposite charged particles. The outgoing tracks from the V^0 vertices must not be connected to any primary vertex and the position of the V^0 vertices has to be downstream of the primary vertex, i.e. $Z_{sec.vtx.} - Z_{prim.vtx.} > 0$, to be sure that the neutral particles are created at the primary vertex. Later on a cut on this distance is applied as described afterwards.
In the K^0 analysis only K^0_S ($K^0 \mathrel{\widehat{=}} 50\%\ K^0_S,\ 50\%\ K^0_L$) are considered and here only the decay into π^+ and π^- can be detected clearly under our conditions. The fraction of the decay mode for this reaction $K^0_S \to \pi^+ + \pi^-$is $(30.69 \pm 0.05)\%$ [9].
The outgoing tracks of the V^0 vertices have to fulfill the following criteria similarly to those for the tracks of the charged hadrons from the primary vertex:

- $\chi^2_{red} < 10$ for the reconstruction quality of the hadron track.
- Radiation length $nX/X_0 < 10$.
- $Z_{last} > 350$ cm to discard tracks only reconstructed in the fringe field of SM1.
- To remove muons, the clusters in the HCALs connected to hadrons with a momentum P_h larger than 2.5 GeV/c are tested for the following conditions:
  - If there is more than one cluster, the particle is rejected.
  - Particles with no cluster at all are accepted.
  - In the case of exactly one cluster in the hadronic calorimeters, a cut depending on the particle momentum is performed: In a momentum range of P_h from 2.5 GeV/c to 22.5 GeV/c the condition for the cluster energy to fulfill is $E_{clus} > (P_h - 2.5\ \text{GeV}/c) \cdot 0.5\ \text{GeV}/c^2$ corresponding to a linear slope in P_h, while for momenta $P_h > 22.5$ GeV/c the cut remains constant with $E_{clus} > 10$ GeV/c^2) (see fig. 4.7).

If one of the two charged hadrons doesn't satisfy any of those conditions, the corresponding V^0 vertex is excluded.
To test the association of the secondary vertex from the K^0 decay, the angle θ between the reconstructed momentum of the hadron pair and the vector, which connects the primary and the secondary vertex, is calculated. The distributions of the angles for all V^0 (in blue), only for those V^0 with a well separated primary vertex (in red) and for the identified K^0 with all cuts except the one for this angle (in black) can be seen in fig. 4.8. The condition chosen to accept the particle is $\theta < 10$ mrad. It has to be mentioned here that the latter cut on the invariant mass of the assumed pion pair near to the K^0 mass includes this target

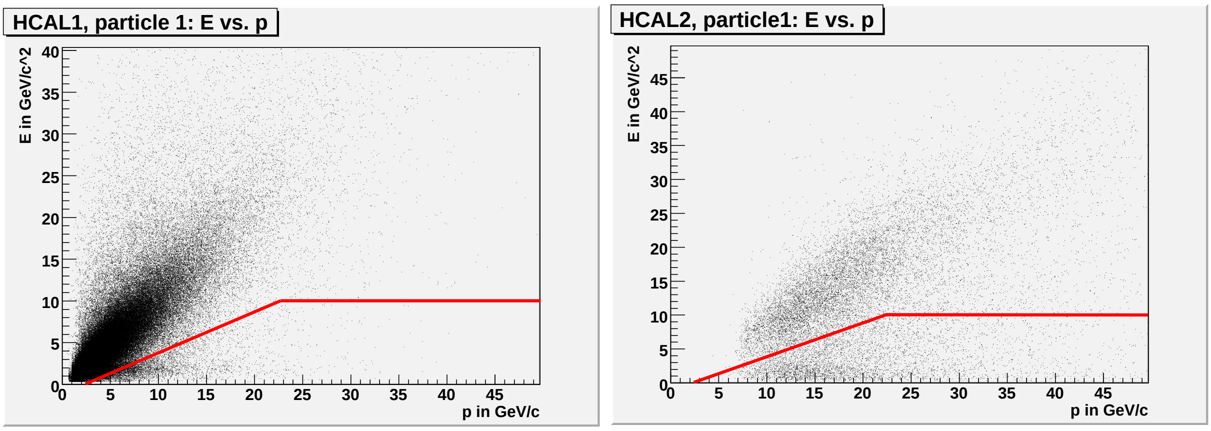

Figure 4.7: *Correlation between the energy measured in HCAL1 (left-hand side) and HCAL2 (right-hand side), respectively and the momentum measured in the spectrometer in one period of the 2004 data. The cut to remove muons in the sample (see text) is marked by a red line.*

pointing cut. Nevertheless the cut is necessary to identify other neutral hadrons produced at the primary vertex to calculate the sum of the energy fractions z of all hadrons coming from the primary vertex. For the leading hadron analysis also the hadron with the largest z has to be found.
To get a good distinction between the primary and the secondary vertex a cut on the distance between primary and secondary vertex, where the K^0 decays, is applied. The $c\tau$ distribution of the reconstructed pion pairs, which gives the range of the K^0 before decaying, boosted into the laboratory system can be seen in fig. 4.9. Due to this and the dependance of the signal-to-background-ratio for the K^0 signal from the distance between primary and secondary vertex a cut at a distance of 10 cm was chosen. A cut at a larger value does not improve the signal-to-background-ratio and results in a poorer signal statistics (see fig. 4.10).
In fig. 4.11 the Armenteros-Podolanski plot of the hadron pair is shown. In this type of plots the transverse momentum fraction p_t of one hadron (transverse relativ to the hadron momentum sum) is plotted vs. the difference of the longitudinal momenta of the two hadrons over their sum $\frac{p_{l1}-p_{l2}}{p_{l1}+p_{l2}}$ [71]. The K^0 band can be seen clearly as well as the Λ and $\bar{\Lambda}$ bands. The background from e^+e^- pairs is reduced by a cut of $p_t > 25$ MeV/c.
For the final identification of the K^0 a cut on the invariant mass of the pion pair is done. The reconstructed invariant mass has to be within ± 20 MeV/c^2 of the literature value of 497.614 ± 0.024 MeV (PDG: [9]) as one can see in fig. 4.12. Because the fitted peak has a width of $\sigma \approx 6$ MeV/c^2, more than 99% of the signal is covered by the region of ± 20 MeV/c^2.
At lower values of the fraction z of the photon energy transferred to the struck quark (and subsequently to the produced hadron) impurities occur by secondary interactions of the

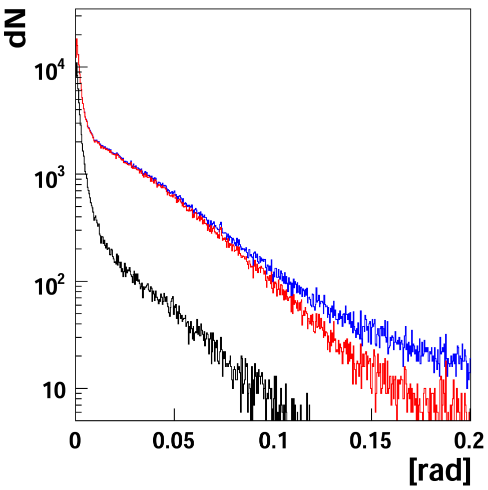

Figure 4.8: *Angle between the reconstructed V^0 momentum and the vector connecting primary and secondary vertex. Blue: all V^0, red: only those with a well separated primary vertex and black: only identified K^0.*

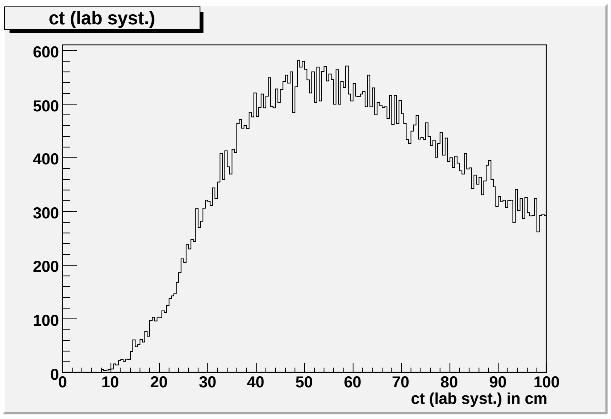

Figure 4.9: *$c\tau$ distribution of the reconstructed pion pairs, which gives the range of the K^0 before decaying, boosted into the laboratory system.*

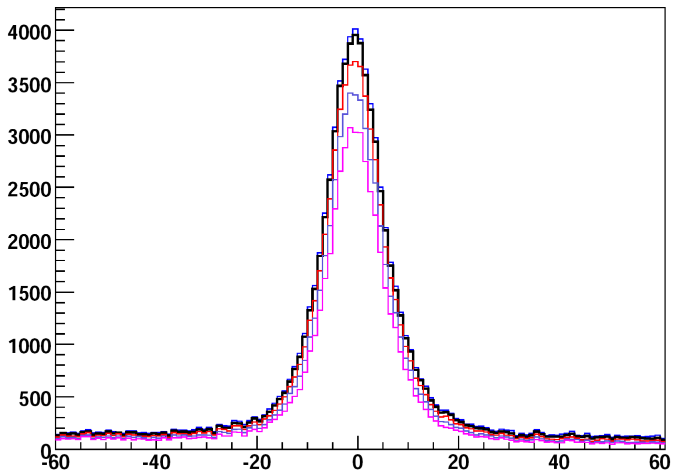

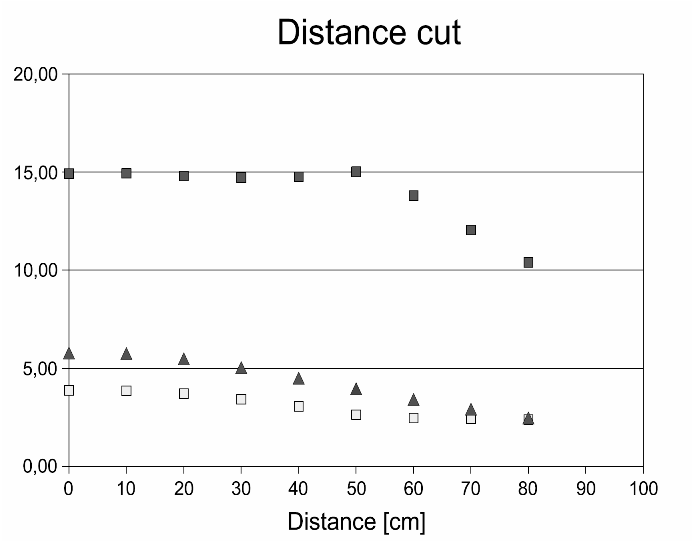

Figure 4.10: *Upper plot: Invariant mass spectra (in* MeV/c^2*) for different distances between primary and secondary vertex. The spectra correspond with falling statistics to* 0cm, 10cm, 20cm, 30cm *and* 40cm. *Lower plot: Signal-to-background-ratio (filled squares), signal strength (filled triangles) and background (open squares) vs. the distance between primary and secondary vertex.*

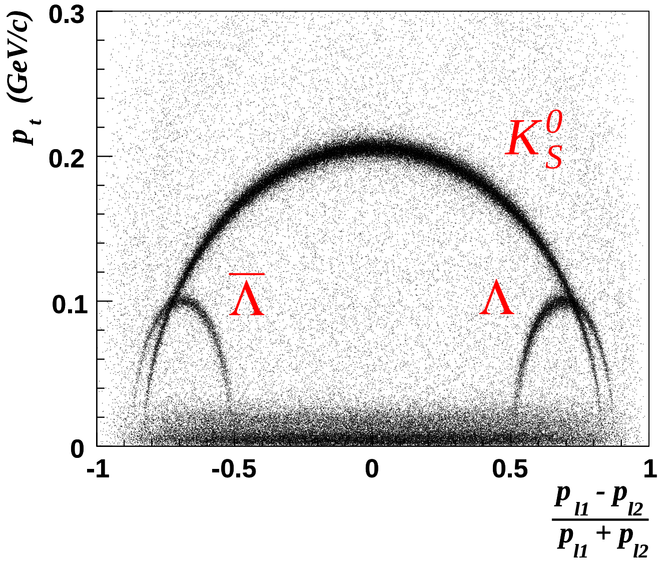

Figure 4.11: *Armenteros-Podolanski plot of the hadron pair. The K^0 band as well as the Λ and $\bar{\Lambda}$ bands can be clearly seen.*

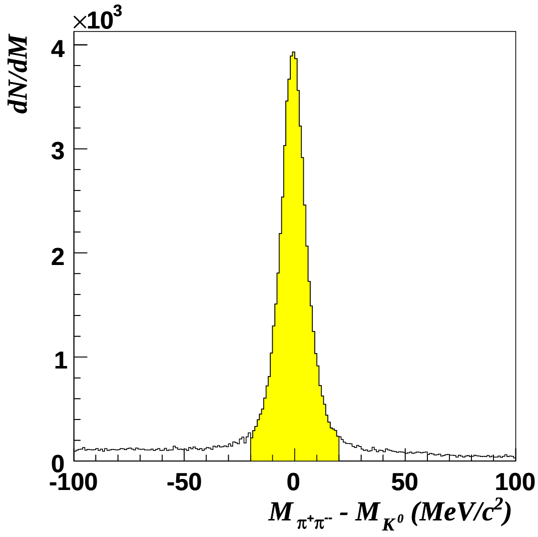

Figure 4.12: *Difference of the invariant mass of the hadron pair after cuts to the literature value of the K^0 mass [9]. The yellow region marks the accepted K^0.*

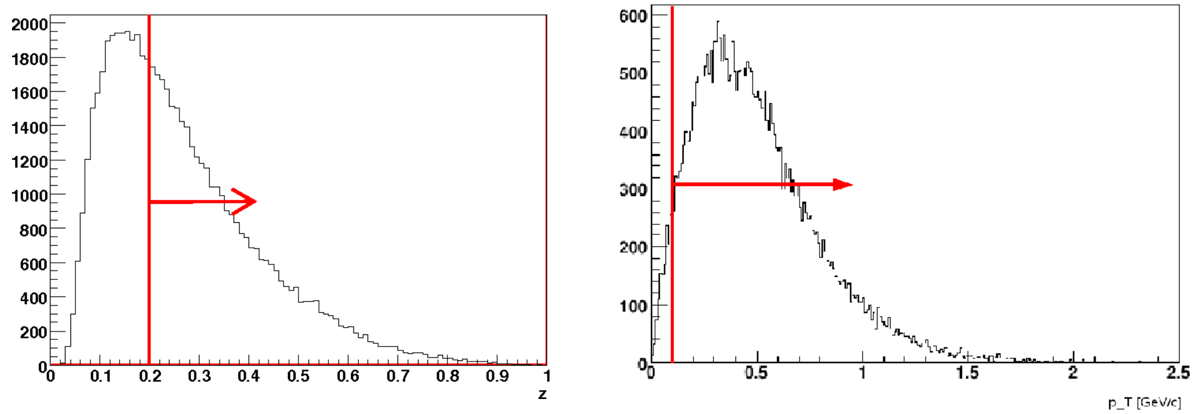

Figure 4.13: *Left: z distribution of the selected K^0 in the all hadron analysis in one period of the 2004 data with the corresponding cut at $z > 0.2$ marked in red (which is $z > 0.25$ in the leading K^0 analysis). Right: P_T^h distribution of the selected K^0 in the all hadron analysis in one period of the 2004 data with the corresponding cut at $P_T^h > 0.1$ marked in red.*

fragmented hadron with the target material. This can provoke a false identification of the hadron. Therefore a lower cut on z of the K^0 is implimented, requiring $z > 0.2$ for the all hadron sample and the stricter condition $z > 0.25$ for the leading hadron sample to exclude the possibility that a hadron is wrongly identified as the leading one. An upper cut of $z < 1$ is also performed.
If the sum of z of all particles outgoing from the primary vertex is larger than 1.1 the event is discarded.
In the leading hadron analysis it is also tested, whether there is an unreconstructed (neutral) hadron from the primary vertex with a higher energy as the particle identified as leading hadron. For this the calculated sum of z of all particles from the primary vertex is substracted from 1. In the case, this "missing" z is larger than the z of the identified leading hadron, it is searched in the hadronic calorimeters for clusters of an energy higher than the one of the identified leading hadron added by 2σ of the leading hadron's energy. If such a cluster is found and no track is associated to it – meaning that the cluster is from a neutral particle – the event is removed.
Finally, to assure a good resolution of the azimuthal angle of the K^0, its transverse momentum with respect to the virtual photon direction has to be larger than 0.1 GeV/c.
The distribution of the variables z and P_T^h and the effect of the corresponding cuts is shown in fig. 4.13. It is clearly visible that the z cut has a large influence on the accepted statistics.
After applying all these cuts the signal-to-background ratio is about 15, constant over the whole kinematic range.

Year	Period	Leading K^0 sample	All K^0 sample
2002	1	14374	20766
2002	2	9448	13732
Sum 2002		23822	34498
2003		51657	76518
2004	1	43058	63482
2004	2	56363	83260
Sum 2004		99421	146742
Total sum		174900	257758

Table 4.2: *Final statistics for the K^0 data from the deuteron target runs.*

x	z	P_T^h
$0.003 < x < 0.013$	$0.200 \leqq z < 0.250$	0.10 GeV$/c < P_T^h \leqq 0.35$ GeV$/c$
$0.013 \leqq x < 0.032$	$0.250 \leqq z < 0.325$	0.35 GeV$/c < P_T^h \leqq 0.55$ GeV$/c$
$0.032 \leqq x < 0.080$	$0.325 \leqq z < 0.425$	0.55 GeV$/c < P_T^h \leqq 0.75$ GeV$/c$
$0.080 \leqq x < 0.130$	$0.425 \leqq z < 0.550$	0.75 GeV$/c < P_T^h \leqq 1.00$ GeV$/c$
$0.130 \leqq x < 1.000$	$0.550 \leqq z < 0.700$	1.00 GeV$/c < P_T^h$
	$0.700 \leqq z < 1.000$	

Table 4.3: *Bins in the variables x, z and P_T^h.*

4.2.4 Final Data Sample

The final statistics entering the asymmetry evaluation after all cuts is given in table 4.2. for the leading K^0 as well as for the all K^0 sample corresponding to all (sub-)periods of the deuteron data taking in 2002, 2003 and 2004.

4.3 Extraction of the Asymmetries

4.3.1 Binning

As can be seen in eq. (2.93) and (2.100) the Collins as well as the Sivers asymmetry depend on the product of a x-dependant distribution and a z-dependent fragmentation function. To analyse the dependance on x, z and P_T^h, the asymmetries were calculated as functions of one of these variables after integration over the two other ones. For this the kinematical range of the variables was divided into bins with variable width to have a comparable statistics in each of them. In total in x and P_T^h there are five bins for both samples, while in z there are six for the all K^0 analysis and five for the leading K^0 analysis (see table 4.3).

4.3.2 Extraction of the Raw Asymmetries

In section 2.4 and 2.5 the single spin asymmetries for Collins and Sivers were defined by comparing the cross-section for the two different spin directions. It can be seen from eq. (2.92) and (2.99) that the angular modulations for Collins and Sivers are different and independent, so that both effects can be extracted separately. For both effects the number of hadrons depends on an azimuthal angle $\Phi_{C,S}$ (with C for Collins and S for Sivers):

$$N(\Phi_{C,S}) = Fn\sigma a(\Phi_{C,S})(1 + A^{raw}_{C,S}\sin(\Phi_{C,S})) \tag{4.2}$$

where F is the muon flux, n the number of target particles, σ the spin averaged cross-section, $A^{raw}_{C,S}$ the raw Collins and Sivers asymmetry, respectively and $a(\Phi_{C,S})$ the product of the angular acceptance and the spectrometer efficiency. Spectrometer acceptance and efficiency are largely unknown and have therefore to be compensated in the data analysis. Here it has also to be taken into account that they are different for the upstream and downstream target cells.

For the compensation of those acceptance effects the measurement is always split into two sub-periods with opposite spin-direction as already mentioned.

As a technicality the angles are always calculated assuming spin up, which results in two different rate distributions depending on the real spin orientation, because this assumption induces a phase of π in the angle definitions:

$$N^{\uparrow}(\Phi_{C,S}) = Fn\sigma a^{\uparrow}(\Phi_{C,S})(1 + A^{raw}_{C,S}\sin(\Phi_{C,S})) \tag{4.3}$$

$$N^{\downarrow}(\Phi_{C,S}) = Fn\sigma a^{\downarrow}(\Phi_{C,S})(1 - A^{raw}_{C,S}\sin(\Phi_{C,S})) \tag{4.4}$$

For the deuteron data the so-called “double ratio” method was used to extract the asymmetries. Here the information of both target cells (upstream: u, downstream: d) and both sub-periods (p_1, p_2) with opposite target spin configuration (see fig. 4.1) is used simultaneously by defining the ratio:

$$F(\Phi_{C,S}) = \frac{N_u^{\uparrow,p_2}(\Phi_{C,S})N_d^{\uparrow,p_1}(\Phi_{C,S})}{N_u^{\downarrow,p_1}(\Phi_{C,S})N_d^{\downarrow,p_2}(\Phi_{C,S})} \tag{4.5}$$

Using the above equations we get:

$$\begin{aligned}
F(\Phi_{C,S}) &= \\
&\frac{F_{p_2}n_u\sigma a_u^{\uparrow,p_2}(\Phi_{C,S})(1 + A^{raw}_{C,S}\sin(\Phi_{C,S}))F_{p_1}n_d\sigma a_d^{\uparrow,p_1}(\Phi_{C,S})(1 + A^{raw}_{C,S}\sin(\Phi_{C,S}))}{F_{p_1}n_u\sigma a_u^{\downarrow,p_1}(\Phi_{C,S})(1 - A^{raw}_{C,S}\sin(\Phi_{C,S}))F_{p_2}n_d\sigma a_d^{\downarrow,p_2}(\Phi_{C,S})(1 - A^{raw}_{C,S}\sin(\Phi_{C,S}))} \\
&= C\frac{a_u^{\uparrow,p_2}(\Phi_{C,S})a_d^{\uparrow,p_1}(\Phi_{C,S})(1 + A^{raw}_{C,S}\sin(\Phi_{C,S}))(1 + A^{raw}_{C,S}\sin(\Phi_{C,S}))}{a_u^{\downarrow,p_1}(\Phi_{C,S})a_d^{\downarrow,p_2}(\Phi_{C,S})(1 - A^{raw}_{C,S}\sin(\Phi_{C,S}))(1 - A^{raw}_{C,S}\sin(\Phi_{C,S}))} \\
&\approx C\frac{a_u^{\uparrow,p_2}(\Phi_{C,S})a_d^{\uparrow,p_1}(\Phi_{C,S})}{a_u^{\downarrow,p_1}(\Phi_{C,S})a_d^{\downarrow,p_2}(\Phi_{C,S})} \cdot (1 + 4A^{raw}_{C,S}\sin(\Phi_{C,S}))
\end{aligned} \tag{4.6}$$

at the first order in $A_{C,S}^{raw}$. This is sufficient due to the small raw asymmetries expected to be of the order of a fraction of 10^{-4}.
This ratio is calculated in eight bins of equal width over the range of $\Phi_{C,S}$ and plotted against those angles. The statistical error from the error propagation of eq. (4.6) is:

$$\sigma^2_{F(\Phi_{C,S})} = [F(\Phi_{C,S})]^2 \cdot \left[\frac{1}{N_u^{\uparrow,p_2}} + \frac{1}{N_d^{\uparrow,p_1}} + \frac{1}{N_u^{\downarrow,p_1}} + \frac{1}{N_d^{\downarrow,p_2}}\right] \tag{4.7}$$

The ratio as a function of $\Phi_{C,S}$ is fitted with a sin amplitude in a two parameter fit:

$$par(0) \cdot (1 + par(1)\sin(\Phi_{C,S})) \tag{4.8}$$

The raw asymmetry is then extracted from $par(1)$ as $A_{C,S}^{raw} = par(1)/4$.
To get the asymmetries with this method without a systematic effect caused by the method the following "reasonable" assumption has to be valid:

$$\frac{a_u^{\uparrow,p_2}(\Phi_{C,S})a_d^{\uparrow,p_1}(\Phi_{C,S})}{a_u^{\downarrow,p_1}(\Phi_{C,S})a_d^{\downarrow,p_2}(\Phi_{C,S})} = const. \tag{4.9}$$

or

$$\frac{a_u^{\uparrow,p_2}(\Phi_{C,S})}{a_d^{\downarrow,p_2}(\Phi_{C,S})} = const. \frac{a_u^{\downarrow,p_1}(\Phi_{C,S})}{a_d^{\uparrow,p_1}(\Phi_{C,S})} \tag{4.10}$$

This condition means therefore that the ratio of the acceptances of the upstream and downstream cell remains constant during both sub-periods.
The assumption of constant acceptances can be tested by calculating the following ratio:

$$R(\Phi_{C,S}) = \frac{N_u^{\uparrow,p_2}(\Phi_{C,S})N_d^{\downarrow,p_2}(\Phi_{C,S})}{N_u^{\downarrow,p_1}(\Phi_{C,S})N_d^{\uparrow,p_1}(\Phi_{C,S})} \tag{4.11}$$

where the term containing the asymmetries vanishes:

$$R(\Phi_{C,S}) \approx C\frac{a_u^{\uparrow,p_2}(\Phi_{C,S})a_d^{\downarrow,p_2}(\Phi_{C,S})}{a_u^{\downarrow,p_1}(\Phi_{C,S})a_d^{\uparrow,p_1}(\Phi_{C,S})} \tag{4.12}$$

The condition that R is constant is a stricter condition than the "reasonable" assumption itself. If R is constant, there are no changes in the acceptances between both sub-periods and therefore the "reasonable" assumption holds. If this is not the case, there are changes in the acceptances, but the "reasonable" assumption nevertheless can be valid. This R-test is done in section 4.4.3.

4.3.3 From Raw to Collins and Sivers Asymmetries

To get the final Collins and Sivers asymmetry one has to take into account the polarization P_T and the dilution factor f of the target as well as the depolarization factor D_{NN}.
The Collins asymmetry one then receives through:

$$A_{Coll} = \frac{A_C^{raw}}{D_{NN} f P_T} \tag{4.13}$$

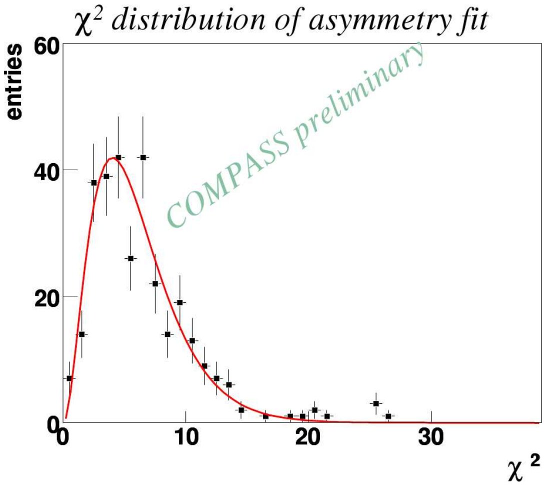

Figure 4.14: χ^2 *distribution of the performed asymmetry fits compared to the curve theoretically expected for six degrees of freedom.*

The depolarization factor in the Collins case (see section 2.4) is given by:

$$D_{NN} = \frac{1-y}{1-y+y^2/2} = \frac{2(1-y)}{1+(1-y)^2} \tag{4.14}$$

It is calculated from the kinematics from each event and the mean value in each bin is taken for the asymmetry extraction.
The dilution factor of the target, which gives the fraction of the target material that can be polarized, is taken constant as $f = 0.38$ (see section 3.2).
The target polarization cannot be measured directly in the transverse mode at COMPASS. So the polarization was measured in the longitudinal field of 2.5 T at the beginning and the end of each data taking sub-period. The measured values of the target polarization P_T in the transverse deuteron runs in 2002-04 were about 50% (see appendix A.1).
The Sivers final asymmetry one can extract analog to the Collins one:

$$A_{Siv} = \frac{A_S^{raw}}{D_{NN} f P_T} = \frac{A_S^{raw}}{f P_T} \tag{4.15}$$

Here the depolarization factor $D_{NN} = 1$ (see section 2.5).
The Collins and Sivers asymmetries were extracted individually for each data taking period and then combined by a weighted mean. To test the quality of the fits the χ^2 of each fit in eight $\Phi_{C,S}$ bins were calculated and plotted together with the theoretically expected χ^2 curve for six degrees of freedom (8 $\Phi_{C,S}$ bins and 2 extracted parameters: $ndf = 8-2 = 6$). Alltogether there are 5 periods of data taking with Collins and Sivers asymmetries in $5x$, $6z$ and $5P_T^h$ bins for the all K^0 sample and $5x$, $5z$ and $5P_T^h$ bins for the leading K^0 sample corresponding to 310 entries. It can be seen in fig. 4.14 that a good agreement between the χ^2 distribution from the performed fit and the theoretical expectation was obtained.

4.3.4 Results

The results of the Collins and Sivers asymmetries for K^0 from the 2002-04 deuteron data taking are shown in fig. 4.15 for the all K^0 analysis and in fig. 4.16 for the leading K^0 analysis. The error bars show the statistical errors only, the systematic errors are found to be considerably smaller (see next section, 4.4). Both the Collins and the Sivers asymmetries are all small and compatible with zero. The interpretation of the results is done in chapter 6 together with those from the proton target described in chapter 5.

4.4 Systematic Studies

It is essential for the data analysis to examine the stability of the spectrometer. Many tests to evaluate possible false asymmetries and to investigate the stability of the physics results were done for the analysis of the asymmetries of charged hadrons. It is not necessary to repeat all those tests, because the data were already shown to be stable. So only the most significant studies and particularly checks for the analysis of the K^0 were done here. The main goal of the tests is the evaluation of the sources and the size of the systematic errors of the asymmetries.
The systematic checks performed for this analysis are:

- Compatibility of the results in the different periods
- Studies on background asymmetries
- Stability of the acceptance ratio

4.4.1 Compatibility of the Different Periods

As explained in section 3.3.3 the measured asymmetries are given by the weighted mean of the results of all single periods. Therefore the compatibility of the asymmetries in each bin of x_{bj}, z and P_T^h of all five periods in the years 2002-04 was checked by evaluating the following quantity:

$$\frac{A_i - \langle A \rangle}{\sqrt{\sigma_i^2 - \sigma_{\langle A \rangle}^2}}; \quad i = 1, 2, 3, 4, 5 \tag{4.16}$$

where A_i are the asymmetries in a single bin and period and $\langle A \rangle$ the corresponding weighted mean of this bin. In the denominator the difference of the single asymmetry values and those of the weighted mean was used to take into account the correlation between A_i and $\langle A \rangle$.
The number of entries for the overall distribution of this quantity for all asymmetries, Collins and Sivers in five periods in all bins is 160 for the all K^0 sample corresponding to 2 (Collins/Sivers) $\cdot$ 5 (periods) $\cdot$ $(5 + 6 + 5)$ (x_{bj}, z and P_T^h bins) and 150 for the leading K^0 sample corresponding to 2 (Collins/Sivers) $\cdot$ 5 (periods) $\cdot$ $(5 + 5 + 5)$ (x_{bj}, z and P_T^h bins).

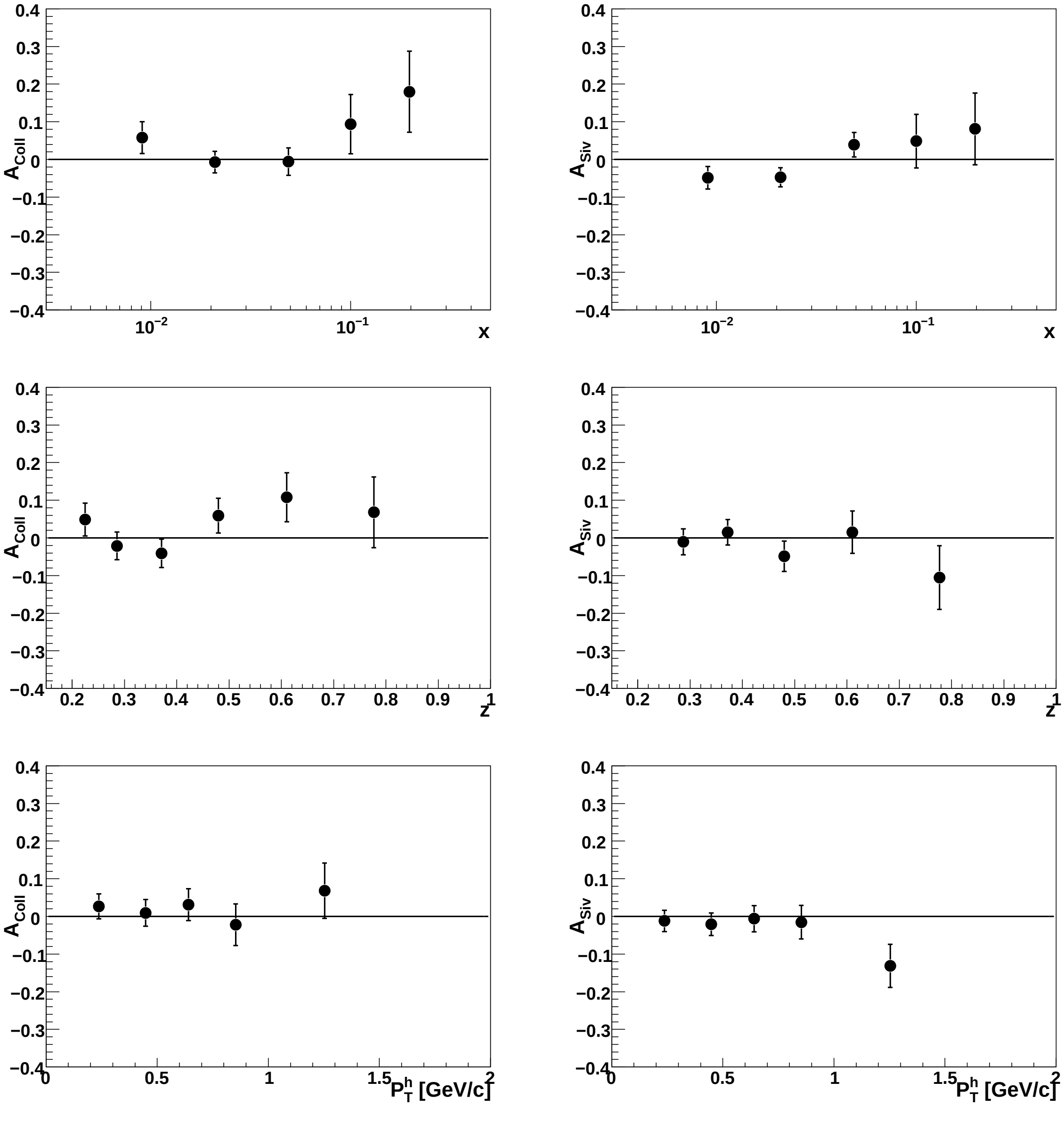

Figure 4.15: *The Collins (left) and Sivers (right) asymmetries for the all K^0 analysis as function of x, z and P_T^h from a deuteron target at the COMPASS experiment. Only statistical errors are shown.*

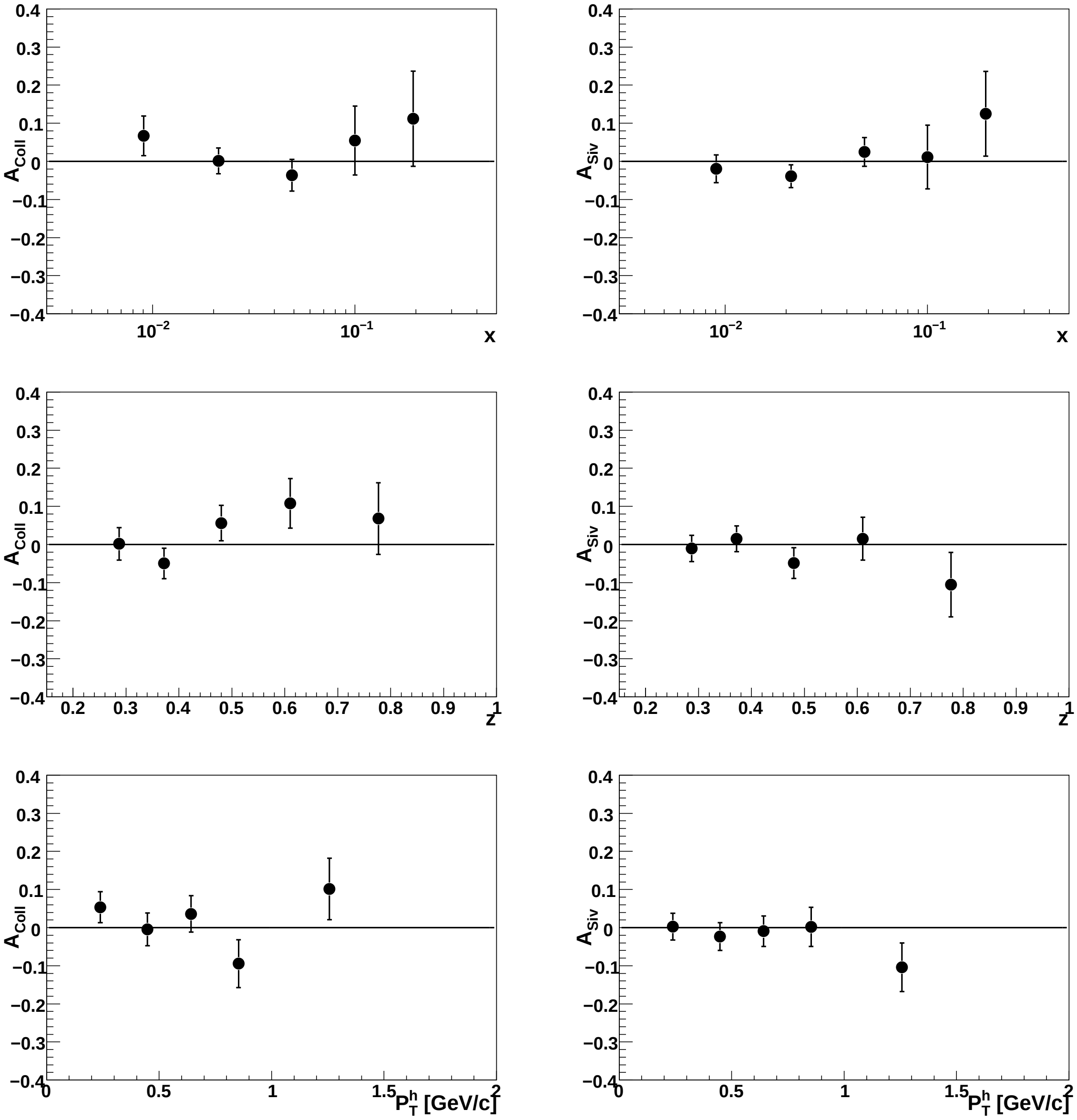

Figure 4.16: *The Collins (left) and Sivers (right) asymmetries for the leading* K^0 *analysis as function of* x*,* z *and* P_T^h *from a deuteron target at the COMPASS experiment. Only statistical errors are shown.*

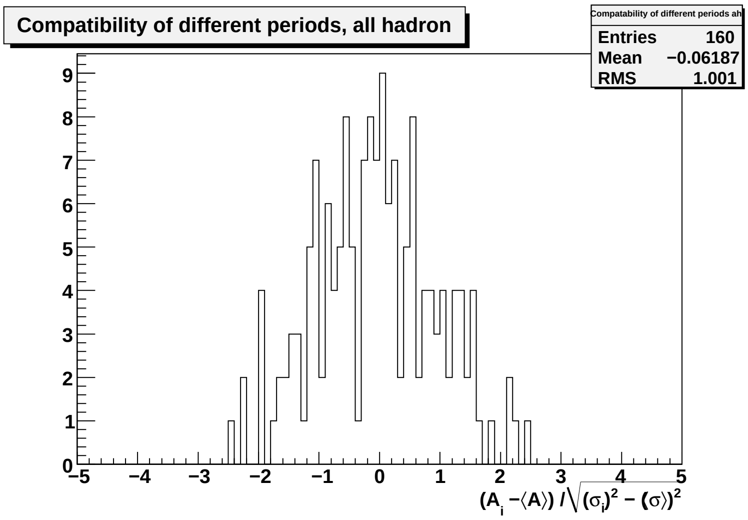

Figure 4.17: *Distribution of the asymmetries for K^0 on deuteron for all values (Collins/Sivers, x_{bj}, z and P_T^h, five periods) in the all hadron analysis.*

As expected the asymmetries for both analysis follow the standard normal distributions with a mean value compatible with 0 and a RMS near 1 of 1.001 for the all K^0 and 0.982 for the leading K^0 case. The distribution for the all K^0 analysis is shown as example in fig. 4.17, for the one for the leading K^0 analysis see appendix A.2.1.
This test was also done separately for the Collins and Sivers asymmetries. Also here it resulted in standard normal distributions with mean values compatible with 0 and RMS with values between 0.96 and 1.04 near the expected value of 1 (for the figures see appendix A.2.1).
So it can be concluded that the results gained from the different periods are compatible.

4.4.2 Background Asymmetries

Another check was the extraction of asymmetries in the same way as described before, but in a mass range widely outside the one of the K^0-signal. As a distance of $|50|$ MeV in the mass spectrum of the K^0 corresponds to 6-7 σ of the K^0-signal, a range of $[-50, -350] \cup [50, 350]$ MeV in the difference of the measured K^0-mass and the literature value was chosen for those background asymmetries. The sample was devided in three bins in x_{bj}, z and P_T^h with:

$0.003 \leqq x_{bj} < 0.028$	$0.0 \leqq z < 0.325$	$0.0 < P_T^h \leqq 0.40$
$0.028 \leqq x_{bj} < 0.100$	$0.325 \leqq z < 0.55$	$0.40 < P_T^h \leqq 0.80$
$0.100 \leqq x_{bj} < 1.000$	$0.55 \leqq z < 1.00$	$0.80 < P_T^h \leqq 10.0$

The resulting asymmetries in the sidebands are consistent with zero. One example is given in fig. 4.18 for the Collins asymmetries in the sidebands vs. x_{bj} weighted over all periods

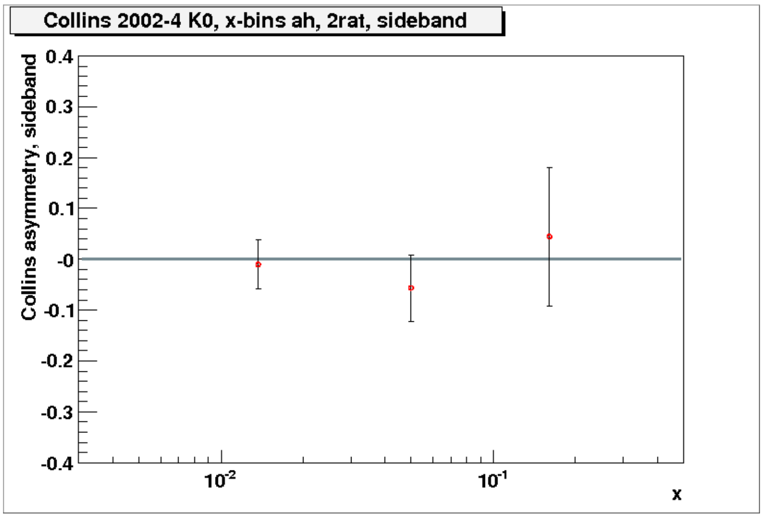

Figure 4.18: *Collins asymmetries in the sidebands vs.* x_{bj} *for the 2002-04 data in the all hadron analysis.*

in the all K^0 analysis. For the other background asymmetries see appendix A.2.2.
To test the compatibility with zero also the following quantity analog to the one in eq. (4.16) was evaluated:

$$\frac{A_{i,background} - 0}{\sigma_{i,background}}; \quad i = 1, 2, 3, 4, 5 \tag{4.17}$$

If the distribution of this quantity for all Collins and Sivers asymmetries together is regarded, for the all K^0 sample a RMS of 1.037 and for the leading K^0 sample a RMS of 1.044 is obtained, both near 1 as expected for a standard normal distribution and the mean is also for both near 0 as expected. As an example the distribution for the all K^0 sample is shown in fig. 4.19, for the one for the leading K^0 sample see appendix A.2.2.
Also the distributions separated for Collins and Sivers have all mean values near 0 and RMS values with 0.92 to 1.14 near 1. For the cooresponding figures see appendix A.2.2.
The compatibility of the background asymmetries with zero is therefore clear confirmed.
For getting a mean background asymmetry the sidebands asymmetrys were also evaluated integrating over all bins in x_{bj}, z and P_T^h. The results integrated over x_{bj} are given in fig. 4.20 for Collins and fig. 4.21 for Sivers for all measuring periods in the all K^0 analysis. As one can see the asymmetries are in good agreement to each other as well as to zero.
For the weighted mean of the integrated background asymmetries over all periods see table 4.4. For both, Collins and Sivers, they are well consistent with zero.

4.4.3 Stability of the Acceptance Ratio

As described in section 4.3.2 the ratio R was built from the event numbers:

$$R(\Phi_{C,S}) = \frac{N_u^{\uparrow}(\Phi_{C,S}) N_d^{\downarrow}(\Phi_{C,S})}{N_u^{\downarrow}(\Phi_{C,S}) N_d^{\uparrow}(\Phi_{C,S})} \tag{4.18}$$

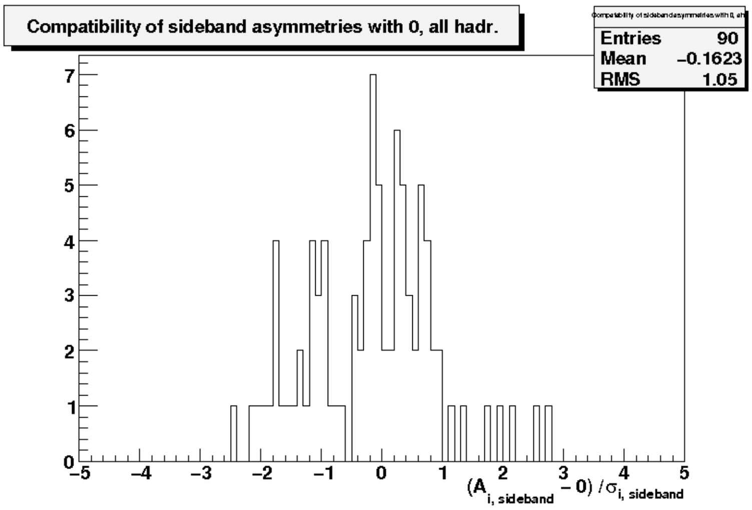

Figure 4.19: *Compatibility of the single K^0 asymmetries on deuteron in the sidebands with zero, for all values (Collins/Sivers, x_{bj}, z and P_T^h, five periods) for the all hadrons analysis.*

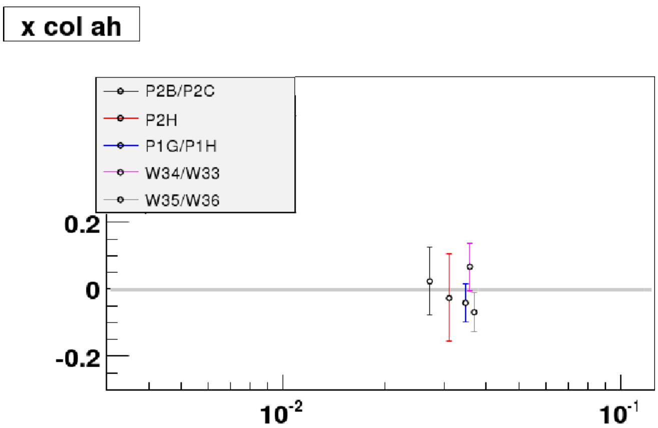

Figure 4.20: *Collins asymmetries in the sidebands for the 2002-04 data integrated over x_{bj} in the all K^0 analysis for the different periods.*

Integrated sideband asymmetry	All K^0 sample 2002-04
Collins	-0.021 ± 0.038
Sivers	0.002 ± 0.030

Table 4.4: *Weighted mean of the integrated background asymmetries over all periods 2002-04.*

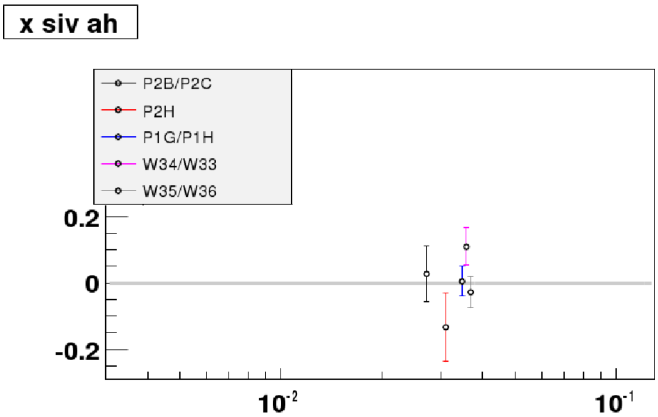

Figure 4.21: *Sivers asymmetries in the sidebands for the 2002-04 data integrated over x_{bj} in the all K^0 analysis for the different periods.*

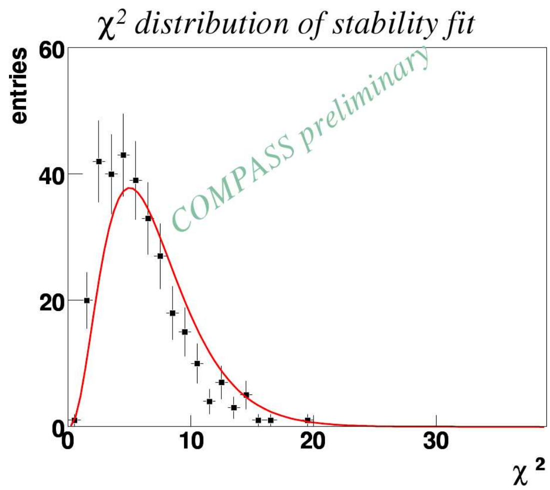

Figure 4.22: *χ^2 distribution of the performed fits of the ratio R compared to the curve theoretically expected for seven degrees of freedom.*

A constant R over the range of $\Phi_{C,S}$ implies that also the acceptance ratio is constant.
The ratio R was calculated for all eight bins of the Collins and Sivers angles in each bin in x_{bj}, z and P_T^h for all five periods, for the all and the leading K^0 sample and fitted with a constant function.
To test the quality of these constant fits and so the constancy of the acceptance ratios the received distribution of the χ^2 of the fits was compared with the theoretically expected curve for seven degrees of freedom (eight bins in $\Phi_{C,S}$ and a one parameter fit). Like for the χ^2 distribution of the double ratio F there were 310 entries corresponding to the number of all bins for Collins and Sivers for the all and the leading K^0 analysis in all periods. The result is shown in fig. 4.22. A good agreement between the calculated χ^2 values and the expected curve can be seen.

4.4.4 Summary of the Systematic Studies

There are no visible indications of systematic effects with consequence on the observables of interest in our tests. Therefore it can be concluded that the systematic errors from acceptance and efficiency effects are considerably smaller than the statistical errors.
The uncertainty of the target polarization P_T is about 5% and the one of the dilution factor f due to the uncertainty in the composition of the target about 6%. So by combining in quadrature and taking the square root a combined systematic error of about 8% is obtained from these effects.

Chapter 5

Collins and Sivers Asymmetries from a Proton Target

> La vraie définition de la science, c'est qu'elle est l'étude de la beauté du monde.
>
> The true definition of science is that it is the study of the beauty of the world.
>
> S. Weil (1909-1943), French philosopher

In the year 2007 the COMPASS experiment has taken data on a transversely polarized proton target. In this chapter the analysis of the Collins and Sivers asymmetries from those data is described. Asymmetries in the production of charged hadrons without identification as well as for the neutral K^0 and charged hadrons with identification will be presented.

5.1 Transverse Data from 2007 on the Proton Target

The data taking at COMPASS on the polarized proton (NH_3) target in 2007 was nearly equally shared between longitudinal and transverse polarization, corresponding to an amount of $\approx 40 \cdot 10^{12}$ and $\approx 42 \cdot 10^{12} \mu^+$ recorded, respectively. In the transverse run we had eleven sub-periods, each of them corresponding to about five days of data taking: W25, W26, W27, W28, W30, W31, W39, W40, W41, W42 and W43. Consecutive sub-periods have an opposite spin configuration and are combined for the analysis. An exception is here W42, which was splitted in two parts, W42-1 and W42-2, in a way that those have similar statistics as their chosen partner periods W41 and W43, respectively. The spin configuration for the three target cell setup used in 2007 is illustrated in fig. 5.1. An overview of the different (sub-)periods and their spin orientation is given in table 5.1.
The "data production" was analog to the one for the data from 2002-04 (see section 4.1.1).

Sub-period	Polarization		
	upstream	central	downstream
W25	$\Downarrow$	$\Uparrow$	$\Downarrow$
W26	$\Uparrow$	$\Downarrow$	$\Uparrow$
W27	$\Downarrow$	$\Uparrow$	$\Downarrow$
W28	$\Uparrow$	$\Downarrow$	$\Uparrow$
W30	$\Downarrow$	$\Uparrow$	$\Downarrow$
W31	$\Uparrow$	$\Downarrow$	$\Uparrow$
W39	$\Uparrow$	$\Downarrow$	$\Uparrow$
W40	$\Downarrow$	$\Uparrow$	$\Downarrow$
W41	$\Downarrow$	$\Uparrow$	$\Downarrow$
W42	$\Uparrow$	$\Downarrow$	$\Uparrow$
W43	$\Downarrow$	$\Uparrow$	$\Downarrow$

Table 5.1: *The transversity data taking (sub-)periods for the 2007 proton run and their spin configurations.*

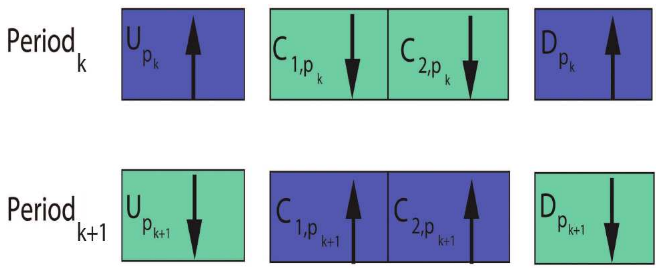

Figure 5.1: *Schematic illustration of the target cells and their polarization in transverse mode with longitudinally polarized muon beam for the three cell setup. The upstream and downstream cells have always an opposite polarization to the central cell. The polarization is reversed between two sub-periods. Figure taken from [72].*

The complete amount of data from the 2007 transverse run is $0.49 \cdot 10^3$PByte.
To get fast preliminary results the first production of the first half of data taking in 2007 (periods W25-W31, see table 5.1) was done quasi-online. Therefore not all final alignment and calibration constants were already available. This results in an insufficient quality and stability of the data from this first part of data taking. Because of this a second production with a new alignment and the missing calibration files was performed some time later, which was used for the analysis of this first half of the data, W25-31. The second half of the data, W39-43, was analyzed with the data from the first production, as those turned out to be well conditioned.

5.1.1 Data Selection and Quality

I repeat my request: non multa sed multum. Fewer figures, but more matter.

W. I. Lenin (1870-1924), Russian revolutionary and politician

As stressed in section 3.1.2 for the deuteron data, stable data taking conditions in time are essential for the measurement of transverse cross-section asymmetries. Like for the deuteron data firstly runs or groups of runs with obvious problems marked in the logbook were rejected. Afterwards the following checks were applied:

- Bad spill rejection
- K^0 stability test
- Bad trigger rejection
- Kinematic stability

Bad Spill Rejection

At spill level the variation of variables like number of primary vertices, number of secondary vertices or number of clusters in the different calorimeters were evaluated over each sub-period. For the second analysis done after the re-production for both produced data samples, the first and the second one, in addition the trigger rates and the variables of the RICH detector e.g. mean likelihoods, angles were checked for each sub-period. To reject bad spills the following method was used:
For each spill the number of neighbours, which lie within a box of 3 RMS for all the regarded distributions around the values of this spill, was counted. A spill is regarded as bad, if it has less than 600 neighbours to both sides, timely before and after. If spills have less than $75 \cdot 10^6$ muons, they were categorized as bad and got zero neighbours by definition.

K^0 Stability Test

A very sensitive tool to check the stability of the data is the K^0 reconstruction with which the quality of the alignment and more general the track reconstruction is tested. In this check the mass of the K_S^0 is reconstructed from the mDSTs with the analysis programm PHAST from the decay $K_S^0 \rightarrow \pi^+ + \pi^-$. For this V^0 vertices at least 87cm downstream of the origin of the COMPASS reference system were searched. This means $\approx$ 20cm downstream of the last target cell. By assuming the two decay particles to be pions an invariant mass was calculated. The difference between this K^0 mass and the literature

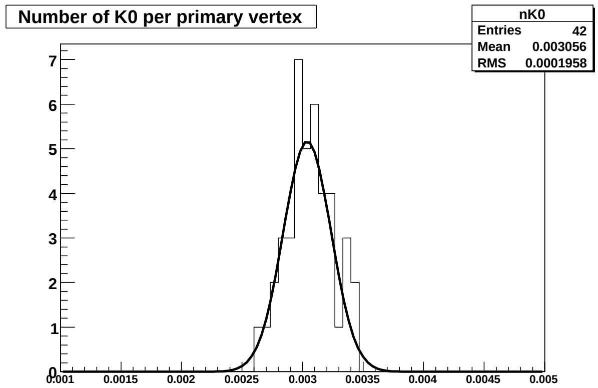

Figure 5.2: *Distribution of the number of K^0 per primary vertex over the runs of a period (here: W40), fitted with a Gaussian function.*

value was then fitted with a Gaussian [9].
The relevant parameters for the data stability are the shift between the mean value of the calculated mass and the literature value, the mass resolution (width of the distribution) and the number of K^0 per primary vertex.
The last one was plotted versus the runs for every period and again fitted with a Gaussian (see fig. 5.2). A run was rejected, if the number of K^0 per primary vertex is more than 3 sigma away from the mean value of the distribution. The fraction of bad runs is about 3%.
The stability of the three parameters mass shift, mass resolution and number of K^0 per primary vertex was also tested together for the sub-periods, which will be combined in the analysis. As examples the results for the period W25/26 (second production) and W41/42/43 (first production) are shown in fig. 5.3 and 5.4, respectively. For W25/26 the evaluated variables are clearly stable, while for the weeks W41/42/43 there is a jump in the number of K^0 per primary vertex between the single weeks. Most probably this is due to a not optimal alignment.

Bad Trigger Rejection

In the first analysis after the first production the identification of possible trigger malfunctioning was done by calculating the ratio R described in section 4.4.3 for the different triggers and fitting those ratios for every bin in $\Phi_{C,S}$ with a constant function. For a more detailed description of this R-test on the proton data see section 5.4.5. If for a particular trigger the confidence level associated to the χ^2 value of the fit is smaller than $\approx 10^{-4}$, this trigger is excluded for the corresponding period. For the first analysis for the second half of data taking this was the case for the outer trigger in the period W41/42-1.
In the second analysis after the re-production of the data the stability of the trigger conditions was evaluated by examining the trigger rates. Spills with a deviation in a subtrigger rate inside one week clearly visible as a step were rejected. If the trigger rates show a step

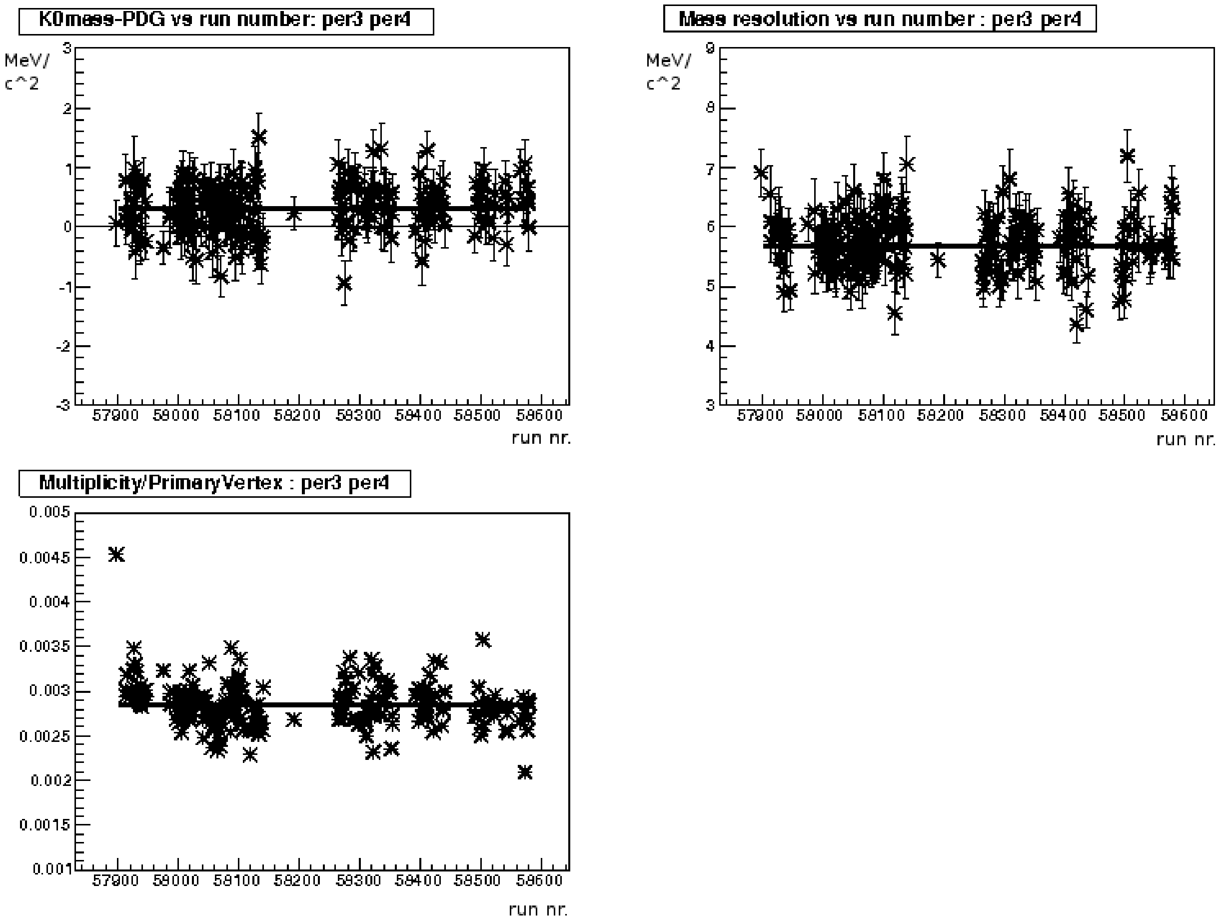

Figure 5.3: K^0 *stability test in W25/26 (second production). Upper left: mass difference* $m_{\pi^+\pi^-} - m_{K^0}$ *vs. runs, upper right: mass resolution vs. runs, down: number of* K^0 *per primary vertex. The evaluated variables are stable.*

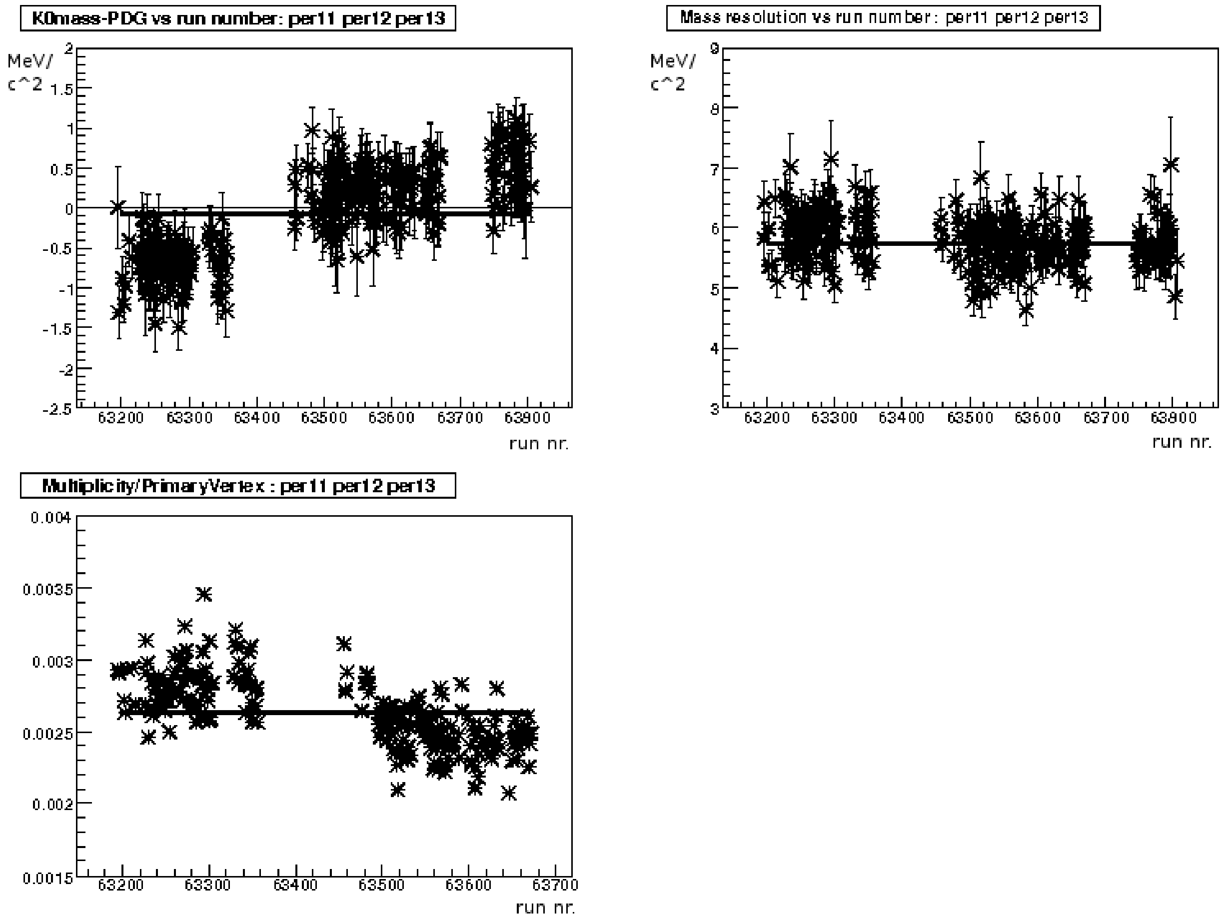

Figure 5.4: *K^0 stability test in W41/42/43 (first production). Upper left: mass difference $m_{\pi^+\pi^-} - m_{K^0}$ vs. runs, upper right: mass resolution vs. runs, down: number of K^0 per primary vertex. A jump between W41 and W42/43 is clearly visible.*

between two weeks of a period, the corresponding trigger was excluded. This was done for the pure ECAL1 trigger in the periods W27/28, W40/39 and W41/42-1.

Kinematic Stability

To remove possible instabilities not detected in the other tests the stability of various kinematical quantities was evaluated. For the first analysis of the data a method was developed based on the comparison of the distributions of the regarded variables in each single run with the general trend in one sub-period. For this for each variable the ratio between the distribution in each single run and the distribution of the total sub-period was calculated. The ratio was fitted with a constant function and the distribution of the resulting χ^2 values was fitted with a gaussian to extract the mean value. Runs with deviations of more than three sigma from the mean values were removed from the sample used for the physics analysis.
The monitored variables are:
- the z coordinate of the primary vertex
- Q^2: the momentum transfer of the virtual photon
- W: the invariant mass of the hadronic end-product
- x_{bj}: the Bjørken scaling variable
- y: the fractional energy transfer
- E': the energy of the scattered muon
- $\theta_{\mu'}$: the polar angle of the scattered muon in the laboratory system
- P_T^h: the transverse momentum of the hadron in the GNS ("gamma-nucleon-system")
- ϕ_h^{LAB}: the azimuthal angle of the hadron in the laboratory system
- θ_h^{LAB}: the polar angle of the hadron in the laboratory system
- ϕ_h^{GNS}: the azimuthal angle of the hadron in the GNS system
- ϕ_S^{GNS}: the azimuthal angle of the nucleon spin in the GNS system

This test was repeated to check also the kinematic stability between coupled sub-periods by doing the same for the ratio between the distribution of each single run of the first sub-period and the distribution of the whole second sub-period. Again a deviation of three sigma was the criterion to reject a run.
In the second analysis of the data also another method to evaluate the kinematic stability was applied. Here the same variables and in addition the azimuthal angle of the scattered muon in the laboratory system $\phi_{\mu'}$, the energy of the hadron E_h and the momentum fraction carried by the hadron z were monitored.
In this method the distributions of the kinematical variables were drawn for all runs in a coupled period. Afterwards the normalized distributions for each combination of pairs of runs were substracted from each other and then it was investigated by a χ^2-test, if the resulting distribution is compatible with zero. Those χ^2 values were extracted and drawn in a histogram for each distribution and run. For a good run one should get for its χ^2 distribution a mean value of 1 and a certain RMS depending on the number of degrees of freedom. All runs, which have in at least one kinematic distribution a mean value of the

χ^2 distribution $\langle\chi^2_{run,i}\rangle$ larger than 3.5 σ off from the mean χ^2 distribution were excluded. As there are no significant differences in the quality from those two methods and the "substraction" method was the one with less requirements, this one was chosen for the second analysis.

5.2 Event Reconstruction and Selection

The event reconstruction and selection is mainly analog to the one for the deuteron data (see section 4.2). As for the deuteron analysis we look into DIS events, where at least one hadron is produced. In the following we will shortly describe all cuts used in the event selection with the focus on differences to the analysis of the deuteron data. For more details of the cuts already used in the deuteron analysis, particularly for more information on the motivation of the cuts, see section 4.2.

5.2.1 General DIS Cuts

As in the case of the deuteron target we did a cut on $Q^2 > 1$ (GeV/c)^2 to get a deep-inelastic sample, a cut on the relative energy transfer via the virtual photon $0.1 < y < 0.9$ and a cut on the mass of the hadronic final state $W > 5$ GeV/c^2. As the first bin in x_{bj} begins at a value of 0.003 (see section 5.3.1) in addition a cut on $x_{bj} > 0.003$ was applied to guarantee exactly the same statistics in all the three different variables x_{bj}, z and P_T^h vs. which the asymmetries are drawn.
The final distributions of Q^2, y and x_{bj} for the charged hadrons after all cuts described in this section can be seen in fig. 5.5 and the distribution of W with the corresponding cut in fig. 5.6.

5.2.2 Muon and Primary Vertex Cuts

The best primary vertex is selected with the corresponding PHAST function (see section 4.2.2). The vertex has to be inside one of the three target cells, which requires its z coordinate to be between -62.5 cm and -32.5 cm (upstream cell), between -27.5 cm and 32.5 cm (central cell) or between 37.5 cm and 67.5 cm (downstream cell). As the target cells, which had a radius of 2 cm in 2007, are displaced in x and y direction a radial cut with $r < 1.9$ cm was chosen for the primary vertex.
It is also checked, if the projection of the muon track to the most upstream and the most downstream end of the target is inside this radius to ensure an identical beam intensity for all the target cells.
The resulting distribution of the z coordinate of the primary vertex can be found in fig. 5.7.
We take the incoming particle connected to the best primary vertex as the beam muon. It is accepted, if its momentum is below 200 GeV/c and its associated track has a $\chi^2_{red} < 10$. The same cut on χ^2_{red} is used for the scattered muon and in addition a radiation length

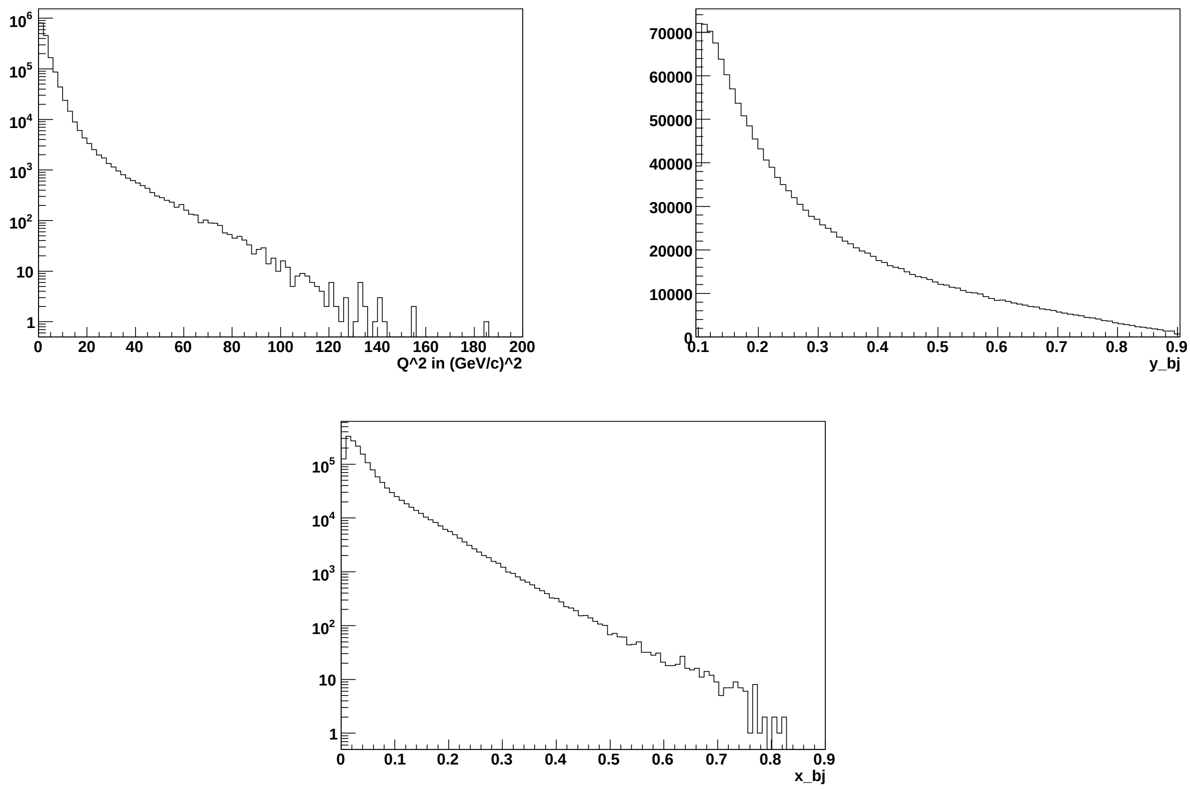

Figure 5.5: *From upper left to down: final distributions of Q^2, y and x_{bj} after all cuts for the charged hadrons.*

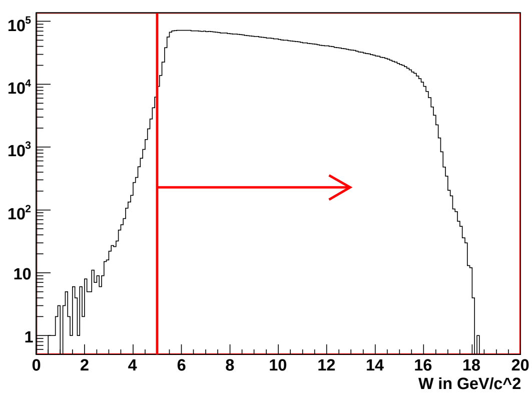

Figure 5.6: *Distribution of the mass of the hadronic final state W with the used cut in red.*

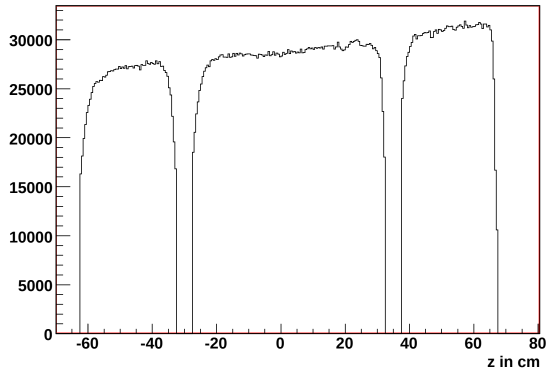

Figure 5.7: *Distribution of the z coordinate of the primary vertex after the corresponding cuts described in the text. The increase of the events with an increasing z coordinate is due to the different geometrical acceptances of the target cells.*

of $nX/X_0 > 30$ is required. If we find a positive outgoing particle from the best primary vertex not recognized as scattered muon, which in Muon Wall 1 caused four or more hits in front of and six or more hits behind the hadron absorber, we assume it to be a muon scattered at large angles outside the kinematic range of the COMPASS trigger hodoscopes. To accept it, this particle has also to fulfill the conditions $\chi^2_{red} < 10$ and $nX/X_0 > 30$. If the identification of the scattered muon is not unique, i.e., we have more than one muon "recovered" in this way in the LAS, a "recovered" and a "normal" flagged muon or more than one "normal" flagged muons, the event is discarded.

5.2.3 Hadron Identification

All other particles connected to the best primary vertex beside the beam and the scattered muons are regarded as hadrons. The criterions for accepting the hadron candidate are:

- $\chi^2_{red} < 10$.
- To allow the momentum computation of the hadron, the associated track has to have its first measured hit at the z coordinate at $Z_{first} < 350$ cm.
- To guarantee a good reconstruction of the tracks those only reconstructed in the fringe field of SM1 were discarded with a lower cut on the z coordinate of the last measured hit associated with the track. Furthermore also an upper cut on the last measured z coordinate was applied to avoid a high contamination of muons. The criterion for the last measured z coordinate was chosen as 350 cm $< Z_{last} <$ 3300 cm.
- Radiation length $nX/X_0 < 10$.
- A minimum energy deposition for clusters in HCAL1 and HCAL2 associated with the hadron: $E^{HCAL1} > 4$ GeV and $E^{HCAL2} > 5$ GeV (see fig. 5.8). Hadrons with

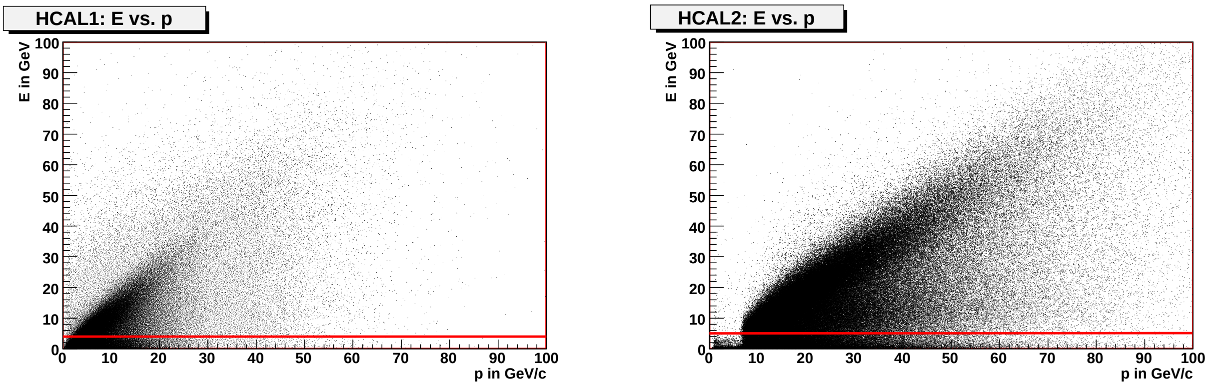

Figure 5.8: *Correlation between the energy measured in HCAL1 (left-hand side) and HCAL2 (right-hand side), respectively and the momentum measured in the spectrometer for unidentified charged hadrons in one period of the 2009 data. The cuts to remove muons in the sample (see text) are marked by the horizontal red line.*

more than one cluster are sorted out, but if no cluster at all is found, the hadron is accepted.

As in the deuteron data there is also in the proton data a peak in the y distribution at high y for positive hadrons in the last z bin ($0.8 < z < 1$) due to the misidentification of scattered muon, which pass through a hole in the muon absorber, as positive hadrons (see section 4.2.3 and description in [69]). To reject those wrongly reconstructed events we used for the proton data from the year 2007 the method suggested in [70]: The track of a positive charged hadron candidate is extrapolated to the iron absorber and if it passes through the hole, the corresponding event is discarded. If though the track passes through the active zone of the inner trigger hodoscope HI05 and we found no hits there, the event is accepted.

SM2 Magnet Yoke Cuts

It may happen that the scattered muon or a produced hadron cross the yoke of the spectrometer magnet SM2. Because the magnet field is not known here, the momentum reconstruction is not possible. In the case of a hadron crossing the SM2 yoke we had to exclude this particle, while in the case that the scattered muon crosses the yoke of SM2 we had to remove the complete event [73].
We did a lower cut of $z > 0.2$ on the fraction of the photon energy carried by the produced hadrons to ensure that the identification of the hadrons is not distorted by secondary interactions and an upper cut of $z < 1$ as z is by definition not larger than 1 (see eq. (2.65)). For the transverse momentum of the hadrons with respect to the virtual photon direction we required $P_T^h > 0.1$ GeV/c to guarantee a good resolution of the hadrons' azimuthal angles.

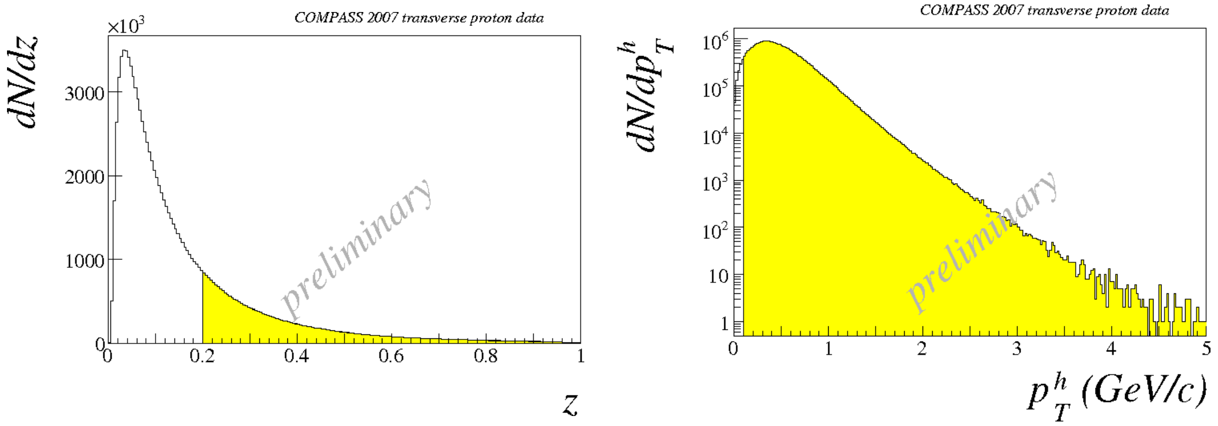

Figure 5.9: *Left: z distribution of the unidentified charged hadrons with the corresponding cut at $z > 0.2$. Right: P_T^h distribution of the unidentified charged hadrons with the corresponding cut at $P_T^h > 0.1$. The yellow region marks in both cases the accepted particles.*

The distribution of the variables z and P_T^h and the large effect of the z cut on the accepted statistics is shown in fig. 5.9.

Selection of the K^0

The selection of the K^0 was analog to the one for the deuteron data to search for the decay of K_S^0 into $\pi^+\pi^-$. The cuts were carefully reviewed.
The principle of the selection was again the search for V^0 vertices downstream of the primary vertex ($Z_{sec.vtx.} - Z_{prim.vtx.} > 0$), whose tracks must not be connected to any primary vertex.
The outgoing tracks from the V^0 vertex have to fulfill the following conditions, which are basically the same as for the tracks of the charged hadrons from the primary vertex:

- $\chi^2_{red} < 10$.
- The tracks must not cross the magnet yoke of SM2.
- $Z_{first} < 350$ cm to ensure the momentum computation.
- $350 < Z_{last} < 3300$ cm to exclude tracks only reconstructed in the fringe field of SM1 and to get a good reconstruction.
- Radiation length $nX/X_0 < 10$.
- To sort out muons we require for clusters in the HCALs connected to the hadrons outgoing from the V^0:

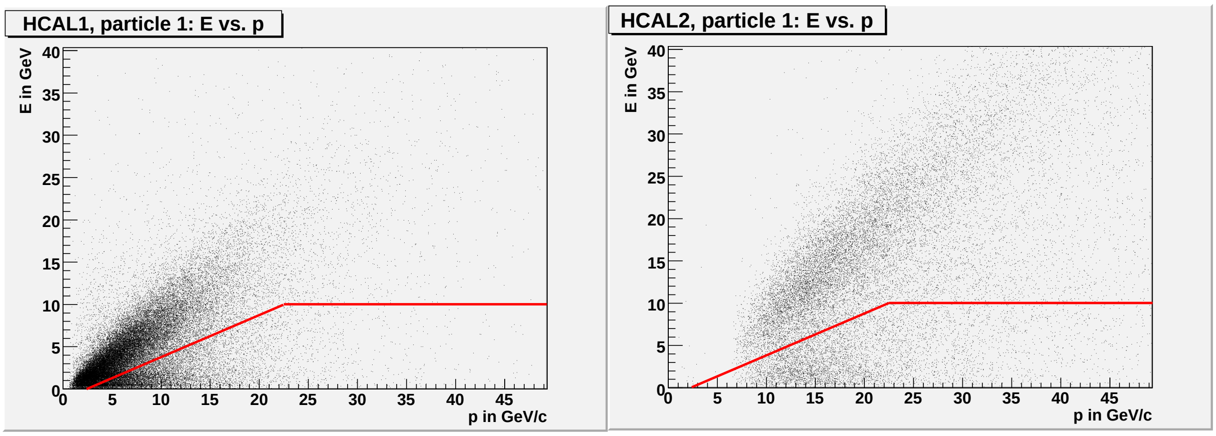

Figure 5.10: *Correlation between the energy measured in HCAL1 (left-hand side) and HCAL2 (right-hand side), respectively and the energy measured in the spectrometer for pions from a V^0 vertex in one period of the 2004 data. The cut to remove muons in the sample (see text) is marked by a red line.*

– Particles with a momentum of $P_h > 2.5$ GeV/c that have more than one connected cluster in the HCALs are rejected.

– Particles with no cluster at all are accepted.

– If there is exactly one cluster in the HCALs, a cut depending on the particle momentum is applied: For a momentum P_h from 2.5 GeV/c to 22.5 GeV/c the condition to fulfill is $E_{clus} > (P_h - 2.5\ \text{GeV}/c) \cdot 0.5\ \text{GeV}/c^2$ corresponding to a linear slope in P_h, while for momenta $P_h > 22.5$ GeV/c we leave the cut constant with $E_{clus} > 10$ GeV/c^2) (for an illustration see fig. 5.10).

If any of those conditions is not fulfilled by one of the two particles the corresponding V^0 vertex is rejected.
Like for the deuteron data the angle θ between the reconstructed momentum of the K^0 and the vector connecting the primary and the secondary vertex was calculated to test the connection between the secondary vertex of the K^0 decay and the primary vertex. As it can be seen in fig. 5.11 a cut of $\theta < 10$ mrad is again a suggestive choice for the cut.
As minimum for the distance between the primary and the secondary vertex also for the proton data a value of 10 cm was set by regarding the $c\tau$ distribution of the reconstructed decay pion pairs (see fig. 5.12).
The Armenteros-Podolanski-Plot for the hadron pairs from the V^0 in the proton data is shown in fig. 5.13. To reduce the background from e^+e^- pairs we accepted only transverse momenta of $p_t > 40$ MeV/c. Furthermore to sort out also impurities due to Λ and $\bar{\Lambda}$ we excluded also the region $80 < p_t < 110$ MeV/c.
To complete the identfication of the K^0 we require that the reconstructed invariant mass of the pion pair is within ± 20 MeV of the literature value of the K^0 (PDG: [9]). The

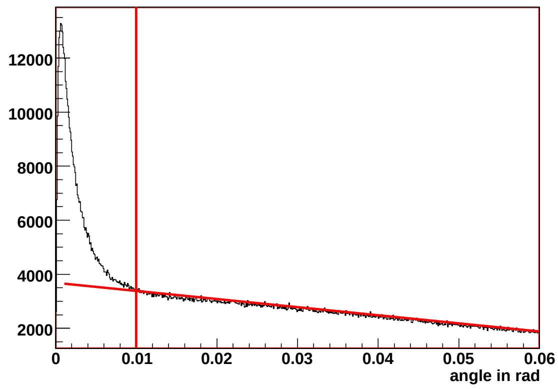

Figure 5.11: *Angle between the reconstructed V^0 momentum and the vector connecting primary and secondary vertex. The cut chosen as* $\theta < 0.01$ rad$(= 10$ mrad$)$ *is marked by the vertical red line.*

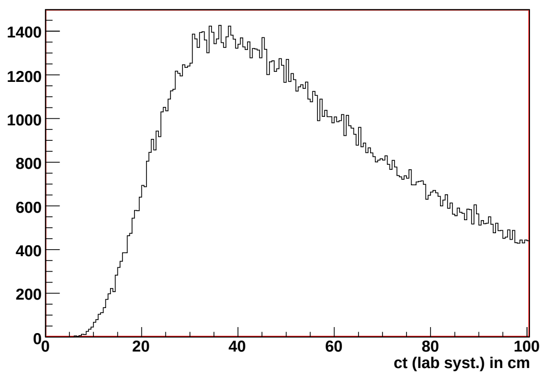

Figure 5.12: *$c\tau$ distribution of the reconstructed pion pairs, which gives the range of the K^0 before decaying, boosted into the laboratory system.*

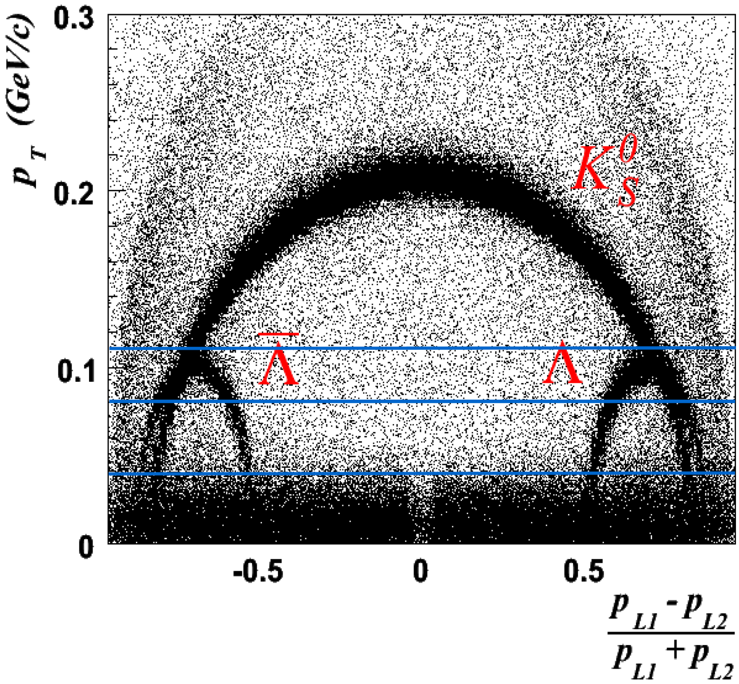

Figure 5.13: *Armenteros-Podolanski plot of the hadron pair. The* K^0 *band as well as the* Λ *and* $\bar{\Lambda}$ *bands can be clearly seen. The cuts to require a transverse momentum of* $p_t > 40$ MeV/c *and to sort out impurities due to* Λ *and* $\bar{\Lambda}$ *by excluding the region* $80 < p_t < 110$ MeV/c *are marked by the blue lines.*

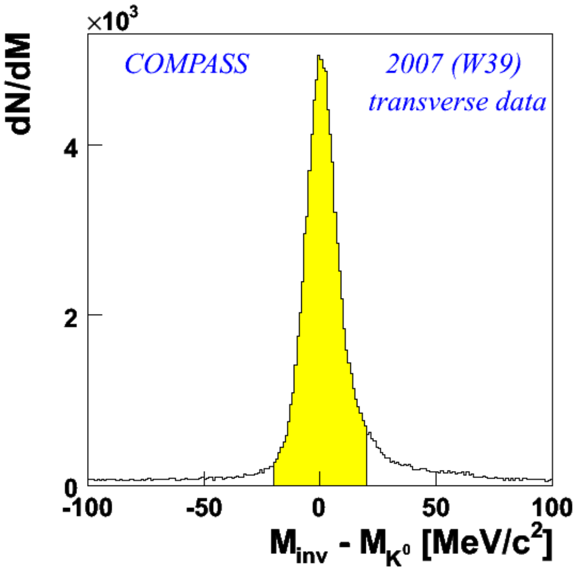

Figure 5.14: *Difference of the invariant mass of the hadron pair after cuts to the literature value of the K^0 mass [9]. The yellow region marks the accepted K^0.*

corresponding distribution can be seen in fig. 5.14.
As for the analysis of the charged hadrons (and for the analysis of the deuteron data) we cut on the fraction of the photon energy transferred to the hadron : $0.2 < z < 1$ as well as on the sum of z of all particles outgoing from the primary vertex, for which we demand $\sum_{i=0}^{N(outg.\ prim.\ vtx.)} z_i \leqq 1.1$. A cut is also done on the K^0's transverse momentum with respect to the direction of the virtual photon by demanding $P_T^h > 0.1$ GeV/c to assure a good resolution of the azimuthal angle.

5.2.4 Particle Identification with the RICH

For the identification of charged pions and kaons the Ring Imaging Cherenkov (RICH) detector is used at COMPASS (see section 3.4.1). The parameters for the particle identification as e.g. the likelihood values for the mass hypothesis are saved in the mDST files produced via the CORAL software (see section 3.7).
In this data "production" the particle tracks of the corresponding events and the hits in the photon detectors are used to identify the particles.
The reconstruction process begins with a clustering procedure. Here individual hits in the photon detectors are combined to clusters, for which we expect that they correspond to the real impact point of the photons. The coordinates of the clusters are transformed to the $\phi - \theta_{Ch}$ Cherenkov plane, where θ_{Ch} is the polar (Cherenkov) angle and ϕ the azimuthal angle of the photons relative to the trajectory of the particle. Then in this plane the clusters from a given particle are distributed uniformly in ϕ along a fixed θ_{Ch}. The search for a ring in the detector plane is therefore equivalent to the search for a peak in θ_{Ch}.

With this information a likelihood is constructed for five mass hypothesis, namely for pion, kaon, proton, electron and muon:

$$L_N^i = \prod_{k=1}^{N} [(1-\eta)G(\theta_k, \phi_k, \theta_i^{expec}) + B(\theta_k, \phi_k)] \quad i \in \{\pi, K, p, e, \mu\} \tag{5.1}$$

Here the product runs over all N photons associated to the signal, θ_k is the angle of the k-th photon, θ_i^{expec} is the Cherenkov angle expected for a certain mass hypothesis i, η gives the probability to loose a photon due to the dead zones of the RICH, $G(\theta_k, \phi_k, \theta_i^{expec})$ parametrizes the signal and $B(\theta_k, \phi_k)$ the background contributions.
The signal contribution $G(\theta_k, \phi_k, \theta_i^{expec})$ to the likelihood can generally be described as a Gaussian distribution with the center at the expected angle θ_i^{expec} and the width $\sigma_\theta(\phi_k)$. The advantage we get from the likelihood method is that here the background contribution is taken explicitly into account. Possible contributions to the background are electric noise, photons from other particles belonging to the same or to other events except for the upgraded central part of the RICH, where Multi-Anode Photomultipliers (MAPMT) allowing to separate events in time very effectively are used for the read-out (see section 3.4.1).

Cuts on Momentum and Likelihood

To ensure a good identification the following cuts on the particle momentum and the likelihood values were applied.
Cut on Momentum: Corresponding to a 1.5σ seperation between pions and kaons an upper limit for accepted momenta of 50 GeV/c has been applied. To reject particles with no Cherenkov photons also a lower cut at the Cherenkov threshold (p_{thr}) is done. This threshold is calculated for a certain particle mass and the refractive index of the used radiator gas by:

$$p_{th} = \frac{m}{\sqrt{n^2-1}} \tag{5.2}$$

The threshold is computed on a run-by-run basis separately for pions and kaons.
Cut on Likelihood Values: We cut on the variable $\frac{LH_{max}}{LH2ndmax}$, which gives the ratio between the highest likelihood corresponding to the identity assumed and the second highest likelihood for another mass hypothesis. If the value is near 1, the likelihood of the identified particle and that of the particle with the second highest likelihood are close together meaning that a clear distinction between those two particles is not possible. The cuts on those distributions had therefore to be determined by finding a good compromise between the sample's purity and efficiency (see fig. 5.15).
To recognize a particle as pion the cut on the ratio of the two highest likelihoods was chosen as:

$$\frac{LH_{max=\pi}}{LH2ndmax} \leqq 1.02 \tag{5.3}$$

and for kaons as:

$$\frac{LH_{max=K}}{LH2ndmax} \leqq 1.06 \tag{5.4}$$

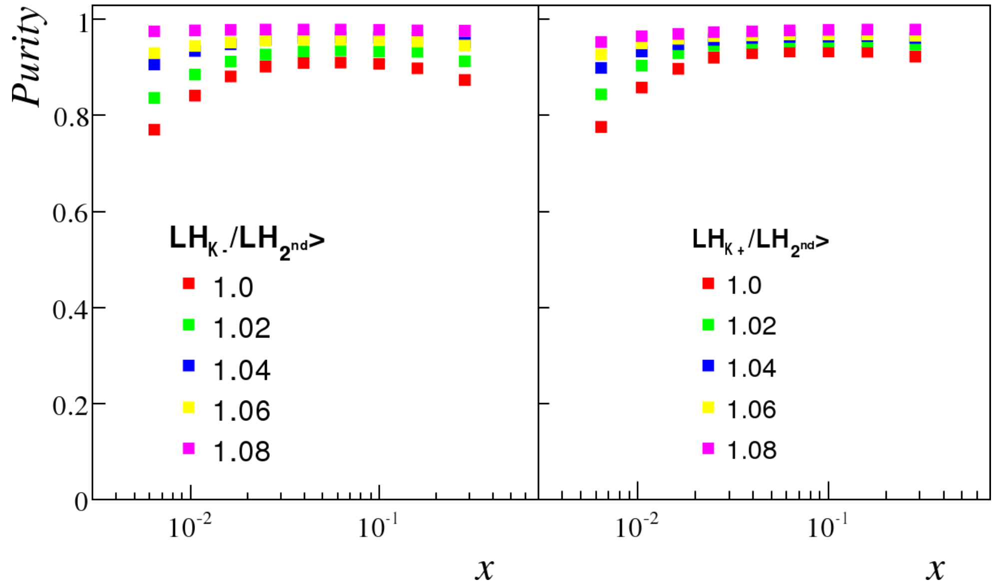

Figure 5.15: *Purity of the K^- (left) and K^+ (right) samples as function of the cut* $\frac{LH_{max=K}}{LH2ndmax}$.

5.2.5 Final Data Sample

As we gained for the first half of the run with the second "data production" a higher quality and more stable data, it was possible to analyze the Collins effect for the whole 2007 run, not only for the second half of the data taking, for which the first "data production" as the better one was used. Until now we didn't finally succeed in analyzing also the complete data set for the Sivers asymmetries, because those are more sensitive to instabilities in the spectrometer.
The final statistics after all cuts is given in table 5.2 for unidentified charged hadrons, in table 5.3 for K^0 and in table 5.4 for identified charged hadrons ($\pi^{\pm}$, $K^{\pm}$). The full data set from all periods, W25-43, could up to now be used finally only for the analysis of the Collins effect, for the Sivers effect the analysis was at least not yet finally possible for all periods, but only for W25/26, W30/31, W39/40 and W42-2/43.

5.3 Extraction of the Asymmetries

5.3.1 Binning

As for the deuteron data the asymmetries were evaluated in bins in x, z and P_T^h with variable intervals to have similar statistics in each of them. The binning chosen can be seen in table 5.5 for the charged hadrons (unidentified and identified ones) and in table 5.6 for K^0, which is the same as in the analysis of the deuteron data (see table 4.3). For the

Period	Positive hadrons	Negative hadrons
W25/26	2436012	1956088
W27/28	2361388	1874941
W30/31	3689172	2922582
W39/40	2765941	2167777
W41/42-1	2592834	2050423
W42-2/43	1320743	1045075
Sum of W25/26 + W30/31 + W39/40 + W42-2/43	10211868	8091522
Total sum of all periods	15166090	12016886

Table 5.2: *Final statistics for the unidentified charged hadrons from the 2007 proton run. While the analysis of the Collins effect was possible for the full data set from all periods, W25-43, could be used, for the one of the Sivers effect until now only the periods W25/26, W30/31, W39/40 and W42-2/43 could be used.*

Period	K^0 sample
W25/26	57910
W27/28	54971
W30/31	89675
W39/40	78297
W41/42-1	56810
W42-2/43	28509
Sum of W25/26 + W30/31 + W39/40 + W42-2/43	254391
Total sum of all periods	366172

Table 5.3: *Final statistics for K^0 from the 2007 proton run. For the analysis of the Sivers effect only the priods W25/26, W30/31, W39/40 and W42-2/43 could be used.*

Period	π^+	π^-	K^+	K^-
W25/26	1762246	1512055	363254	220747
W27/28	1695320	1439437	338417	202903
W30/31	2665992	2257973	517891	309190
W39/40	1985242	1661714	396795	234251
W41/42-1	1866303	1585023	377293	223781
W42-2/43	956242	812260	188974	111855
Sum of W25/26 + W30/31 + W39/40 + W42-2/43	7369722	6244002	1466914	876043
Total sum of all periods	10931345	9268462	2182624	1302727

Table 5.4: *Final statistics for the identified charged hadrons ($\pi^\pm$, $K^\pm$) from the 2007 proton run. For the analysis of the Sivers effect only the priods W25/26, W30/31, W39/40 and W42-2/43 could be used.*

x	z	P_T^h
$0.003 < x < 0.008$	$0.200 \leqq z < 0.250$	0.10 GeV/$c < P_T^h \leqq 0.20$ GeV/c
$0.008 \leqq x < 0.013$	$0.250 \leqq z < 0.300$	0.20 GeV/$c < P_T^h \leqq 0.30$ GeV/c
$0.013 \leqq x < 0.020$	$0.300 \leqq z < 0.350$	0.30 GeV/$c < P_T^h \leqq 0.40$ GeV/c
$0.020 \leqq x < 0.032$	$0.350 \leqq z < 0.400$	0.40 GeV/$c < P_T^h \leqq 0.50$ GeV/c
$0.032 \leqq x < 0.050$	$0.400 \leqq z < 0.500$	0.50 GeV/$c < P_T^h \leqq 0.60$ GeV/c
$0.050 \leqq x < 0.080$	$0.500 \leqq z < 0.650$	0.60 GeV/$c < P_T^h \leqq 0.75$ GeV/c
$0.080 \leqq x < 0.130$	$0.650 \leqq z < 0.800$	0.75 GeV/$c < P_T^h \leqq 0.90$ GeV/c
$0.130 \leqq x < 0.210$	$0.800 \leqq z < 1.000$	0.90 GeV/$c < P_T^h \leqq 1.30$ GeV/c
$0.210 \leqq x < 1.000$		1.30 GeV/$c < P_T^h$

Table 5.5: *Bins in the variables x, z and P_T^h for the charged hadrons (unidentified and identified ones).*

charged hadrons nine bins in x and P_T^h and eight in z have been used, while for K^0 five bins in x and P_T^h and six in z were chosen.

5.3.2 Unbinned Maximum Likelihood Estimator

The extraction of the asymmetries was done with a newly developed unbinned maximum likelihood estimator. The results were compared to those obtained with the "double ratio" method described in 4.3.2. The technique of the likelihood method is based on the evaluation of the probability for a certain set of parameters to observe the measured data set. The set of parameters, which maximizes the probability, is chosen as the best one.
For simplicity in the following a setup with two target cells with opposite polarization is regarded. The expressions for more complicated setups are analog.

x	z	P_T^h
$0.003 < x < 0.013$	$0.200 \leqq z < 0.250$	0.10 GeV/$c < P_T^h \leqq 0.35$ GeV/c
$0.013 \leqq x < 0.032$	$0.250 \leqq z < 0.325$	0.35 GeV/$c < P_T^h \leqq 0.55$ GeV/c
$0.032 \leqq x < 0.080$	$0.325 \leqq z < 0.425$	0.55 GeV/$c < P_T^h \leqq 0.75$ GeV/c
$0.080 \leqq x < 0.130$	$0.425 \leqq z < 0.550$	0.75 GeV/$c < P_T^h \leqq 1.00$ GeV/c
$0.130 \leqq x < 1.000$	$0.550 \leqq z < 0.700$	1.00 GeV/$c < P_T^h$
	$0.700 \leqq z < 1.000$	

Table 5.6: *Bins in the variables x, z and P_T^h for K^0.*

For every bin in x, z and P_T^h we have in our case N^+ hadrons coming from the cell with positive polarization and N^- hadrons coming from the cell with negative polarization and consider the variables (ϕ_S, ϕ_h). We get the probability to observe the set of $N^+ + N^-$ variables (ϕ_S, ϕ_h) for a combination of parameters a_1, ..., a_m from the product of the probability for each hadron:

$$\mathcal{L} = \prod_{i=0}^{N^+} P^+(\phi_S^i, \phi_h^i; a_1, ..., a_m) \prod_{i=0}^{N^-} P^-(\phi_S^i, \phi_h^i; a_1, ..., a_m) \tag{5.5}$$

It is then e.g. possible to normalize the probabilities $P^\pm$ over the range of (ϕ_S, ϕ_h) to 1 by:

$$\int P^\pm(\phi_S, \phi_h; a_1, ..., a_m) d\phi_S d\phi_h = 1 \tag{5.6}$$

Because with this "standard" likelihood method in very few cases the fit did not converge or, what was also proved by Monte Carlo simulations, showed some small bias, the likelihood in this analysis was constructed in an alternative way, with an extended maximum likelihood method. Here we instead build the term $\mathcal{N}^\pm$:

$$\int p^\pm(\phi_S, \phi_h; a_1, ..., a_m) d\phi_S d\phi_h = \mathcal{N}^\pm \tag{5.7}$$

which we use to normalize the likelihood expression:

$$\mathcal{L} = \left(e^{-\mathcal{N}^+} \prod_{i=0}^{N^+} p^+(\phi_S^i, \phi_h^i; a_1, ..., a_m) \right)^{\frac{1}{N^+}} \left(e^{-\mathcal{N}^-} \prod_{i=0}^{N^-} p^-(\phi_S^i, \phi_h^i; a_1, ..., a_m) \right)^{\frac{1}{N^-}} \tag{5.8}$$

where the two exponents $\frac{1}{N^+}$ and $\frac{1}{N^-}$ are a kind of a further normalization between hadrons from the cell with positive and those from the cell with negative polarization to avoid any bias from different statistics in the oppositely polarized cells.
The functions $p^\pm$ consist of two parts, namely the acceptance $\mathcal{A}$ and the cross-section σ:

$$p^\pm(\phi_S, \phi_h; a_1, ..., a_m) \propto \mathcal{A}(\phi_S, \phi_h; a_1, ..., a_l) \cdot \sigma(\phi_S, \phi_h; a_{l+1}, ..., a_m) \tag{5.9}$$

which depend on different parameters.
The acceptance can be described with a Fourier series:

$$\mathcal{A}(\phi_S, \phi_h; a_1, ..., a_l) \propto \left[1 + \sum_{j,k} \left(c_{j,k}\cos(j\phi_S \pm k\phi_h) + s_{j,k}\sin(j\phi_S \pm k\phi_h)\right)\right] \tag{5.10}$$

with $c_{j,k}$ and $s_{j,k}$ as the free parameters.
The cross-section consists of the polarized and the unpolarized part[1]:

$$\begin{aligned}\sigma \propto 1 + U_1\cos\phi_h + U_2\cos(2\phi_h) \pm fP_T\,(\epsilon_1\sin(\phi_h + \phi_S - \pi) + \epsilon_2\sin(3\phi_h - \phi_S) \\ +\epsilon_3\sin(\phi_h - \phi_S) + \epsilon_4\cos(\phi_h - \phi_S) + \epsilon_5\sin\phi_S + \epsilon_6\cos(2\phi_h - \phi_S) \\ +\epsilon_7\cos\phi_S + \epsilon_8\sin(2\phi_h - \phi_S))\end{aligned} \tag{5.11}$$

where U_1 and U_2 are the unpolarized asymmetries (the modulation in $\cos\phi_h$ is mainly connected to the so-called "Cahn" effect) and ϵ_1, ..., ϵ_8 are the single spin asymmetries, which can be measured with a transversely polarized target. ϵ_1 corresponds to the Collins and ϵ_3 to the Sivers asymmetry.
To obtain the parameters of interest the likelihood has to be maximized. Equivalent to this is to minimize the expression $-\ln\mathcal{L}$.
The method used for this work is based on the MINUIT (MIGRAD and IMPROVE algorithms) minimization software package provided by the CERN and developed at the Università degli Studi di Trieste by Paolo Schiavon and Federica Sozzi. The fit is done in two iterations, where the first one has the aim to get good starting values for the parameters.

5.3.3 From Raw to Collins and Sivers Asymmetries

As for the data from the deuteron we have for the final asymmetries to take into account the polarization P_T, the dilution factor f of the target and the depolarization factor D_{NN} (see section 4.3.3).
The Collins asymmetry is then again given by:

$$A_{Coll} = \frac{A_C^{raw}}{D_{NN} f P_T} \tag{5.12}$$

For D_{NN} the mean value for all events in one kinematical bin is taken for the asymmetry calculation in this bin. The same is done for the dilution factor f of the proton target as function of x. For the mean values of f versus x, which is ≈ 0.15, see fig. 5.16.
As for the deuteron run the polarization could not be measured directly in the transverse mode at COMPASS. So the polarization again was measured in the longitudinal mode at the beginning and the end of each sub-period and extrapolated. The values were about 80

[1] This equation is equivalent to eq. (2.78).

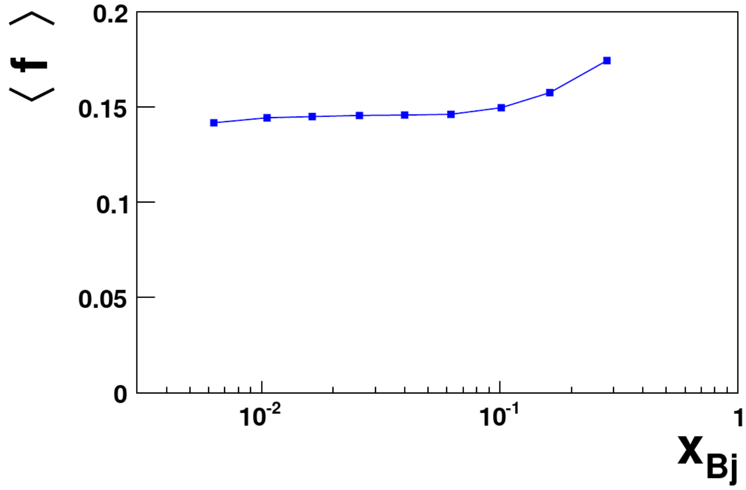

Figure 5.16: *Mean dilution factor versus x for the 2007 proton run.*

- 90% (see appendix B.1).
The Sivers final asymmetry we obtain as for the deuteron data by:

$$A_{Siv} = \frac{A_S^{raw}}{f P_T} \tag{5.13}$$

as $D_{NN} = 1$ for Sivers.
The results were extracted separately for each data taking period and afterwards combined with a weighted mean.

5.3.4 Results

Unidentified Charged Hadrons

The final asymmetries from the 2007 proton run for unidentified charged hadrons extracted with the unbinned maximum likelihood method can be seen in fig. 5.17 for Collins and 5.18 for Sivers, respectively. Only statistical errors are shown, the estimation of the systematical errors is done in the sections 5.4 and 5.5.
For low x up to $x < 0.05$ the Collins asymmetry is small and compatible with zero, while for $x > 0.05$ a signal is visible, opposite in sign for positive and negative hadrons. For z and P_T^h we cannot see a clear dependance, but a negative tendency of the asymmetry values for positive hadrons and a positive tendency for those for negative hadrons.
The Sivers asymmetries are small but non-zero for larger x in the case of positive hadrons, while they are statistically compatible with zero over the whole range of x for negative hadrons.

Identified Charged Pions and Kaons

The asymmetries for the charged pions identified with the RICH detector are shown in fig. 5.19 for Collins and 5.20 for Sivers. As about 85% of the charged hadrons are pions,

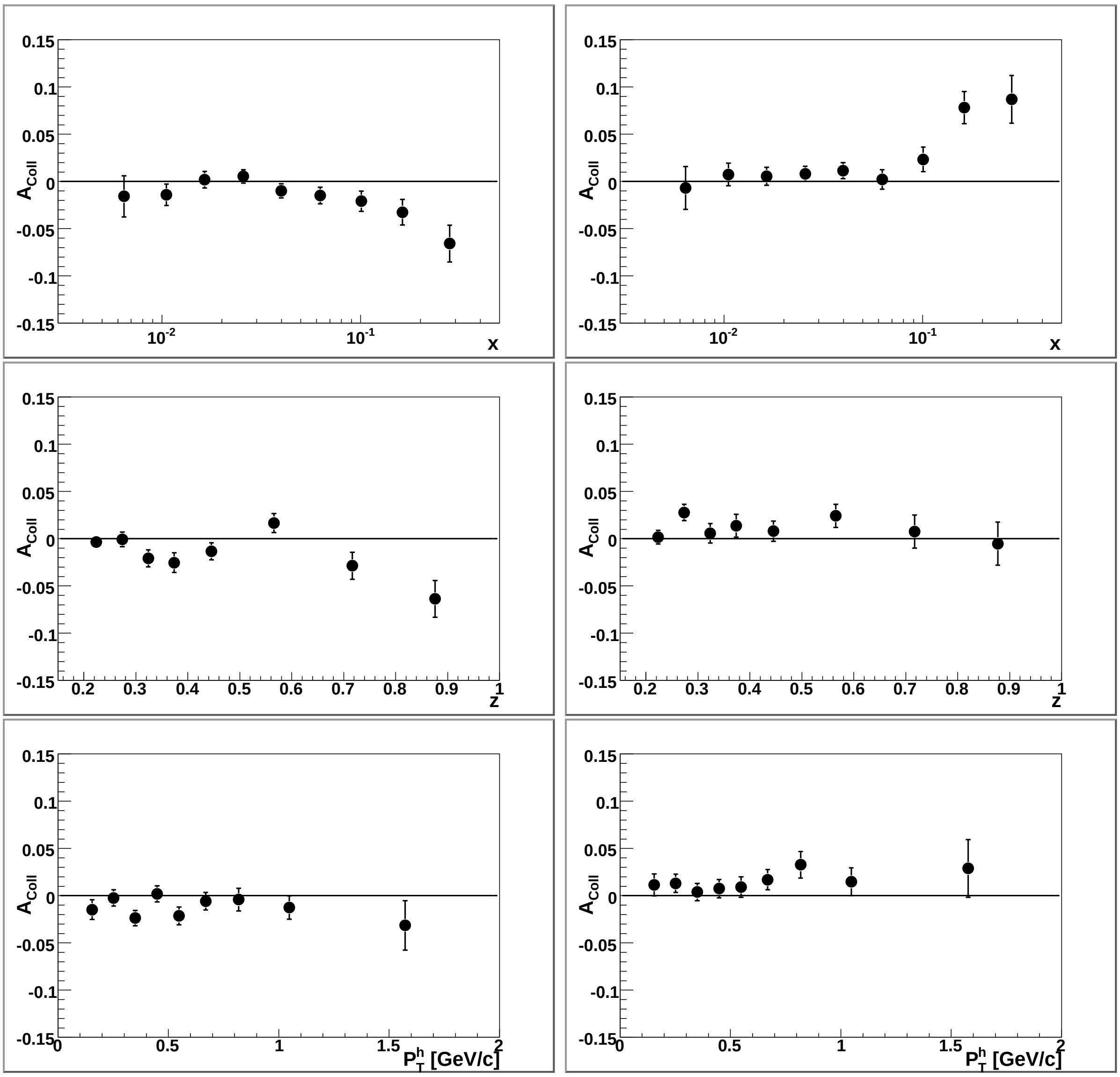

Figure 5.17: *Collins asymmetries for positive (left) and negative (right) unidentified hadrons as function from x, z and P_T^h from a proton target at COMPASS. Only statistical errors are shown.*

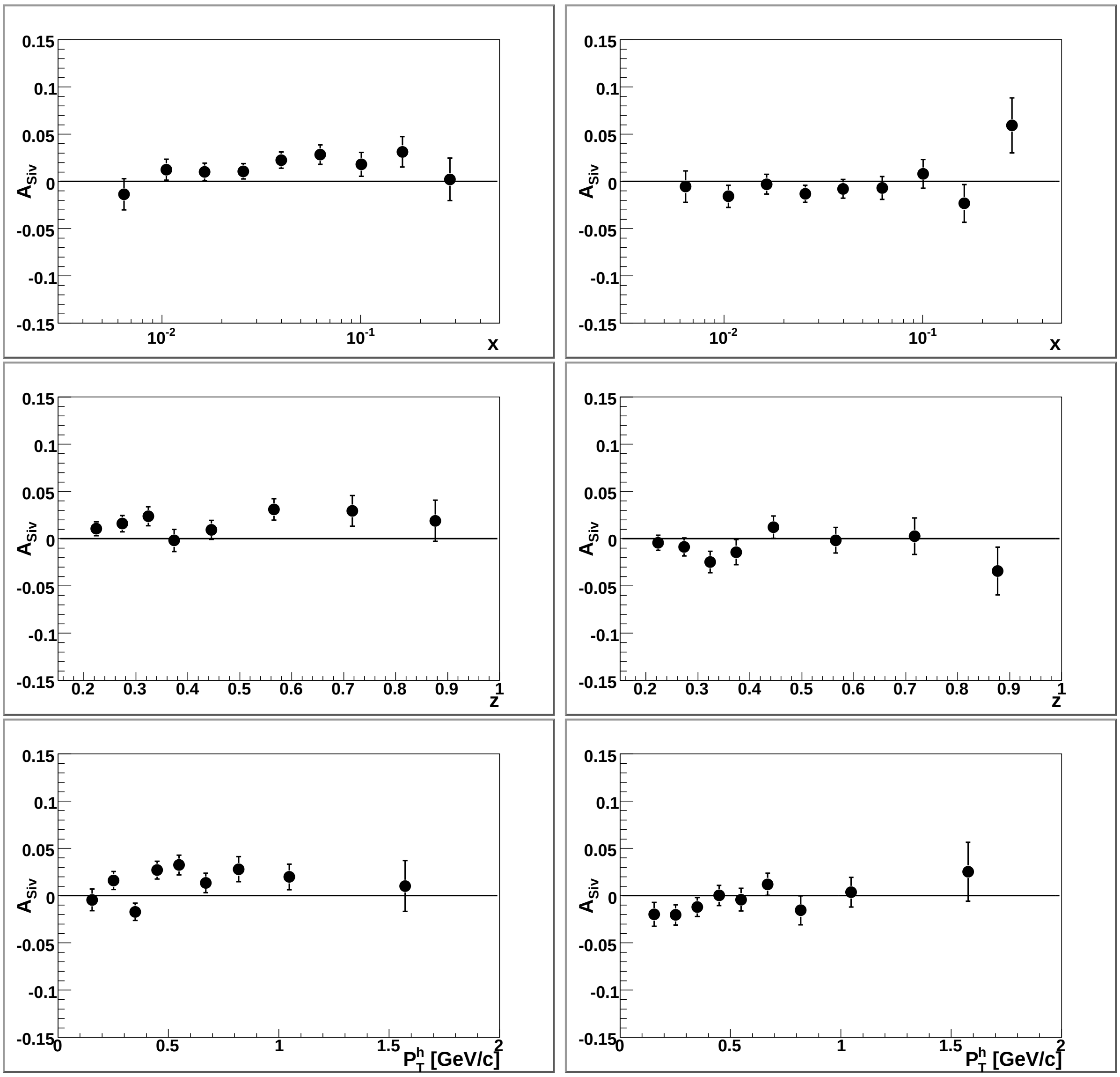

Figure 5.18: *Sivers asymmetries for positive (left) and negative (right) unidentified hadrons as function from x, z and P_T^h from a proton target at COMPASS. Only statistical errors are shown.*

the asymmetries of the identified charged pions are similar to the asymmetries of the unidentified hadrons.
For the charged kaons the Collins and Sivers asymmetries can be seen in fig. 5.21 and 5.22, respectively. Because of the limited statistics (see table 5.4) the error bars are relatively large. For Collins the data show a negative trend in x for K^+ and a positive trend for K^- as it can be seen also for the charged pions and the unidentified charged hadrons, respectively. For Sivers the asymmetries for K^- are compatible with zero, while they seem to be a little bit larger but still compatible with zero for K^+.
It has to be mentioned here that beside the large statistical errors also the purity of the charged kaon samples has to be taken into account. The trends could be amplified by impurities from pions.

Neutral K^0

For the neutral K^0 the Collins and Sivers asymmetries are shown in fig. 5.23. All asymmetries are small and compatible with zero, but these results are limited due to the small statistics (see table 5.3).

5.4 Systematic Studies

As for the deuteron data possible systematic effects on the physics results were investigated to evaluate the sources and the size of the systematic errors of the asymmetries. Because this procedure plays a crucial rôle in the investigation of the physics asymmetries, it is described in detail in this section. The reader not interested in all details can leave out this chapter 5.4 as well as the following 5.5.
The tests performed on the unidentified hadron sample are:

- Evaluation of false asymmetries
- Dependence on the target cells
- Compatibility of the results in the different periods
- Stability of acceptances
- Comparison of different estimators

In addition for the analysis of the K^0 the following tests were done:

- Compatibility of the results in the different periods
- Studies on background asymmetries
- Stability of acceptance ratios
- Evaluation of false asymmetries
- Comparison of different estimators

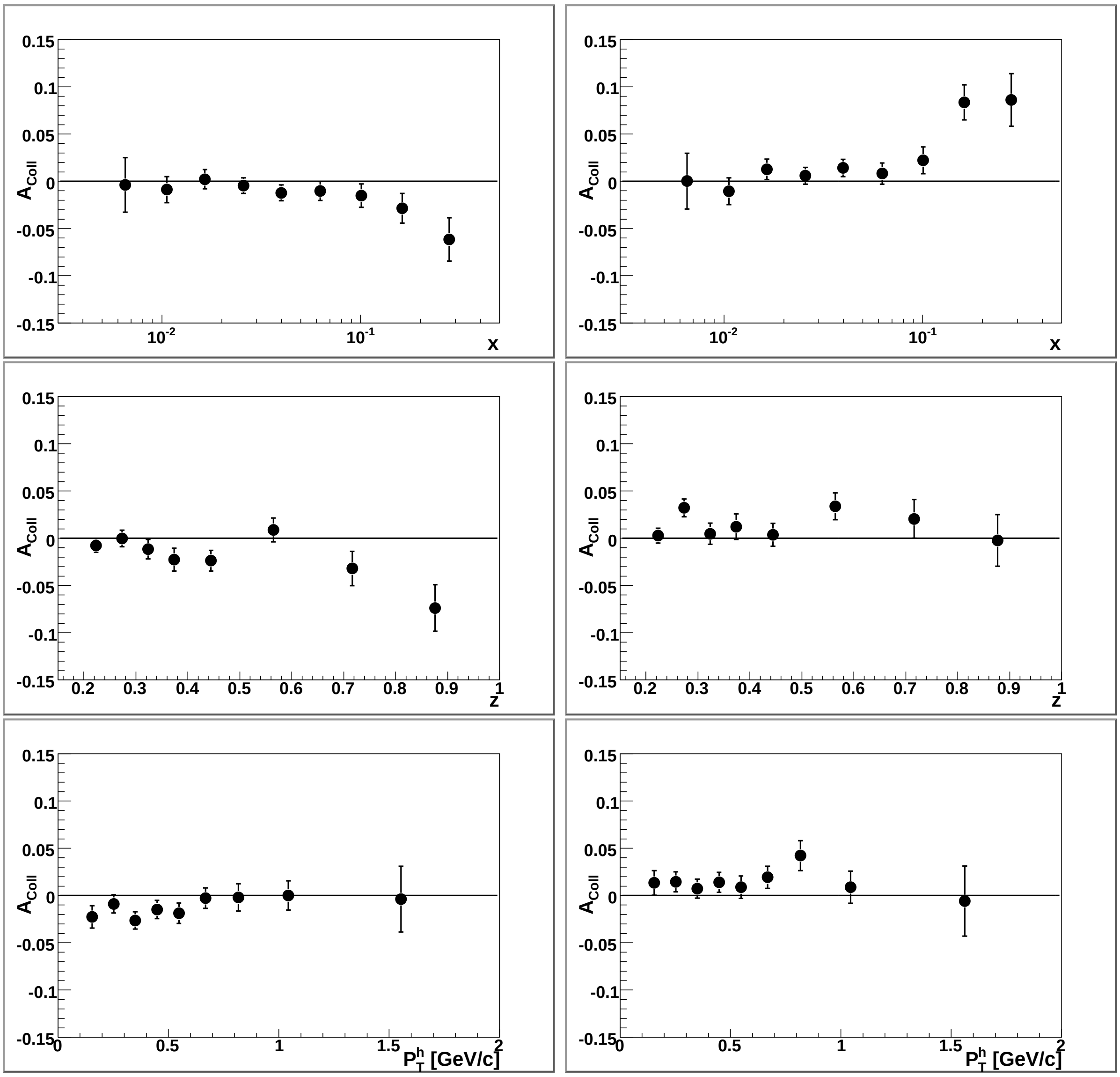

Figure 5.19: *Collins asymmetries for positive (left) and negative (right) pions as function from x, z and P_T^h from a proton target at COMPASS. Only statistical errors are shown.*

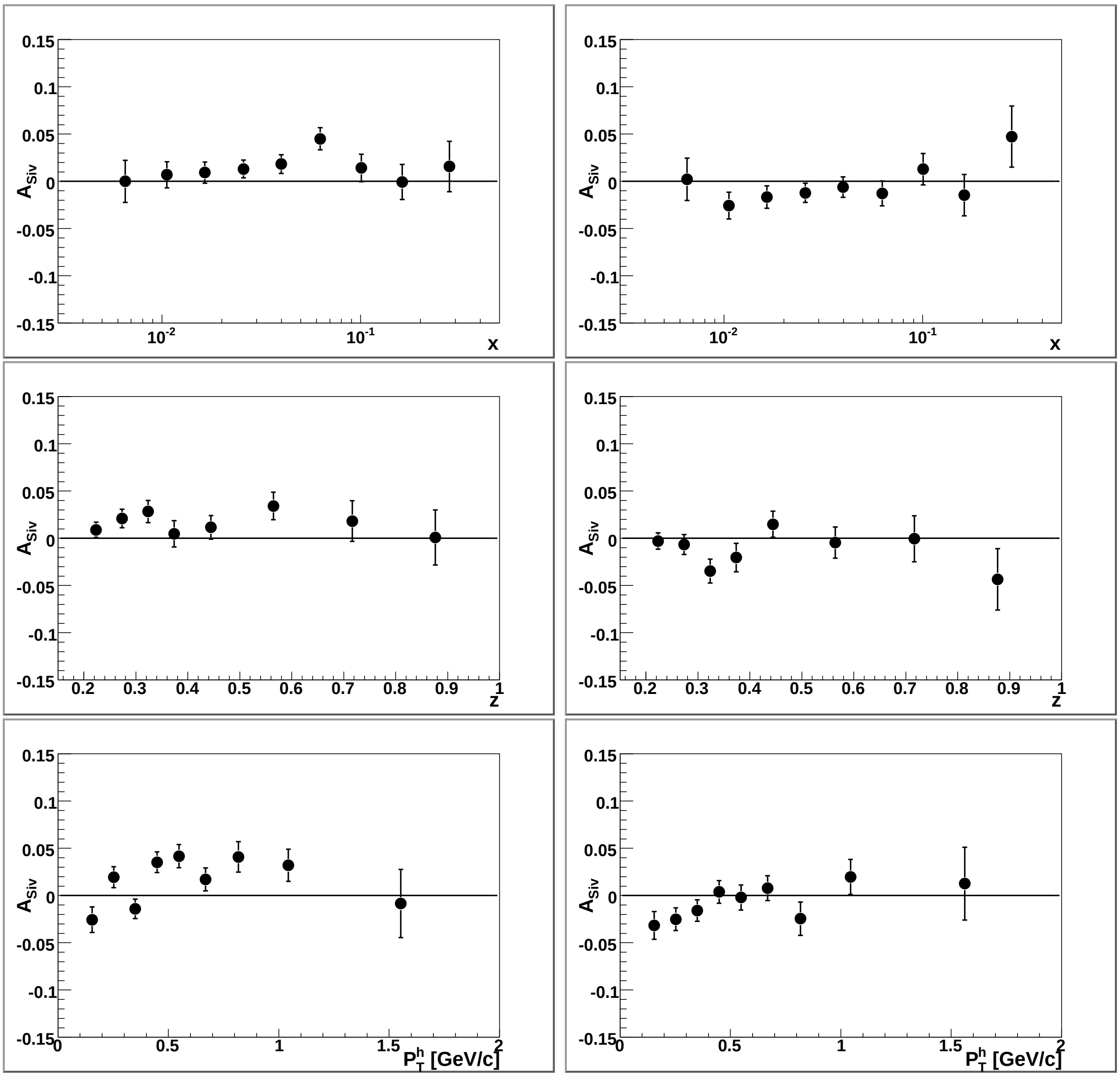

Figure 5.20: *Sivers asymmetries for positive (left) and negative (right) pions as function from x, z and P_T^h from a proton target at COMPASS. Only statistical errors are shown.*

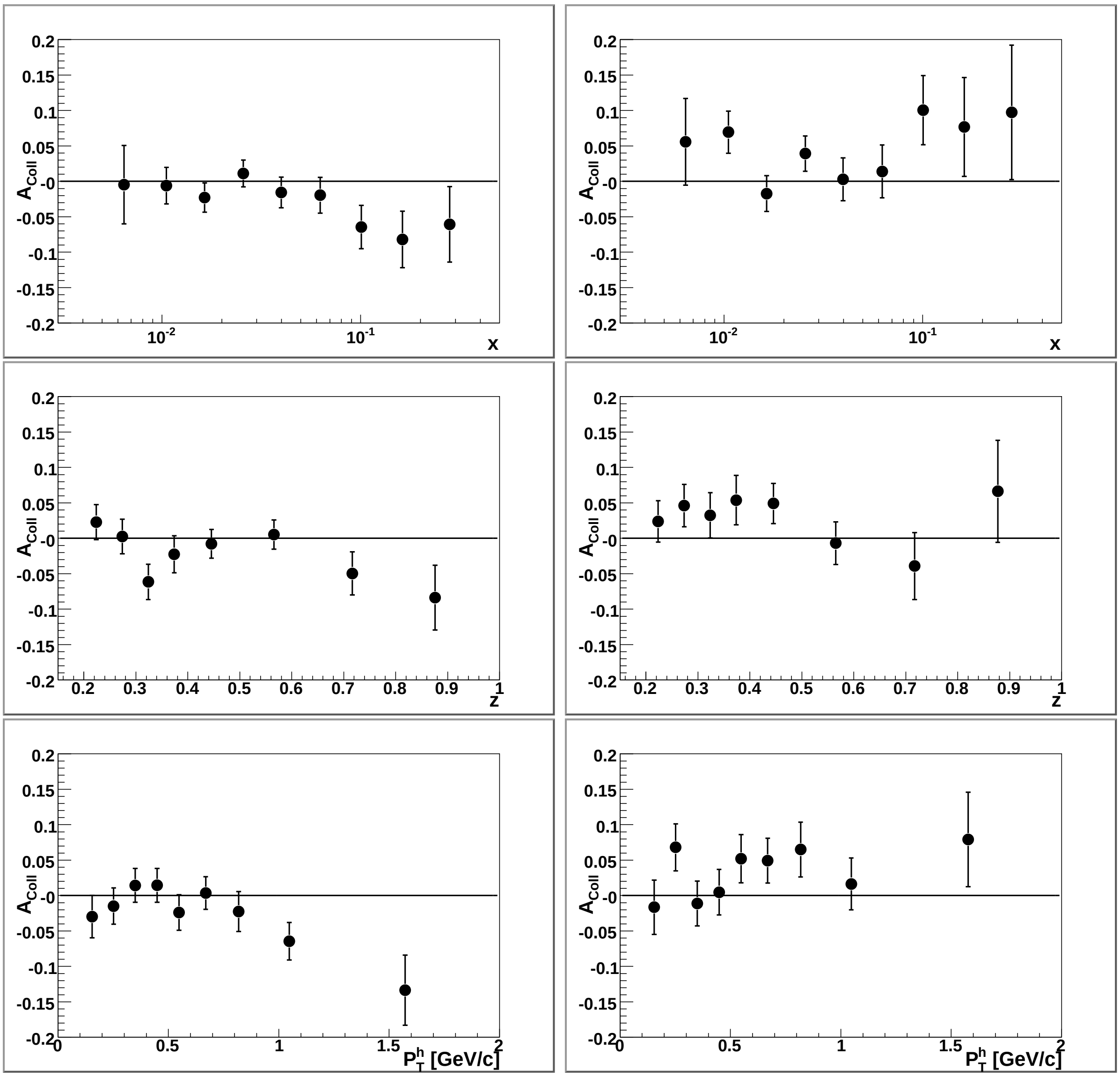

Figure 5.21: *Collins asymmetries for positive (left) and negative (right) kaons as function from* x, z *and* P_T^h *from a proton target at COMPASS. Only statistical errors are shown.*

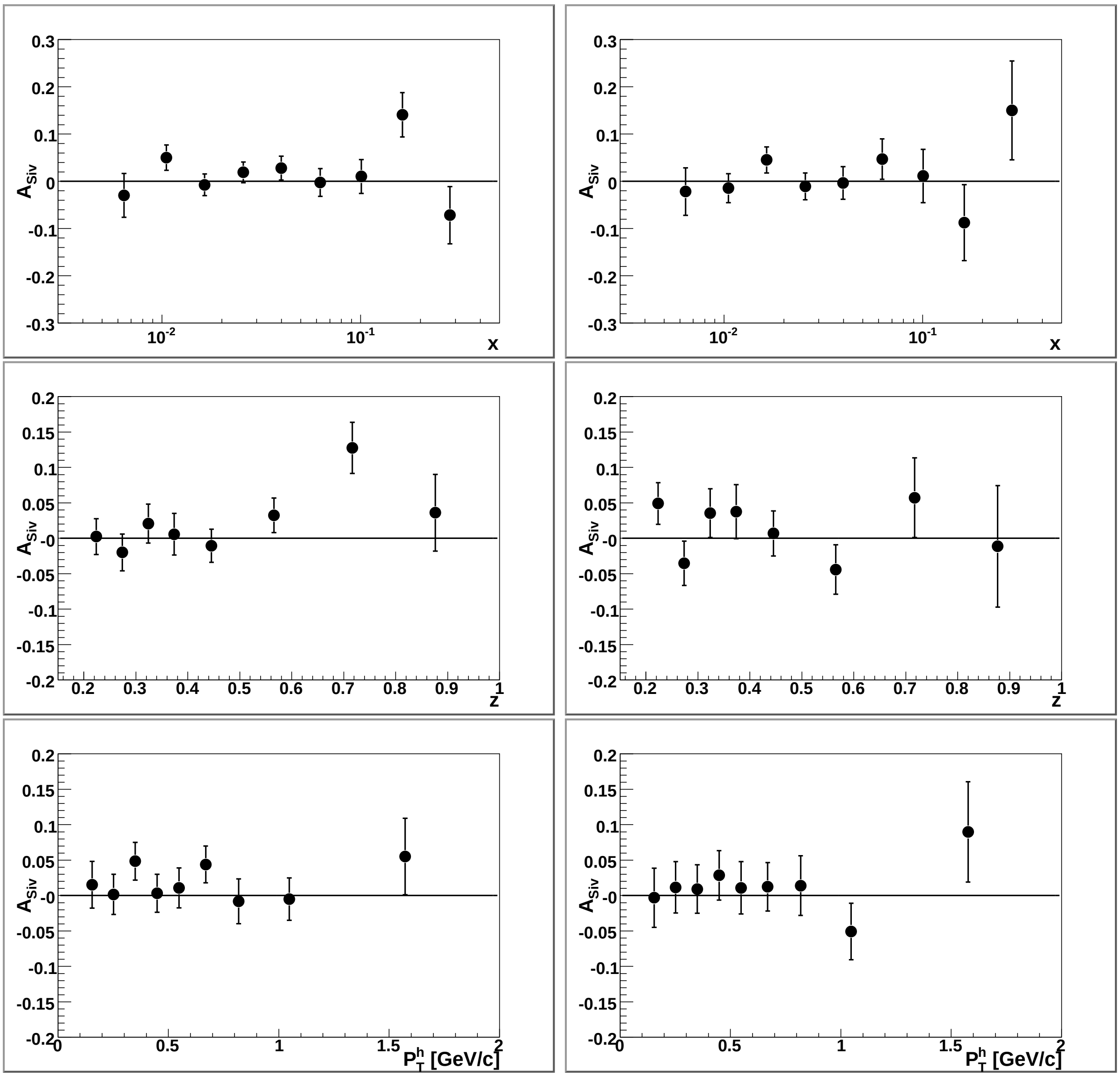

Figure 5.22: *Sivers asymmetries for positive (left) and negative (right) kaons as function from x, z and P_T^h from a proton target at COMPASS. Only statistical errors are shown.*

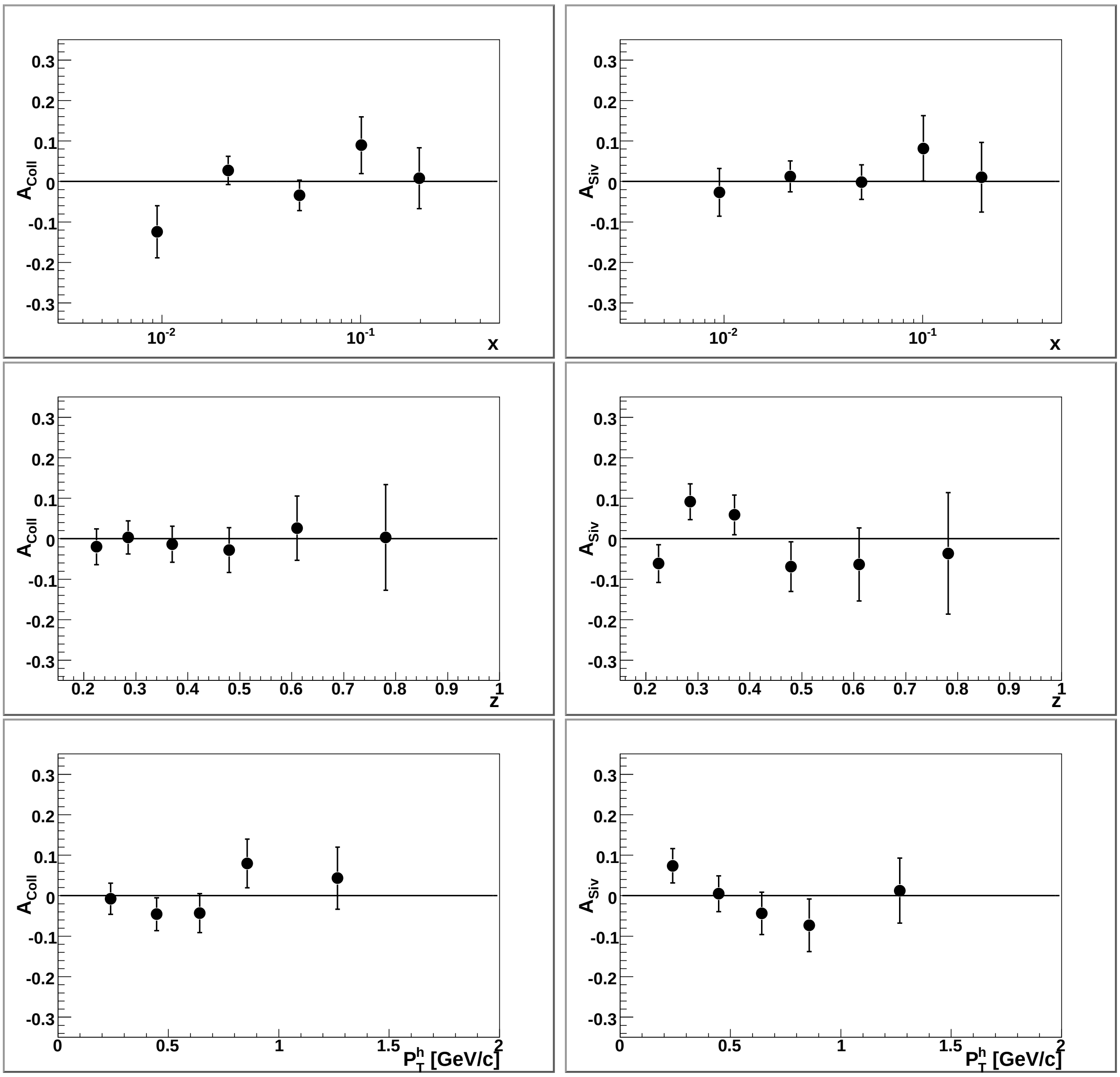

Figure 5.23: *Collins (left) and Sivers (right) asymmetries from K^0 production on a proton target at the COMPASS experiment as function of x, z and P_T^h. Only statistical errors are shown.*

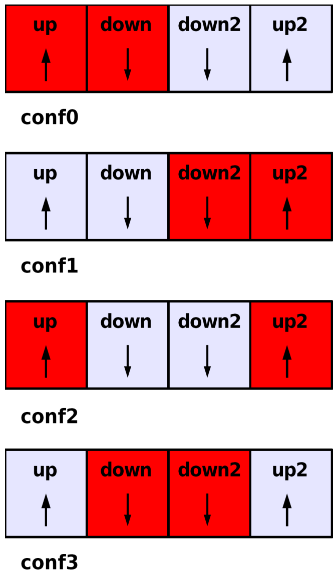

Figure 5.24: *Definition of the target cell configurations. The red colored cells are used in the analysis of the real or false asymmetries by combining the events of two consecutive sub-periods with the opposite target spin.*

5.4.1 Definition of Target Configurations

Because we had for the 2007 run three target cells, we can split the central cell into two parts so that we can work with four cells effectively and get therefore four possible combinations (see fig. 5.24): conf_0 built from the upstream and the first half of the central cell and conf_1 built from the second half of the central cell and the downstream cell can be used for the extraction of the physics asymmetries by combining the events of two consecutive sub-periods with the opposite target spin.
In contrary the configurations conf_2 built from the upstream and the downstream cell corresponding to the external part of the target and conf_3 built from the two halfs of the central cell corresponding to the internal part of the target, which have the same sign of polarization, can be used to calculate false asymmetries by combining the events from two consecutive sub-periods assuming the wrong sign of polarization in one of the two target cells.
As conf_4 we call in the following the combination of conf_0 and conf_1, where the data of all four cells are be used simultaneously. Thus to extract the physics asymmetries there are two alternatives: building the mean of the asymmetries from conf_0 and conf_1 or using conf_4.

5.4.2 False Asymmetries

The false Collins and Sivers asymmetries obtained by using the definitions in the section before, are for both configurations, conf_2 and conf_3, small and scattered around zero. One example is shown in fig. 5.25 for the false Collins asymmetries for positive hadrons from

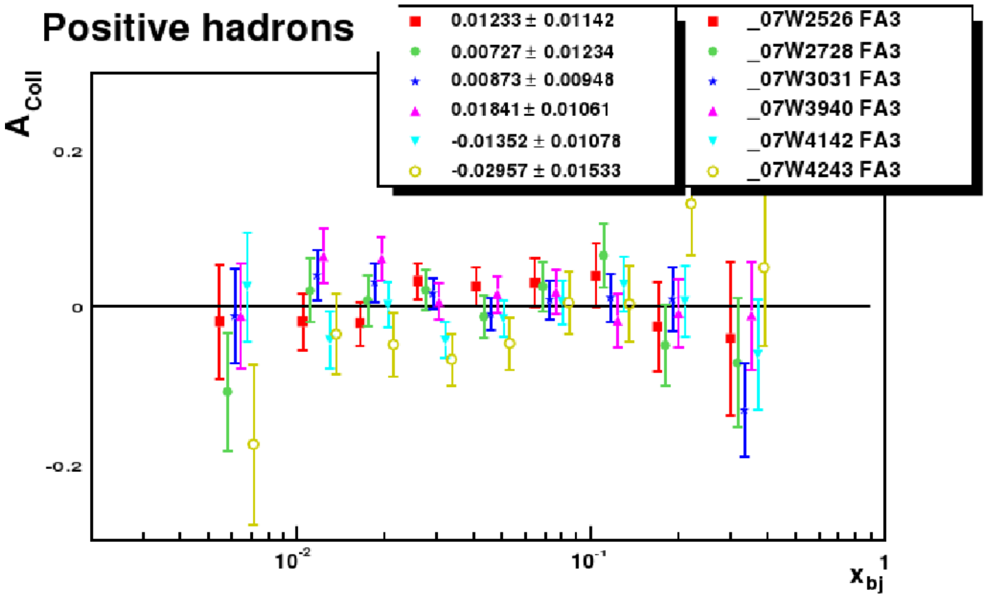

Figure 5.25: *False Collins asymmetries from* conf_3 *(called here: FA3 for false asymmetries,* conf_3*) for positive hadrons.*

conf_3. The other false asymmetries are shown in appendix B.2.1. A further evaluation of those false asymmetries will follow in section 5.4.8.

5.4.3 Dependence on the Target Cells

To check the dependance of the asymmetries from the target cells the pulls P_{0-1} between the asymmetries extracted separately from conf_0 and conf_1 were calculated for all bins in x, z and P_T^h:

$$P_{0-1} = \frac{A_{\mathrm{conf}_0} - A_{\mathrm{conf}_1}}{\sqrt{\sigma^2_{\mathrm{conf}_0} + \sigma^2_{\mathrm{conf}_1}}} \tag{5.14}$$

where $A_{\mathrm{conf_i}}$ are the asymmetries for the corresponding configuration $\mathrm{conf_i}$ in a single bin and period. In the denominator we have the sum of the variances, because the samples are independent.

The sigma[2] values of the distributions are in all cases very close or at least sufficiently near to zero as expected for a standard normal distribution. The mean values for the Collins distributions for positive and negative hadrons are compatible with zero, while they are shifted for the Sivers distributions by -0.48 for positive and by 0.073 for negative hadrons. For the worst case, for Sivers, negative hadrons, the pulls can be seen in fig. 5.26, the other three distributions are shown in appendix B.2.2.

Those dependances of the asymmetries from the target cells are further evaluated in section 5.4.8, where the contributions to the systematic errors are calculated.

[2] $\sigma = \sqrt{\sigma^2_{\mathrm{conf}_0} + \sigma^2_{\mathrm{conf}_1}}$

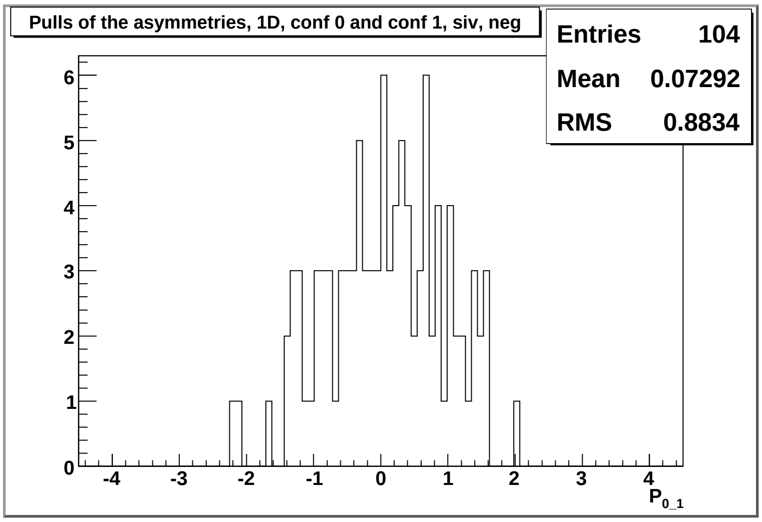

Figure 5.26: *Top: Pulls P_{0-1} for Sivers asymmetries between* conf_0 *and* conf_1 *for negative hadrons.*

As described in section 5.4.1 conf_4, where the data of all four effective target cells are used simultaneously, provides an alternative possibility to obtain the physics asymmetries. To test the compatibility of the results from conf_0 and conf_1 and those from conf_4, the following quantity P_{01-4} was evaluated for all periods and in all bins in x, z and P_T^h separately for Collins and Sivers and positive and negative hadrons:

$$P_{01-4} = \frac{\langle A_{01} \rangle - A_{\mathrm{conf}_4}}{\left(\sigma_{\langle A_{01} \rangle} + \sigma_{\mathrm{conf}_4}\right)/2} \tag{5.15}$$

where

$$\langle A_{01} \rangle = \frac{A_{\mathrm{conf}_0}/\sigma^2_{\mathrm{conf}_0} + A_{\mathrm{conf}_1}/\sigma^2_{\mathrm{conf}_1}}{1/\sigma^2_{\mathrm{conf}_0} + 1/\sigma^2_{\mathrm{conf}_1}}; \qquad \sigma_{\langle A_{01} \rangle} = \frac{1}{\sqrt{1/\sigma^2_{\mathrm{conf}_0} + 1/\sigma^2_{\mathrm{conf}_1}}} \tag{5.16}$$

is the weighted mean of the asymmetries from conf_0 and conf_1 in a single period and bin and the corresponding error, respectively.
Contrary to eq. (5.14) one has to take here the mean of the errors $\sigma_{\langle A_{01} \rangle}$ and σ_{conf_4}, because the samples from conf_0 and conf_1 and the one from conf_4 are not independent.
The mean and sigma values of the distributions of the quantity P_{01-4} are all near 0 as expected. For one example (Collins asymmetries for negative hadrons) see fig. 5.27, for the other distributions see appendix B.2.2. So we can conclude that the extraction from conf_0 and conf_1 is compatible with the one from conf_4. In this work the extraction of the asymmetries was done with conf_4.

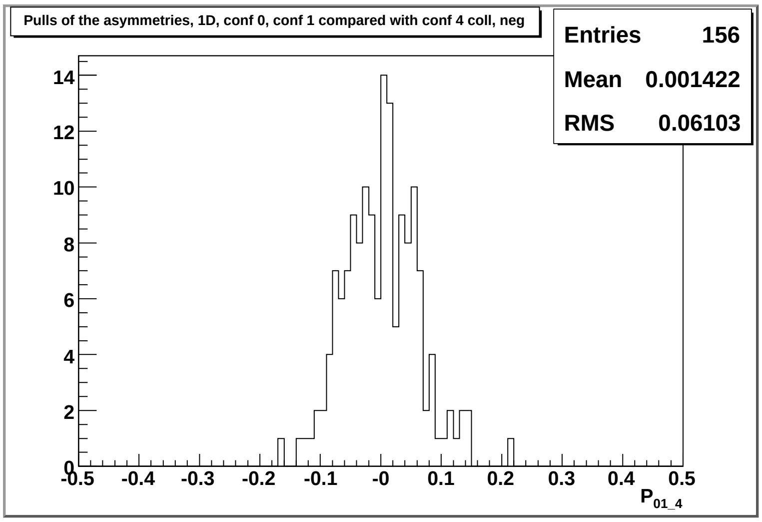

Figure 5.27: *Distribution of the quantity P_{01-4} defined in eq. (5.15) to test the compatibility between the results from* conf_0 *and* conf_1 *and those from* conf_4 *for Collins, negative (right) hadrons.*

5.4.4 Compatibility of the Different Periods

Like for the deuteron data the compatibility of the asymmetries in all bins of x, z and P_T^h for all periods were tested by checking the distribution of the following quantity:

$$\frac{A_i - \langle A \rangle}{\sqrt{\sigma_i^2 - \sigma_{\langle A \rangle}^2}}; \quad i = 1, 2, 3, 4, 5, 6 \tag{5.17}$$

A_i are again the asymmetries in a single bin and period and $\langle A \rangle$ the corresponding weighted mean of this bin.

The distributions for the asymmetries are evaluated separately for Collins and Sivers and positive and negative hadrons. For the Collins distributions there are 156 entries corresponding to 6 (periods) $\cdot$ $(9 + 8 + 9)$ (x, z and P_T^h bins), while for the Sivers distributions we have 104 entries corresponding to 4 (periods) $\cdot$ $(9 + 8 + 9)$ (x, z and P_T^h bins).

In all cases we got standard normal distributions with mean values compatible with zero and a RMS sufficently near 1 as expected, meaning that the results of the different periods are compatible. One example (Collins asymmetries for negative hadrons) is shown in fig. 5.28, for all distributions it is refered to appendix B.2.3.

Compatibility of first and second part of the run

For Sivers slight differences between the first and the second part of the run were found in the case of positive hadrons as can be seen in fig. 5.29, where the asymmetries using all four weeks with those only from the first part (W25/26 and W30/31) and only from the second part of the run (W39/40 and W42/43) were plotted together. The mean asymmetry

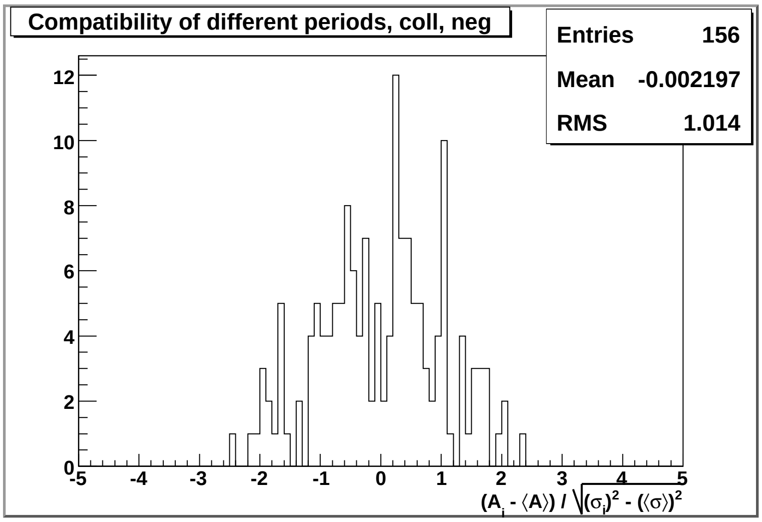

Figure 5.28: *Distribution of the quantity defined in eq. (5.17) to test the compatibility of the results from the different periods for the Sivers asymmetries for positive hadrons.*

values over the x bins are 0.024 ± 0.005 for the first part and 0.004 ± 0.006 for the second part. In contrast for Sivers, negative hadrons (see also fig. 5.29), as well as for the Collins asymmetries (see appendix B.2.3) the differences were smaller.
To take this effect into account, half the difference of the two mean asymmetry values for positive hadrons, namely 0.01, was added as a scale factor to the systematic error. In contrast to the other contributions to the systematic error in this analysis this number is not given as a fraction of the statistical error, but as an absolute value.

Splitting of sub-periods into two parts

Another test of the stability of the asymmetries inside one week was to split the sub-periods into two parts, combine each of the parts with the coupled sub-period and extract the asymmetries. For all periods used in this analysis for Collins and Sivers the extracted asymmetries for positive and negative hadrons were well compatible beside for Sivers for positive hadrons in W30/31. The systematic effect obtained by splitting W30 and combine it with W31 is shown in fig. 5.30. This effect has to be taken into account for the systematic error in this week by adding the absolute value of the half of the difference between both extraxted asymmetries divided by the statistical error:

$$\frac{\frac{1}{2}|A_{1st\ part} - A_{2nd\ part}|}{\sigma_{|A_{1st\ part} - A_{2nd\ part}|}} \tag{5.18}$$

which turned out to be 0.8 in this case.

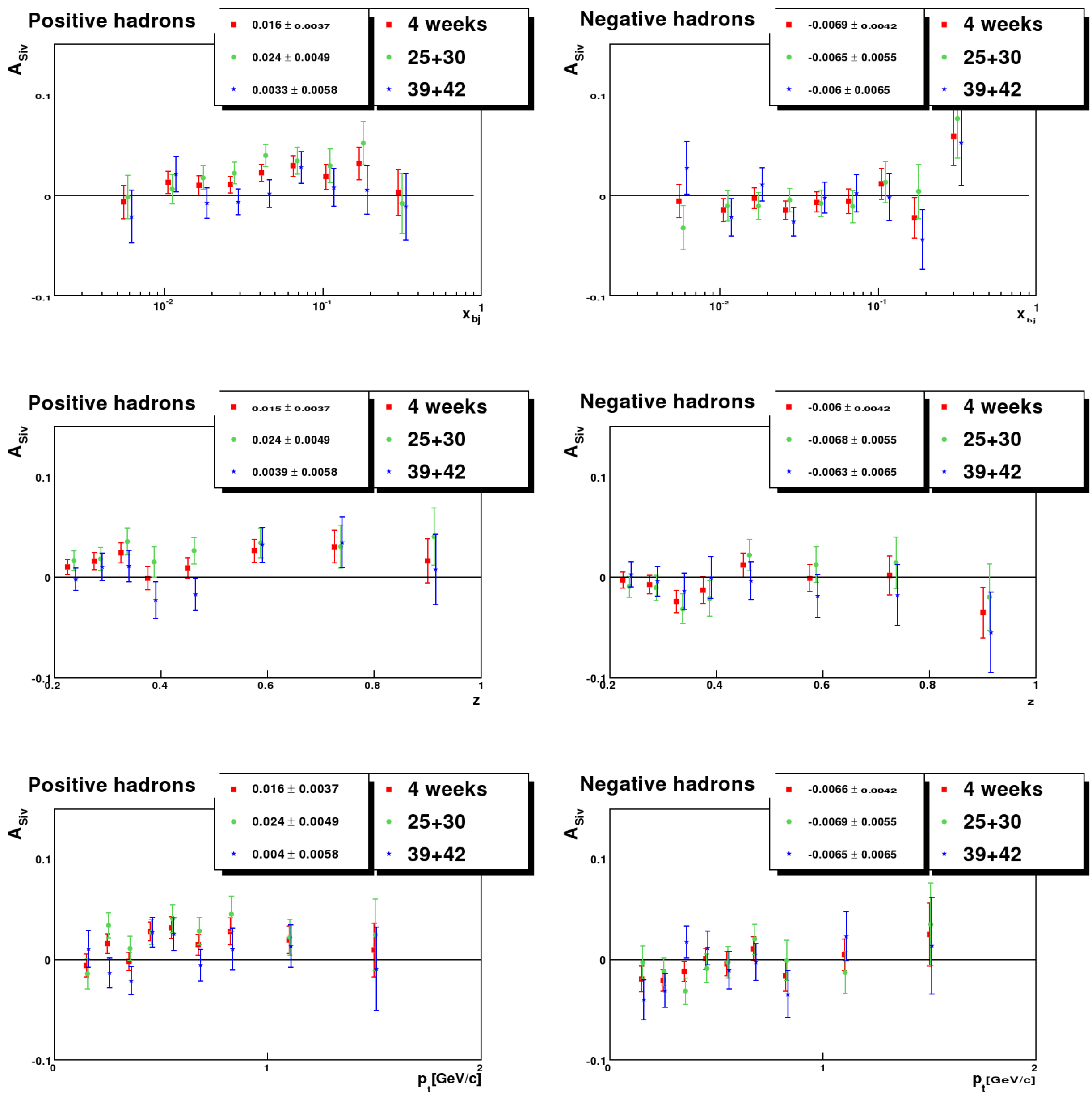

Figure 5.29: *In red: Sivers asymmetries vs. x. z and P_T^h using all four weeks from this analysis, in green: same with only those from the first part (here: W25/26 and W30/31) and in blue: same with only those from the second part of the run (here: W39/40 and W42/43). In all three cases: left: positive, right: negative hadrons.*

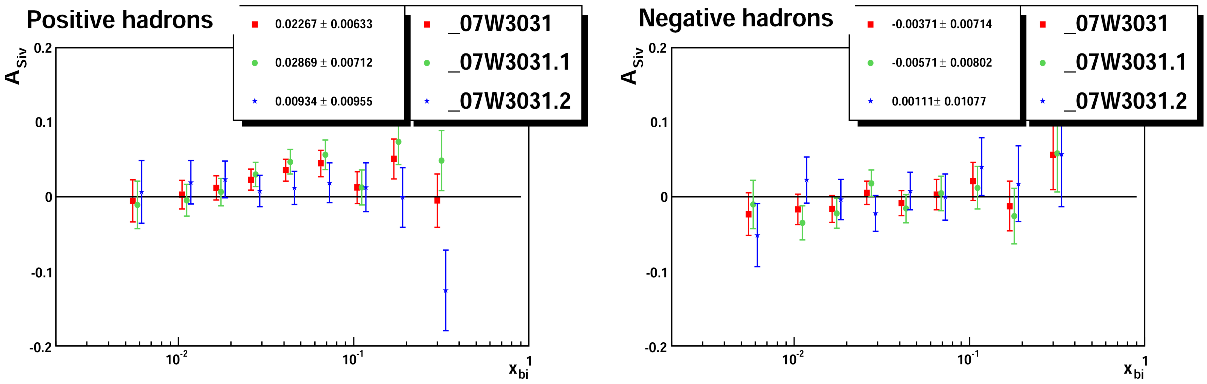

Figure 5.30: *Sivers asymmetries vs. x, splitting W30 into two parts and combining it with W31. Left: positive hadrons. Right: negative hadrons.*

5.4.5 Stability of Acceptances

R-test

The so-called R-test already used for the deuteron data (see sections 4.3.2 and 4.4.3) as a check of the stability of the data inside one period was also performed for the proton data. For simplicity we used for this the "double ratio" method. To evaluate the ratio the middle cell of the target was split into two parts. We therefore have effectively two target cells: upstream (u) plus central 1 ($c1$) with one polarization and central 2 ($c2$) plus downstream (d) with the opposite one.
The equation corresponding to eq. (4.11) and (4.12) is then:

$$\begin{aligned} R(\Phi) &= \frac{(N_u^{\uparrow}(\Phi) + N_d^{\uparrow}(\Phi))(N_{c1}^{\downarrow}(\Phi) + N_{c2}^{\downarrow}(\Phi))}{(N_u^{\downarrow}(\Phi) + N_d^{\downarrow}(\Phi))(N_{c1}^{\uparrow}(\Phi) + N_{c2}^{\uparrow}(\Phi))} \\ &\approx const \cdot \frac{(a_u^{\uparrow}(\Phi) + a_d^{\uparrow}(\Phi))(a_{c1}^{\downarrow}(\Phi) + a_{c2}^{\downarrow}(\Phi))}{(a_u^{\downarrow}(\Phi) + a_d^{\downarrow}(\Phi))(a_{c1}^{\uparrow}(\Phi) + a_{c2}^{\uparrow}(\Phi))} \end{aligned} \tag{5.19}$$

R was calculated for all bins in x, z and P_T^h. Unlike as for the deuteron data, where the ratio was always constant, we had for the proton data some instabilities. One example for the resulting χ^2 distributions of the constant fit of R is shown for Collins for the period W30/31 in bins in x in fig. 5.31 together for positive and negative hadrons, for the other χ^2 distributions in bins in x see appendix B.2.4.
As for the deuteron data in section 4.4.3 the resulting distributions are compared with the curves theoretically expected for seven degrees of freedom (eight bins in $\Phi_{C,S}$ and a one parameter fit). Despite some deviations of the χ^2 distributions from the expected curves an overall agreement was achieved.

T-test

Due to the instabilities described before in addition a new test was implemented for further studies. This new test called "T" for "total" is based on the idea that spin effects should

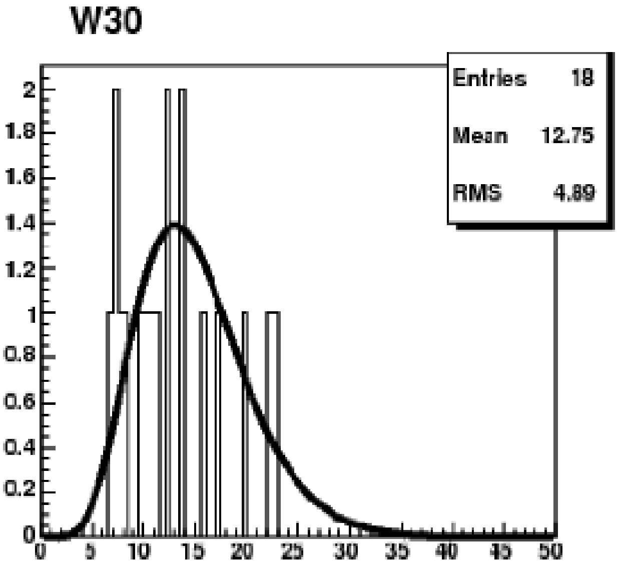

Figure 5.31: χ^2 *distributions of the constant fit of R together for positive and negative hadrons for the bins in x for Collins for the period W30/31 (second "data production" used compared to the curve theoretically expected for seven degrees of freedom.*

disappear at first order under the assumption that the acceptances cancel, if we sum the number of hadrons from all cells in one week:

$$\begin{aligned} T(\Phi) &= \frac{N_u^{\uparrow}(\Phi) + N_d^{\uparrow}(\Phi) + N_{c1}^{\downarrow}(\Phi) + N_{c2}^{\downarrow}(\Phi)}{N_u^{\downarrow}(\Phi) + N_d^{\downarrow}(\Phi) + N_{c1}^{\uparrow}(\Phi) + N_{c2}^{\uparrow}(\Phi)} \\ &\approx const \cdot \frac{a_u^{\uparrow}(\Phi) + a_d^{\uparrow}(\Phi) + a_{c1}^{\downarrow}(\Phi) + a_{c2}^{\downarrow}(\Phi)}{a_u^{\downarrow}(\Phi) + a_d^{\downarrow}(\Phi) + a_{c1}^{\uparrow}(\Phi) + a_{c2}^{\uparrow}(\Phi)} \end{aligned} \tag{5.20}$$

The ratio T should therefore in the ideal case be zero. From the numerous tests performed we can conclude that the only acceptance effect leading to a relevant error in the extraction of the physics asymmetries is a modulation of the same type as in the physics case. Therefore we can express the acceptances in the form $a_i = const \cdot (1 + \alpha_i \cdot \sin\Phi)\,, \quad i \in u, c1, c2, d$ (see eq. (4.6)). We then obtain from eq. (5.20):

$$\begin{aligned} T(\Phi) &= const \cdot \frac{4 + \Big(\alpha_u^{\uparrow}(\Phi) + \alpha_d^{\uparrow}(\Phi) + \alpha_{c1}^{\downarrow}(\Phi) + \alpha_{c2}^{\downarrow}(\Phi)\Big) \cdot \sin\Phi}{4 + \Big(\alpha_u^{\downarrow}(\Phi) + \alpha_d^{\downarrow}(\Phi) + \alpha_{c1}^{\uparrow}(\Phi) + \alpha_{c2}^{\uparrow}(\Phi)\Big) \cdot \sin\Phi} \\ &\approx const \cdot \{1 + \frac{1}{4}\Big[\alpha_u^{\uparrow}(\Phi) + \alpha_d^{\uparrow}(\Phi) + \alpha_{c1}^{\downarrow}(\Phi) + \alpha_{c2}^{\downarrow}(\Phi) \\ &\qquad - \Big(\alpha_u^{\downarrow}(\Phi) + \alpha_d^{\downarrow}(\Phi) + \alpha_{c1}^{\uparrow}(\Phi) + \alpha_{c2}^{\uparrow}(\Phi)\Big)\Big] \cdot \sin\Phi\} \\ &= const \cdot \{1 + \frac{1}{4}\left[e_u(\Phi) + e_d(\Phi) + e_{c1}(\Phi) + e_{c2}(\Phi)\right] \cdot \sin\Phi\} \end{aligned} \tag{5.21}$$

with $e_i = \alpha_i^{period1} - \alpha_i^{period2}, \quad i \in u, c1, c2, d$.
If we use the same hypothesis for R we get the relation $T = R/2$. To verify this we have fitted the values of T and R, respectively, with $const \cdot (1 + \epsilon_{T/R} \sin\Phi)$. Here $\epsilon_T = e_u + e_d + e_{c1} + e_{c2}$ and ϵ_R should be $\epsilon_R = 2 \cdot (e_u + e_d + e_{c1} + e_{c2})$. In the most cases the relation $T = R/2$ is valid for our data. For an example see appendix B.2.4.
For the physics asymmetries we get with the double ratio method analog to eq. (4.6) by splitting the middle cell and summing up the data from cells with the same polarization:

$$F(\Phi) \approx const \frac{(a_u^{\uparrow}(\Phi) + a_d^{\uparrow}(\Phi)) \cdot (a_{c1}^{\uparrow}(\Phi) + a_{c2}^{\uparrow}(\Phi))}{(a_u^{\downarrow}(\Phi) + a_d^{\downarrow}(\Phi)) \cdot (a_{c1}^{\downarrow}(\Phi) + a_{c2}^{\downarrow}(\Phi))} \cdot (1 + 4\epsilon \sin\Phi) \tag{5.22}$$

with $\epsilon = A_{C,S}^{raw}$ as the raw Collins and Sivers asymmetry, respectively.
If we transform eq. (5.22) we obtain:

$$\begin{aligned} F(\Phi) &\approx const \frac{1 + \left(\alpha_u^{\uparrow}(\Phi) + \alpha_d^{\uparrow}(\Phi) + \alpha_{c1}^{\uparrow}(\Phi) + \alpha_{c2}^{\uparrow}(\Phi) + 2\epsilon\right) \cdot \sin\Phi}{1 + \left(\alpha_u^{\downarrow}(\Phi) + \alpha_d^{\downarrow}(\Phi) + \alpha_{c1}^{\downarrow}(\Phi) + \alpha_{c2}^{\downarrow}(\Phi) + 2\epsilon\right) \cdot \sin\Phi} \\ &\approx const \cdot \{1 + [e_u(\Phi) + e_d(\Phi) - (e_{c1}(\Phi) + e_{c2}(\Phi)) + 4\epsilon] \cdot \sin\Phi\} \end{aligned} \tag{5.23}$$

Thus the estimated physics asymmetry is $\epsilon_F = \epsilon + [e_u + e_d - (e_{c1} + e_{c2})]/4$. This shows a bias, which is not obviously zero. Because the bias does not depend directly from ϵ_T, it can also be zero in the case of a non-zero ϵ_T under the assumption that the “reasonable” assumption (eq. (4.9), (4.10)) holds. Due to the smallness of the spin effects we are looking for, we will not use any data, which exhibit very large values of ϵ_T, so that we are on the safe side.
For a further description and examples for this T-test and also the further development of the R- and the T-test it is refered to appendix B.2.4.

Test of the “reasonable” assumption

The “reasonable” assumption defined in eq. (4.9), which can be formulated as $e_u = e_{c1} = e_{c2} = e_d$, is tested also in the following way: By coupling two sub-periods with opposite spin configurations it is possible to extract four independent asymmetry values, one for each target cell. Those measured asymmetries are given by the sum of the physics asymmetry ϵ and the change of acceptance for this cell e_i with $i \in u, c1, c2, d$:

$$\begin{aligned} A_1 &= \epsilon + \frac{e_1}{2} \\ A_2 &= \epsilon - \frac{e_2}{2} \\ A_3 &= \epsilon - \frac{e_3}{2} \\ A_4 &= \epsilon + \frac{e_4}{2} \end{aligned} \tag{5.24}$$

If the "reasonable" assumption is valid, the acceptance variations in each target cell have to be compatible with their mean value $\langle e\rangle$, which can be tested by calculating the following χ^2:

$$\chi^2_{RA} = \sum \left(\frac{A_i - (\epsilon \pm \langle e\rangle)}{\sigma_i} \right)^2 \tag{5.25}$$

where A_i are the measured asymmetries and σ_i their sigma values. The distribution of the χ^2_{RA} has two degrees of freedom because of the four measurements and two estimated mean values ϵ and $\langle e\rangle$.
For the calculation of the mean asymmetry ϵ and the mean variation of the acceptance $\langle e\rangle$ it is refered to appendix B.2.4.

Quality tables for acceptance variations

To evaluate the acceptance variations the results of the T-test and the test of the "reasonable" assumption have to be combined. χ^2_T for the T-test we define as comparison of the measured T value with the hypothesis $T = 0$, meaning that the acceptance does not vary between two coupled sub-periods:

$$\chi^2_T = \sum \left(\frac{T}{2\sigma} \right)^2 \tag{5.26}$$

The factor 2 is motivated by the fact that the condition $T = 0$ is a stricter requirement than the "reasonable" assumption.
χ^2_{tot} we than obtain by:

$$\chi^2_{tot} = \chi^2_{RA} + \chi^2_T \tag{5.27}$$

The χ^2_{tot} values calculated separately for positive and negative hadrons are afterwards summed up to get an overall confidence level of the regarding period or sub-period.
To get a decision, which of the two different data productions has a better quality for the second part of the run, the χ^2_{tot} values for both productions are compared. The test on the "reasonable" assumption gives nearly the same results for both productions, while the T-test is significantly worse for the second production. For this reason the first data production was used to extract the asymmetries from the second part of the run.
For the χ^2 values, the overall confidence levels and more details see appendix B.2.4.

Cuts on the acceptances

To test the target cell acceptances a cut was performed to reject the large angle tracks, which resulted in acceptances similar to that of the 2004 deuteron data, where those tracks were not detected. In this cut the tracks were extrapolated to a z coordinate of 600cm just before the RICH entrance and cut in the region $|x| > 40$cm and $|y| > 40$cm.
For Sivers of positive hadrons in W30/31 a systematic effect was found as can be seen in fig. 5.32 for the raw asymmetries, where the corresponding asymmetries with and without this cut on the acceptances are plotted. For comparison the corresponding plot for Sivers

for negative hadrons is shown in fig. 5.33. The error added therefore for Sivers for positive hadrons in period W30/31 was calculated analog to the case of the test of splitting the sub-periods in section 5.4.4:

$$\frac{\frac{1}{2}|A_{without\ acc\ cut} - A_{with\ acc\ cut}|}{\sigma_{|A_{without\ acc\ cut} - A_{with\ acc\ cut}|}} = 0.7 \tag{5.28}$$

The value of 0.7 is added to the systematic error.

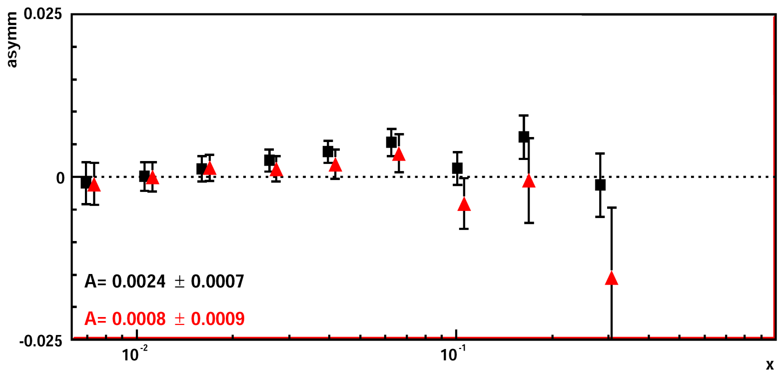

Figure 5.32: *Sivers raw asymmetries in period W30/31 vs. x for positive hadrons without (black symbols) and with (red symbols) the cut on the acceptances described in the text.*

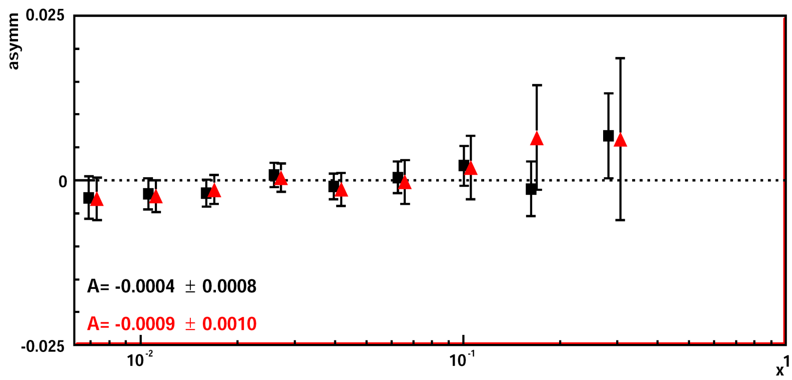

Figure 5.33: *Sivers raw asymmetries in period W30/31 vs. x for negative hadrons without (black symbols) and with (red symbols) the cut on the acceptances described in the text.*

5.4.6 Comparison of Different Estimators

As already mentioned the asymmetries were extracted with different methods. Here we compare the unbinned maximum likelihood method with the "double ratio" method by

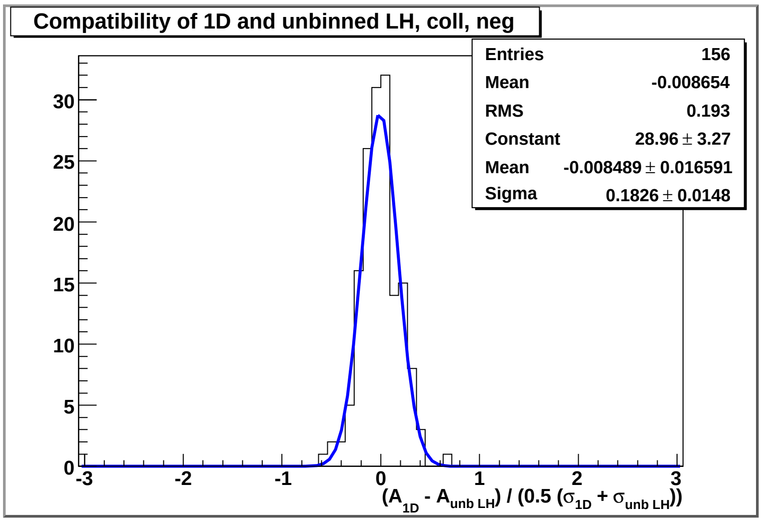

Figure 5.34: *Distribution of the quantity defined in eq. (5.29) to compare the results from the "double ratio" and the ones from the unbinned maximum likelihood method for Collins for negative hadrons.*

building the following distribution:

$$\frac{A_{DR} - A_{unbLH}}{(\sigma_{DR} + \sigma_{unbLH})/2} \tag{5.29}$$

where A_{DR} are the asymmetries calculated with the "double ratio" and A_{unbLH} those with the unbinned maximum likelihood method. These distributions were calculated separately for Collins and Sivers, for positive and negative hadrons. One example (Collins asymmetries for negative hadrons) is given in fig. 5.34, for the other distributions it is referred to appendix B.2.5. The two methods differ by $0.2 - 0.3$ of the statistical error. It was therefore decided to assign for a value of 0.15 σ as contribution of the asymmetry estimator to the systematic error.

5.4.7 Systematic Studies for K^0 Asymmetries

For the analysis of the K^0 asymmetries it is not necessary to repeat all tests already done for the analysis of the unidentified charged hadrons. Those systematic tests, which were performed additional for the K^0 analysis, are described in the following.

Compatibility of the Results in the Different Periods

As done for the unidentified hadrons (section 4.4.3) and for the K^0 analysis of the deuteron data (section 4.4.1) the compatibility of the asymmetries in all bins of x, z and P_T^h for all periods used in this analysis was examined. For this again the distribution of the following

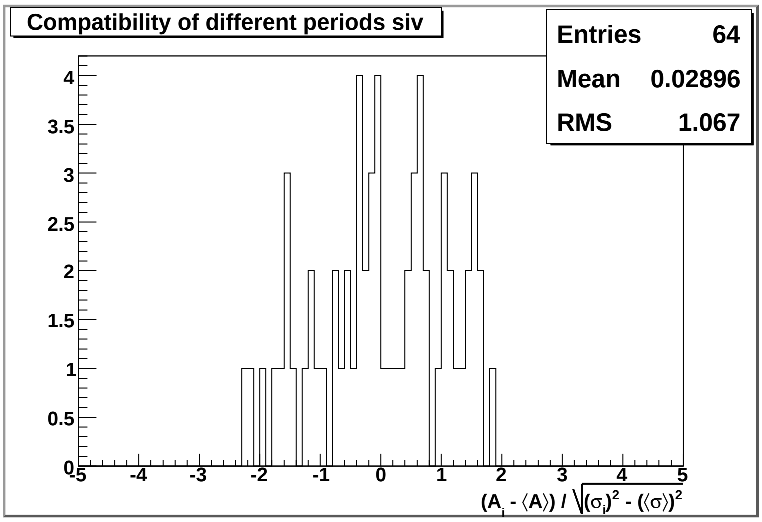

Figure 5.35: *Distribution of the quantity defined in eq. (5.30) to test the compatibility of the results from the different periods for Sivers for K^0 production.*

quantity was evaluated:

$$\frac{A_i - \langle A \rangle}{\sqrt{\sigma_i^2 - \sigma_{\langle A \rangle}^2}}; \quad i = 1, 2, 3, 4, 5, 6 \tag{5.30}$$

where A_i are again the asymmetries in each bin and period and $\langle A \rangle$ the corresponding weighted mean.
Those distributions are evaluated separately for the Collins and Sivers asymmetries. The number of entries in the case of Collins is 96 corresponding to 6 (periods) $\cdot$ $(5+6+5)$ (bins in x_{bj}, z and P_T^h), while it is for Sivers 64 corresponding to 4 (periods) $\cdot$ $(5+6+5)$ (bins in x_{bj}, z and P_T^h). As example the distribution for Sivers is shown in fig. 5.35, for the distribution for Collins see appendix B.2.6. The resulting mean values are for both, Collins and Sivers, close to 0 and the RMS close to 1 as expected for a standard normal distribution. So we can conclude that the results from the different periods are compatible.

Studies on Background Asymmetries

It was also necessary to check, whether there are background asymmetries. For this like for the deuteron data (see section 4.4.2) asymmetries in a mass range outside the one of the K^0-signal were extracted. Here a range of $[-40, -200] \cup [40, 200]$ MeV in the difference of the measured invariant mass and the literature value was chosen. The binning is the same like for the analysis of the asymmetries for K^0 production itself (see table 5.6).
For simplicity the "double ratio" method was used for the extraction of those sideband asymmetries. As it is known that particularly for a zero asymmetry the "double ratio" method has only evanescent differences to the unbinned likelihood method, this is justified for a test of the compatibility with zero like it is done here.

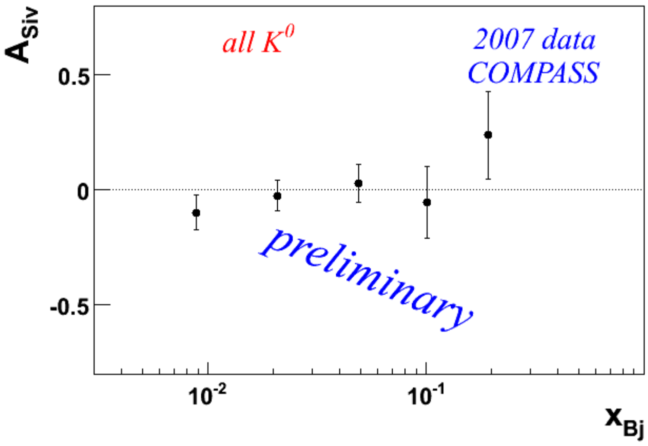

Figure 5.36: *Weighted mean of the Sivers asymmetries in the sidebands vs.x for the 2007 proton data from COMPASS.*

As example for the weighted mean of the resulting background asymmetries for all six periods the one for Sivers is shown as function vs. x in fig. 5.36. For the other sideband asymmetries see appendix B.2.6. All those sideband asymmetries are consistent with zero.

Stability of Acceptance Ratios

To test the stability of the data inside one period the R-test was also done for the K^0 analysis of the proton data. The test was analog to the one performed in section 5.4.5 for the analysis of the unidentified charged hadrons. Again, for simplicity, the "double rato" method was used.
The calculation of R is like in eq. (5.19):

$$R(\Phi) = \frac{(N_u^{\uparrow}(\Phi) + N_d^{\uparrow}(\Phi))(N_{c1}^{\downarrow}(\Phi) + N_{c2}^{\downarrow}(\Phi))}{(N_u^{\downarrow}(\Phi) + N_d^{\downarrow}(\Phi))(N_{c1}^{\uparrow}(\Phi) + N_{c2}^{\uparrow}(\Phi))}$$

The ratio was calculated for all eight bins of the Collins and Sivers angles in each bin in x_{bj}, z and P_T^h for all six periods and fitted with a constant function.
The quality of those fits is tested by comparing the resulting distribution of the χ^2 values of the fits with the theoretically expected curve for seven degrees of freedom (eight bins in $\Phi_{C,S}$ and a one parameter fit). As we see in fig. 5.37 there is a good agreement between the calculated χ^2 values and the expected curve.

Evaluation of false asymmetries

Possible false results due to systematic effects were evaluated by calculating the asymmetries inside one week from two data samples created by giving numbers to all events of this

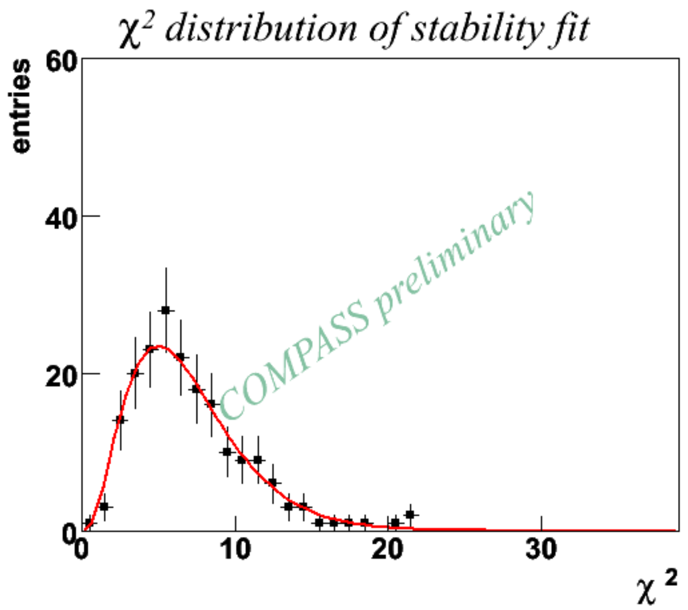

Figure 5.37: χ^2 *distribution of the fits of the ratio* R *performed for all eight bins of the Collins and Sivers angles in each bin in* x_{bj}, z *and* P_T^h *for all six periods compared to the curve theoretically expected for seven degrees of freedom.*

week and dividing the data sample of this week into two parts, one with the odd and one with the even event numbers. One sample is than treated like one sub-period (week) and the other one as the corresponding one with opposite polarization. As for the background asymmetries also for this test it was justified to use the "double ratio" method.
Then the weighted mean of these false asymmetries vs. x, z and P_T^h was built one time using from all weeks W25-43 for Collins and Sivers, respectively, only those with one target spin configuration, here those with + - + were taken, namely W25, W27, W31, ... (see table 5.1), another time the weighted mean with all weeks was built. The false asymmetries are in both cases compatible with zero. As example the weighted mean of all weeks of the false Collins asymmetries vs. x is shown in fig. 5.38. All weighted false asymmetries can be seen in appendix B.2.6.

Comparison of Different Estimators

Another test repeated for the analysis of the K^0 asymmetries was the comparison of the two different estimators used in this work, the unbinned maximum likelihood and the "double ratio" method. Examined was the distribution:

$$\frac{A_{DR} - A_{unbLH}}{(\sigma_{DR} + \sigma_{unbLH})/2} \tag{5.31}$$

here evaluated together for Collins and Sivers asymmetries. In fig. 5.39 we can see that the mean value of the distribution is with 0.08 close to zero and from the RMS we can

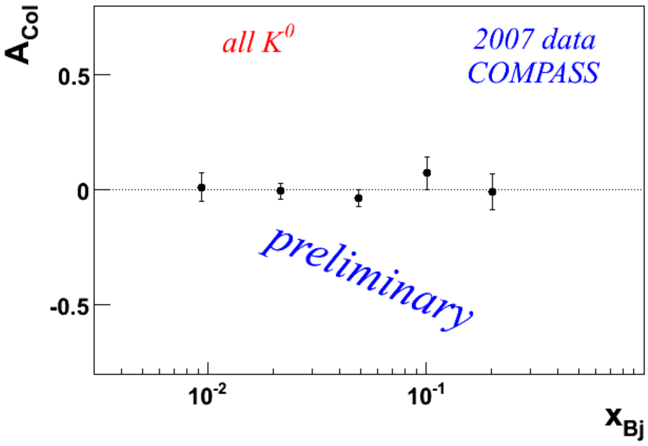

Figure 5.38: *Weighted mean of all weeks of the false Collins asymmetries from odd and even event numbers vs. x.*

conclude that the two methods differ by 0.3 of the statistical error.

5.4.8 Systematic Error from Acceptance Variation

To estimate the systematic errors from acceptance variation between the sub-periods a method based on different measurements of those effects was developed. These methods and their results are described in the following.

Error Estimation from False and Physics Asymmetries

The bias on the measured asymmetries introduced by the acceptance variation can be derived e.g. from eq. (5.22) as:

$$BIAS = \frac{(e_u + e_d) - (e_{c1} + e_{c2})}{8} \tag{5.32}$$

As it is not possible to calculate the bias directly from the data, it can only be estimated by different combinations of the e_i terms in eq. (5.32).
One combination of those e_i terms can be extracted with the false asymmetries from conf$_2$ and conf$_3$ (see sections 5.4.1 and 5.4.2). In section 5.4.5 we showed that, if we use the "double ratio":

$$F(\Phi) = \frac{(N_u^{\uparrow} + N_d^{\uparrow})(N_{c1}^{\uparrow} + N_{c2}^{\uparrow})}{(N_u^{\downarrow} + N_d^{\downarrow})(N_{c1}^{\downarrow} + N_{c2}^{\downarrow})} \approx 1 + [e_u + e_d - (e_{c1} + e_{c2}) + 4\epsilon] \cdot \sin\Phi$$

we get for the estimated "physics" asymmetry $\epsilon_F = \epsilon + [e_u + e_d - (e_{c1} + e_{c2})]/4$.
In the same way we can use the following quantities:

$$X_{\mathrm{conf}_2} = \frac{N_u^{\uparrow} \cdot N_d^{\downarrow}}{N_u^{\downarrow} \cdot N_d^{\uparrow}} \approx 1 + [e_u - e_d] \cdot \sin\Phi \tag{5.33}$$

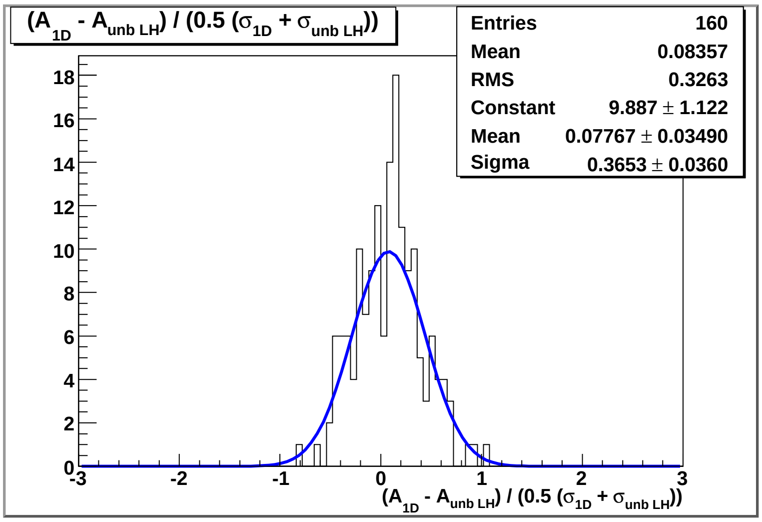

Figure 5.39: *Distribution of the quantity defined in eq. (5.31) to compare the results from the "double ratio" and the unbinned maximum likelihood method.*

$$X_{\mathrm{conf3}} = \frac{N_{c1}^{\downarrow} \cdot N_{c2}^{\uparrow}}{N_{c1}^{\uparrow} \cdot N_{c2}^{\downarrow}} \approx 1 + [e_{c1} - e_{c2}] \cdot \sin\Phi \tag{5.34}$$

to extract the false asymmetries $A^{false}_{\mathrm{conf}_2}$ and $A^{false}_{\mathrm{conf3}}$ and get access to the e_i terms by summing those false asymmetries:

$$A^{false}_{\mathrm{conf}_2} + A^{false}_{\mathrm{conf3}} = \frac{(e_u - e_d) + (e_{c1} - e_{c2})}{4} \tag{5.35}$$

Another method to access the e_i is the calculation of the difference of the two independent measurements of the physics asymmetry from the cell configurations conf_0 and conf_1 (see section 5.4.1). Analog as for ϵ_F in section 5.4.5 and as in eq. (5.33) and (5.34) the two independent physics asymmetries A_{conf_0} and A_{conf_1} can be extracted from the corresponding "double ratios":

$$F_{\mathrm{conf}_2} = \frac{N_u^{\uparrow} \cdot N_{c1}^{\uparrow}}{N_u^{\downarrow} \cdot N_{c1}^{\downarrow}} \approx 1 + [e_u - e_{c1}] \cdot \sin\Phi \tag{5.36}$$

$$F_{\mathrm{conf3}} = \frac{N_d^{\uparrow} \cdot N_{c2}^{\uparrow}}{N_d^{\downarrow} \cdot N_{c2}^{\downarrow}} \approx 1 + [e_d - e_{c2}] \cdot \sin\Phi \tag{5.37}$$

as:

$$A_{\mathrm{conf}_0} = \epsilon + \frac{1}{4}(e_u - e_{c1}), \quad A_{\mathrm{conf}_1} = \epsilon + \frac{1}{4}(e_d - e_{c2}) \tag{5.38}$$

The difference of the asymmetries gives then another combination of the e_i:

$$A_{\mathrm{conf}_0} - A_{\mathrm{conf}_1} = \frac{e_u - e_d - e_{c1} + e_{c2}}{4} \tag{5.39}$$

As estimators of the systematic errors we use the quantities b_i^{FA} and b_i^{conf} defined as $b_i^{FA} = \frac{|A^{false}_{\mathrm{conf}_2} + A^{false}_{\mathrm{conf3}}|}{2}$ and $b_i^{conf} = \frac{|A_{\mathrm{conf}_0} - A_{\mathrm{conf}_1}|}{2}$ in the i^{th} x bin. b_i^{FA} and b_i^{conf} are variations in units

Collins		
	$h+$	$h-$
W25/26	0.56	1.30
W27/28	0.89	0.46
W30/31	0.72	1.10
W39/40	1.03	0.70
W41/42-1	1.04	1.30
W42-2/43	0.76	0.92

Sivers		
	$h+$	$h-$
W25/26	0.93	0.98
W30/31	0.97	0.55
W39/40	0.83	0.66
W42-2/43	0.65	0.70

Table 5.7: *Systematic errors in unit of the statistical errors for Collins (left) and Sivers (right) estimated with the false asymmetries from the cell configurations* conf_2 *and* conf_3.

of the statistical errors σ_i. Therefore we get for the two estimations the systematic errors in unit of the statistical ones by a weighted mean of the ratio $\frac{b_i^{FA}}{\sigma_i}$ and $\frac{b_i^{conf}}{\sigma_i}$, respectively:

$$\frac{\sigma_{sys}}{\sigma_{stat}} = \frac{\sum_i \left(\frac{b_i^{FA/conf}}{\sigma_i}\right) \frac{1}{\sigma_i^2}}{\sum_i \frac{1}{\sigma_i^2}} \tag{5.40}$$

The systematic errors obtained by using b_i^{FA} of the estimation from the false asymmetries are shown in table 5.7 and those obtained by using b_i^{conf} of the estimation from the physics asymmetries in table 5.8. To be on the safe side as values for the systematic errors from the acceptance variation always the larger one of both values was taken. The corresponding values are given in table 5.9. For the error on the Sivers asymmetries for positive hadrons in W30/31 this final value includes also the contributions from the test of splitting the periods into two parts (see 5.4.3) and the test with the acceptance cut (see 5.4.5), which were added in quadrature.
The decision to take for the systematic errors always the larger one of both estimations has the consequence that the values given in table 5.9 are the maximum possible errors. In the meanwhile there have been new efforts by the COMPASS collaboration to get a more precise estimation, which would reduce further the systematic errors. As those considerations were not finalized in the time of writing of this work, they are not further explained here.

Final Systematic Error from Acceptance Variation

As final systematic error for the Collins and the Sivers asymmetries, respectively, the mean value of the values over the periods used in the analysis was taken.
Therefore those errors are: 0.9 σ_{stat} for Collins, positive hadrons, 1.1 σ_{stat} for Collins, negative hadrons, 1.3 σ_{stat} for Sivers, positive hadrons and 0.8 σ_{stat} for Sivers, negative hadrons.

Collins		
	$h+$	$h-$
W25/26	0.84	0.61
W27/28	0.57	0.69
W30/31	0.75	0.66
W39/40	0.75	0.80
W41/42-1	0.48	0.73
W42-2/43	0.95	1.10

Sivers		
	$h+$	$h-$
W25/26	1.30	0.63
W30/31	0.75	0.73
W39/40	0.80	0.70
W42-2/43	1.30	0.41

Table 5.8: *Systematic errors in unit of the statistical errors for Collins (left) and Sivers (right) estimated with the physics asymmetries from the cell configurations* conf_0 *and* conf_1.

Collins		
	$h+$	$h-$
W25/26	0.84	1.30
W27/28	0.89	0.69
W30/31	0.75	1.10
W39/40	1.03	0.80
W41/42-1	1.04	1.30
W42-2/43	0.95	1.10

Sivers		
	$h+$	$h-$
W25/26	1.30	0.98
W30/31	1.44	0.73
W39/40	0.83	0.70
W42-2/43	1.30	0.70

Table 5.9: *Systematic errors from acceptance variation in unit of the statistical errors for Collins (left) and Sivers (right) taking the maximum of the two estimations from false and physics asymmetries. For Sivers asymmetries for positive hadrons in W30/31 this value includes also the contributions from the test of splitting the periods into two parts (see 5.4.3) and the test with the acceptance cut (see 5.4.5).*

Collins		
	error	
systematic effect	$h+$	$h-$
estimator for extraction of asymmetries (unit of σ_{stat})	0.15 σ_{stat}	0.15 σ_{stat}
acceptance variations (unit of σ_{stat})	max: 0.9 σ_{stat}	max: 1.1 σ_{stat}
period compatibility (unit of final asymmetry)	0	0
target polarization (unit of final asymmetry)	0.05	0.05
Sivers		
	error	
systematic effect	$h+$	$h-$
estimator for extraction of asymmetries (unit of σ_{stat})	0.15 σ_{stat}	0.15 σ_{stat}
acceptance variations (unit of σ_{stat})	max: 1.3 σ_{stat}	max: 0.8 σ_{stat}
period compatibility (unit of final asymmetry)	0.01	0
target polarization (unit of final asymmetry)	0.05	0.05

Table 5.10: *Contributions to the systematic error for Collins (top) and Sivers (bottom) asymmetries. For the contribution from the acceptance variations it has to be mentioned that the values given are an estimation of the maximum error.*

That means that in all cases the systematic error is very close to the respective statistical error.

5.5 Overall Systematic Error

The systematic error of the target polarization we estimated as 5% corresponding to a conservative assumption.
The various contributions to the systematic error for the Collins and Sivers asymmetries can be seen in table 5.10. For the contribution from the acceptance variations it has to be mentioned that the values given are an estimation of the maximum error. If we consider this the overall systematic errors, for which the various contributions have to be added in quadrature, are similar to the statistic errors.
The systematic errors are illustrated in fig. 5.40 for Collins and fig. 5.41 for Sivers. The semi-difference between the first and the second part of the 2007 run (see section 5.4.3) for each data point is drawn as a yellow band in these figures.
Beside calculating the weighted mean of the asymmetries only with the statistical errors as done before (see section 5.3.3) in addition a weighted mean taking also the systematic errors obtained for each period (table 5.9) into account by adding them in quadrature was performed. As can be seen in fig. 5.40 and 5.41 there is not a large difference between both methods to calculate the weighted mean. The overall systematic error for each bin is then obtained by $\sigma_{sys,\,tot} = \sqrt{\sigma^2_{mean} - \sigma^2_{stat}}$ shown as a blue band in these figures.

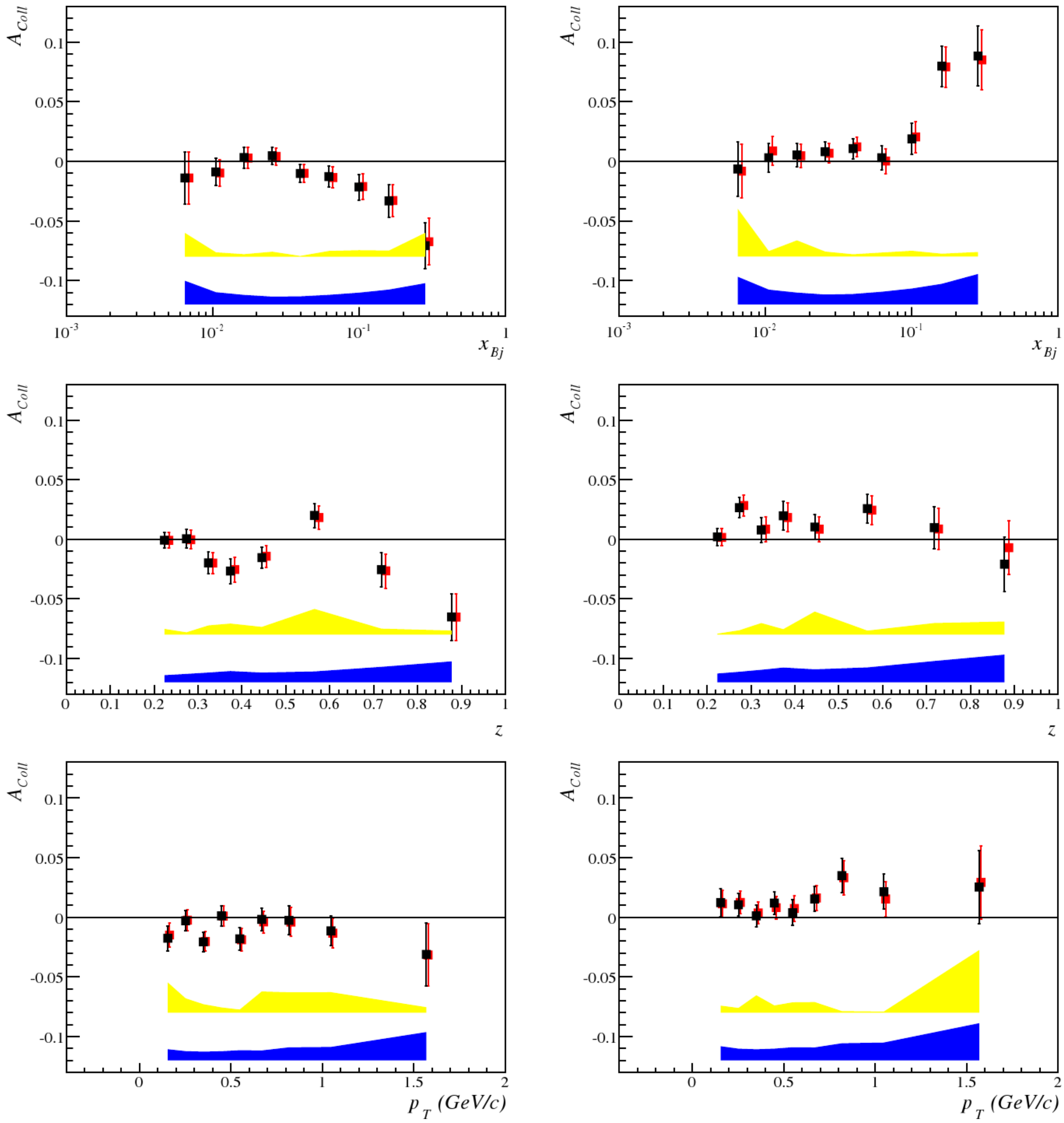

Figure 5.40: *Systematic errors of the Collins asymmetries: Left: positive hadrons, right: negative hadrons. The mean of the asymmetries vs. x, z and P_T^h over the periods weighted with the statistical errors as in section 5.3.3 are given by the red points, the mean of the asymmetries taking into account also the systematic errors from acceptance variation for each period are given by the black points. The yellow band illustrates the error given by the semi-difference between the first and the second part of the 2007 run. The blue band shows the overall systematic error obtained for each bin by $\sigma_{sys,\,tot} = \sqrt{\sigma^2_{mean} - \sigma^2_{stat}}$. Remark: In this plot the asymmetries from another analysis at COMPASS are shown, which may have minimal deviations to the asymmetries presented in this work.*

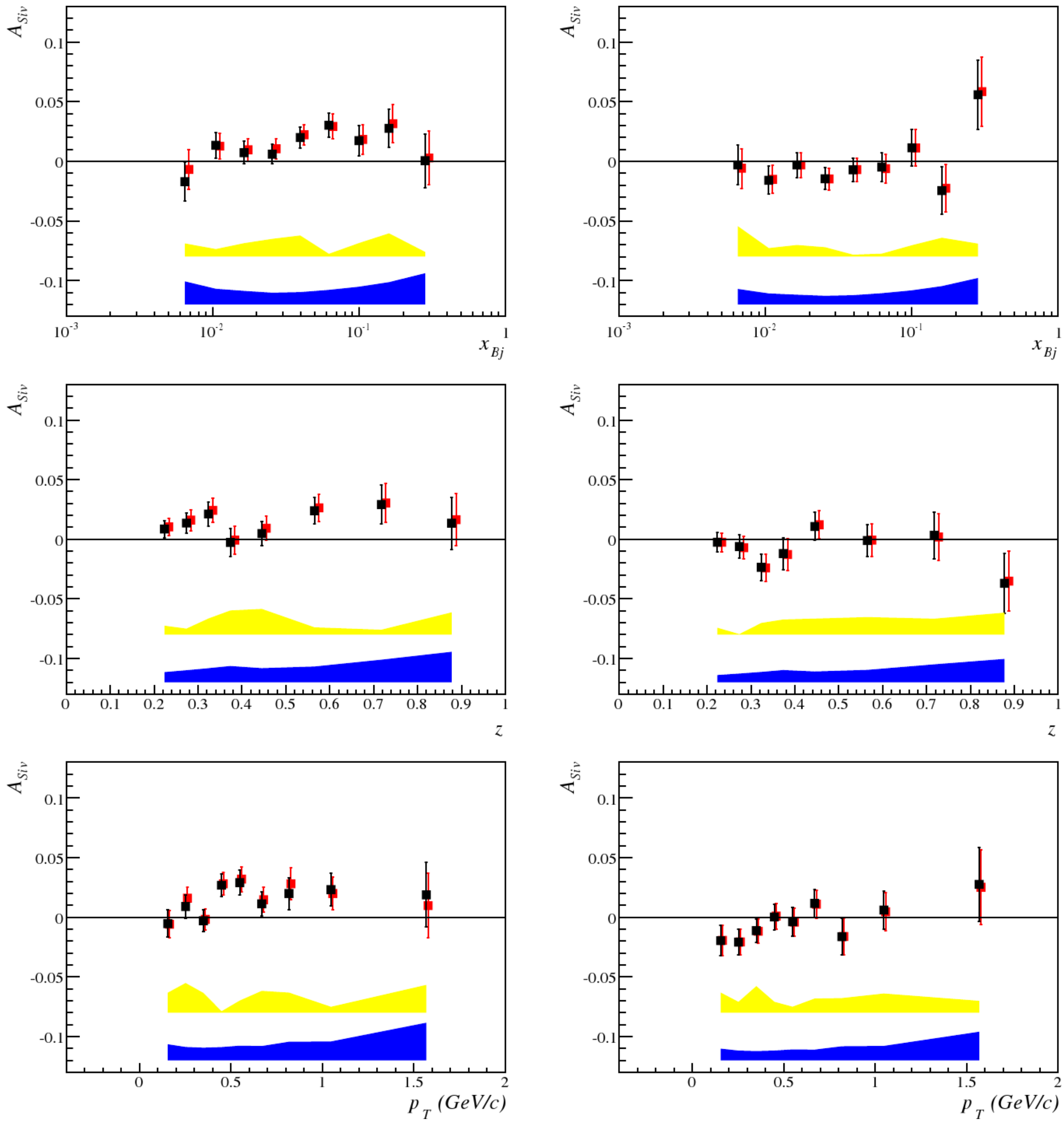

Figure 5.41: *Systematic errors of the Sivers asymmetries: Left: positive hadrons, right: negative hadrons. The mean of the asymmetries vs. x, z and P_T^h over the periods weighted with the statistical errors as in section 5.3.3 are given by the red points, the mean of the asymmetries taking into account also the systematic errors from acceptance variation for each period are given by the black points. The yellow band illustrates the error given by the semi-difference between the first and the second part of the 2007 run. The blue band shows the overall systematic error obtained for each bin by $\sigma_{sys,\,tot} = \sqrt{\sigma^2_{mean} - \sigma^2_{stat}}$. Remark: In this plot the asymmetries from another analysis at COMPASS are shown, which may have minimal deviations to the asymmetries presented in this work.*

Chapter 6

Interpretation of the Results

A good scientific theory should be explicable to a barmaid.

E. Rutherford (1871-1937),
British-New Zealand physicist,
Nobel Prize 1908

In this chapter an interpretation of the COMPASS results for Collins and Sivers asymmetries on deuteron (see section 2.6 for the charged hadrons and chapter 4 for K^0) and proton (see chapter 5) as well as a comparison of the proton results of COMPASS with those of HERMES is given. Furthermore the results are compared to theoretical models. Particulary the results of the first extraction of the transversity distribution functions based on the COMPASS deuteron, the HERMES proton and the BELLE e^+e^- annihilation results are shown as well as those of the first extraction of the Sivers distribution functions with the COMPASS deuteron and the HERMES proton data.
Only with the combined deuteron and proton data it is possible to do a flavor separation and to get therefore access to the transversity and to the Sivers functions of the u and d quarks, separately. Because COMPASS has meanwhile measured both, proton and deuteron data, it is also possible to extract the Sivers functions only from COMPASS data and the transversity functions by using only COMPASS data and the independent information from BELLE on the Collins fragmentation function.

6.1 Collins Asymmetry

The result that the Collins asymmetries on a deuteron target are small (see section 2.6 and chapter 4) was expected, because it was assumed to have an opposite contribution from u and d quarks, which should cause a large cancelation in the case of an isoscalar deuteron target in the kinematical region of COMPASS. Nevertheless there was no clear expectation that the Collins asymmetries on the deuteron target are even compatible with zero.

Contrary to this as shown in chapter 5 the COMPASS experiment has measured a signal for the Collins asymmetry of charged hadrons on the proton target, visible for large $x > 0.05$, in the valence quark region, while for small x the asymmetries are compatible with zero. For z and P_T^h a negative tendency of the asymmetry values for positive hadrons and a positive tendency for those for negative hadrons can be seen. To check the z and P_T^h dependance an event subsample with $x > 0.05$ was selected. The result is shown in fig. 6.1: The signal is now more visible and there seems not to be an obvious dependence on z or P_T^h.
To extract the transversity distribution function for u and d quarks it is necessary to have both, data on deuteron and proton. Before the 2007 measurement of COMPASS on a proton target the HERMES collaboration had measured a non-zero Collins asymmetry on the proton meaning that the transversity distribution (here: $\Delta_T u$ because of u quark dominance in the target) as well as the Collins mechanism with its fragmentation function (here: $\Delta_T^0 D_u^h(z)$) are existing and non-zero [46]. Independently also the results of the Belle collaboration, which has measured a non-zero Collins fragmentation function in e^+e^- annihilation, give evidence for the Collins effect [51].
To compare the COMPASS results on the proton target with those of HERMES the different definitions of the Collins angle $\Phi_{Coll}^{COMPASS} = -\Phi_{Coll}^{HERMES}$ have to be taken into account. It also has to be mentioned that the two experiments have different kinematic ranges (x, y), which results also in a different depolarization factor $D_{NN}(y)$. While in the COMPASS analysis the term D_{NN} was factorized out during the extraction of the asymmetries (see section 4.3.3 and 5.3.3), which was not done in the analysis of HERMES.
For the comparison of the asymmetries as a function of z and P_T^h the COMPASS data cut at $x > 0.05$ are more suitable, because therefore the kinematical region of the HERMES data is largely covered. As can be seen in fig. 6.1 the COMPASS results confirm the previous results by HERMES. The sign as well as the size of the asymmetries are comparable with those of HERMES despite the difference in the kinematical region.
From Collins asymmetries in the production of charged and neutral kaons it is in principle possible to get informations about the s quark and $\bar{s}$ antiquark transversity. The results on the proton target for charged kaons shown in fig. 6.2 for COMPASS and HERMES are more difficult to compare and to interprete due to the large error bars. (Again the results of HERMES have the opposite sign in the figure because of the definition of the Collins angle.) While the COMPASS data show in x a negative trend for K^+ and a small positive trend for K^- going for both in the same direction as for the charged pions, the K^+ asymmetries from the HERMES measurements are tentatively positive and those for K^- tentatively negative (with the definition of Φ_{Coll} from COMPASS).
Beside the large statistical errors also the purity of the charged kaon samples has to be taken into account. It is possible that the trends in the COMPASS data are amplified by impurities from pions in the kaon samples. For the purity of the samples see fig. 5.15.
For the interpretation of the Collins asymmetries from kaon production also the quark

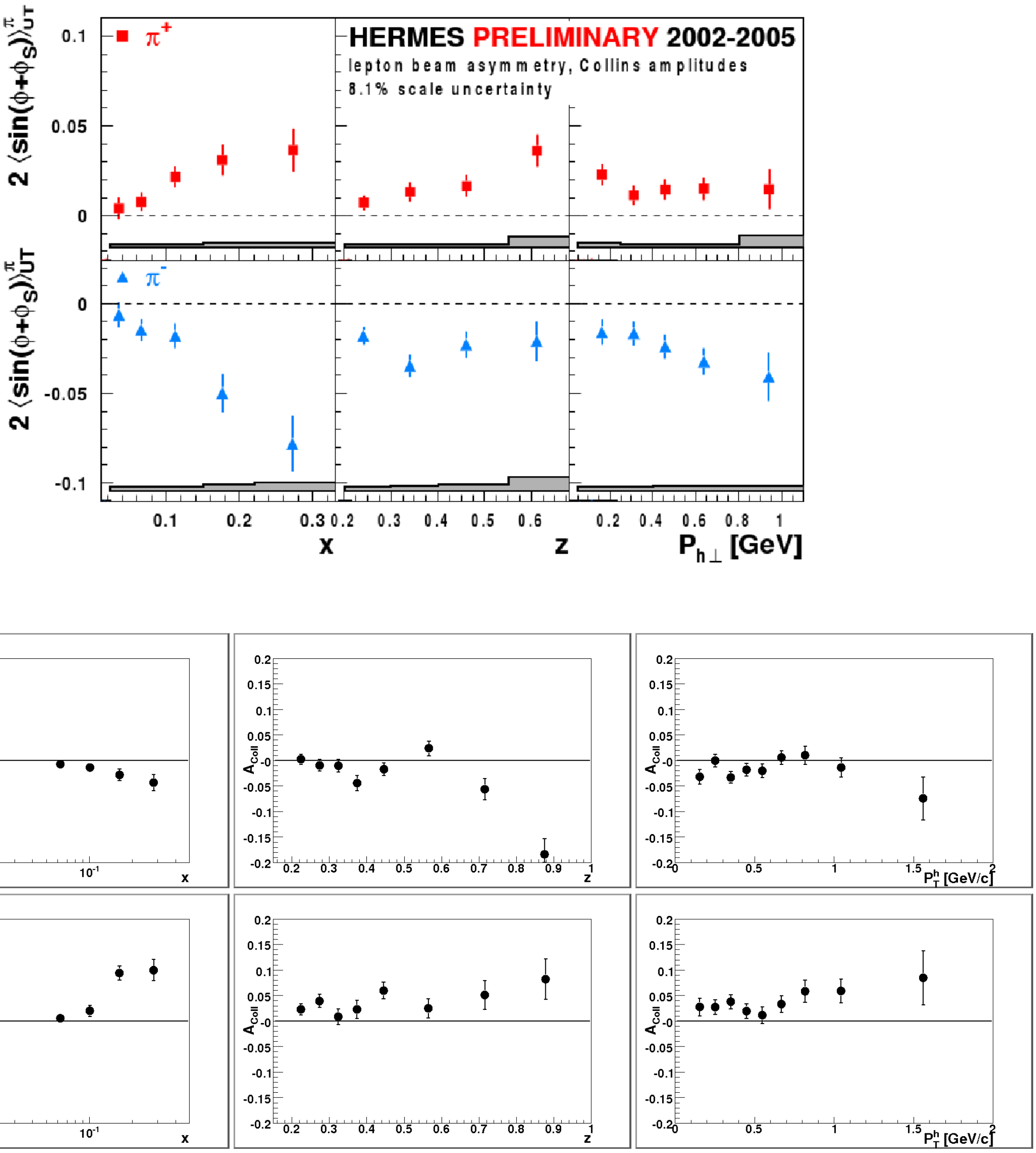

Figure 6.1: *Top: Collins asymmetries for charged and neutral pions from a proton target at HERMES [46]. Bottom: Collins asymmetries for positive (upper row) and negative (lower row) unidentified hadrons as function from x, z and P_T^h from a proton target at COMPASS. Only statistical errors are shown. The COMPASS data were cut at $x > 0.05$ (valence quark region) to show better the z and P_T^h dependance and to get a larger overlap with the region of HERMES.*

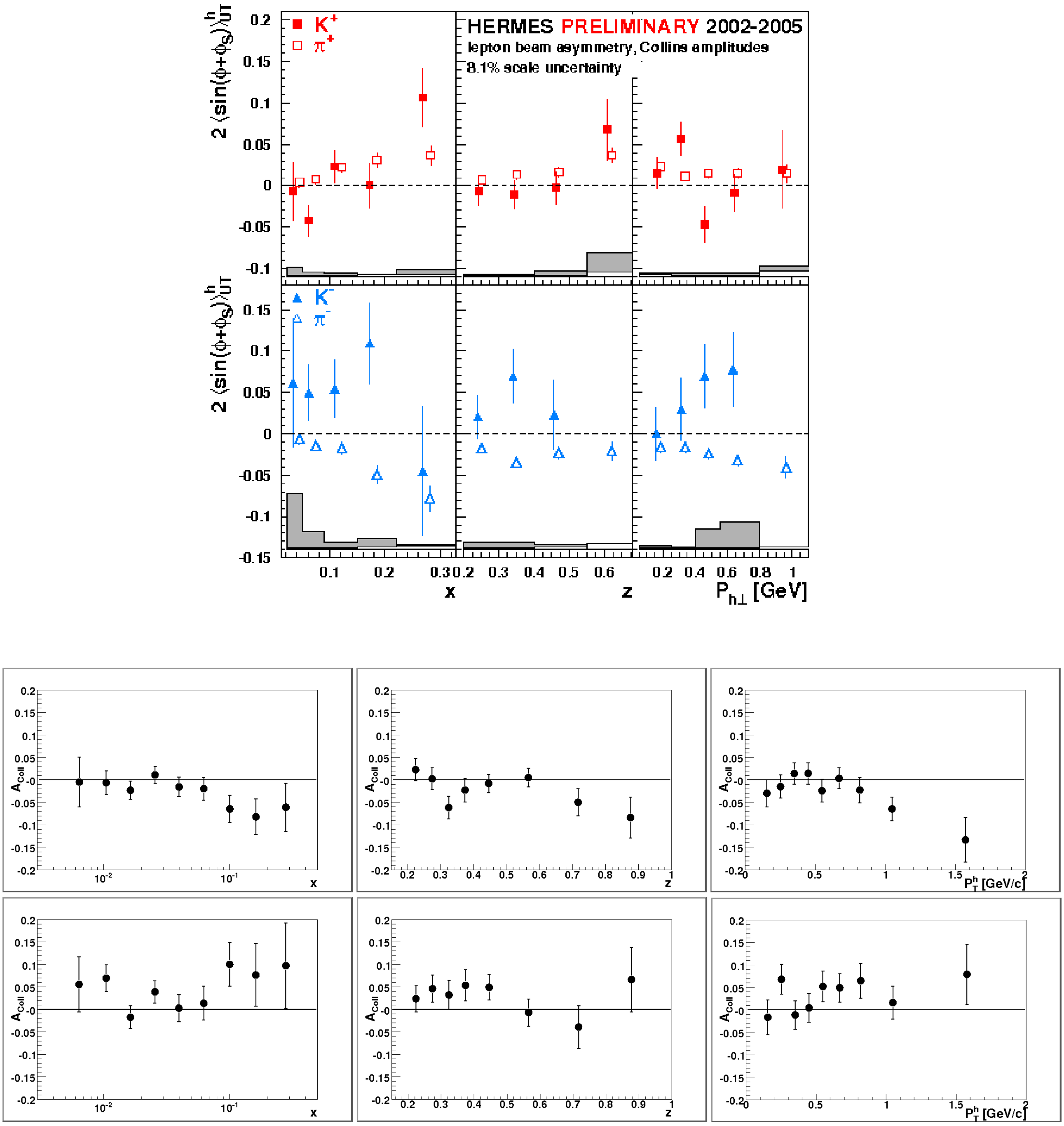

Figure 6.2: *Top: The Collins asymmetries for charged kaons (closed symbols) and charged pions (open symbols) as function of x, z and P_T^h from a proton target at the HERMES experiment [46]. Bottom: The Collins asymmetries for charged kaons (first row: positive, second row: negative) as function of x, z and P_T^h from a proton target at the COMPASS experiment.*

content of the kaons has to be taken into account:

$$\begin{aligned} K^+ = u\bar{s} \quad K^- = \bar{u}s \\ K^0 = d\bar{s} \quad \bar{K^0} = \bar{d}s \end{aligned} \tag{6.1}$$

At COMPASS only K^0_S ($K^0 \hat{=} 50\%\ K^0_S,\ 50\%\ K^0_L$) from the decay channel $K^0_S \rightarrow \pi^+ + \pi^-$ were analyzed (see section 4.2.3) and that therefore it is not possible to distinguish between K^0 and $\bar{K^0}$ in the data.
As the Collins asymmetries for the charged hadrons measured on deuteron by COMPASS are compatible with zero, the result that also the K^0 asymmetries are compatible with zero was expected from isospin symmetry given that the sea quark contributions are small.
The Collins asymmetries for K^0 on a proton target measured at COMPASS are also small and compatible with zero, but are statistically limited.
With the measured asymmetries on the proton target the results on the deuteron target for charged pions in the parton model can be interpreted naïvely in the following way. We consider here only the valence quark region ($0.1 < x < 0.3$) and neglect the sea quark contribution ($\bar{q} = s = 0$ and $\Delta_T\bar{q} = \Delta_T s = 0$). Naming now the unpolarized favored fragmentation function (eq. (2.69)) D_1 and the unpolarized unfavored one (eq. (2.70)) D_2, where $D_1 = D_u^{\pi^+} = D_d^{\pi^-}$ and $D_2 = D_d^{\pi^+} = D_u^{\pi^-}$ and assuming accordingly $\Delta_T^0 D_1 = \Delta_T^0 D_u^{\pi^+} = \Delta_T^0 D_d^{\pi^-}$ and $\Delta_T^0 D_2 = \Delta_T^0 = D_d^{\pi^+} = \Delta_T^0 D_u^{\pi^-}$ we obtain for the Collins asymmetry in eq. (2.93) for π^+ on a proton target:

$$A_{Coll}^{p,\pi^+} \approx \frac{4\Delta_T u_v \Delta_T^0 D_1 + \Delta_T d_v \Delta_T^0 D_2}{4u_v D_1 + d_v D_2} \tag{6.2}$$

and for π^- on proton:

$$A_{Coll}^{p,\pi^-} \approx \frac{4\Delta_T u_v \Delta_T^0 D_2 + \Delta_T d_v \Delta_T^0 D_1}{4u_v D_2 + d_v D_1} \tag{6.3}$$

The PDF[1] parametrizations usually refer to a proton target. Therefore we have to note the following relationships due to isospin symmetry, if we consider a deuteron target:

$$\begin{aligned} u^d(x) = u^p(x) + u^n(x) = u^p(x) + d^p(x) \\ d^d(x) = d^p(x) + d^n(x) = d^p(x) + u^p(x) \end{aligned} \tag{6.4}$$

which means:

$$u^d(x) = d^d(x) = u^p(x) + d^p(x) \tag{6.5}$$

Then we get for the Collins asymmetry in eq. (2.93) for π^+ on a deuteron target:

$$A_{Coll}^{d,\pi^+} \approx \frac{\Delta_T u_v + \Delta_T d_v}{u_v + d_v} \frac{4\Delta_T^0 D_1 + \Delta_T^0 D_2}{4D_1 + D_2} \tag{6.6}$$

and correspondingly for π^-:

$$A_{Coll}^{d,\pi^-} \approx \frac{\Delta_T u_v + \Delta_T d_v}{u_v + d_v} \frac{\Delta_T^0 D_1 + 4\Delta_T^0 D_2}{D_1 + 4D_2} \tag{6.7}$$

[1]PDF: parton distribution function

From the proton data we can deduce that $\Delta_T^0 D_1 \approx -\Delta_T^0 D_2$ (see also below). Together with the information obtained from the unpolarized data $D_2 \approx 0.5 D_1$, $d_v \approx 0.5 u_v$ we get for the asymmetries on proton for π^+ and π^-, respectively, neglecting the d quark transversity contribution:

$$A_{Coll}^{p,\pi^+} \approx \frac{\Delta_T u_v}{u_v} \frac{\Delta_T^0 D_1}{D_1} \tag{6.8}$$

$$A_{Coll}^{p,\pi^-} \approx -\frac{4}{2.5} \frac{\Delta_T u_v}{u_v} \frac{\Delta_T^0 D_1}{D_1} \tag{6.9}$$

and for the asymmetries on deuteron, where the d quark transversity has to be considered:

$$A_{Coll}^{d,\pi^+} \approx \frac{3}{7} \frac{\Delta_T u_v + \Delta_T d_v}{u_v} \frac{\Delta_T^0 D_1}{D_1} \tag{6.10}$$

$$A_{Coll}^{d,\pi^-} \approx -\frac{3}{4.5} \frac{\Delta_T u_v + \Delta_T d_v}{u_v} \frac{\Delta_T^0 D_1}{D_1} \tag{6.11}$$

As we see from eq. (6.5), (6.6) and (6.9), (6.10), respectively, the Collins asymmetry on deuteron is for both, π^+ and π^-, proportional to $\Delta_T u_v + \Delta_T d_v$. The very small Collins asymmetries compatible with zero in the case of the deuteron target are therefore a strong indication that $\Delta_T u_v \approx -\Delta_T d_v$.

Until now there were three different global analyses, which combine the COMPASS deuteron, HERMES proton and BELLE e^+e^- data. The COMPASS proton data have not yet been included.

In the work of Vogelsang and Yuan [74] the HERMES data on proton were fitted with simple parametrizations of the Collins fragmentation function by using the QCD factorization approach for small transverse momenta. The transversity distribution is parametrized by assuming the saturation of the Soffer bound $|\Delta_T q(x)| = (q(x) + \Delta q(x))/2$. Vogelsang and Yuan have considered two scenarios for the favored and unfavored Collins fragmentation functions by two different sets of parametrizations, which always resulted in the relation $\Delta_T^0 D_1 \approx -\Delta_T^0 D_2$. Afterwards the resulting predictions were compared with the published COMPASS deuteron data from 2002 ([48], unidentified leading hadron sample) and show a rather good agreement (see fig. 6.3).

A different approach can be found in the works of Efremov, Goeke and Schweitzer [75, 76]. Here a Gaussian model is assumed for the distribution of the parton transverse momenta and a chiral quark-soliton model for the transversity distribution. The Collins fragmentation function was extracted separately from HERMES SIDIS and Belle e^+e^- annihilation data resulting in a good agreement. The prediction for the COMPASS deuteron data obtained from the fit on the HERMES data is shown to be consistent with the published 2002-04 COMPASS deuteron data for unidentified hadrons [48, 49] (see fig. 6.4).

In the third analysis done by Anselmino et al. [77] for the first time the extraction of the transverse spin distribution function was performed. For this a global fit of HERMES proton, COMPASS deuteron [49] (unidentified hadron sample) and Belle e^+e^- data was performed to extract the Collins fragmentation function and the transversity distribution function for u and d quarks simultaneously.

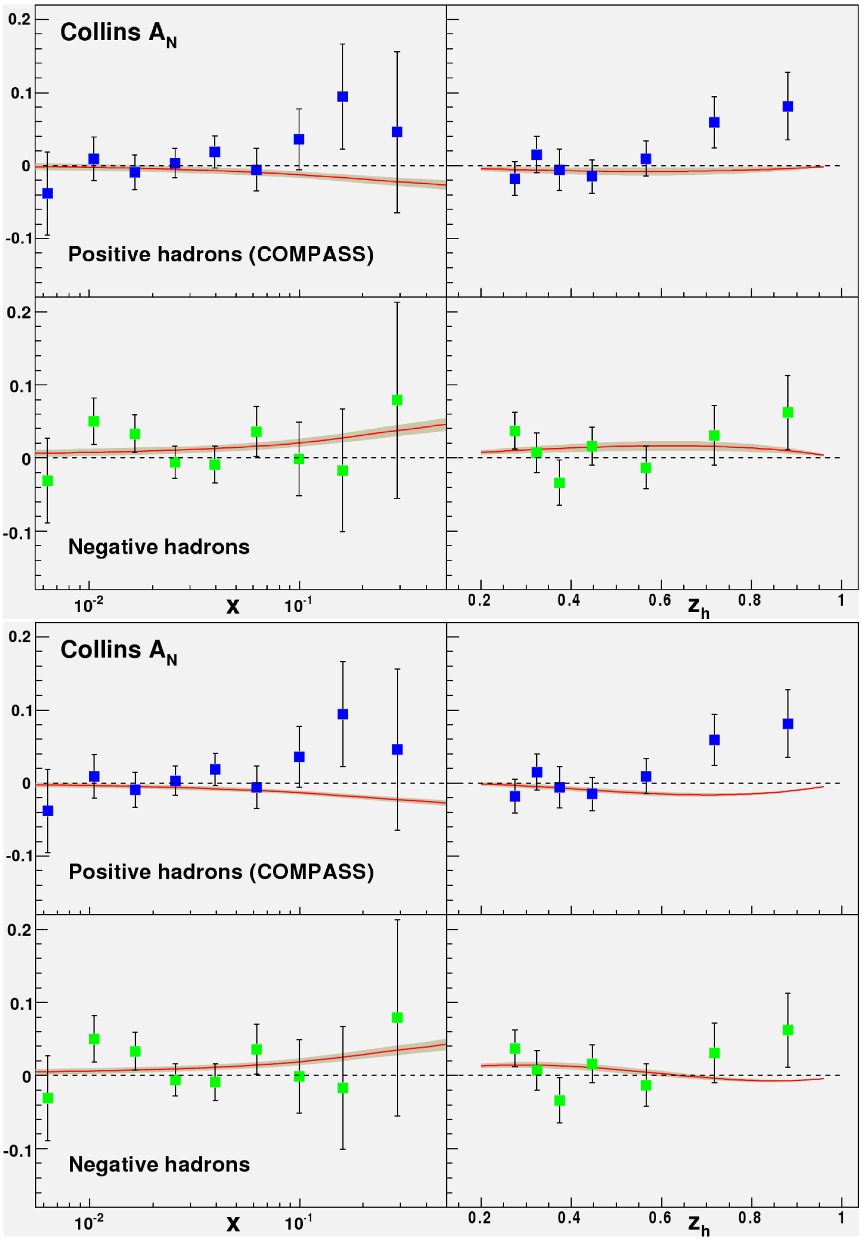

Figure 6.3: *Comparison of the fit in [74] with two different parametrization sets (upper plot: Set I, lower plot: Set II) with the Collins asymmetries from the COMPASS deuteron data from 2002 ([48], unidentified leading hadron sample).*

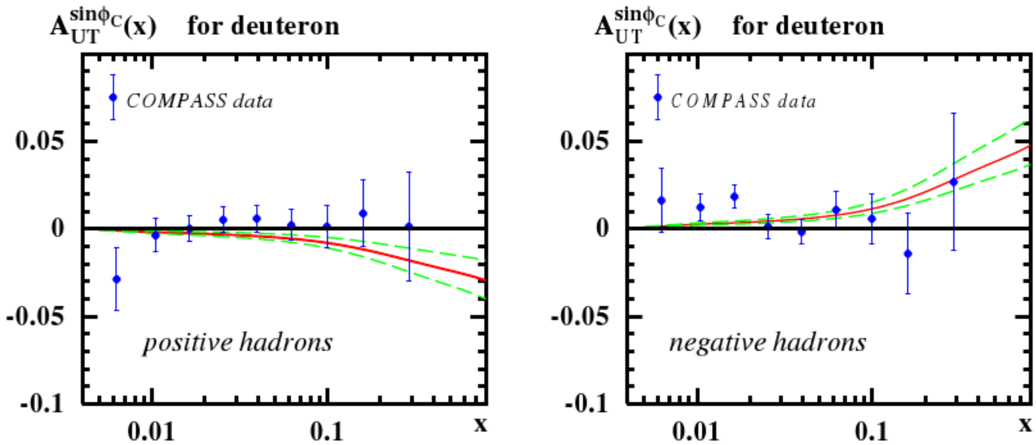

Figure 6.4: *Comparison of the fit in [76] with the Collins asymmetries on deuteron from COMPASS [48, 49].*

A more recent analysis by Anselmino et al. [79] includes the complete HERMES 2002-05 pion sample [46], new Belle data [51] and the COMPASS asymmetries of the identified pion sample published in [50]. It resulted in an improved extraction of the transversity distribution functions. The description of the COMPASS deuteron data by the fit in [79] can be seen in fig. 6.5. Also here good agreement is found within the errors.

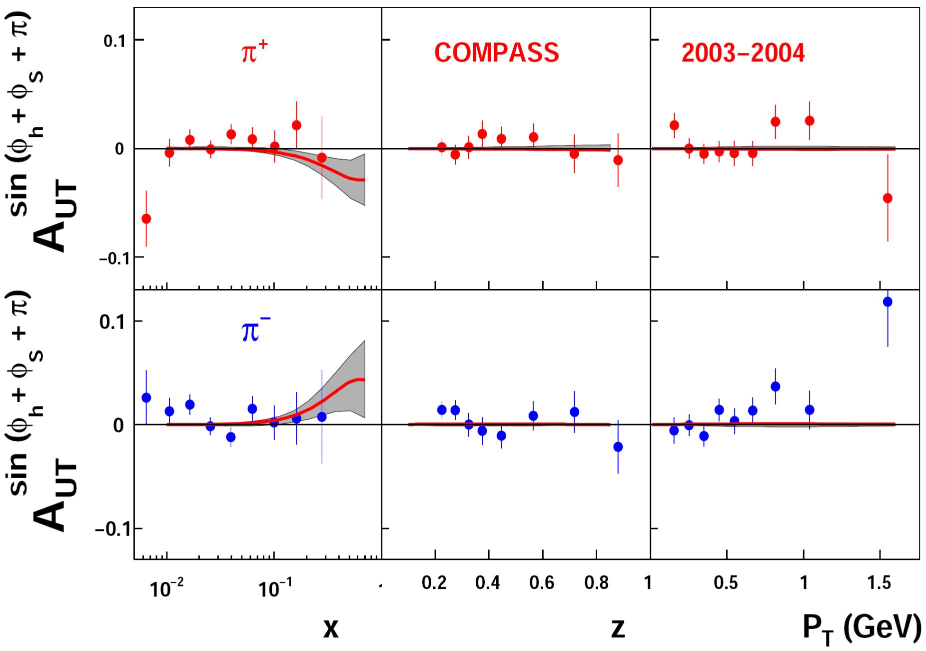

Figure 6.5: *Fit of Anselmino et al. [79] on the COMPASS deuteron data [50]. The shaded area marks the uncertainty in the parameter values.*

The favored and unfavored Collins fragmentation functions $\Delta_T^0 D_1$ and $\Delta_T^0 D_2$ extracted in [79] (named there $\Delta^N D_{fav}$ and $\Delta^N D_{unf}$) are plotted in fig. 6.6 as function of z in the

P_T^h integrated version and as function of P_T^h at a fixed value of z. The positivity bound $|\Delta_T^0 D_{h/q}(z, P_T^h)| \leqq 2D_{h/q}(z, P_T^h)$ is also shown and the Collins fragmentation functions are compared to those extracted in the previous analysis [77]. The obtained transversity dis-

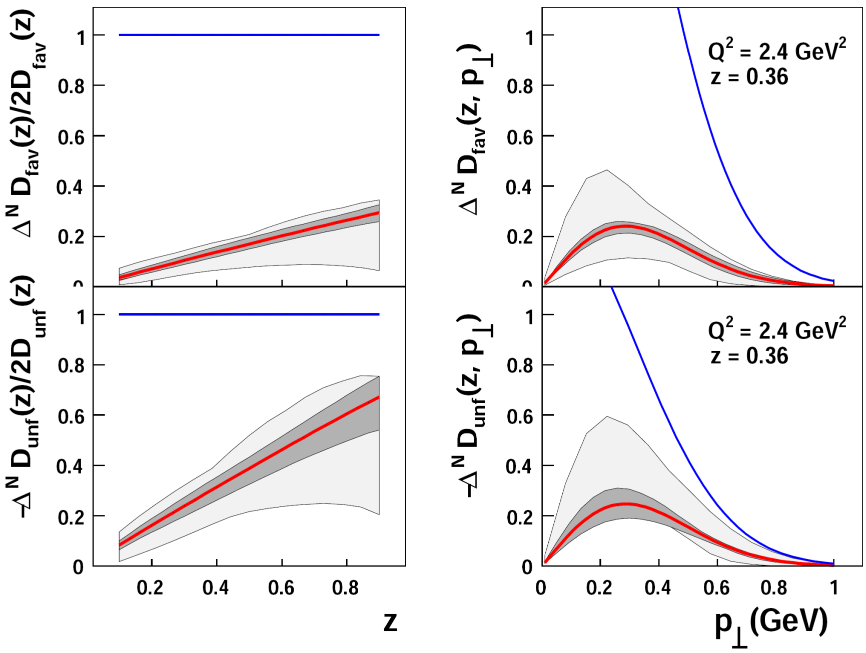

Figure 6.6: *Favored and unfavored Collins fragmentation functions at* $Q^2 = 2.62\,(\mathrm{GeV}/c)^2$ *extracted in [79]. Left: The Collins fragmentation functions normalized to twice the corresponding unpolarized fragmentation functions vs. z. Right: The Collins fragmentation functions vs. P_T^h at a fixed value of z (P_T^h unintegrated version). Also shown is the positivity bound $|\Delta^N D_{h/q^\uparrow}(z, P_T^h)| \leqq 2D_{h/q}(z, P_T^h)$ (upper blue lines). The wider uncertainty band from the previous analysis of Anselmino et al. [77] is also shown. Figure taken from [78].*

tribution functions $\Delta_T u$ and $\Delta_T d$ from [77, 79] are given in fig. 6.7 as a function of x as well as function of k_T at a fixed value of x ($\vec{k}_T$ unintegrated transversity functions). The Soffer bound is shown as blue line and the uncertainty in the parameter values is marked as shaded area. It can be seen that $\Delta_T u$ and $\Delta_T d$ are opposite in sign, that the magnitude of $\Delta_T u$ is larger than that of $\Delta_T d$ and that the absolute value of both transverse distribution functions is significantly smaller than the corresponding Soffer bound.

From the conclusion that the absolute value of $\Delta_T u$ is larger than the one of $\Delta_T d$ one can see the limitation of the naïve interpretation done before, which resulted in $\Delta_T u_v \approx -\Delta_T d_v$. The result of those two global fits was used for predictions for the COMPASS proton data. In fig. 6.8 one can see the comparison of the latest predictions from Anselmino et al. [78] (lower part) with the corresponding COMPASS measurements (upper part). Obviously the data and the predictions agree well within the errors.

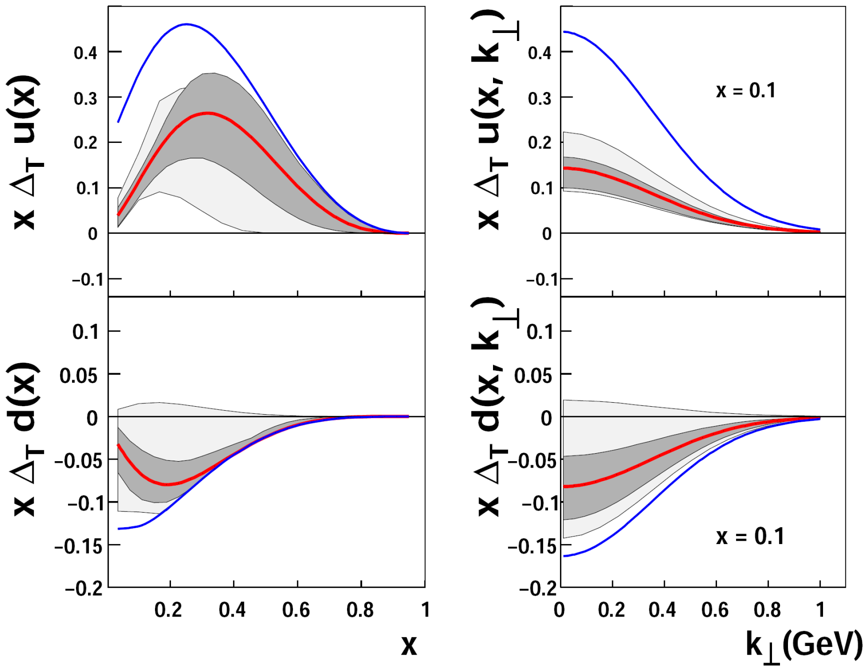

Figure 6.7: *The transversity distribution functions for u and d quarks at Q^2 = $2.62\,(\mathrm{GeV}/c)^2$ extracted from Anselmino et al. [79], on the left-hand side $\Delta_T u$ and $\Delta_T d$ as a function of x, on the right-hand side the $\vec{k}_T$ unintegrated transversity functions as function of k_T at a fixed value of x. The Soffer bound is shown as blue line and the uncertainty in the parameter values is marked as shaded area. The wider uncertainty band is the one of the first extraction from [77].*

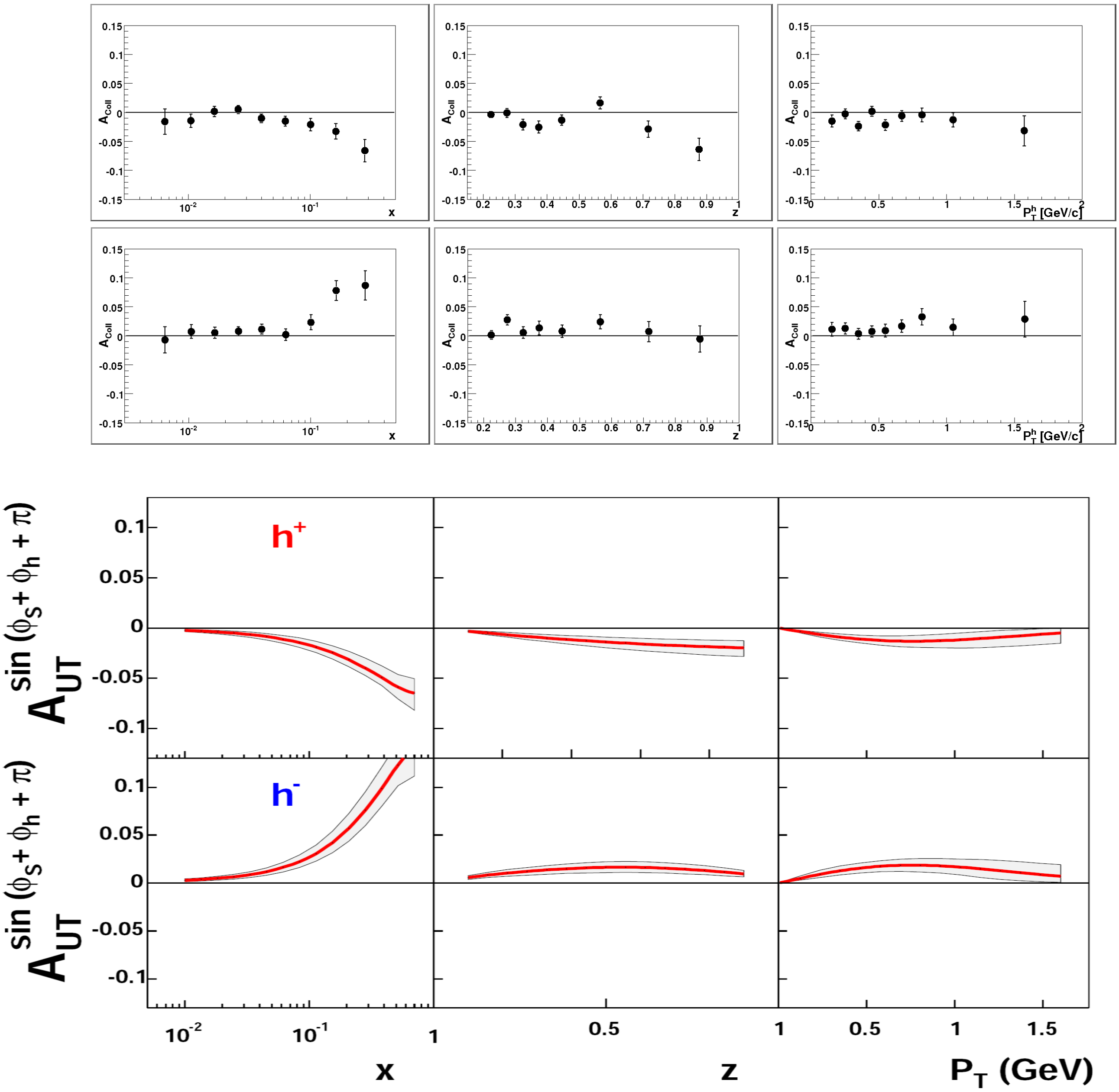

Figure 6.8: *Top: Collins asymmetries for unidentified hadrons on proton from COMPASS. Bottom: The latest predictions of Anselmino et al. [78] for those measurements.*

6.2 Sivers Asymmetry

As shown in section 2.6 and chapter 4 the Sivers asymmetries measured by COMPASS on the deuteron target are very small and compatible with zero, similar as the Collins asymmetries.
On a proton target HERMES has obtained a positive Sivers asymmetry for π^+ and a very small asymmetry, consistent with zero, for π^-. Compared to those results the asymmetries measured at the COMPASS 2007 run on the proton target (chapter 5) for Sivers are smaller than expected in the case of π^+, but inside the statistical error bars not in contradiction to the HERMES ones. For π^- the COMPASS Sivers asymmetries on proton confirm the results of HERMES. The comparison is shown in fig. 6.9. It has to be noted here that for the comparison of the Sivers asymmetries between COMPASS and HERMES on proton a correction like for the Collins asymmetry (see section 6.1) is not necessary, because for Sivers $D_{NN} = 1$ (see eq. (2.101)).
Also in the case of the Sivers effect it is in principle possible to get informations about the s and $\bar{s}$ Sivers function from the corresponding asymmetries in the production of charged and neutral kaons. The results for positive kaons from a proton target show in the COMPASS measurements a slight tendency to positive values, but are smaller than the asymmetries measured by HERMES, while for negative kaons the results of both experiments, HERMES and COMPASS, are compatible with zero as the asymmetries for π^- are (see fig. 6.10). Of course also for Sivers the COMPASS results for charged kaons are limited by the large errors.
For K^0 production the result that the Sivers asymmetries on deuteron are compatible with zero is again in agreement with the expectation from isospin symmetry coming from the fact that the Sivers asymmetries measured by COMPASS on deuteron for the charged hadrons are compatible with zero and assuming that the sea quark contributions are small. On the proton target the K^0 Sivers asymmetries measured at COMPASS were also small and compatible with zero, but also those results are limited due to the small statistics.
Analog to the Collins case a naïve consideration outgoing from the Sivers asymmetry in eq. (2.100) is possible. Restricting us to the valence region, neglecting the sea quark contribution ($\bar{q} = s = 0$ and $\Delta_0^T \bar{q} = \Delta_0^T s = 0$) and taking the definition $D_1 = D_u^{\pi^+} = D_d^{\pi^-}$ and $D_2 = D_d^{\pi^+} = D_u^{\pi^-}$ from section 6.1, we get for the Sivers asymmnetry in eq. (2.100) for π^+ on a proton target:

$$A_{Siv}^{p,\pi^+} \approx \frac{4\Delta_0^T u_v D_1 + \Delta_0^T d_v D_2}{4u_v D_1 + d_v D_2} \tag{6.12}$$

and for π^- on proton:

$$A_{Siv}^{p,\pi^-} \approx \frac{4\Delta_0^T u_v D_2 + \Delta_0^T d_v D_1}{4u_v D_2 + d_v D_1} \tag{6.13}$$

For PDF parametrizations refering to a proton target (as in section 6.1) we obtain for the Sivers asymmetry for π^+ on a deuteron target:

$$A_{Siv}^{d,\pi^+} \approx \frac{\left(\Delta_0^T u_v + \Delta_0^T d_v\right)(4D_1 + D_2)}{(u_v + d_v)(4D_1 + D_2)} = \frac{\Delta_0^T u_v + \Delta_0^T d_v}{u_v + d_v} \tag{6.14}$$

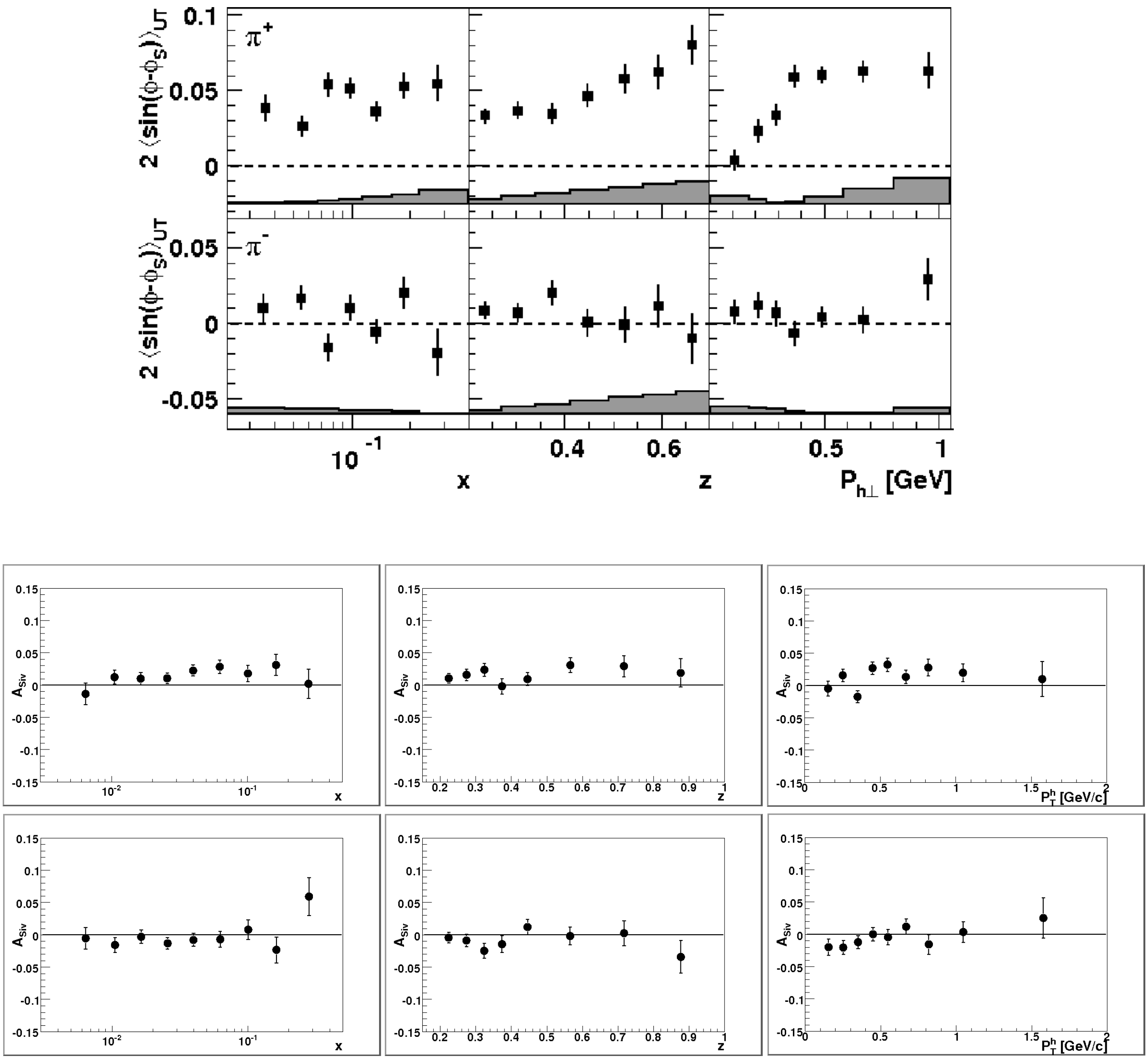

Figure 6.9: *Top: The Sivers asymmetries for charged pions (first row: positive, second row: negative) as function of x, z and P_T^h from a proton target at the HERMES experiment [46]. Bottom: The Sivers asymmetries for unidentified charged hadrons (first row: positive, second row: negative) as function of x, z and P_T^h from a proton target at the COMPASS experiment.*

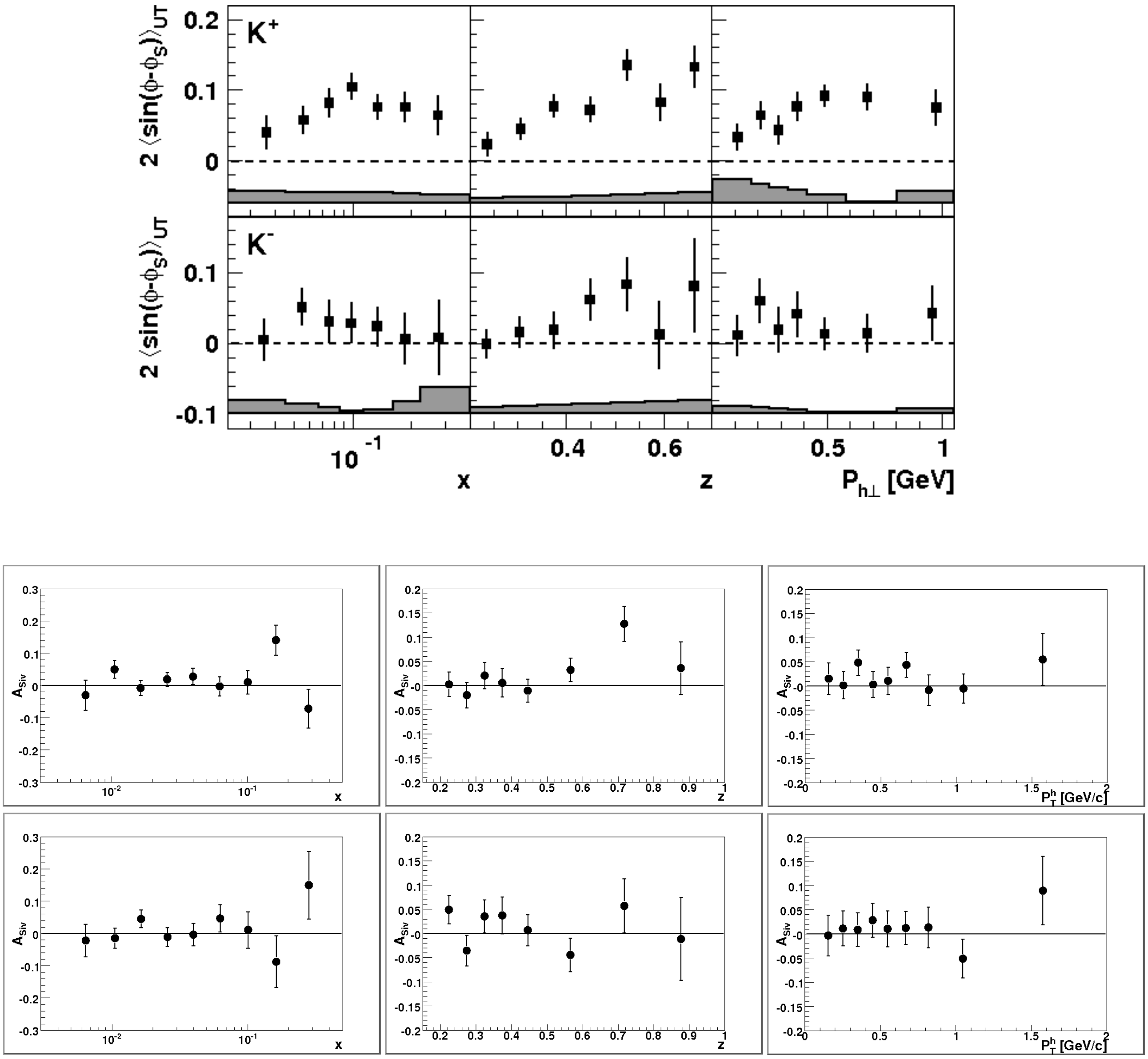

Figure 6.10: *Top: The Sivers asymmetries for charged kaons (first row: positive, second row: negative) as function of* x*,* z *and* P_T^h *from a proton target at the HERMES experiment [46]. Bottom: The Sivers asymmetries for charged kaons (first row: positive, second row: negative) as function of* x*,* z *and* P_T^h *from a proton target at the COMPASS experiment.*

and for π^-:

$$A_{Siv}^{d,\pi^-} \approx \frac{\left(\Delta_0^T u_v + \Delta_0^T d_v\right)(4D_2 + D_1)}{(u_v + d_v)(4D_2 + D_1)} = \frac{\Delta_0^T u_v + \Delta_0^T d_v}{u_v + d_v} \tag{6.15}$$

This means that $A_{Siv}^{d,\pi^+} \approx A_{Siv}^{d,\pi^-}$. From the approximately zero asymmetries on the deuteron data at COMPASS we get:

$$\Delta_0^T d_v \approx -\Delta_0^T u_v \tag{6.16}$$

By using again the information $D_2 \approx 0.5D_1$ and $d_v \approx 0.5u_v$ it is possible to simplify the Sivers asymmetries on proton for π^+ neglecting the d quark Sivers function (because the ratio of the quark contributions in this equation is $u : d \approx 4 : 1$) as:

$$A_{Siv}^{p,\pi^+} \approx \frac{\Delta_0^T u_v}{u_v} \tag{6.17}$$

and correspondingly for π^-, where the ratio between the u and d quark contributions is $2 : 1$ and therefore not neglectible:

$$A_{Siv}^{p,\pi^-} \approx \frac{2\Delta_0^T u_v + \Delta_0^T d_v}{2.5u_v} \tag{6.18}$$

As the HERMES as well as the COMPASS experiment have measured on a proton target a Sivers asymmetry for π^- of about zero, we can conclude:

$$\Delta_0^T d_v \approx -2\Delta_0^T u_v \tag{6.19}$$

which is a clear difference to eq. (6.16) obtained from the COMPASS deuteron data. Therefore we can conclude that this naïve consideration is not sufficient to describe the data and a global analysis of all available data is needed also for the Sivers effect.

Several of such global analysis were performed combining the HERMES proton and the COMPASS deuteron Sivers asymmetries. The newer COMPASS asymmetries on the proton could not yet be considered.

In the work [74] by Vogelsang and Yuan already mentioned the QCD factorization approach at small transverse momenta was used and a simple fit on the HERMES data for the Sivers functions of u and d quarks was performed. The very well working fit resulted in $\Delta_0^T d_v \approx -\Delta_0^T u_v$. From the fit results the expected Sivers asymmetries for π^+ and π^- on deuteron were calculated for the kinematic region of COMPASS and compared afterwards with the published 2002 results from COMPASS [48]. As can be seen in fig. 6.11 there is a rather good agreement.

The group of Collins, Efremov et al. used for their extraction of the Sivers function from the HERMES data a simple Gaussian model for the distribution of parton transverse momenta in the Sivers function [80]. They show also that their results are consistent with the COMPASS deuteron asymmetries near to zero (see fig. 6.12).

The first extraction of the Sivers functions of the u and d quarks by a common fit to both, HERMES proton (for charged pion production [83]) and COMPASS deuteron asymmetries

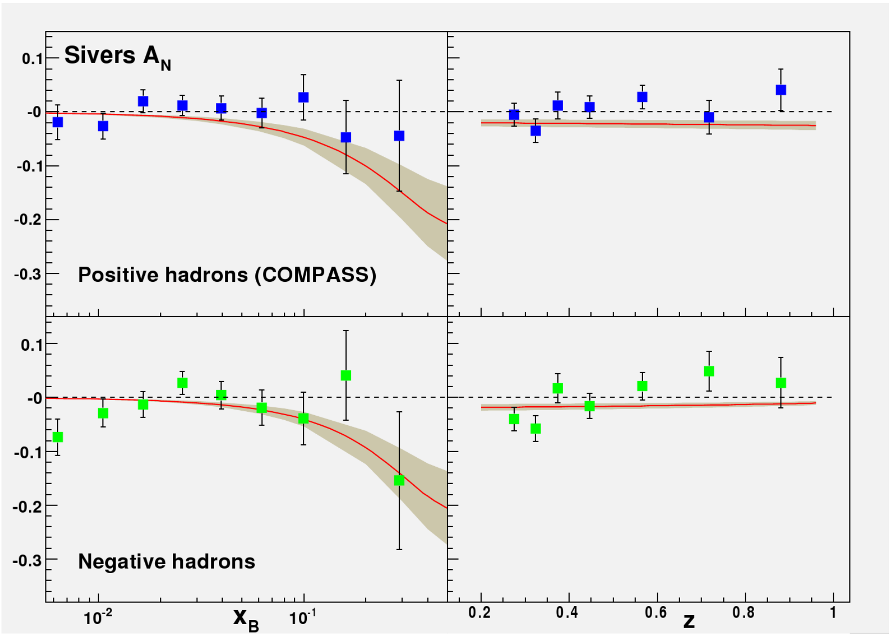

Figure 6.11: *Comparison of the fit in [74] with the Sivers asymmetries from the COMPASS deuteron data from 2002 ([48], unidentified leading hadron sample).*

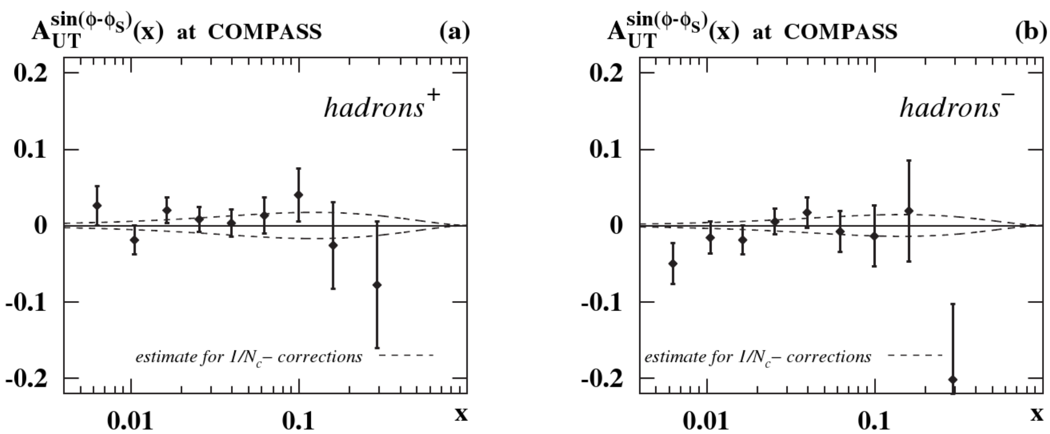

Figure 6.12: *Comparison of the estimation in [80] (dashed line) with the Sivers asymmetries from COMPASS on deuteron.*

(unidentified charged hadrons [48]), was done by Anselmino et al. [81]. This analysis was performed within the leading order (LO) parton model using unintegrated parton distribution and fragmentation functions.

In a more recent analysis by Anselmino et al. [82] the asymmetries for identified hadrons (pions and kaons) of the HERMES proton [46] and COMPASS deuteron data [50] (see fig. 6.13) were fitted and the Sivers functions for quarks/antiquarks with flavors u, d, s, $\bar{u}$, $\bar{d}$, $\bar{s}$ were extracted. The COMPASS data of the K^0 production were not included in this global fit, because the corresponding fragmentation functions are not so well known and have to be taken from those for $K^{\pm}$ applying further assumptions. Instead of this the Sivers asymmetry for K^0 is estimated by using all Sivers functions extracted from all other data and assuming exact $SU(2)$ invariance to get the fragmentation functions for K^0.

The Sivers functions obtained are shown in fig. 6.14[2].

From the global fit in [82] also predictions for the COMPASS Sivers asymmetries on the proton target were performed (see fig. 6.15). As already mentioned the measured asymmetries are for positive hadrons lower than the expected ones, while for negative ones they are compatible with zero as it was predicted. For K^0 the expectation that the Sivers asymmetries are compatible with zero was confirmed, but as mentioned this result is still limited by the large error bars.

A second common fit to HERMES proton and COMPASS deuteron data for identified hadrons (without the COMPASS K^0 data) together was done by Arnold et al. [84]. The fit, which was performed vs. x, can be seen for the COMPASS data in fig. 6.16, where in addition the predictions for the COMPASS deuteron asymmetries vs. z are shown. The extracted Sivers functions are given in fig. 6.17.

The expectations from this global fit in [84] show the same disagreement for the positive hadrons as those of Anselmino et al. [82] (see fig. 6.18 for the predictions of Arnold et al. and 6.15 for the COMPASS results). For differences between HERMES and COMPASS results Arnold et al. already give a possible explanation. They stress that HERMES and COMPASS have a comparable mean value of $\langle Q^2 \rangle \approx (2-3)\,(\mathrm{GeV}/c)^2$, but that nevertheless at a fixed x value Q^2 can vary significantly between those experiments. As example they set:

$$\begin{aligned} \text{HERMES:} \quad \langle x \rangle = 0.115, \quad \langle Q^2 \rangle = 2.62\,(\mathrm{GeV}/c)^2 \\ \text{COMPASS:} \quad \langle x \rangle = 0.1205, \quad \langle Q^2 \rangle = 12.9\,(\mathrm{GeV}/c)^2 \end{aligned} \tag{6.20}$$

If the Sivers effect at HERMES would be due to the leading twist contributions, power corrections should be not so important and thus the Q^2 dependance small. If this is not the case, one has to add the power corrections:

$$A_{Siv}^{measured} = \{\text{twist-2 Sivers effect}\} + C(Q)\frac{M^2}{Q^2} \tag{6.21}$$

[2]For the notation in [82] a remark is in place: Anselmino et al. use for the quark transverse momentum $k_\perp$, what in this work is named k_T. The notation of the Sivers function and of its first moment in [82] can be expressed by $f_{1T}^{\perp;q}(x,k_\perp)$ introduced in section 2.3.3 through: $\Delta^N f_{q/p^\uparrow}(x,k_\perp) = -2\frac{|\vec{k}_\perp|}{M} f_{1T}^{\perp;q}(x,k_\perp)$ (see also eq. (2.96)) and for the first moment: $\Delta^N f^1_{q/p^\uparrow}(x) = \int d^2\vec{k}_\perp \frac{k_\perp}{4M} \Delta^N f_{q/p^\uparrow}(x,k_\perp)$.

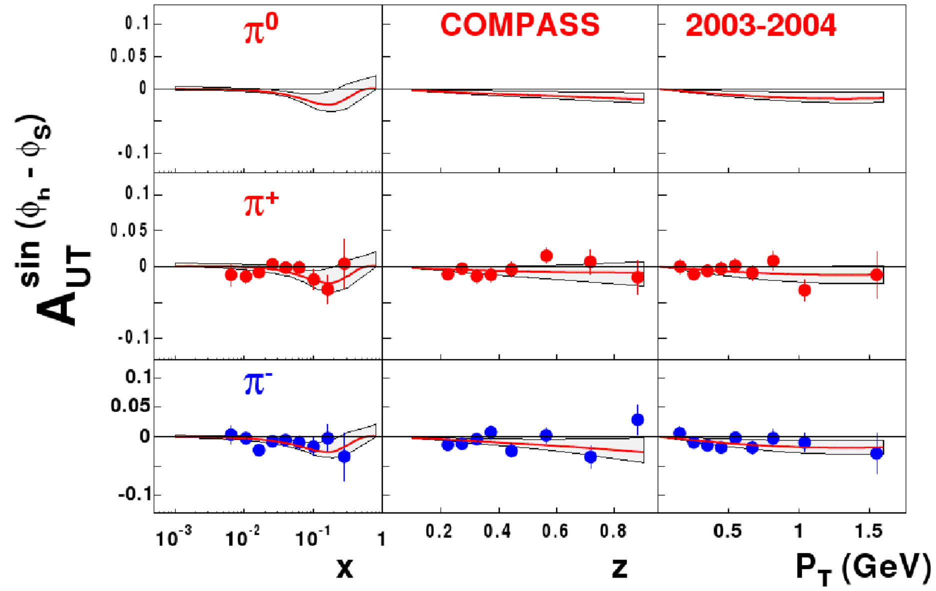

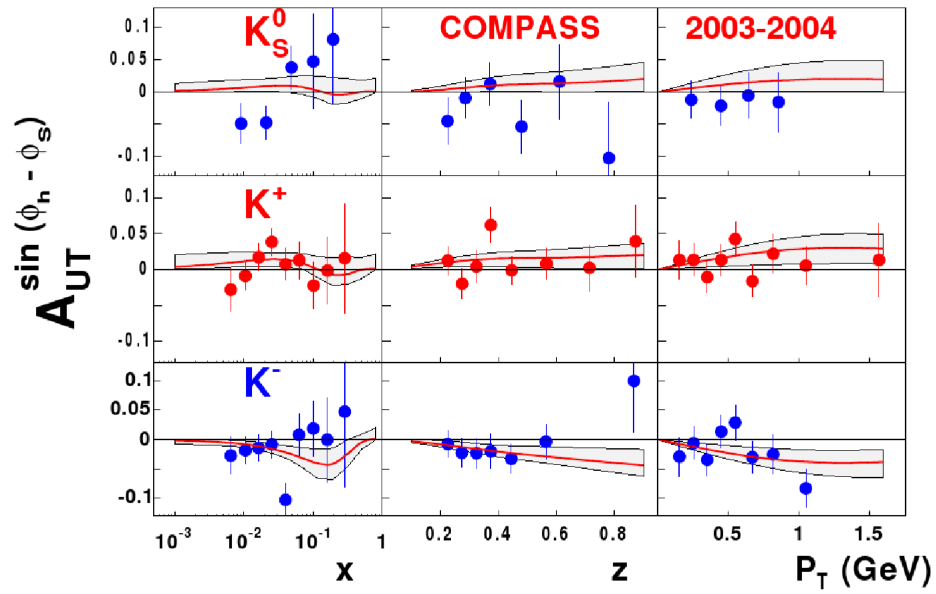

Figure 6.13: *Fit of Anselmino et al. [82] on the Sivers asymmetries on deuteron for charged pion (upper plot) and charged kaon production (lower plot) at COMPASS. The shaded area shows the statistical uncertainty of the parameters.*

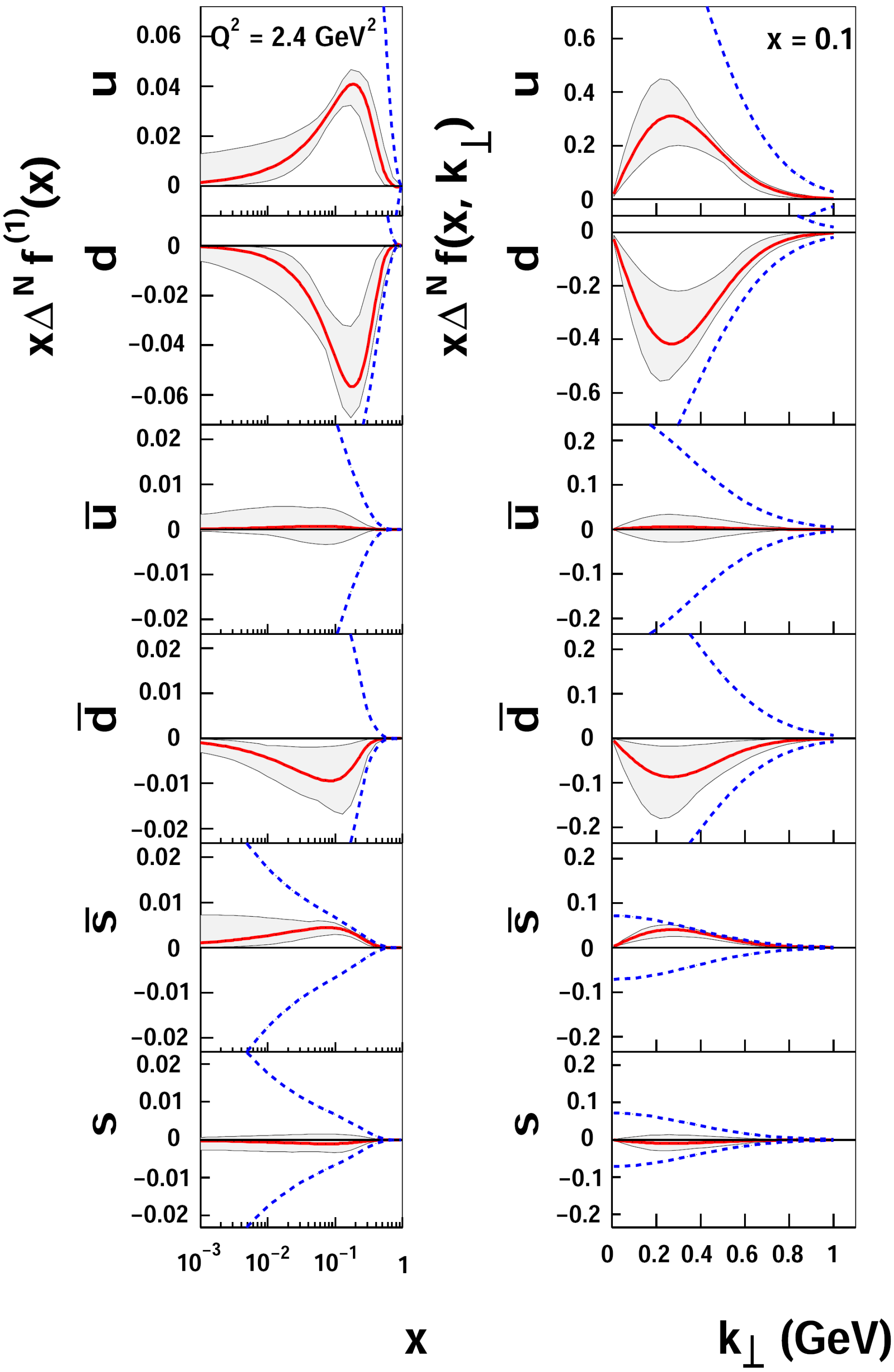

Figure 6.14: *Sivers functions for u, d, s, $\bar{u}$, $\bar{d}$ and $\bar{s}$ flavors extracted by Anselmino et al. [82] on the left-hand side as a function of x and on the right-hand side as function of k_T at a fixed value of x. The blue dashed lines mark the positivity limits $|\Delta^N f| = 2f$. For the notation see the footnote.*

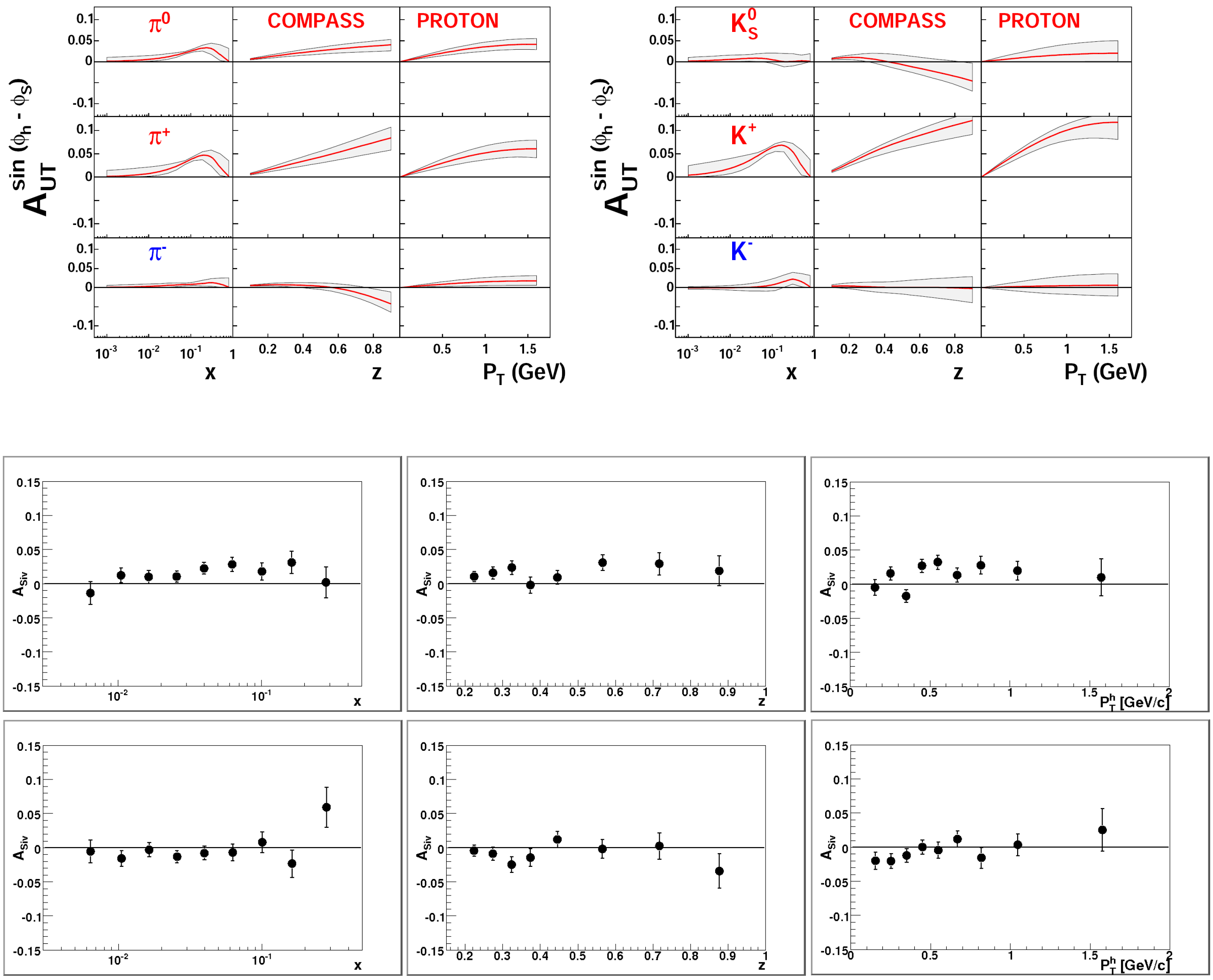

Figure 6.15: *Upper plots: Predictions of Anselmino et al. [82] for the Sivers asymmetries on proton at COMPASS for pions (left) and kaons (right). Lower plot: Sivers asymmetries for unidentified hadrons on proton from COMPASS to compare with the expectations.*

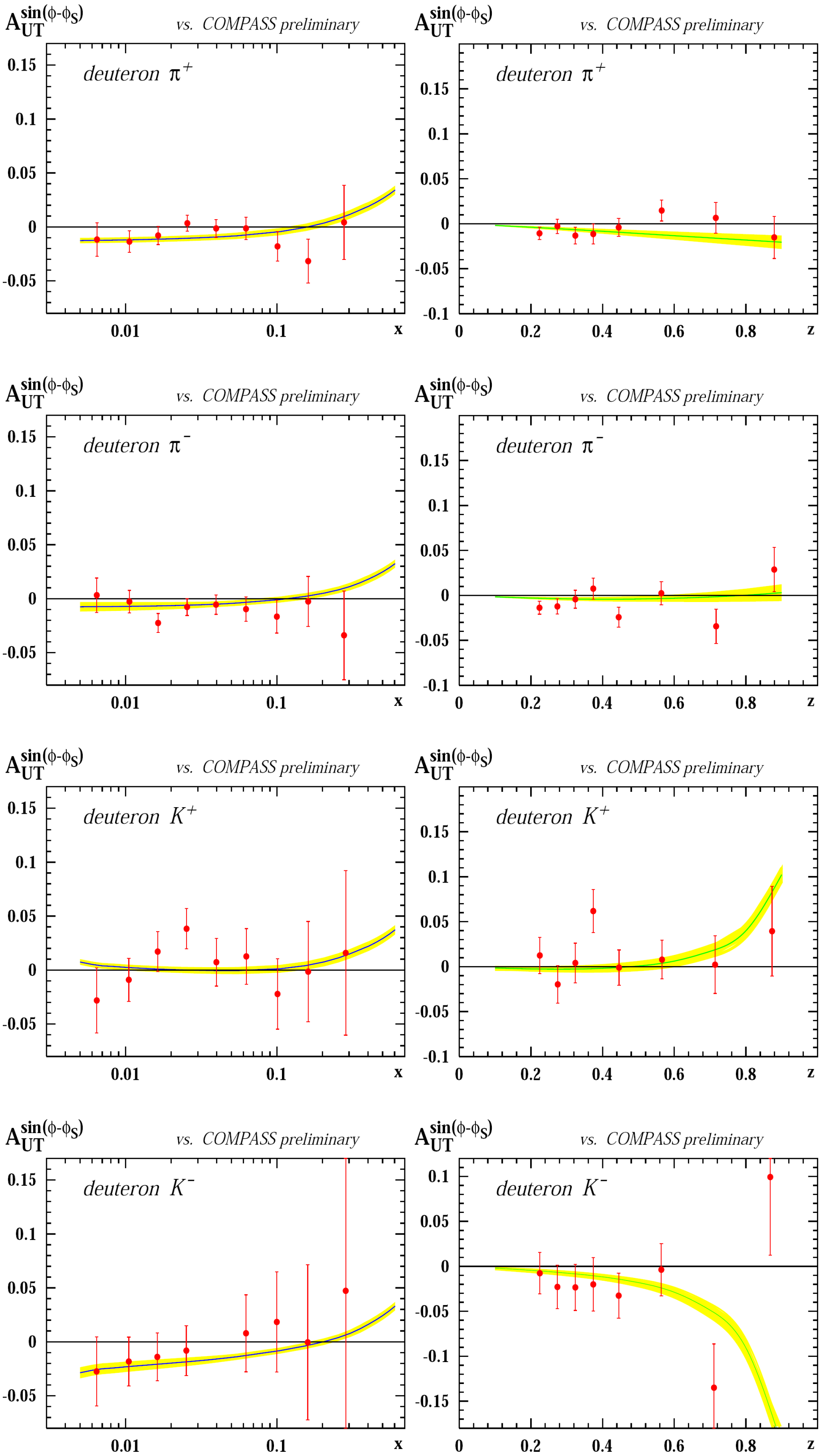

Figure 6.16: *Left: Fit of Arnold et al. [84] on the Sivers asymmetries on deuteron at COMPASS vs. x. Right: Predictions of Arnold et al. [84] from the fit for COMPASS Sivers asymmetries on deuteron at COMPASS vs. z.*

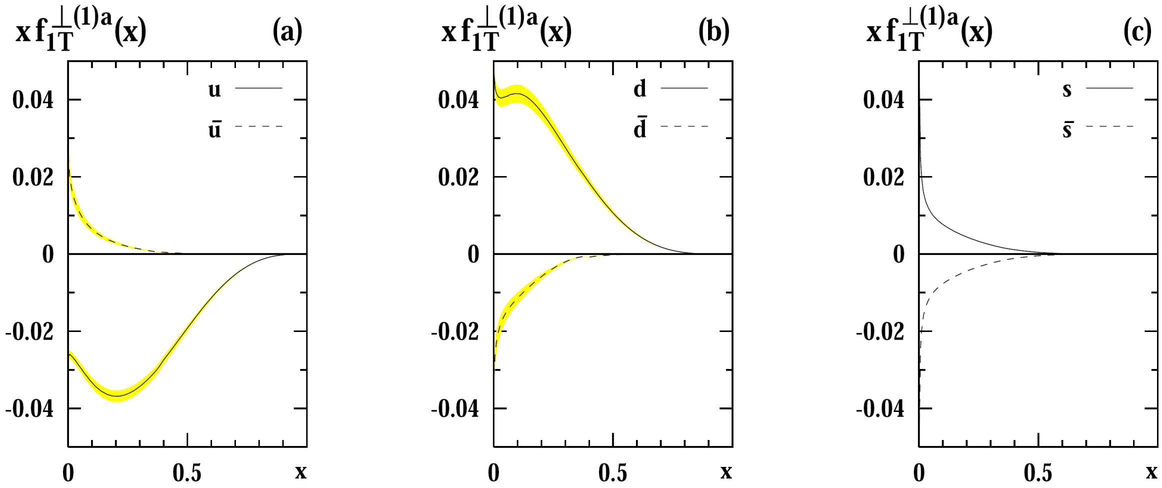

Figure 6.17: *Sivers functions vs.* x *extracted by Arnold et al. [84] a) for* u *and* $\bar{u}$*, b) for* d *and* $\bar{d}$*, c)* s *and* $\bar{s}$*, which were fixed to* $\pm$ *the positivity bounds. The yellow shaded areas in a) and b) mark the respective* 1-σ*-uncertainties.*

The coefficient $C(Q)$ could be flavor-dependent, dependent on x, z etc. and typically depends logarithmically on scale.
Another important aspect for the interpretation and the rôle of the Sivers effect comes from the fact that this process involves a k_T unintegrated quark distribution function inside a transversely polarized nucleon. From this dependence of the quark intrinsic transverse momentum k_T one can conclude that the Sivers effect is connected to the quark orbital angular momentum [86].
Therefore, should the non-zero results on the proton target seen by HERMES and indicated by COMPASS for positive hadrons persist, these results can be interpreted as experimental evidence for orbital angular momenta of the quarks $L_z^q \neq 0$ [87, 88]. Nevertheless the quantitative contribution of the L_z^q to the nucleon spin would still be unclear. This is a question, which could be solved by measuring the more complex Generalized Parton Distributions (GPDs), which give a full three-dimensional picture of the nucleon.
The orbital angular momentum of quarks as well as of gluons is also object in the study of Brodsky and Gardner [89] about the Sivers mechanism. In their theoretical considerations they deduce that the single spin asymmetries on a deuteron target for the fragmentation of a u quark into a positive leading hadron and the fragmentation of a d quark into a negative leading hadron are both small, which is confirmed by the COMPASS measurements. This cancelation of the u and d quark Sivers functions is interpreted as evidence of the absence of (at least a large) gluon orbital angular momentum in the nucleon.

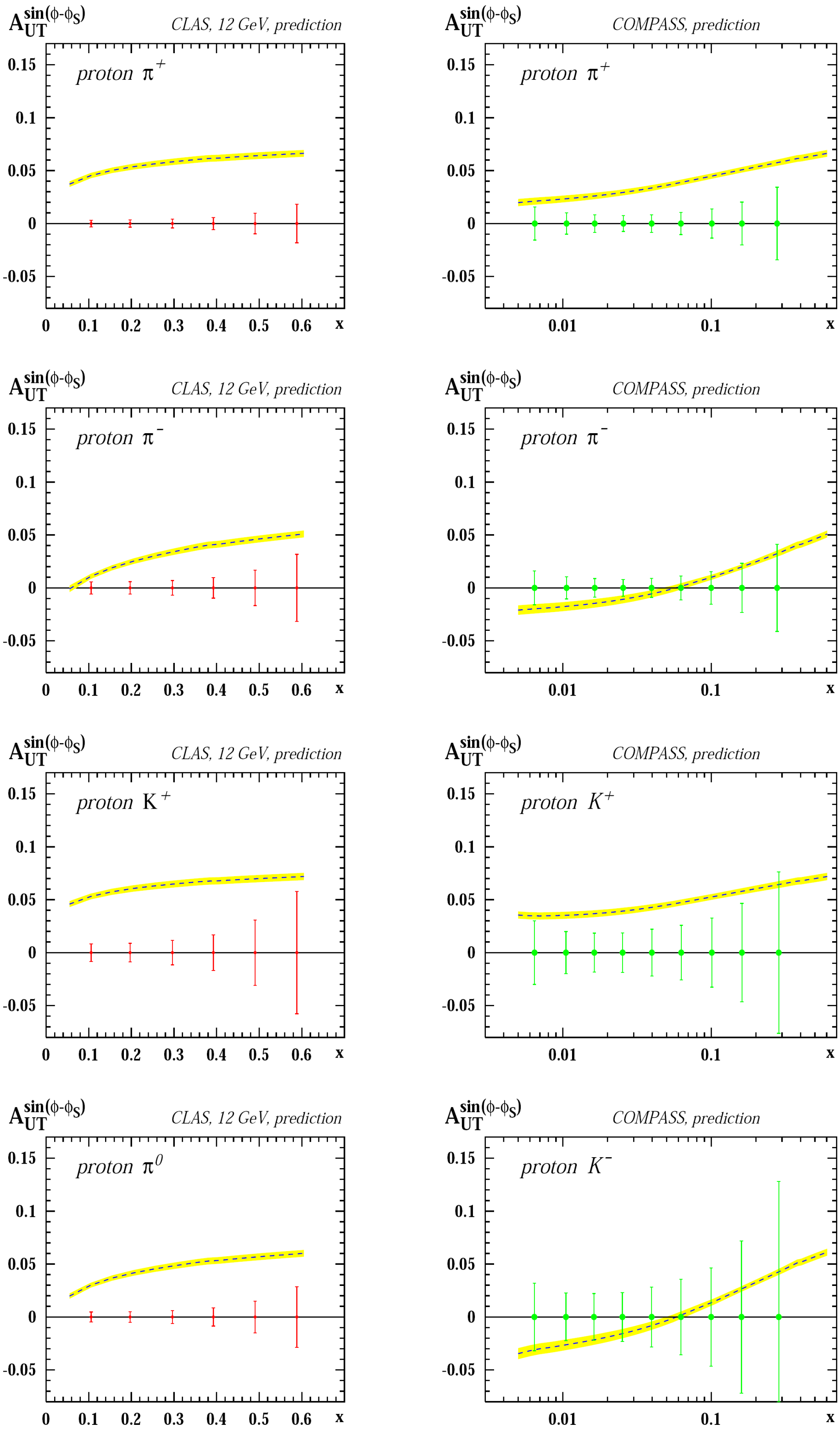

Figure 6.18: *The predictions of Arnold et al. [84] for the Sivers asymmetries vs. x on proton at COMPASS. The error bars are taken from [85].*

Chapter 7

Conclusion and Outlook

> Science is like sex: sometimes something useful comes out, but that is not the reason we are doing it.
>
> R. Feynman (1918-1988), American physicist, Nobel Prize 1965

During the last years a large progress has been made in the field of transverse spin effects on both, the theoretical and the experimental side. The transversity distribution functions, which together with the Bakker Leader Trueman sum rule for a transversely polarized nucleon give also an independent access to the contribution of the orbital angular momentum of quarks, antiquarks and gluons to the nucleon spin, are an additional important piece to solve the *"spin puzzle"*.
For the first time also transverse momentum dependent (TMD) parton distribution functions (PDFs), which could explain observed transverse spin phenomena and shed light on the nucleon spin structure, were measured.
In this work the analysis of the Collins and Sivers asymmetries for K^0 on a transversely polarized deuteron target taken at COMPASS in 2002-04 was presented. Furthermore the analysis of the Collins and Sivers asymmetries from the COMPASS 2007 run on a transversely polarized proton target for charged hadrons without and with identification as well as for the neutral K^0 was described.
The K^0 Collins and Sivers asymmetries on deuteron turned out to be small and compatible with zero. As also for charged hadrons the Collins and Sivers asymmetries measured at COMPASS on deuteron were compatible with zero, this result confirms the expectation from isospin symmetry. The very small Collins asymmetries for charged hadrons on deuteron are interpreted as a cancelation between u and d quark transversity.
The signal seen for charged hadrons in the case of the Collins effect on a proton target at COMPASS, which confirmes the results of HERMES on proton, implies a non-zero transversity distribution $\Delta_T q(x)$. With the proton data of COMPASS and/or HERMES in combination with the COMPASS data on the deuteron and the independent information from BELLE on the Collins fragmentation function a flavor separation and therefore the

extraction of the u and d quark transversity is possible.
The Sivers asymmetries measured in the COMPASS proton run in 2007 are for negative hadrons compatible with zero like the HERMES results, while for positive hadrons they are smaller than those measured by HERMES. Nevertheless the Sivers asymmetries for positive hadrons are inside the errors not in contradiction to the HERMES ones. Here only further measurements at COMPASS in 2010 can give clarity. Amongst others one of the open questions is, if those differences are e.g. due to the different kinematical regimes of HERMES and COMPASS.
Also in the case of the Sivers effect an extraction of the u and d quark Sivers functions by flavor separation is only possible using both, data on proton and on deuteron.
If the non-zero results seen by HERMES on proton will be confirmed, also the Sivers asymmetries on deuteron compatible with zero should be interpreted as the cancelation between u and d quark contributions, i.e. $\Delta_T^0 d \approx \Delta_T^0 u$.
Furthermore such a cancelation of the u and d quark Sivers functions is interpreted as evidence of the absence of (at least a large) gluon orbital angular momentum in the nucleon [89].
The Collins and Sivers asymmetries for K^0 production on proton are compatible with zero within the errors. Also here the ongoing measurements hopefully can provide more clarity resulting in the possibility to extract also the contributions of the s quarks contained in the K^0.
More statistics will reduce also the error bars of the asymmetries for the strange-containing $K^{\pm}$ and thus should contribute to more insights into the rôle of the s quarks. The COMPASS data on proton show in the case of Collins for $K^{\pm}$ the same trend as the corresponding $\pi^{\pm}$ asymmetries, while this at least for K^- is not the case in the HERMES measurements. The Sivers asymmetries from COMPASS on proton are for K^+ compatible with zero in contrast to the positive asymmetries measured by HERMES, while for K^- the Sivers asymmetries from both experiments are compatible with zero.
Alltogether the COMPASS experiment until now has given a large contribution to map out the transverse spin structure of the nucleon and as a running experiment surely will deliver still new insights.

Appendix A

Collins and Sivers Analysis on Deuteron

A.1 Target Polarization Values

Sub-period	Runs	Polarization (%)	
		upstream	downstream
P2B	21178-21207	-49.79	+54.58
P2B	21333-21393	-47.79	+47.40
P2B	21407-21495	-47.09	+46.33
P2C	21670-21765	+52.50	-44.09
P2C	21777-21878	+50.36	-43.06
P2H.1	23490-23575	-49.83	+52.11
P2H.2	23664-23839	+47.45	-41.41
P1G	30772-31038	-49.70	+52.78
P1H	31192-31247	+49.39	-42.60
P1H	31277-31524	+51.31	-44.63
W33	38991-39168	+50.70	-43.52
W34	39283-39290	-44.80	+45.97
W34	39325-39430	-38.60	+40.35
W34	39480-39545	-46.14	+47.41
W35	39548-39780	-46.44	+47.44
W36	39850-39987	+49.89	-42.76

Table A.1: *Target polarization values for the 2002-04 transverse data taking (sub-)periods.*

A.2 Systematic Studies

A.2.1 Compatibility of the Different Periods

The compatibility of the asymmetries in each bin of x_{bj}, z and P_T^h of all five periods in the years 2002-04 was checked by evaluating the following quantity:

$$\frac{A_i - \langle A \rangle}{\sqrt{\sigma_i^2 - \sigma_{\langle A \rangle}^2}}; \quad i = 1, 2, 3, 4, 5 \tag{A.1}$$

where A_i are the asymmetries in a single bin and period and $\langle A \rangle$ the corresponding weighted mean of this bin. In the denominator the difference of the single asymmetry values and those of the weighted mean was used to take into account the correlation between A_i and $\langle A \rangle$.

The overall distribution of this quantity for all asymmetries, Collins and Sivers in five periods in all bins is shown in fig. A.1 for the all K^0 analysis and in fig. A.2 for the leading K^0 analysis. The number of entries is 160 for the all K^0 sample corresponding to 2 (Collins/Sivers) $\cdot$ 5 (periods) $\cdot$ $(5 + 6 + 5)$ (x_{bj}, z and P_T^h bins) and 150 for the leading K^0 sample corresponding to 2 (Collins/Sivers) $\cdot$ 5 (periods) $\cdot$ $(5 + 5 + 5)$ (x_{bj}, z and P_T^h bins). As expected the asymmetries for both analysis follow the standard normal distributions with a mean value compatible with 0 and a RMS near 1 of 1.001 for the all K^0 and 0.982 for the leading K^0 case.

This test was also done separately for the Collins and Sivers asymmetries (see fig. A.3 and A.4 for all K^0, fig. A.5 and A.6 for leading K^0 analysis). Also here it resulted in standard normal distributions with mean values compatible with 0 and RMS with values between 0.96 and 1.04 near the expected value of 1.

So it can be concluded that the results gained from the different periods are compatible.

A.2.2 Background Asymmetries

Another check was the extraction of asymmetries in the same way as it was done for the physics asymmetries, but in a mass range widely outside the one of the K^0-signal. As a distance of $|50|$ MeV in the mass spectrum of the K^0 corresponds to 6-7 σ of the K^0-signal, a range of $[-50, -350] \cup [50, 350]$ MeV in the difference of the measured K^0-mass and the literature value was chosen for those background asymmetries. The sample was devided in three bins in x_{bj}, z and P_T^h with:

$0.003 \leqq x_{bj} < 0.028$	$0.0 \leqq z < 0.325$	$0.0 < P_T^h \leqq 0.40$
$0.028 \leqq x_{bj} < 0.100$	$0.325 \leqq z < 0.55$	$0.40 < P_T^h \leqq 0.80$
$0.100 \leqq x_{bj} < 1.000$	$0.55 \leqq z < 1.00$	$0.80 < P_T^h \leqq 10.0$

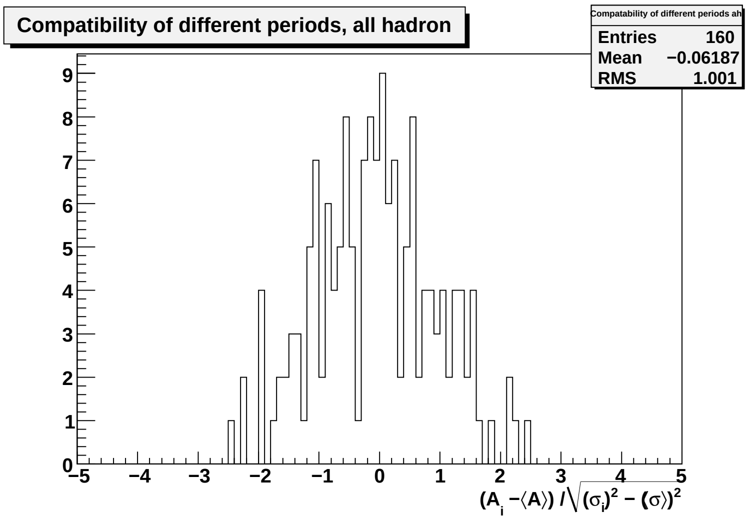

Figure A.1: *Distribution of the asymmetries for K^0 on deuteron for all values (Collins/Sivers, x_{bj}, z and P_T^h, five periods) in the all hadron analysis.*

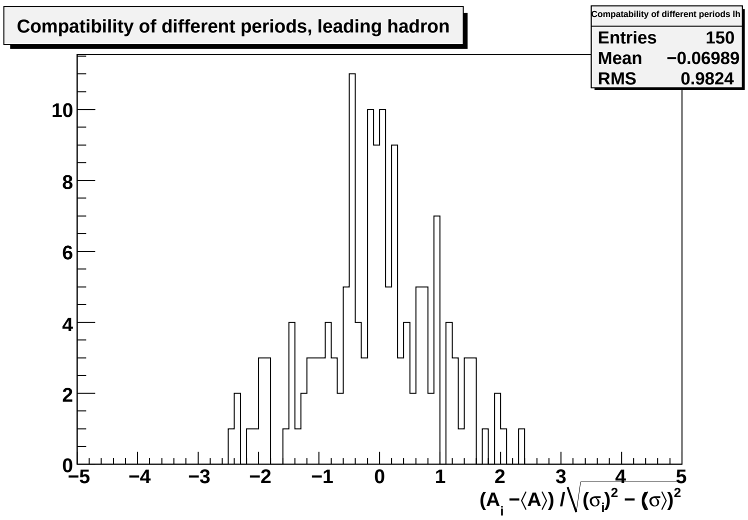

Figure A.2: *Distribution of the asymmetries for K^0 on deuteron for all values (Collins/Sivers, x_{bj}, z and P_T^h, five periods) in the leading hadron analysis.*

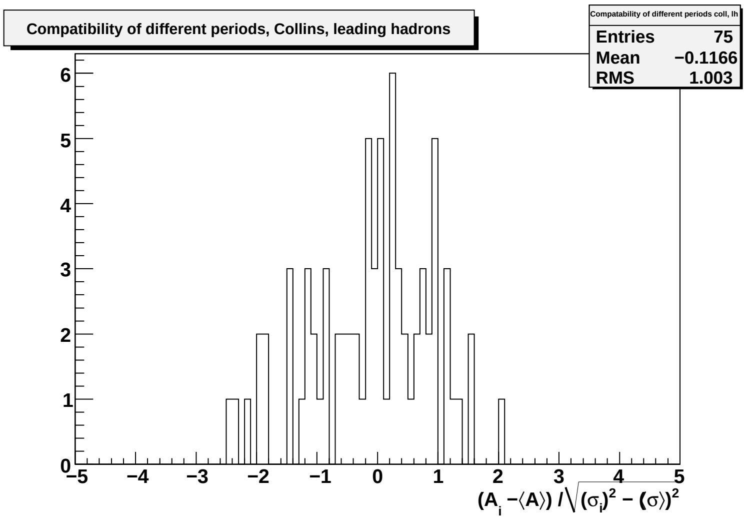

Figure A.3: *Distribution of the Collins asymmetries for K^0 on deuteron (bins in x_{bj}, z and P_T^h, five periods) in the leading hadron analysis.*

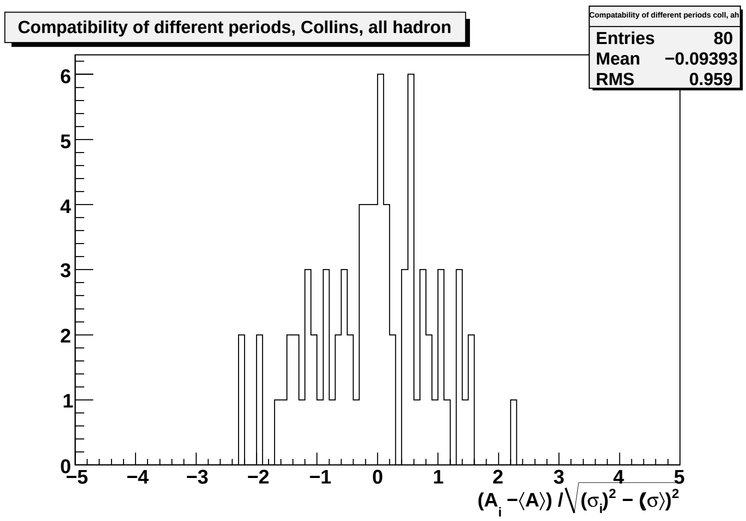

Figure A.4: *Distribution of the Collins asymmetries for K^0 on deuteron (bins in x_{bj}, z and P_T^h, five periods) in the all hadron analysis.*

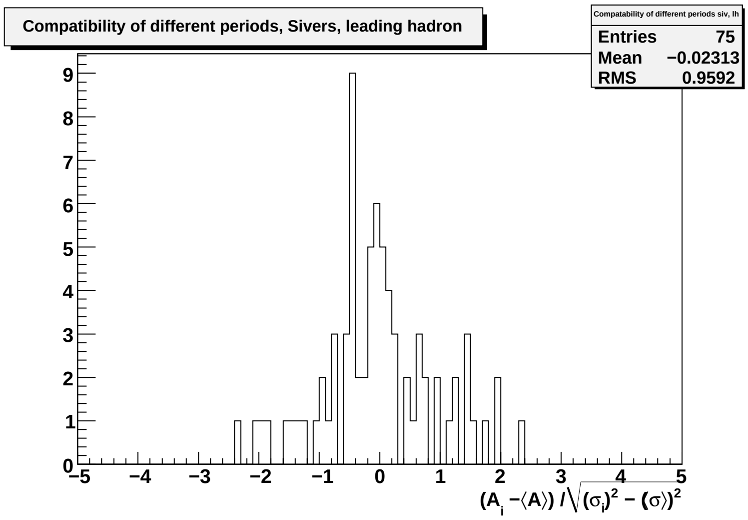

Figure A.5: *Distribution of the Sivers asymmetries for K^0 on deuteron (bins in x_{bj}, z and P_T^h, five periods) in the leading hadron analysis.*

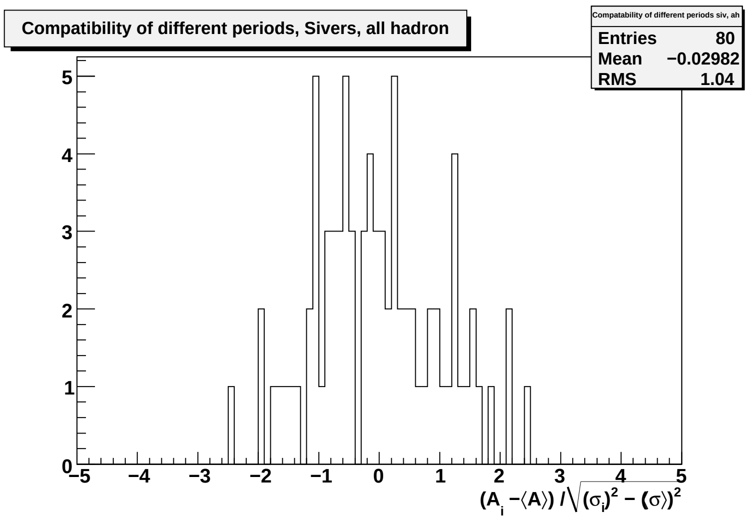

Figure A.6: *Distribution of the Sivers asymmetries for K^0 on deuteron (bins in x_{bj}, z and P_T^h, five periods) in the all hadron analysis.*

Integrated sideband asymmetry	All K^0 sample 2002-04
Collins	-0.021 ± 0.038
Sivers	0.002 ± 0.030

Table A.2: *Weighted mean of the integrated background asymmetries over all periods 2002-04.*

As can be seen in fig. A.7 for the all K^0 analysis and in fig. A.8 for the leading K^0 analysis, the resulting asymmetries in the sidebands are consistent with zero.
To test the compatibility with zero also the following quantity analog to the one in eq. (A.1) was evaluated:

$$\frac{A_{i,background} - 0}{\sigma_{i,background}}; \quad i = 1, 2, 3, 4, 5 \tag{A.2}$$

If the distribution of this quantity for all Collins and Sivers asymmetries together is regarded, for the all K^0 sample a RMS of 1.037 and for the leading K^0 sample a RMS of 1.044 is obtained, both near 1 as expected for a standard normal distribution and the mean is also for both near 0 as expected (see fig. A.9 and A.10).
The distributions separated for Collins and Sivers are shown for the all K^0 case in fig. A.11 (Collins) and A.12 (Sivers) and for the leading K^0 case in fig. A.13 (Collins) and A.14 (Sivers). Also here the mean values are all near 0 and the RMS values with 0.92 to 1.14 near 1.
The compatibility of the background asymmetries with zero is therefore clear confirmed.

For getting a mean background asymmetry the sidebands asymmetrys were also evaluated integrating over all bins in x_{bj}, z and P_T^h. The results integrated over x_{bj} are given in fig. A.15 for Collins and fig. A.16 for Sivers for all measuring periods in the all K^0 analysis. As one can see the asymmetries are in good agreement to each other as well as to zero.
For the weighted mean of the integrated background asymmetries over all periods see tab. A.2. For both, Collins and Sivers, they are well consistent with zero.

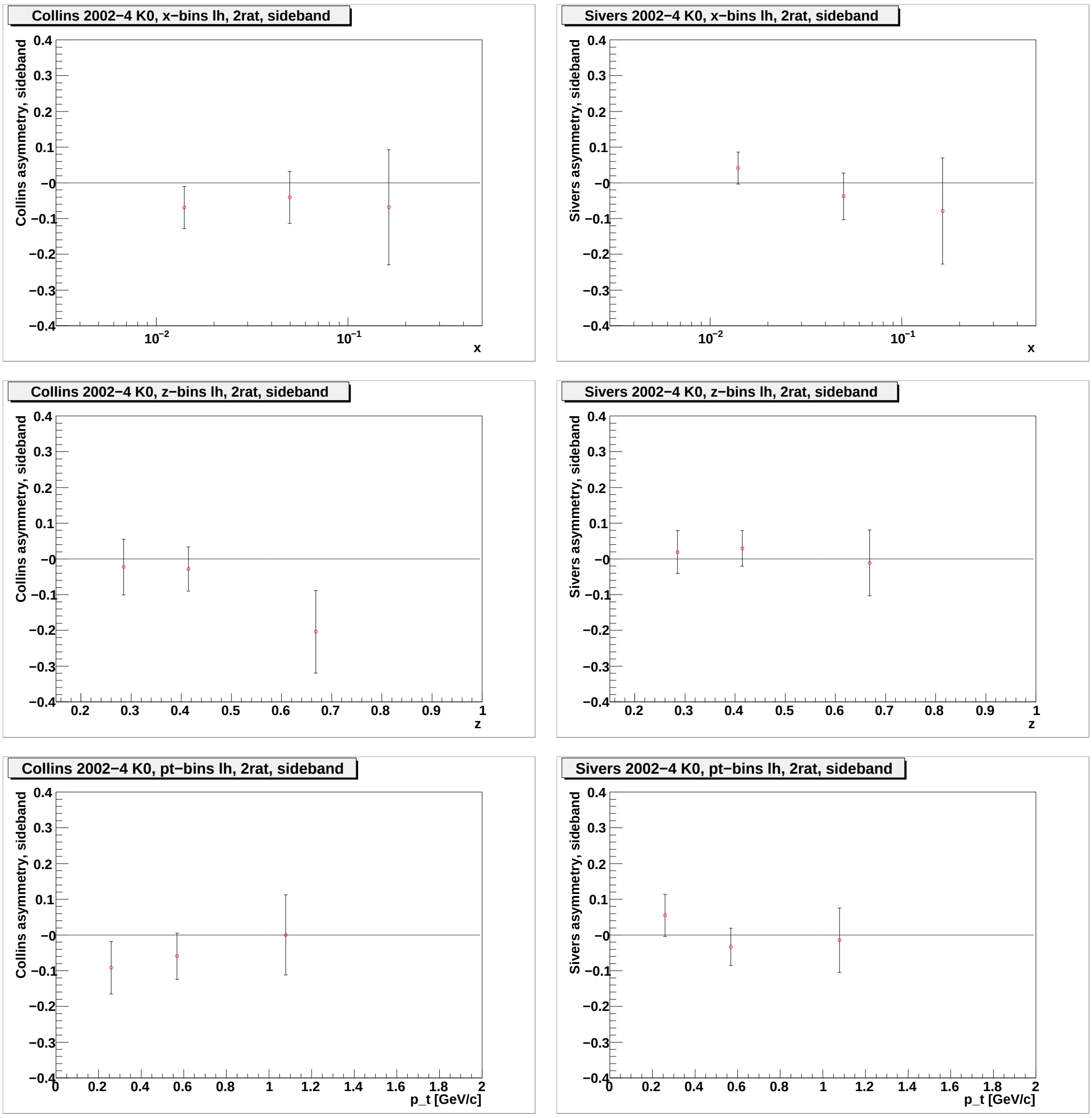

Figure A.7: *Asymmetries in the sidebands for the 2002-04 data in the leading hadron analysis. Left: Collins asymmetry, right: Sivers asymmetry.*

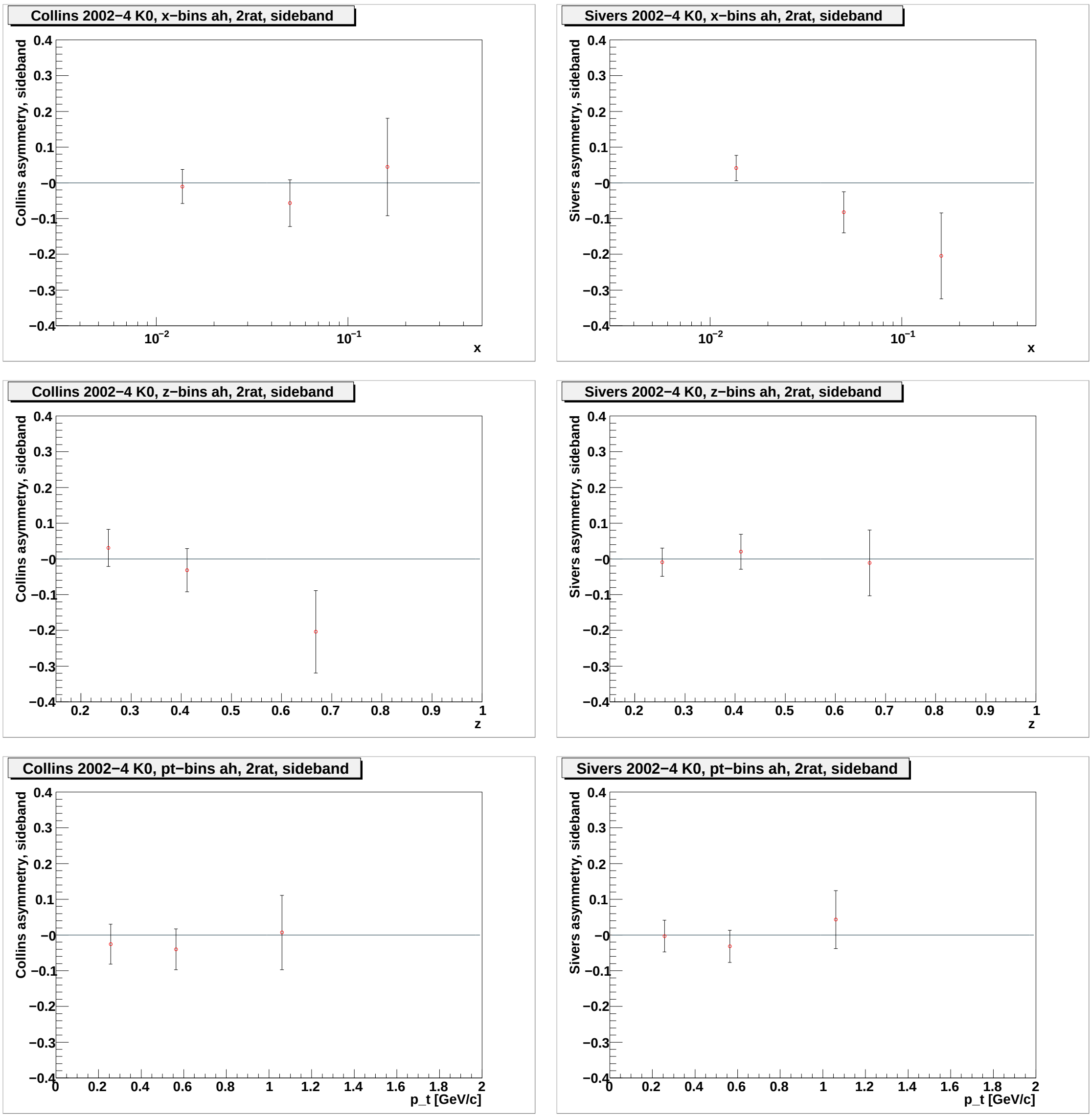

Figure A.8: *Asymmetries in the sidebands for the 2002-04 data in the all hadron analysis. Left: Collins asymmetry, right: Sivers asymmetry.*

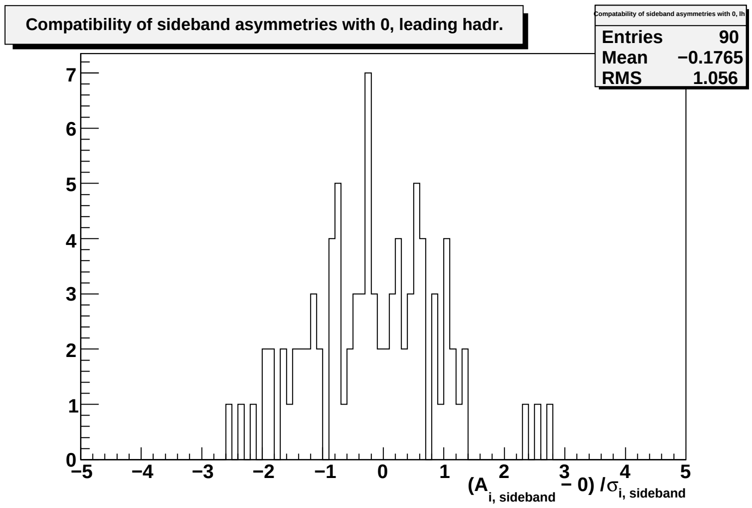

Figure A.9: *Compatibility of the single* K^0 *asymmetries on deuteron in the sidebands with zero, for all values (Collins/Sivers,* x_{bj}*,* z *and* P_T^h*, five periods) for the leading hadron analysis.*

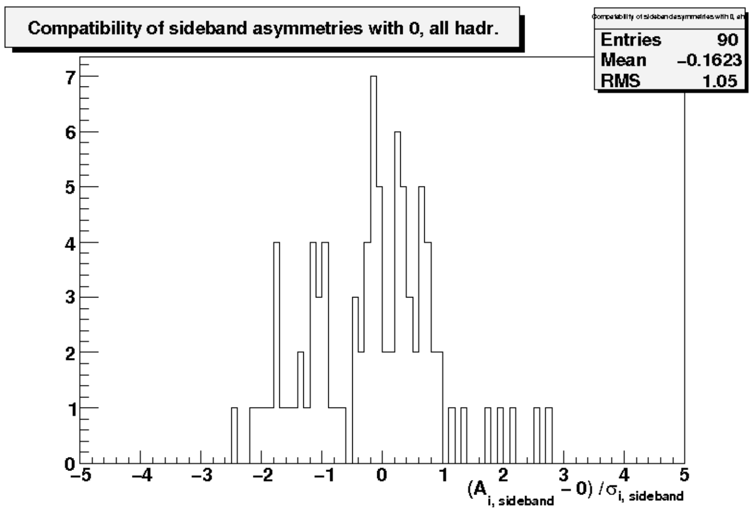

Figure A.10: *Compatibility of the single* K^0 *asymmetries on deuteron in the sidebands with zero, for all values (Collins/Sivers,* x_{bj}*,* z *and* P_T^h*, five periods) for the all hadrons analysis.*

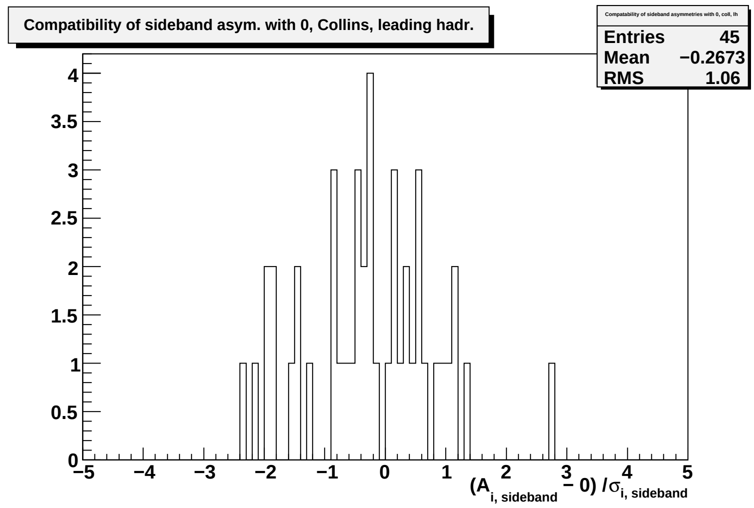

Figure A.11: *Compatibility of the single K^0 asymmetries on deuteron in the sidebands with zero, for Collins asymmetries only (x_{bj}, z and P_T^h, five periods) for the leading hadron analysis.*

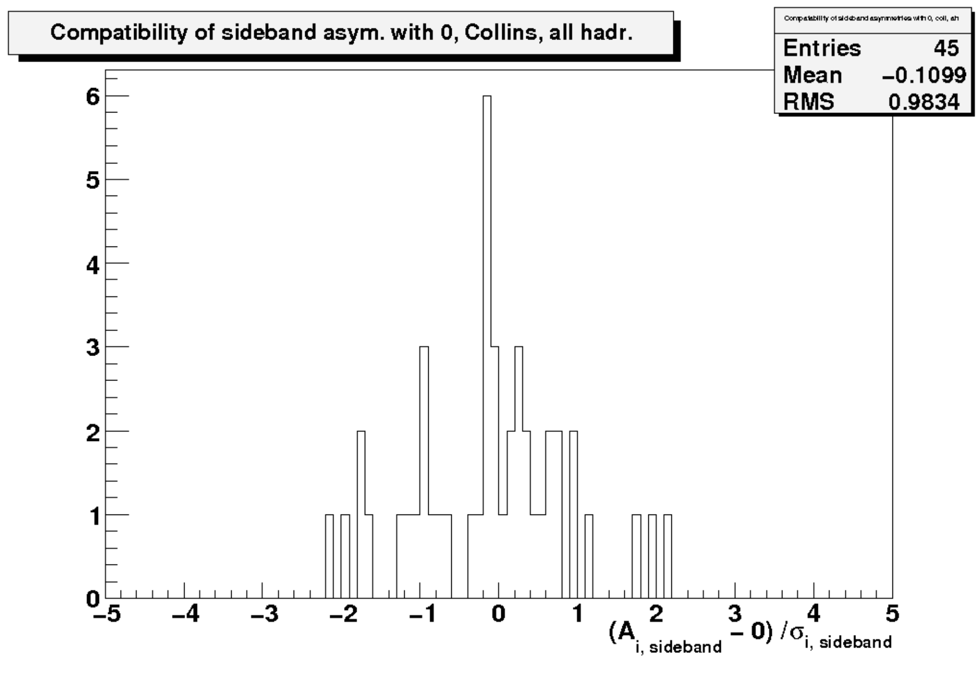

Figure A.12: *Compatibility of the single K^0 asymmetries on deuteron in the sidebands with zero, for Collins asymmetries only (x_{bj}, z and P_T^h, five periods) for the all hadrons analysis.*

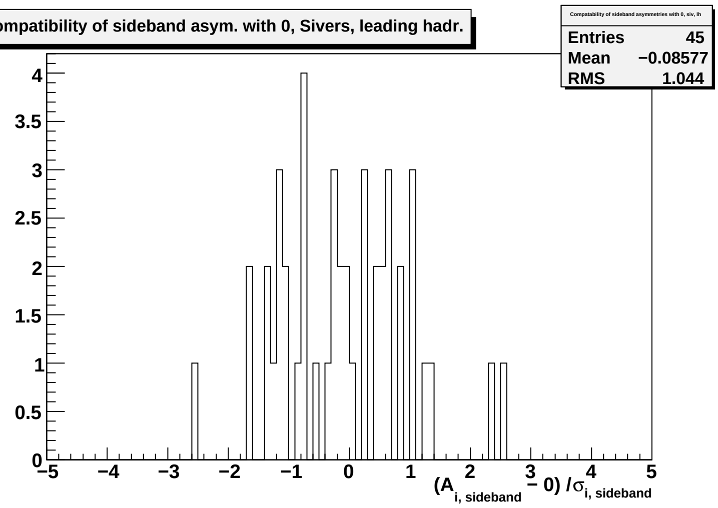

Figure A.13: *Compatibility of the single K^0 asymmetries on deuteron in the sidebands with zero, for Sivers asymmetries only (x_{bj}, z and P_T^h, five periods) for the leading hadron analysis.*

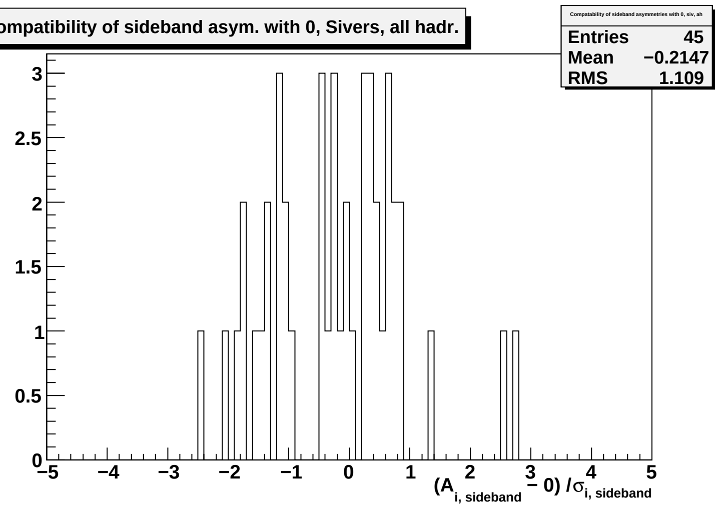

Figure A.14: *Compatibility of the single K^0 asymmetries on deuteron in the sidebands with zero, for Sivers asymmetries only (x_{bj}, z and P_T^h, five periods) for the all hadrons analysis.*

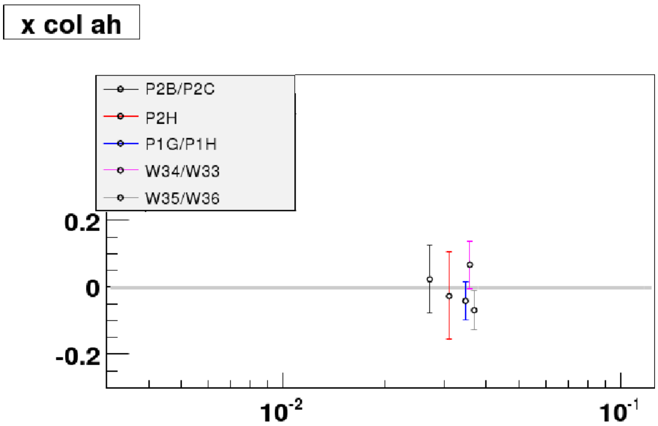

Figure A.15: *Collins asymmetries in the sidebands for the 2002-04 data integrated over x_{bj} in the all K^0 analysis for the different periods.*

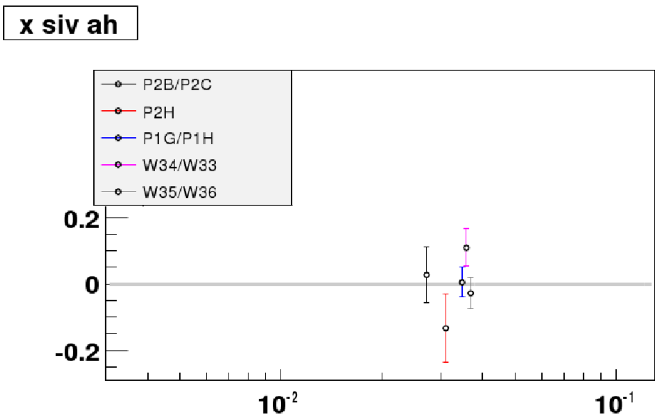

Figure A.16: *Sivers asymmetries in the sidebands for the 2002-04 data integrated over x_{bj} in the all K^0 analysis for the different periods.*

Appendix B

Collins and Sivers Analysis on Proton

B.1 Target Polarization Values

Sub-period	Runs	Polarization (%)		
		upstream	central	downstream
W25	57777-57861	-91.3954	+91.6515	-86.8206
W25	57862-57928	-91.199	+91.4595	-86.6421
W25	57929-57991	-90.6614	+91.0785	-86.1314
W25	57992-58051	-90.1911	+90.6467	-85.6846
W25	58052-58104	-89.5335	+90.0261	-85.0598
W25	58105-58141	-89.0657	+89.6801	-84.6154
W25	58142-58201	-88.7937	+89.4195	-84.357
W26	58263-58295	+84.9562	-86.3551	+78.1448
W26	58296-58346	+85.9222	-87.6602	+79.222
W26	58347-58399	+85.3401	-87.1926	+78.6854
W26	58400-58463	+84.7121	-86.5287	+78.1063
W26	58464-58505	+84.2533	-85.9663	+77.6833
W26	58506-58589	+83.6945	-85.4642	+77.1681
W27	58704-58751	-85.6093	+85.6715	-81.8505
W27	58752-58795	-85.2517	+85.3184	-81.3613
W27	58796-58872	-84.3055	+84.4905	-80.4583
W27	58873-58947	-83.7298	+84.0288	-79.9089
W27	58948-59036	-83.3184	+83.7268	-79.5163
W28	59109-59114	+88.4463	-86.8785	+82.1826
W28	59115-59184	+91.7074	-90.3448	+87.207
W28	59235-59290	+90.8764	-89.9111	+86.4156
W28	59291-59337	+90.298	-89.4533	+85.8656
W28	59338-59382	+89.7811	-89.045	+85.3741
W28	59383-59399	+89.0671	-88.4213	+84.6951

Continued on next page

Continued from previous page

Sub-period	Runs	Polarization (%)		
		upstream	central	downstream
W30	59963-59983	-86.6436	+83.8694	-78.2121
W30	59984-60024	-88.6908	+87.3155	-82.2286
W30	60025-60087	-87.83	+86.4044	-81.4306
W31	60146-60174	+80.5738	-85.8678	+71.4901
W31	60175-60221	+85.0147	-87.8455	+76.4937
W31	60222-60264	+84.5467	-87.558	+76.0725
W31	60265-60317	+84.094	-87.1936	+75.6652
W31	60318-60332	+86.6047	-88.694	+77.9672
W39	62706-62747	+96.6174	-93.8261	+95.1825
W39	62748-62770	+96.347	-93.3217	+94.9161
W39	62771-62806	+95.8361	-92.6466	+94.4127
W39	62807-62843	+95.1906	-92.0481	+93.7768
W39	62844-62899	+94.677	-91.9418	+93.2709
W40	62993	-79.1015	+86.5598	-77.8549
W40	62994-63013	-86.5426	+90.9271	-85.8479
W40	63014-63043	-85.9409	+90.3329	-85.2519
W40	63044-63058	-85.6047	+90.0206	-84.9175
W40	63059-63078	-85.2631	+89.6055	-84.5787
W40	63079-63117	-84.6322	+88.9533	-83.9528
W40	63118-63122	-86.849	+90.8919	-84.7304
W41	63194-63202	-90.2861	+92.6351	-87.7197
W41	63203-63239	-90.9319	+92.738	-87.8739
W41	63240-63272	-90.4662	+92.192	-87.2627
W41	63273-63307	-89.8509	+91.5869	-86.6685
W41	63308-63343	-89.2069	+91.0044	-86.0473
W41	63344-63356	-87.4043	+86.1182	-84.0372
W42	63422-63437	+93.0402	-91.283	+91.2767
W42	63438-63480	+92.9594	-91.5011	+91.2145
W42	63481-63507	+92.1739	-90.8574	+90.4437
W42	63508-63556	+91.6653	-90.4279	+89.9446
W42	63557-63606	+90.9737	-89.7703	+89.266
W42	63607-63657	+90.1072	-88.968	+88.4157
W42	63658-63672	+93.081	-90.6125	+90.1064
W43	63746-63762	-67.4675	+85.6328	-71.4487
W43	63763-63794	-73.4147	+87.757	-76.5012
W43	63795-63808	-79.8792	+89.8366	-81.3501

Table B.1: *Mean target polarization values for the 2007 transverse data taking (sub-)periods.*

B.2 Systematic Studies

B.2.1 False Asymmetries

The false Collins and Sivers asymmetries obtained by using the definitions in section 5.4.1, are for both configurations, conf_2 and conf_3, small and scattered around zero (see fig. B.1 and B.2).

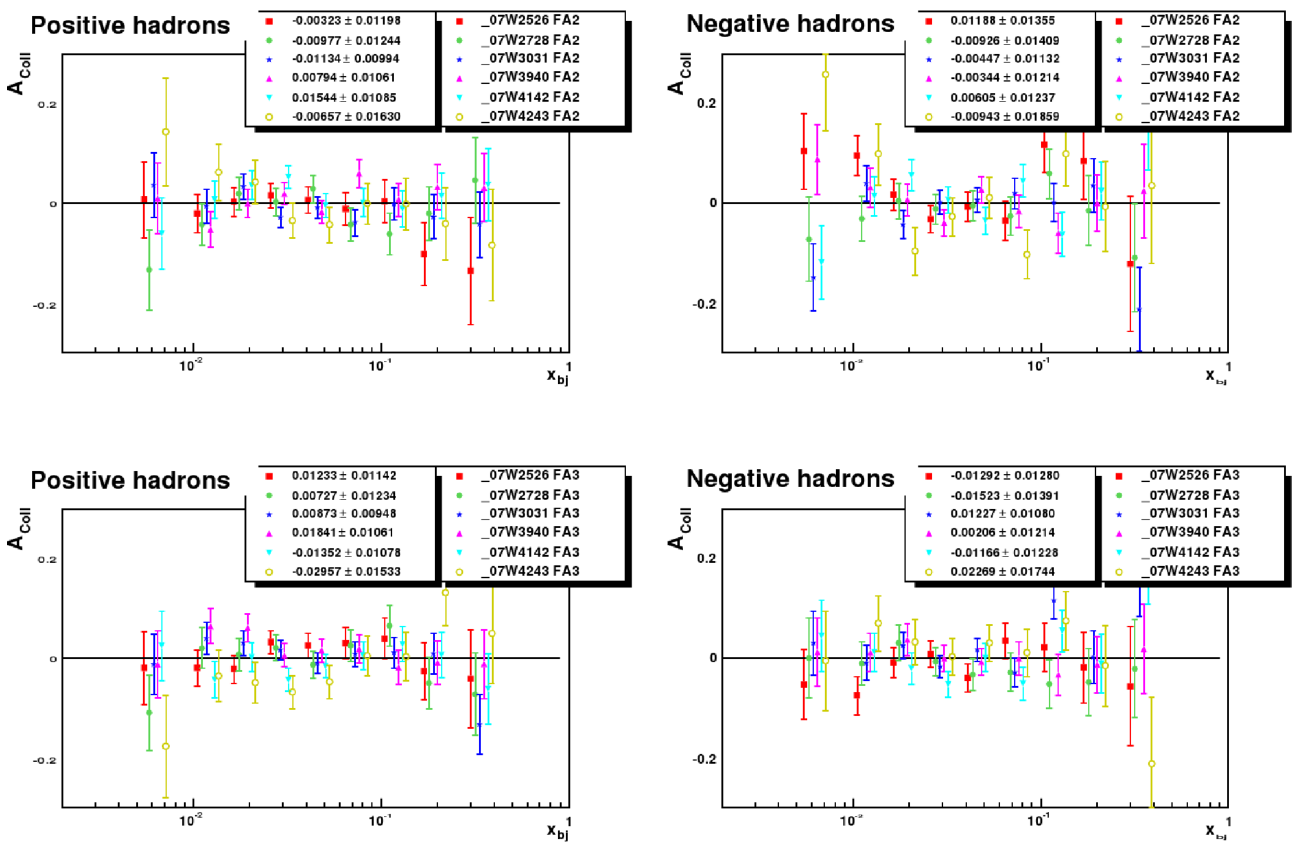

Figure B.1: *False Collins asymmetries, top:* conf_2 *(called here: FA2 for false asymmetries,* conf_2*), bottom:* conf_3 *(called here FA3 for false asymmetries,* conf_3*), left: positive, right: negative hadrons.*

B.2.2 Dependence on the Target Cells

To check the dependance of the asymmetries from the target cells the pulls P_{0-1} between the asymmetries extracted separately from conf_0 and conf_1 were calculated for all bins in x, z and P_T^h:

$$P_{0-1} = \frac{A_{\text{conf}_0} - A_{\text{conf}_1}}{\sqrt{\sigma^2_{\text{conf}_0} + \sigma^2_{\text{conf}_1}}} \tag{B.1}$$

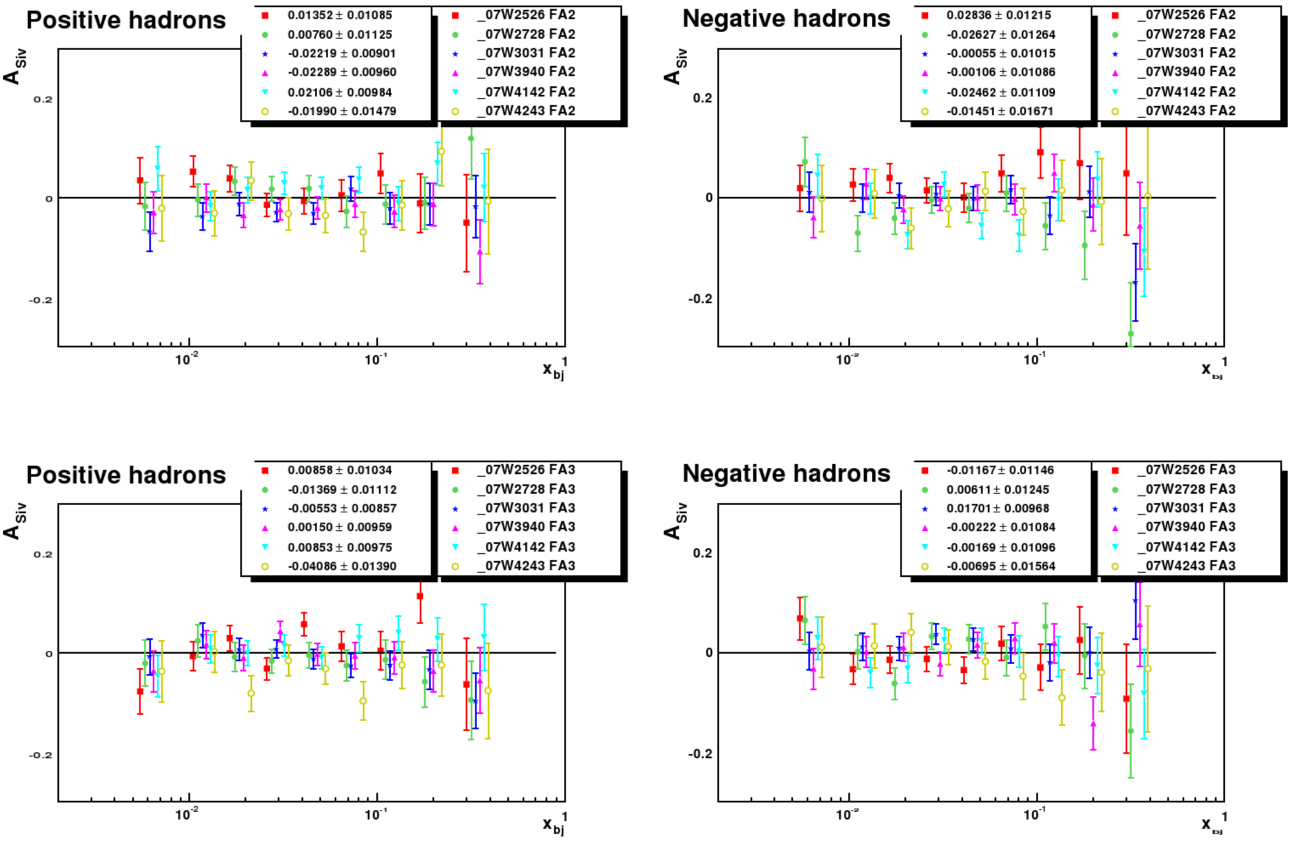

Figure B.2: *False Sivers asymmetries, top:* conf_2 *(called here FA2 for false asymmetries,* conf_2*), bottom:* conf_3 *(called here FA3 for false asymmetries,* conf_3*), left: positive, right: negative hadrons.*

where $A_{\mathrm{conf_i}}$ are the asymmetries for the corresponding configuration $\mathrm{conf_i}$ in a single bin and period. In the denominator we have the sum of the variances, because the samples are independent.
The distributions can be seen in fig. B.3 separately for Collins and Sivers asymmetries and positive and negative hadrons. The sigma[1] values are for Collins, positive and negative hadrons with 0.98 and 1.00, respectively, as well as for Sivers, positive hadrons, with 1.07 very near to 1 as expected for a standard normal distribution, while for Sivers, negative hadrons, the sigma value is with 0.88 not very close to 1, but at least sufficient. The mean values are for Collins with -0.04 for positive hadrons and 0.013 for negative hadrons compatible with zero, while the mean values of the Sivers distributions are shifted by -0.48 for positive hadrons and by 0.073 for negative ones, respectively. To test the compatibility of the results from conf_0 and conf_1 and those from conf_4, the following quantity P_{01-4} was evaluated for all periods and in all bins in x, z and P_T^h separately for Collins and Sivers

[1] $\sigma = \sqrt{\sigma^2_{\mathrm{conf}_0} + \sigma^2_{\mathrm{conf}_1}}$

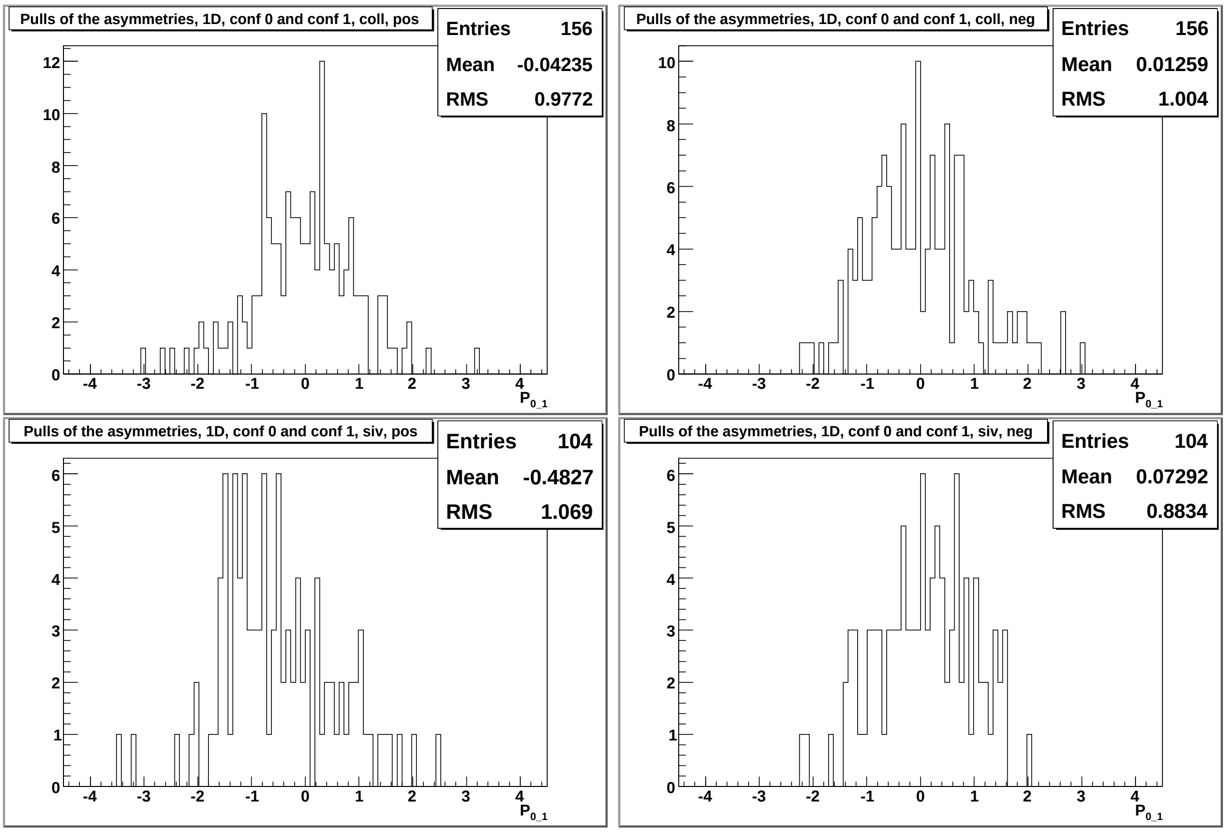

Figure B.3: *Top: Pulls P_{0-1} for Collins asymmetries between* conf_0 *and* conf_1 *for positive (left) and negative (right) hadrons. Bottom: Same for Sivers for positive (left) and negative (right) hadrons.*

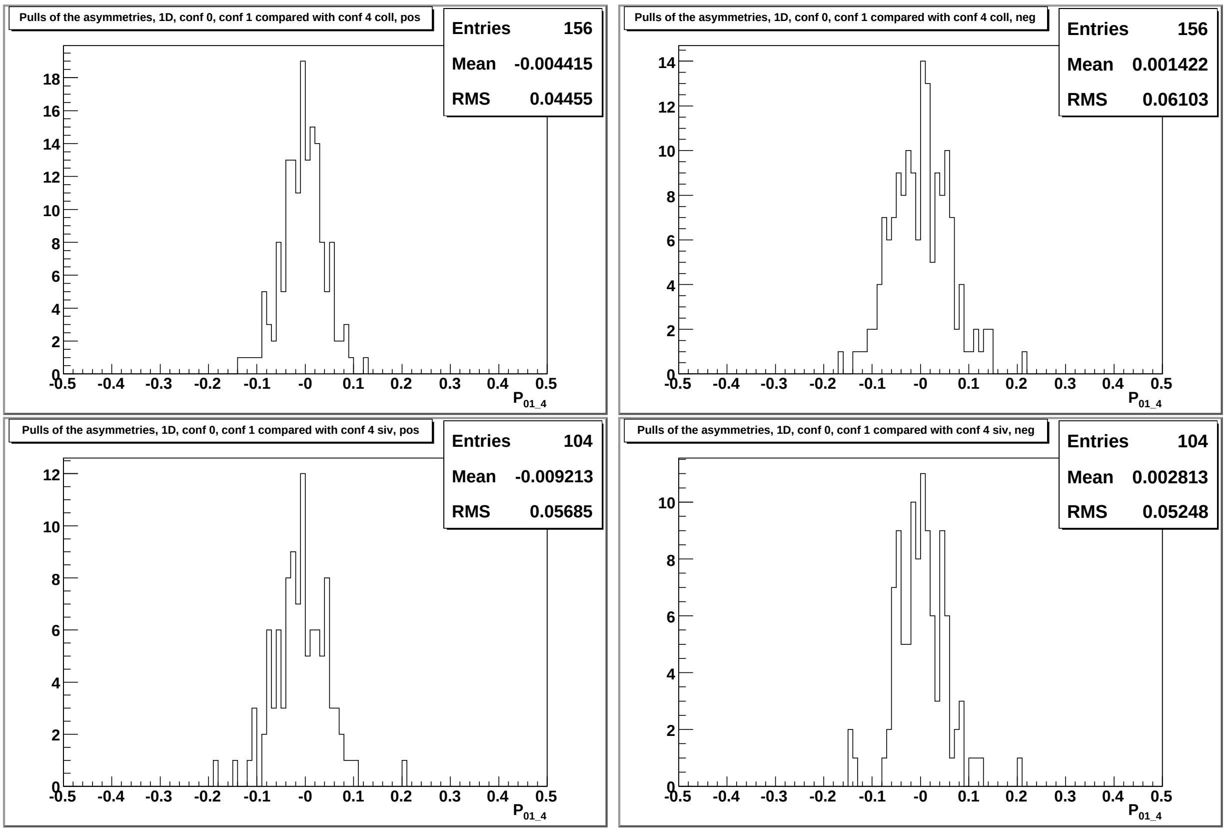

Figure B.4: *Top: Distribution of the quantity P_{01-4} defined in eq. (B.2) to test the compatibility between the results from* conf_0 *and* conf_1 *and those from* conf_4 *for Collins for positive (left) and negative (right) hadrons. Bottom: Same for Sivers for positive (left) and negative (right) hadrons.*

and positive and negative hadrons:

$$P_{01-4} = \frac{\langle A_{01} \rangle - A_{\mathrm{conf}_4}}{\left(\sigma_{\langle A_{01} \rangle} + \sigma_{\mathrm{conf}_4}\right)/2} \tag{B.2}$$

where

$$\langle A_{01} \rangle = \frac{A_{\mathrm{conf}_0}/\sigma^2_{\mathrm{conf}_0} + A_{\mathrm{conf}_1}/\sigma^2_{\mathrm{conf}_1}}{1/\sigma^2_{\mathrm{conf}_0} + 1/\sigma^2_{\mathrm{conf}_1}}; \qquad \sigma_{\langle A_{01} \rangle} = \frac{1}{\sqrt{1/\sigma^2_{\mathrm{conf}_0} + 1/\sigma^2_{\mathrm{conf}_1}}} \tag{B.3}$$

is the weighted mean of the asymmetries from conf_0 and conf_1 in a single period and bin and the corresponding error, respectively. As one can see in fig. B.4 the mean values and the sigma values are all near 0 as expected. The mean and sigma values of the distributions of the quantity P_{01-4} are all near 0 as expected. So we can conclude that the extraction from conf_0 and conf_1 is compatible with the one from conf_4.

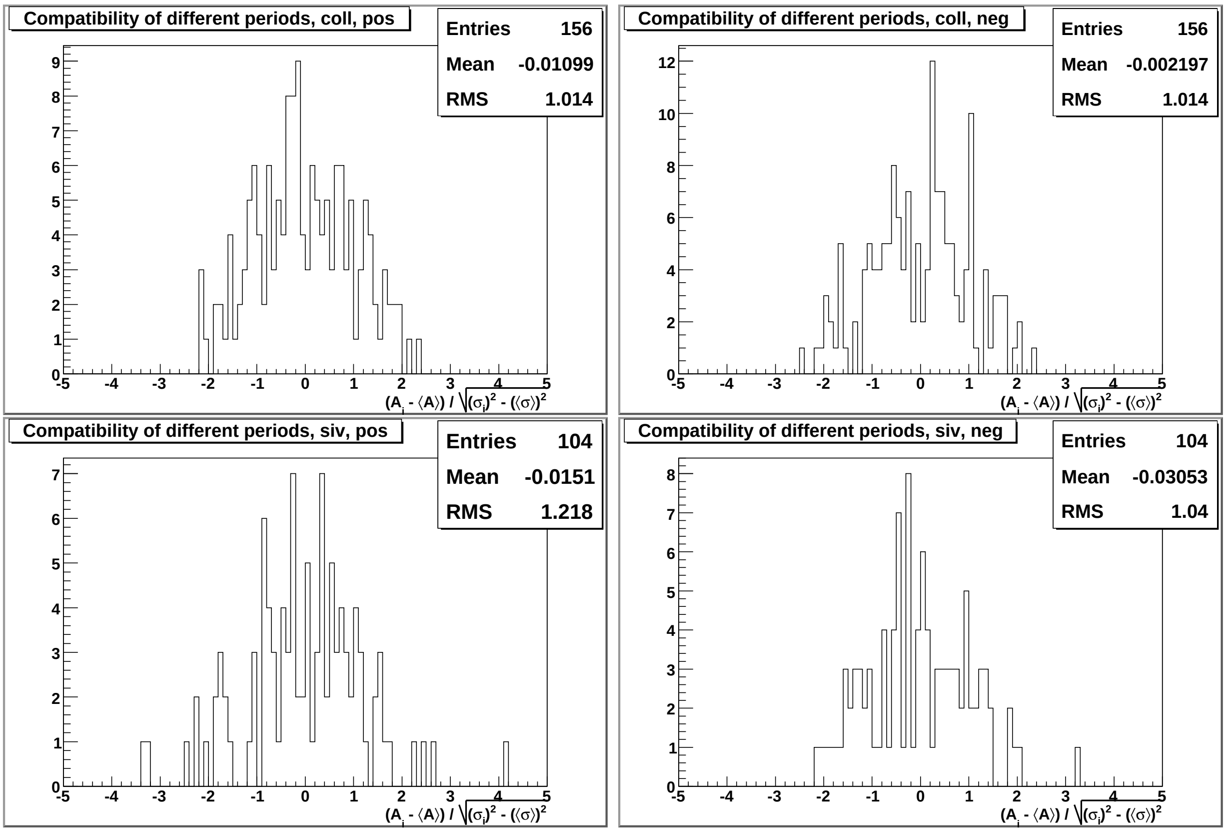

Figure B.5: *Top: Distribution of the quantity defined in eq. (B.4) to test the compatibility of the results from the different periods for the Collins asymmetries for positive (left) and negative (right) hadrons. Bottom: Same for Sivers for positive (left) and negative (right) hadrons.*

B.2.3 Compatibility of the Different Periods

The compatibility of the asymmetries in all bins of x, z and P_T^h for all periods were tested by checking the distribution of the following quantity:

$$\frac{A_i - \langle A \rangle}{\sqrt{\sigma_i^2 - \sigma_{\langle A \rangle}^2}}; \quad i = 1, 2, 3, 4, 5, 6 \tag{B.4}$$

A_i are again the asymmetries in a single bin and period and $\langle A \rangle$ the corresponding weighted mean of this bin. In all cases we got standard normal distributions with mean values compatible with zero and a RMS sufficently near 1 as expected, meaning that the results of the different periods are compatible (see fig. B.5).

Compatibility of first and second part of the run

For Sivers slight differences between the first and the second part of the run were found in the case of positive hadrons (see fig. B.7). The mean asymmetry values over the x bins are 0.024 ± 0.005 for the first part and 0.004 ± 0.006 for the second part. In contrast for Sivers, negative hadrons (see also fig. B.7), as well as for the Collins asymmetries (see fig. B.6) the differences were smaller.

B.2.4 Stability of Acceptances

R-test

The ratio R (see eq. (5.19)) was calculated for all bins in x, z and P_T^h. The resulting distributions are compared with the curves theoretically expected for seven degrees of freedom (eight bins in $\Phi_{C,S}$ and a one parameter fit). Despite some deviations of the χ^2 distributions from the expected curves an overall agreement was achieved (see fig. B.8 and B.9).

T-test

Due to the instabilities in addition a new test was implemented for further studies. This new test called "T" for "total" is based on the idea that spin effects should disappear at first order under the assumption that the acceptances cancel, if we sum the number of hadrons from all cells in one week:

$$\begin{aligned} T(\Phi) &= \frac{N_u^{\uparrow}(\Phi) + N_d^{\uparrow}(\Phi) + N_{c1}^{\downarrow}(\Phi) + N_{c2}^{\downarrow}(\Phi)}{N_u^{\downarrow}(\Phi) + N_d^{\downarrow}(\Phi) + N_{c1}^{\uparrow}(\Phi) + N_{c2}^{\uparrow}(\Phi)} \\ &\approx const \cdot \frac{a_u^{\uparrow}(\Phi) + a_d^{\uparrow}(\Phi) + a_{c1}^{\downarrow}(\Phi) + a_{c2}^{\downarrow}(\Phi)}{a_u^{\downarrow}(\Phi) + a_d^{\downarrow}(\Phi) + a_{c1}^{\uparrow}(\Phi) + a_{c2}^{\uparrow}(\Phi)} \end{aligned} \tag{B.5}$$

The ratio T should therefore in the ideal case be zero. For the further interpretation of the T-test we do the following presumptions:

- We got as conclusion of the numerous tests of all the different methods for asymmetry extraction that the only acceptance effect leading to a relevant error in the extraction of the physics asymmetries is a modulation of the same type as in the physics case.

- Both modulations, from acceptance as well as from physics, are small. Thus we can neglect terms in quadratic.

With the first presumption we can express the acceptances as a modulation like the one expected for the physics asymmetries (see eq. (4.6)): $a_i = const \cdot (1 + \alpha_i \cdot \sin\Phi)\,, \quad i \in$

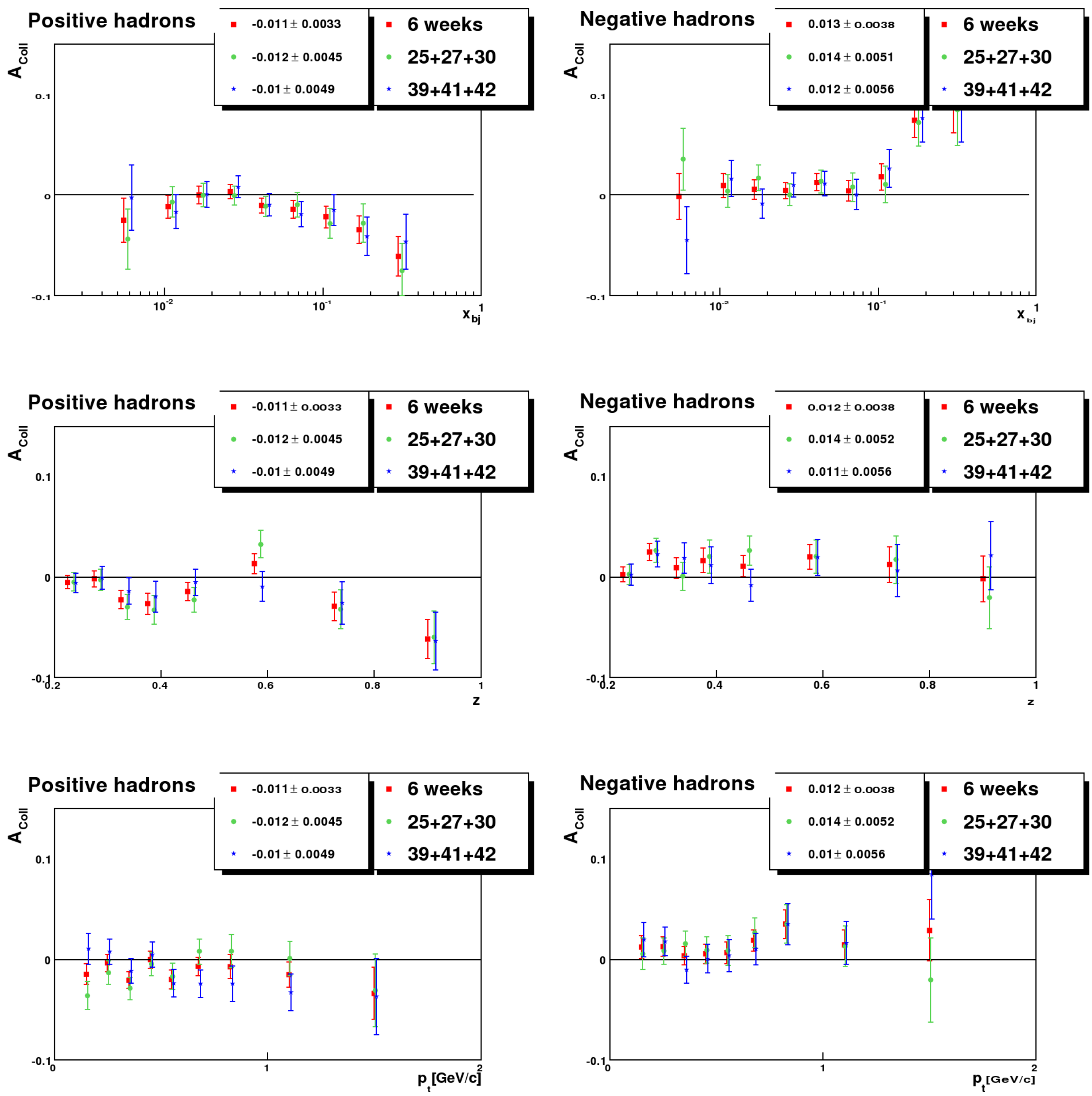

Figure B.6: *In red: Collins asymmetries vs. x. z and P_T^h using all six weeks from this analysis, in green: same with only those from the first part (here: W25/26, W27/28 and W30/31) and in blue: same with only those from the second part of the run (here: W39/40, W41/42-1 and W42/43). In all three cases: left: positive, right: negative hadrons.*

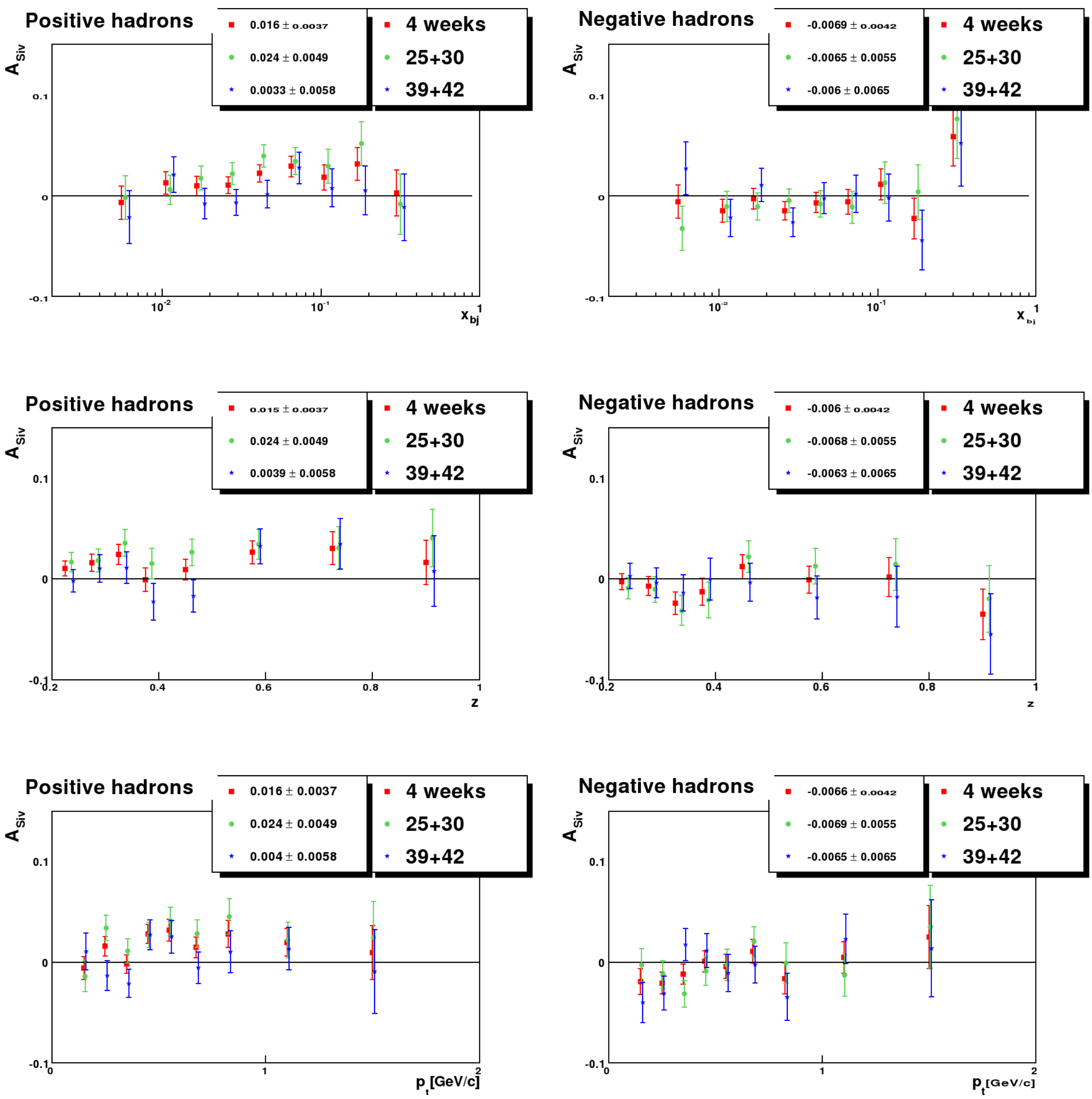

Figure B.7: *In red: Sivers asymmetries vs.* x*.* z *and* P_T^h *using all four weeks from this analysis, in green: same with only those from the first part (here: W25/26 and W30/31) and in blue: same with only those from the second part of the run (here: W39/40 and W42/43). In all three cases: left: positive, right: negative hadrons.*

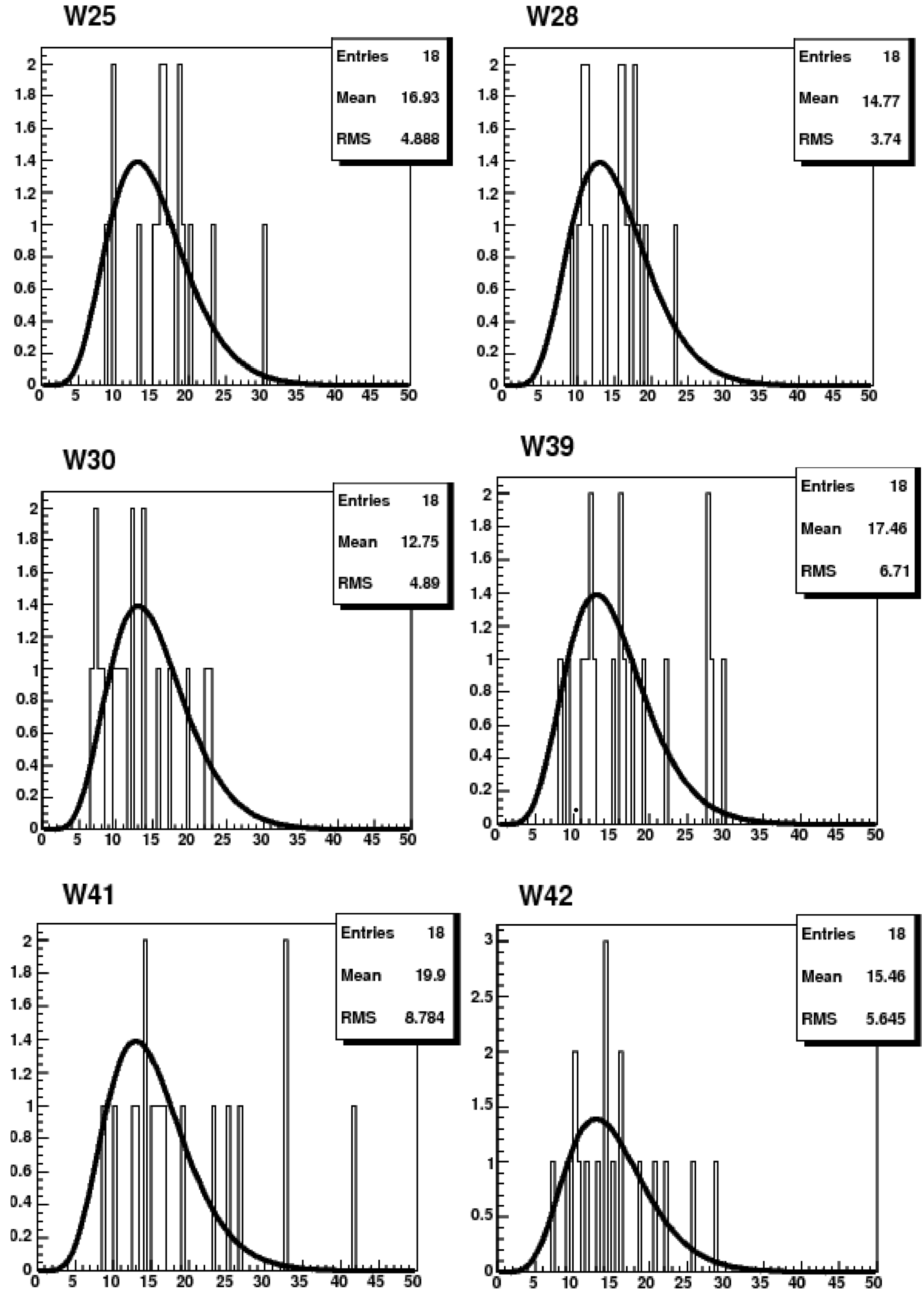

Figure B.8: χ^2 *distributions of the constant fit of* R *together for positive and negative hadrons for the bins in* x *for Collins for all periods: W25/26, W27/28, W30/31 (second "data production" used) and W39/40, W41/42-1, W42-2/43 (first "data production" used) compared to the curve theoretically expected for seven degrees of freedom.*

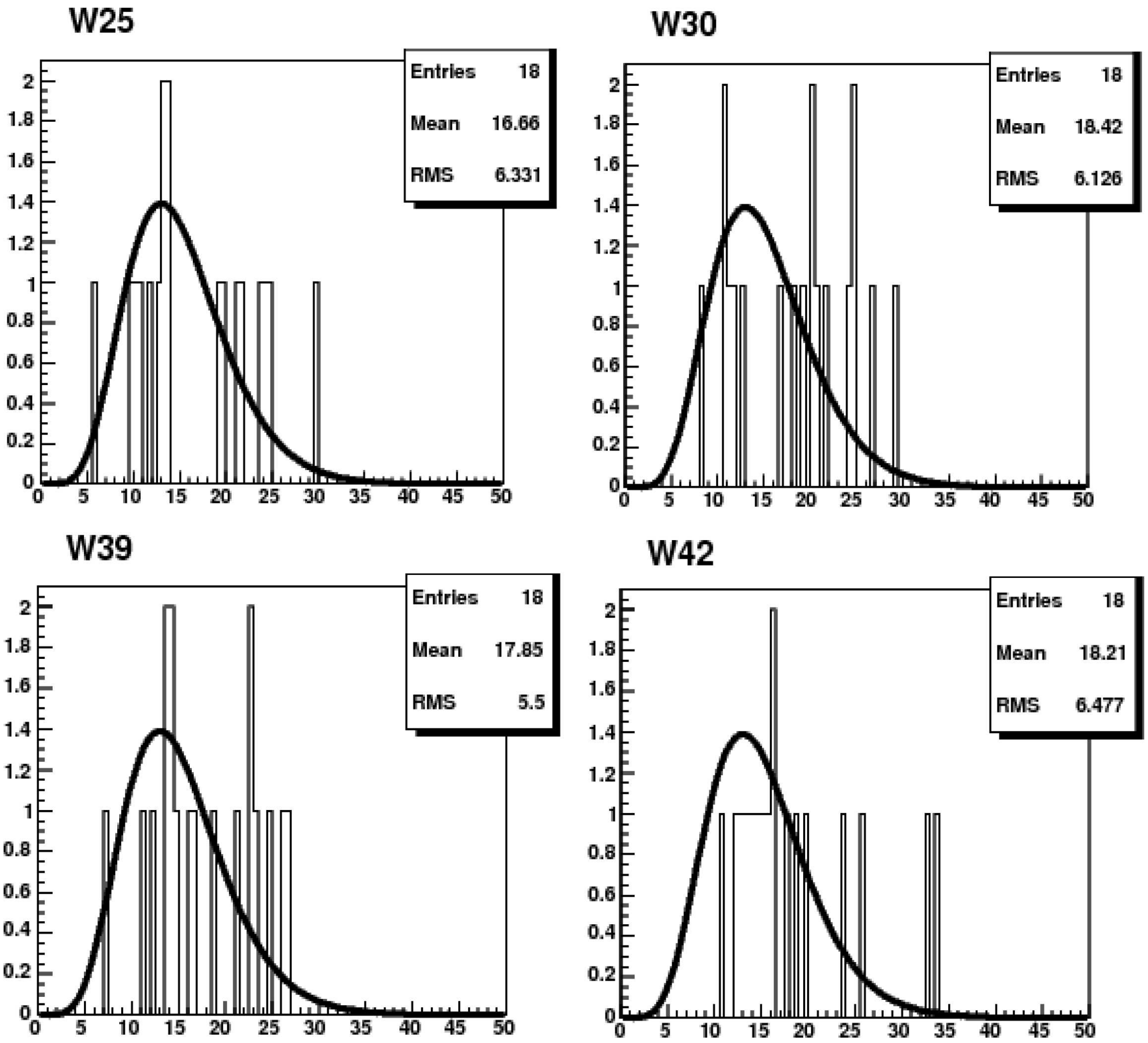

Figure B.9: χ^2 *distributions of the constant fit of* R *together for positive and negative hadrons for the bins in* x *for Sivers for the periods W25/26, W30/31 (second "data production", upper row) and W39/40, W42-2/43 (first "data production", lower row) compared to the curve theoretically expected for seven degrees of freedom.*

$u, c1, c2, d$. We then obtain from eq. (B.5):

$$
\begin{aligned}
T(\Phi) &= const \cdot \frac{4 + \left(\alpha_u^{\uparrow}(\Phi) + \alpha_d^{\uparrow}(\Phi) + \alpha_{c1}^{\downarrow}(\Phi) + \alpha_{c2}^{\downarrow}(\Phi)\right) \cdot \sin\Phi}{4 + \left(\alpha_u^{\downarrow}(\Phi) + \alpha_d^{\downarrow}(\Phi) + \alpha_{c1}^{\uparrow}(\Phi) + \alpha_{c2}^{\uparrow}(\Phi)\right) \cdot \sin\Phi} \qquad \text{(B.6)} \\
&\approx const \cdot \{1 + \frac{1}{4}\Big[\alpha_u^{\uparrow}(\Phi) + \alpha_d^{\uparrow}(\Phi) + \alpha_{c1}^{\downarrow}(\Phi) + \alpha_{c2}^{\downarrow}(\Phi) \\
&\quad - \left(\alpha_u^{\downarrow}(\Phi) + \alpha_d^{\downarrow}(\Phi) + \alpha_{c1}^{\uparrow}(\Phi) + \alpha_{c2}^{\uparrow}(\Phi)\right)\Big] \cdot \sin\Phi\} \\
&= const \cdot \{1 + \frac{1}{4}\left[e_u(\Phi) + e_d(\Phi) + e_{c1}(\Phi) + e_{c2}(\Phi)\right] \cdot \sin\Phi\}
\end{aligned}
$$

with $e_i = \alpha_i^{period1} - \alpha_i^{period2}, \quad i \in u, c1, c2, d.$
If we use the same hypothesis for R we get the relation $T = R/2$. To verify this we have fitted the values of T and R, respectively, with $const \cdot (1 + \epsilon_{T/R}\sin\Phi)$. Here $\epsilon_T = e_u + e_d + e_{c1} + e_{c2}$ and ϵ_R should be $\epsilon_R = 2 \cdot (e_u + e_d + e_{c1} + e_{c2})$. In the most cases the relation $T = R/2$ is valid for our data. One example can be seen in fig. B.10, where ϵ_T and ϵ_R are plotted vs. x.
For the physics asymmetries we get with the double ratio method analog to eq. (4.6) by splitting the middle cell and summing up the data from cells with the same polarization:

$$
F(\Phi) \approx const \frac{(a_u^{\uparrow}(\Phi) + a_d^{\uparrow}(\Phi)) \cdot (a_{c1}^{\uparrow}(\Phi) + a_{c2}^{\uparrow}(\Phi))}{(a_u^{\downarrow}(\Phi) + a_d^{\downarrow}(\Phi)) \cdot (a_{c1}^{\downarrow}(\Phi) + a_{c2}^{\downarrow}(\Phi))} \cdot (1 + 4\epsilon\sin\Phi) \qquad \text{(B.7)}
$$

with $\epsilon = A_{C,S}^{raw}$ as the raw Collins and Sivers asymmetry, respectively.
If we transform eq. (B.7) we obtain:

$$
\begin{aligned}
F(\Phi) &\approx const \frac{1 + \left(\alpha_u^{\uparrow}(\Phi) + \alpha_d^{\uparrow}(\Phi) + \alpha_{c1}^{\uparrow}(\Phi) + \alpha_{c2}^{\uparrow}(\Phi) + 2\epsilon\right) \cdot \sin\Phi}{1 + \left(\alpha_u^{\downarrow}(\Phi) + \alpha_d^{\downarrow}(\Phi) + \alpha_{c1}^{\downarrow}(\Phi) + \alpha_{c2}^{\downarrow}(\Phi) + 2\epsilon\right) \cdot \sin\Phi} \qquad \text{(B.8)} \\
&\approx const \cdot \{1 + \left[e_u(\Phi) + e_d(\Phi) - (e_{c1}(\Phi) + e_{c2}(\Phi)) + 4\epsilon\right] \cdot \sin\Phi\}
\end{aligned}
$$

Thus the estimated physics asymmetry is $\epsilon_F = \epsilon + \left[e_u + e_d - (e_{c1} + e_{c2})\right]/4$. This shows a bias, which is not obviously zero. Because the bias does not depend directly from ϵ_T, it can also be zero in the case of a non-zero ϵ_T under the assumption that the "reasonable" assumption (eq. (4.9), (4.10)) holds. Due to the smallness of the spin effects we are looking for, we will not use any data, which exhibit very large values of ϵ_T, so that we are on the safe side.
The values of ϵ_T vs. x for the case of the Collins asymmetries are given in fig. B.11. On the left-hand side the results for positive and on the right-hand side those for negative hadrons are shown, on the upper side for the first part of the run and on the lower part for the second part of the run. As one can see there are appreciable deviations from zero for ϵ_T indicating that in both, in the acceptances of the single cells and in the global acceptance, there are $\sin\Phi$ modulations varying for the different weeks. Besides this the trend of the

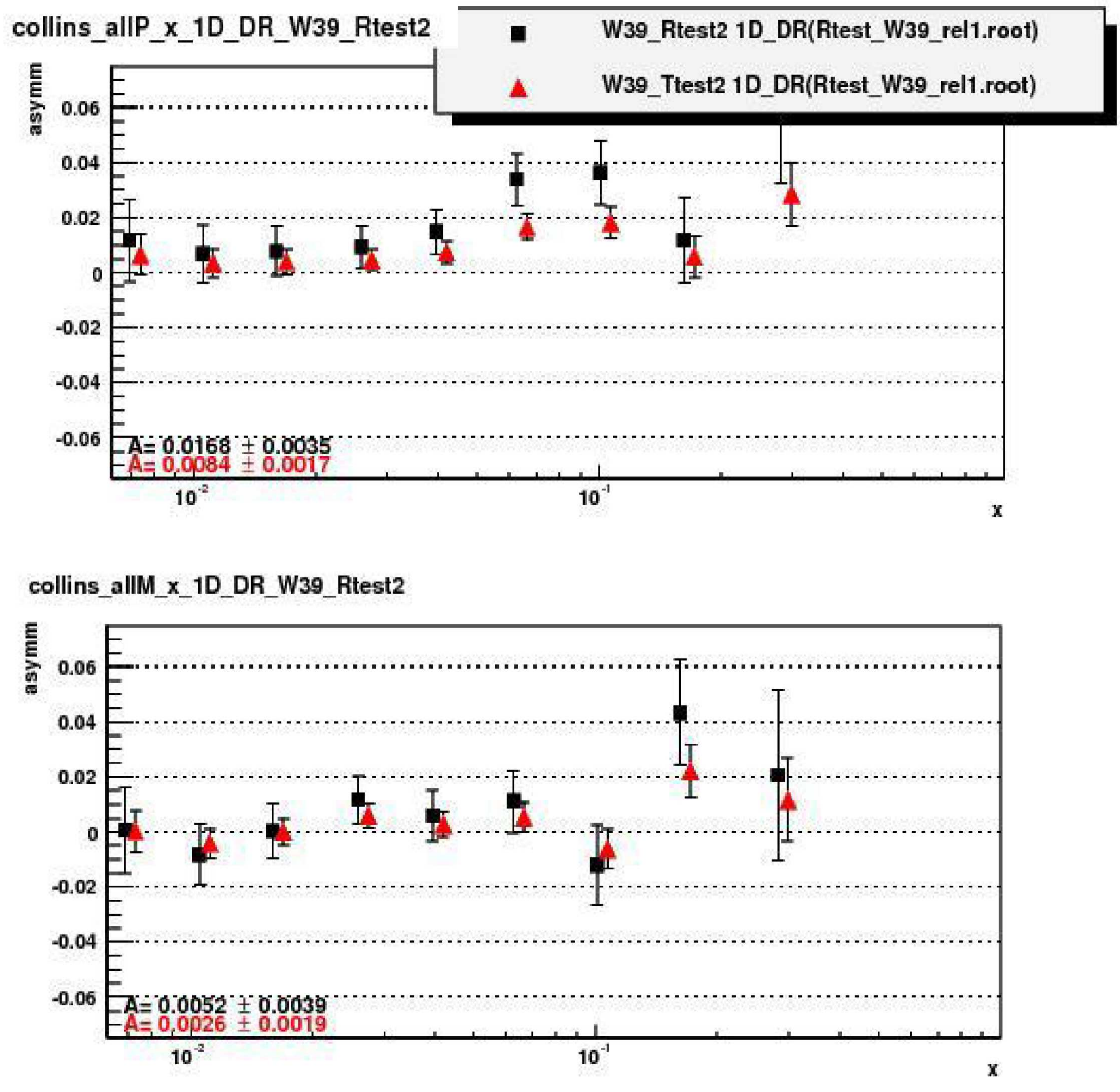

Figure B.10: ϵ_T *(in red) and* ϵ_R *(in black) vs.* x *as example for one period (W39/40) in the case of the Collins asymmetries for positive (upper plot) and negative (lower plot) hadrons.*

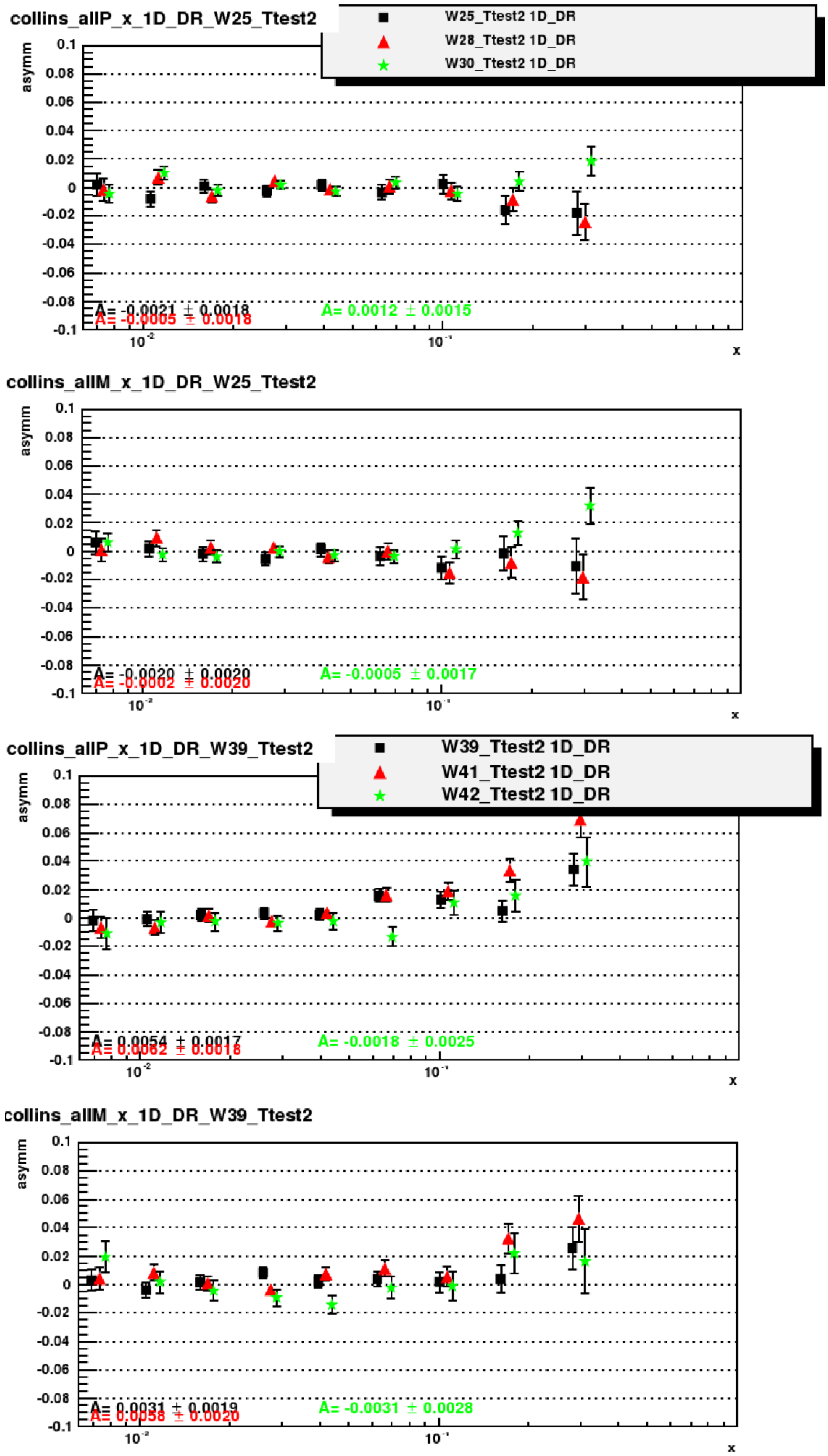

Figure B.11: *First row: ϵ_T vs. x for the case of the Collins asymmetries for positive hadrons for the first half of the 2007 run (in black: W25/26, in red: W27/28, in green: W30/31; second "data production"). Second row: Same for negative hadrons for the first half of the 2007 run. Third row: Same for positive hadrons for the second half of data taking (in black: W39/40, in red: W41/42-1, in green: W42-2/43; first "data production"). Fourth row: Same for negative hadrons for the second half of data taking.*

values is not stable over the different periods, which makes an investigation with a Monte Carlo simulation impossible. For a three cell setup it is also possible instead of building the double ratio to combine the data in a "quad-ratio" method in the following way:

$$\begin{aligned} F^{QR}(\Phi) &= \frac{N_u^{\uparrow}(\Phi)N_{c1}^{\uparrow}(\Phi)N_{c2}^{\uparrow}(\Phi)N_d^{\uparrow}(\Phi)}{N_u^{\downarrow}(\Phi)N_{c1}^{\downarrow}(\Phi)N_{c2}^{\downarrow}(\Phi)N_d^{\downarrow}(\Phi)} \\ &\approx const \cdot \{1 + [e_u(\Phi) - e_{c1}(\Phi) - e_{c2}(\Phi) + e_d(\Phi) + 8\epsilon] \cdot \sin\Phi\} \end{aligned} \tag{B.9}$$

This allows also to define a new T-test. To get a complete cancelation of acceptance effects without any approximation the counting rates were now combined as a product instead as a sum like in eq. (B.5):

$$\begin{aligned} T^{QR}(\Phi) &= \frac{N_u^{\uparrow}(\Phi)N_{c1}^{\downarrow}(\Phi)N_{c2}^{\downarrow}(\Phi)N_d^{\uparrow}(\Phi)}{N_u^{\uparrow}(\Phi)N_{c1}^{\downarrow}(\Phi)N_{c2}^{\downarrow}(\Phi)N_d^{\uparrow}(\Phi)} \\ &\approx const \cdot \frac{a_u^{\uparrow}(\Phi)a_{c1}^{\downarrow}(\Phi)a_{c2}^{\downarrow}(\Phi)a_d^{\uparrow}(\Phi)}{a_u^{\downarrow}(\Phi)a_{c1}^{\uparrow}(\Phi)a_{c2}^{\uparrow}(\Phi)a_d^{\downarrow}(\Phi)} \end{aligned} \tag{B.10}$$

With the assumption from above $a_i = const \cdot (1 + \cdot \sin\Phi)\,,\quad i \in u, c1, c2, d$ we get:

$$T^{QR}(\Phi) = const \cdot \{1 + [e_u(\Phi) + e_{c1}(\Phi) + e_{c2}(\Phi) + e_d(\Phi)] \cdot \sin\Phi\} \tag{B.11}$$

To be compatible with the values of the T-test defined in eq. (B.5) the results of T^{QR} are divided by a factor of 4.

Test of the "reasonable" assumption

The "reasonable" assumption defined in eq. (4.9), which can be formulated as $e_u = e_{c1} = e_{c2} = e_d$, is tested also in the following way: By coupling two sub-periods with opposite spin configurations it is possible to extract four independent asymmetry values, one for each target cell. Those measured asymmetries are given by the sum of the physics asymmetry ϵ and the change of acceptance for this cell e_i with $i \in u, c1, c2, d$:

$$\begin{aligned} A_1 &= \epsilon + \frac{e_1}{2} \\ A_2 &= \epsilon - \frac{e_2}{2} \\ A_3 &= \epsilon - \frac{e_3}{2} \\ A_4 &= \epsilon + \frac{e_4}{2} \end{aligned} \tag{B.12}$$

The mean asymmetry and the mean variation of the acceptance can be extracted with the measured asymmetries A_i and their sigma values σ_i by the equations

$$\epsilon = \frac{\sum \frac{A_i}{\sigma_i^2}}{\sum \frac{1}{\sigma_i^2}} \tag{B.13}$$

and

$$\begin{aligned}
\langle e \rangle = \frac{\sum \frac{e_i}{\sigma_i^2}}{\sum \frac{1}{\sigma_i^2}} = \frac{\sum \frac{\pm 2A_i - \epsilon}{\sigma_i^2}}{\sum \frac{1}{\sigma_i^2}} \\
= \frac{1}{\sum \frac{1}{\sigma_i^2}} \left[(2A_1 - \epsilon)\frac{1}{\sigma_1^2} - (2A_2 - \epsilon)\frac{1}{\sigma_2^2} - (2A_3 - \epsilon)\frac{1}{\sigma_3^2} + (2A_4 - \epsilon)\frac{1}{\sigma_4^2} \right] \\
= \frac{2}{\sum \frac{1}{\sigma_i^2}} \left(A_1 \frac{1}{\sigma_1^2} - A_2 \frac{1}{\sigma_2^2} - A_3 \frac{1}{\sigma_3^2} + A_4 \frac{1}{\sigma_4^2} \right) \\
+ \frac{\epsilon}{\sum \frac{1}{\sigma_i^2}} \underbrace{\left(-\frac{1}{\sigma_1^2} + \frac{1}{\sigma_2^2} + \frac{1}{\sigma_3^2} - \frac{1}{\sigma_4^2} \right)}_{=0 \text{ for about the same statistics}} \\
= \frac{2}{\sum \frac{1}{\sigma_i^2}} \left(A_1 \frac{1}{\sigma_1^2} - A_2 \frac{1}{\sigma_2^2} - A_3 \frac{1}{\sigma_3^2} + A_4 \frac{1}{\sigma_4^2} \right)
\end{aligned} \quad \text{(B.14)}$$

If the "reasonable" assumption is valid, the acceptance variations in each target cell have to be compatible with their mean value, which can be tested by calculating the following χ^2:

$$\chi^2_{RA} = \sum \left(\frac{A_i - (\epsilon \pm \langle e \rangle)}{\sigma_i} \right)^2 \quad \text{(B.15)}$$

with two degrees of freedom because of the four measurements and two estimated mean values ϵ and $\langle e \rangle$.

Quality tables for acceptance variations

To evaluate the acceptance variations the results of the T-test and the test of the "reasonable" assumption have to be combined. χ^2_T for the T-test we define as comparison of the measured T value with the hypothesis $T = 0$, meaning that the acceptance does not vary between two coupled sub-periods:

$$\chi^2_T = \sum \left(\frac{T}{2\sigma} \right)^2 \quad \text{(B.16)}$$

The factor 2 is motivated by the fact that the condition $T = 0$ is a stricter requirement than the "reasonable" assumption.
χ^2_{tot} we than obtain by:

$$\chi^2_{tot} = \chi^2_{RA} + \chi^2_T \quad \text{(B.17)}$$

The χ^2_{tot} values calculated separately for positive and negative hadrons are afterwards summed up to get an overall confidence level of the regarding period or sub-period. This analysis was done separately for the nine x bins as well as for asymmetries and T values extracted after integrating over x. As both approaches are compatible only the results on x integrated values are shown in the following.

Collins						
	W39/40 1st prod		W41/42-1 1st prod		W42-2/43 1st prod	
	$h+$	$h-$	$h+$	$h-$	$h+$	$h-$
χ^2_{RA} (2 NdF)	4.04	0.078	3.77	0.84	4.29	1.58
χ^2_T (1 NdF)	2.4	0.63	3.9	2.25	0.15	0.26
χ^2_{tot}	6.44	0.72	6.86	3.10	4.44	1.85
	7.16 (30 %)		9.96 (12 %)		6.29 (40 %)	
	W39/40 2nd prod		W41/42-1 2nd prod		W42-2/43 2nd prod	
	$h+$	$h-$	$h+$	$h-$	$h+$	$h-$
χ^2_{RA} (2 NdF)	2.92	1.37	2.56	0.51	0.36	1.38
χ^2_T (1 NdF)	1.56	0.19	18	9.75	3.84	2.7
χ^2_{tot}	3.85	1.56	20.50	10.26	4.20	4.08
	5.41 (49 %)		30.76 (0 %)		8.28 (22 %)	

Table B.2: χ^2 *values for Collins-like modulations in the second part of the 2007 run (W39-43), first and second data production, for the test of the "reasonable" assumption, the T-test and both combined as* χ^2_{tot} *as well as the overall confidence level.*

To get a decision, which of the two different data productions has a better quality for the second part of the run, the χ^2_{tot} values for both productions are compared. As one can see in tables B.2 and B.3 the test on the "reasonable" assumption gives nearly the same results for both productions, while the T-test is significantly worse for the second production. For this reason the first data production was used to extract the asymmetries from the second part of the run.
In the tables B.4 and B.5 the χ^2 values for both tests as well as the combined χ^2_{tot} and the overall confidence levels for the first part of the 2007 run are shown. Also here for the Sivers-like modulations only the results for the used periods W25/26 and W30/31 are given.
As for the Sivers-like modulations W42-2/43, W25/26 and W30/31 have sconfidence level of only a few percent, the systematic error for the Sivers asymmetries has to be evaluated very carefully in these cases.
For Collins all periods have confidence levels of 12 to 78%, which is at least sufficient for a reliable analysis.

B.2.5 Comparison of Different Estimators

The unbinned maximum likelihood method and the "double ratio" method to extract the asymmetries were compared by building the following distribution:

$$\frac{A_{DR} - A_{unbLH}}{(\sigma_{DR} + \sigma_{unbLH})/2} \tag{B.18}$$

Sivers				
	W39/40 1st prod		W42-2/43 1st prod	
	$h+$	$h-$	$h+$	$h-$
χ^2_{RA} (2 NdF)	5.83	0.05	10.67	0.94
χ^2_T (1 NdF)	1.13	0	1.82	0.25
χ^2_{tot}	6.90	0.05	12.49	1.19
	6.95 (33 %)		13.68 (3.3 %)	
	W39/40 2nd prod		W42-2/43 2nd prod	
	$h+$	$h-$	$h+$	$h-$
χ^2_{RA} (2 NdF)	1.77	0.49	8.42	2.19
χ^2_T (1 NdF)	2.7	14.7	2.3	7.6
χ^2_{tot}	0.65	15.19	10.72	9.79
	15.84 (1,5 %)		20.51 (0.2 %)	

Table B.3: χ^2 *values for Sivers-like modulations in the second part of the 2007 run, first and second data production, for the test of the "reasonable" assumption, the T-test and both combined as* χ^2_{tot} *as well as the overall confidence level. Only the periods W39/40 and W42-2/43 used in this a analysis are shown.*

Collins						
	W25/26		W27/28		W30/31	
	$h+$	$h-$	$h+$	$h-$	$h+$	$h-$
χ^2_{RA} (2 NdF)	0.99	2.52	1.18	1.86	2.37	1.75
χ^2_T (1 NdF)	0.6	0.12	0.12	0.12	0.13	0.13
χ^2_{tot}	1.59	2.64	1.29	1.98	2.49	1.87
	4.2	(65 %)	3.20	(78 %)	4.30	(63 %)

Table B.4: χ^2 *values for Collins-like modulations in the first part of the 2007 run (W25-31), second data production, for the test of the "reasonable" assumption, the T-test and both combined as* χ^2_{tot} *as well as the overall confidence level.*

Sivers				
	W25/26		W30/31	
	$h+$	$h-$	$h+$	$h-$
χ^2_{RA} (2 NdF)	2.00	6.42	6.89	3.40
χ^2_T (1 NdF)	3.25	0.04	0.11	2.0
χ^2_{tot}	5.25	6.46	7.0	5.4
	11.71	(6.9 %)	12.4	(5.4 %)

Table B.5: χ^2 *values for Sivers-like modulations in the first part of the 2007 run, second data production, for the test of the "reasonable" assumption, the T-test and both combined as* χ^2_{tot} *as well as the overall confidence level. Only the periods W25/26 and W30/31 used in this a analysis are shown.*

where A_{DR} are the asymmetries calculated with the "double ratio" and A_{unbLH} those with the unbinned maximum likelihood method. These distributions were calculated separately for Collins and Sivers, for positive and negative hadrons and are shown in fig. B.12. We can see that the two methods differ by $0.2 - 0.3$ of the statistical error. It was therefore decided to assign for a value of 0.15 σ as contribution of the asymmetry estimator to the systematic error.

B.2.6 Systematic Studies for K^0 Asymmetries

Compatibility of the Results in the Different Periods

For the compatibility of the K^0 asymmetries the distribution of the following quantity was evaluated:

$$\frac{A_i - \langle A \rangle}{\sqrt{\sigma_i^2 - \sigma_{\langle A \rangle}^2}}; \quad i = 1, 2, 3, 4, 5, 6 \tag{B.19}$$

where A_i are again the asymmetries in each bin and period and $\langle A \rangle$ the corresponding weighted mean.
Those distributions are shown separately for the Collins and Sivers asymmetries in fig. B.13. The number of entries in the case of Collins is 96 corresponding to 6 (periods) $\cdot$ $(5 + 6 + 5)$ (bins in x_{bj}, z and P_T^h), while it is for Sivers 64 corresponding to 4 (periods) $\cdot$ $(5 + 6 + 5)$ (bins in x_{bj}, z and P_T^h). The resulting mean values are for both, Collins and Sivers, close to 0 and the RMS close to 1 as expected for a standard normal distribution. So we can conclude that the results from the different periods are compatible.

Studies on Background Asymmetries

It was also checked, if there are background asymmetries. For this asymmetries in a mass range outside the one of the K^0-signal were extracted. Here a range of $[-40, -200] \cup [40, 200]$ MeV in the difference of the measured invariant mass and the literature value was

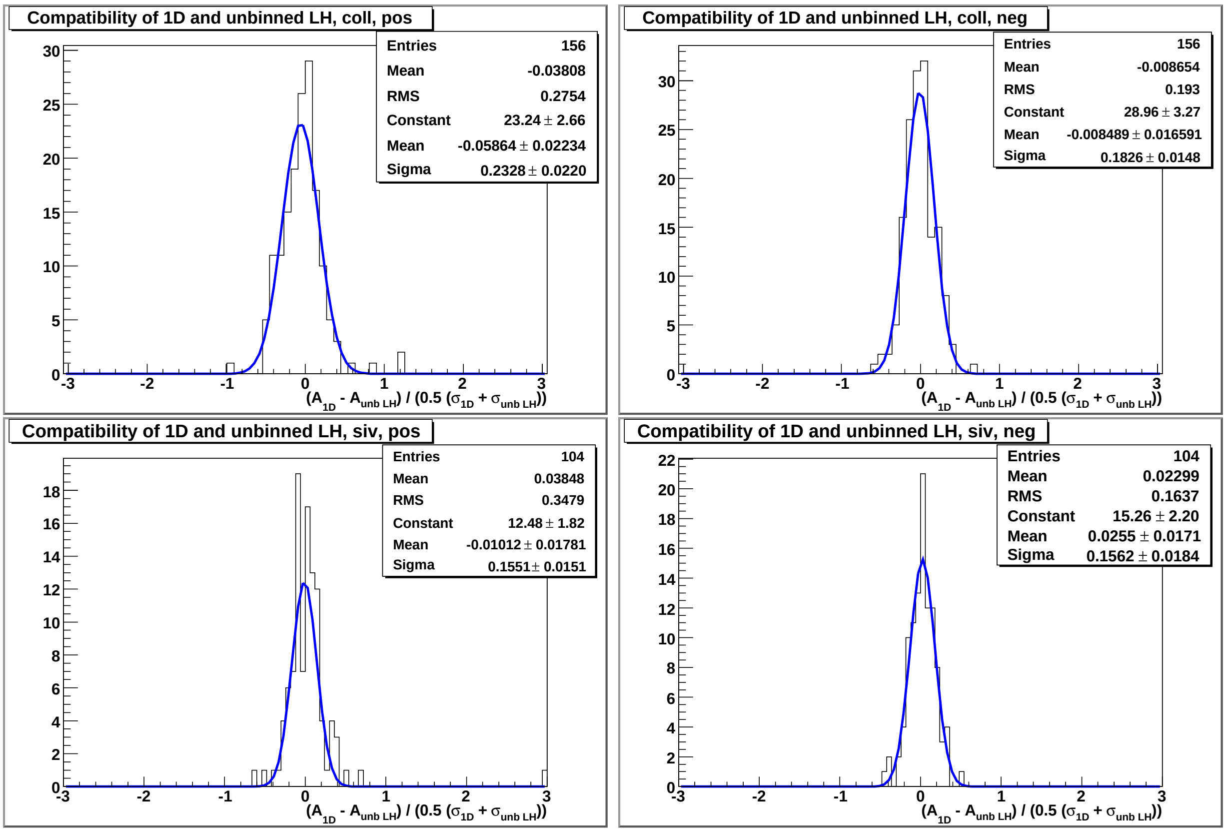

Figure B.12: *Top: Distribution of the quantity defined in eq. (B.18) to compare the results from the "double ratio" and the ones from the unbinned maximum likelihood method for Collins for positive hadrons (left) and negative hadrons (right). Bottom: Same for Sivers for positive hadrons (left) and negative hadrons (right).*

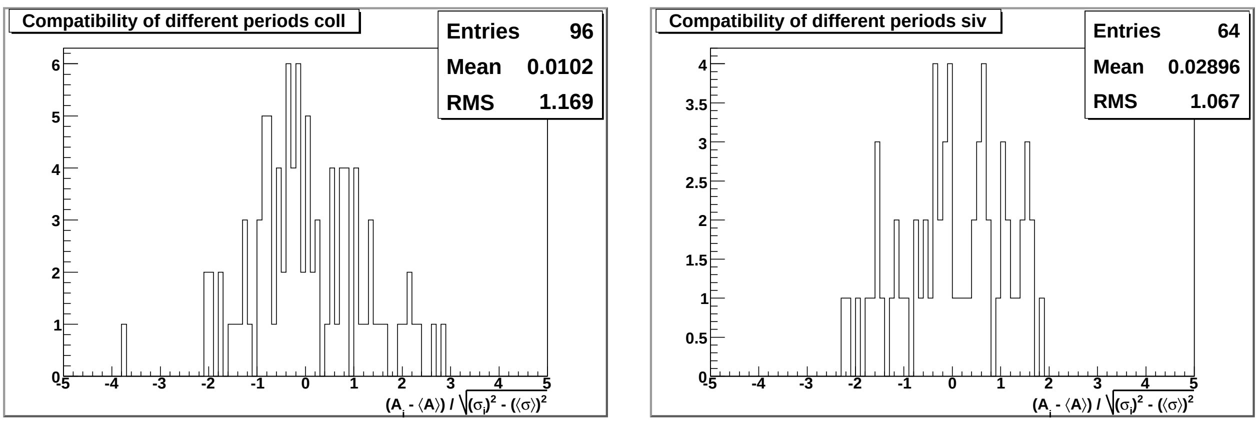

Figure B.13: *Distribution of the quantity defined in eq. (B.19) to test the compatibility of the results from the different periods for Collins (left) and Sivers (right) for K^0 production.*

chosen. The binning is the same like for the analysis of the asymmetries for K^0 production itself (see table 5.6).
For simplicity the "double ratio" method was used for the extraction of those sideband asymmetries. As it is known that particularly for a zero asymmetry the "double ratio" method has only evanescent differences to the unbinned likelihood method, this is justified for a test of the compatibility with zero like it is done here.
The weighted mean of the resulting background asymmetries for all six periods for Collins and Sivers is shown as function vs. x, z and P_T^h in fig. B.14, separately for Collins and Sivers. All those sideband asymmetries are consistent with zero.

Evaluation of false asymmetries

Possible false results due to systematic effects were evaluated by calculating the asymmetries inside one week from two data samples created by giving numbers to all events of this week and dividing the data sample of this week into two parts, one with the odd and one with the even event numbers. One sample is than treated like one sub-period (week) and the other one as the corresponding one with opposite polarization. As for the background asymmetries also for this test it was justified to use the "double ratio" method.
Then the weighted mean of these false asymmetries vs. x, z and P_T^h was built one time using from all weeks W25-43 for Collins and Sivers, respectively, only those with one target spin configuration, here those with + - + were taken, namely W25, W27, W31, ... (see table 5.1), another time the weighted mean with all weeks was built. The results are shown in fig. B.15 for the weighted mean only of the periods with the target spin configuration + - + and in fig. B.16 for the weighted mean of all weeks. It can be seen that the false asymmetries are compatible with zero.

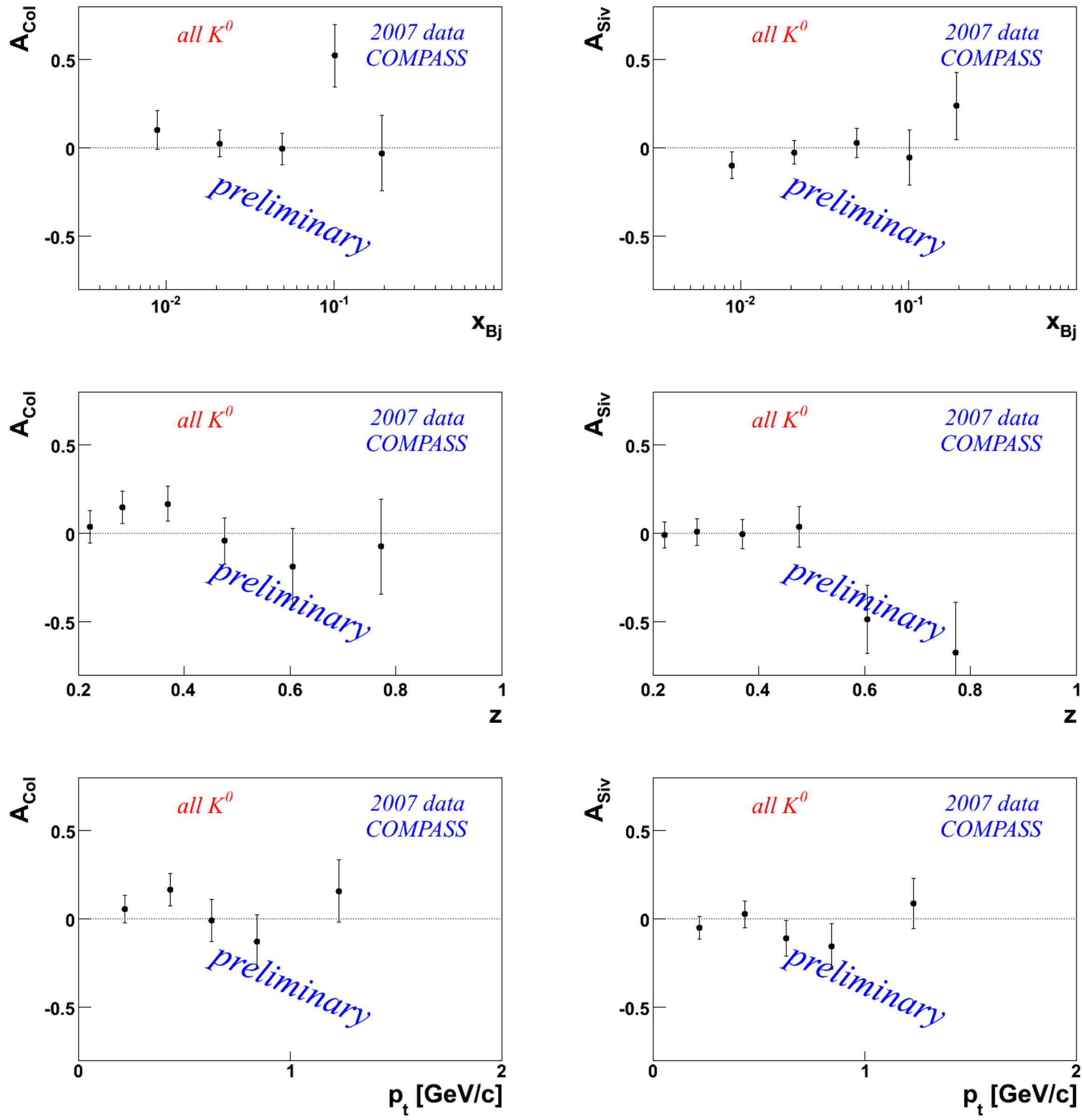

Figure B.14: *Weighted mean of the asymmetries in the sidebands for the 2007 proton data from COMPASS vs. x, z and P_T^h. Left: Collins asymmetry, right: Sivers asymmetry.*

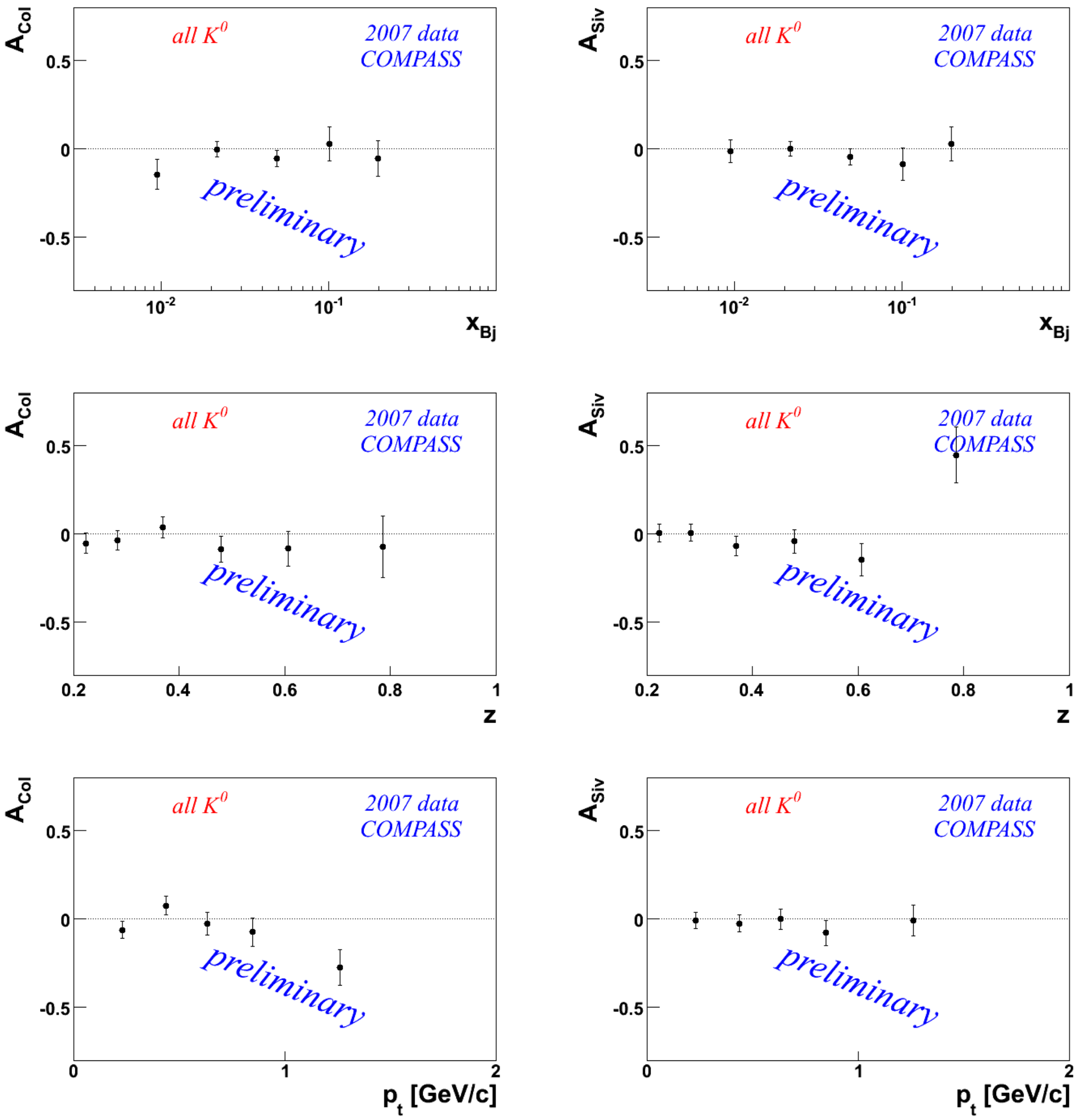

Figure B.15: *Weighted mean of the false asymmetries from odd and even event numbers vs. x, z and P_T^h using only weeks with target spin configuration + - +. Left: False Collins asymmetries, right: False Sivers asymmetries.*

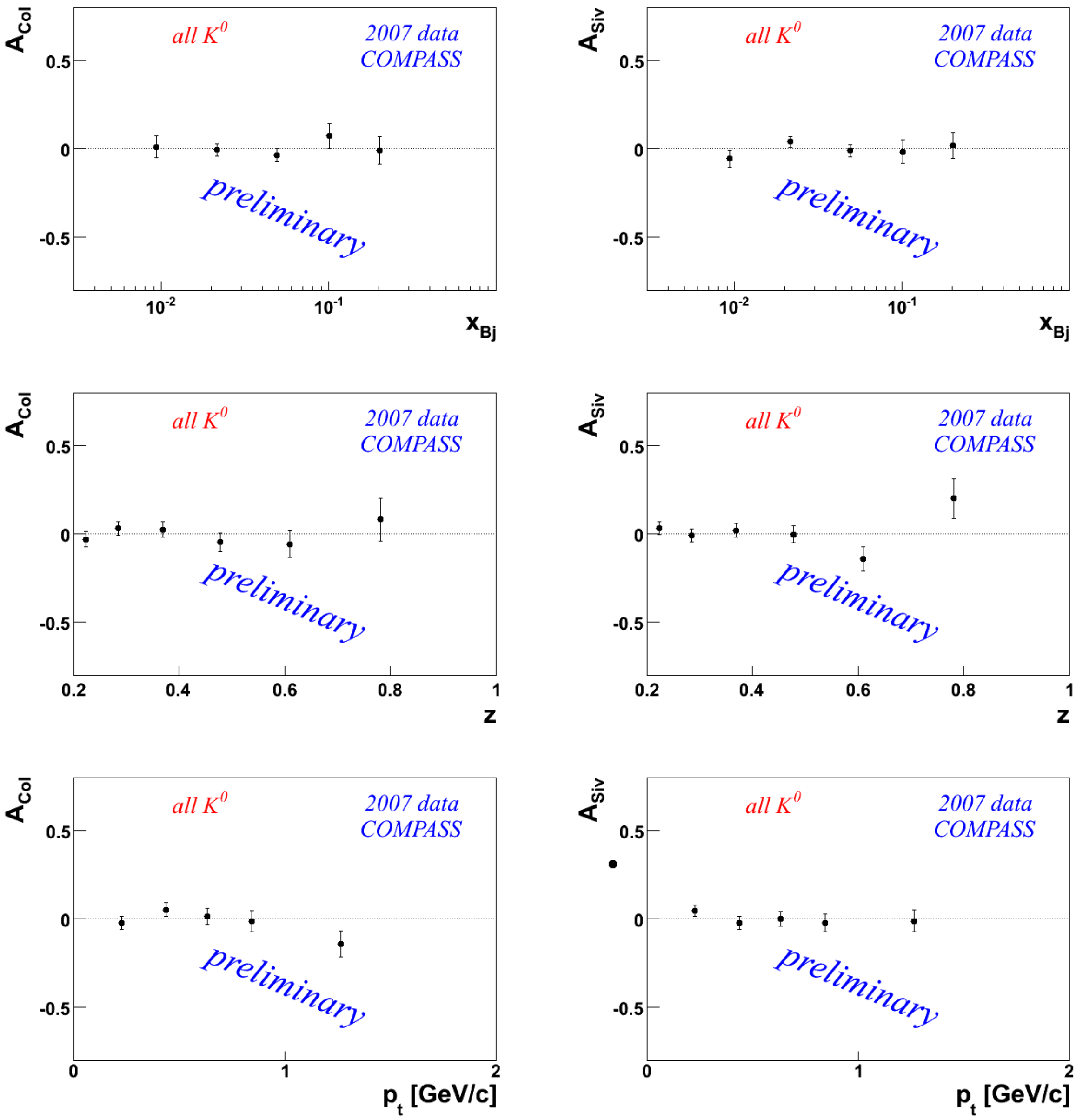

Figure B.16: *Weighted mean of the false asymmetries from odd and even event numbers vs. x, z and P_T^h for all weeks W25-43. Left: False Collins asymmetries, right: False Sivers asymmetries.*

Bibliography

Bookishness drives people mad.

Desiderius Erasmus of Rotterdam
(1466/69-1536),
Dutch Renaissance humanist

[1] J. Ashman et al., [European Muon Collaboration], *A measurement of the spin asymmetry and determination of the structure function* g_1 *in deep inelastic muon-proton scattering.*, (Phys. Lett. B, (206):364, 1988).

[2] J. Ashman et al., [European Muon Collaboration], *An investigation of the spin structure of the proton in deep inelastic scattering of polarised muons on polarised protons.*, (Nucl. Phys. B, (328):1, 1989).

[3] B. L. G. Bakker, E. Leader and T. L. Trueman, *Critique of the angular momentum sum rules and a new angular momentum sum rule.*, (Phys. Rev. D, (70):114001, 2004).

[4] J. C. Collins, *Fragmentation of Transversely Polarized Quarks Probed in Transverse Momentum Distributions.*, (Nucl. Phys. B, (396):161, 1993).

[5] D. W. Sivers, *Single-spin production asymmetries from the hard scattering of pointlike constituents.*, (Phys. Rev. D, (41):83, 1990).

[6] Povh, Rith, Scholz, Zetsche, *Teilchen und Kerne - Eine Einführung in die physikalischen Konzepte.*, (Springer Verlag, 2004).

[7] F. Halzen and A.D. Martin, *Quarks and leptons: an introduction course in modern particle physics.*, (John Wiley & Sons, 1984).

[8] R. G. Roberts., *The Structure of the Proton: Deep Inelastic Scattering.*, (Cambridge Monographs on Mathematical Physics, Cambridge University Press, 1990).

[9] C. Amsler et al., *Particle Physics Booklet.*, (Particle Data Group, July 2008).

[10] R. L. Jaffe, *Spin, twist and hadron structure in deep inelastic processes.*, (arXiv:9602236v1 [hep-ph], 1996).

[11] M. Osipenko et al., *Self-consistent data analysis of the proton structure function g1 and extraction of its moments.*, (arXiv:0409038v1 [hep-ex], 2004).

[12] M. Anselmino, A. Efremov, E. Leader, *The Theory and Phenomenology of Polarized Deep Inelastic Scattering.*, (Phys. Rep., (261):1, 1995).

[13] V. Barone, A. Drago and P. G. Ratcliffe, *Transverse Polarisation of Quarks in Hadrons.*, (Phys. Rep., (359):1, 2002).

[14] S. Chekanov et al., [ZEUS Collaboration], *Measurement of the neutral current cross-section and F_2 structure function for deep inelastic $e + p$ scattering at HERA.*, (Eur. Phys. J. C, (21):443, 2001).

[15] C. Adloff et al., [H1 Collaboration], *Deep-Inelastic Inclusive ep Scattering at Low x and a Determination of α_s.*, (Eur. Phys. J. C, (21):33, 2001).

[16] L. W. Whitlow, E. M. Riordan, S. Dasu, S. Rock and A. Bodek, *Precise measurements of the proton and deuteron structure functions from a global analysis of the SLAC deep inelastic electron scattering cross sections.*, (Phys. Lett. B, (282):475, 1992).

[17] A. C. Benvenuti et al., [BCDMS Collaboration], *A high statistics measurement of the proton structure functions $F_2(x, Q^2)$ and R from deep inelastic muon scattering at high Q^2.*, (Phys. Lett. B, (223):485, 1989).

[18] M. R. Adams et al., [E665 Collaboration], *Proton and deuteron structure functions in muon scattering at* 470GeV., (Phys. Rev. D, (54):3006, 1996).

[19] M. Arneodo et al., [New Muon Collaboration], *Measurement of the proton and deuteron structure functions, F_2^p and F_2^d, and of the ratio σ_L/σ_T.*, (Nucl. Phys. B, (483):3, 1997).

[20] C. Amsler et al., [Particle Data Group], *Review of Particle Physics*, (Phys. Lett. B, (667):1, 2008).

[21] C. G. Callan Jr. and D. J. Gross, (Phys. Rev. Lett., (22):156, 1969).

[22] P. L. Anthony et al., [E142 Collaboration], *Deep inelastic scattering of polarized electrons by polarized ^3He and the study of the neutron spin structure.*, (Phys. Rev. D, (54):6620, 1996).

[23] K. Abe et al., [E143 Collaboration], *Measurements of the proton and deuteron spin structure functions g_1 and g_2.*, (Phys. Rev. D, (58):112003, 1998).

[24] K. Abe et al., [E154 Collaboration], *Precision Determination of the Neutron Spin Structure Function g_1^n.*, (Phys. Rev. Lett., (79):26, (1997).

[25] P. L. Anthony et al., [E155 Collaboration], *Measurement of the deuteron spin structure function $g_1^d(x)$ for* $1(\mathrm{GeV}/c)^2 < Q^2 < 40(\mathrm{GeV}/c)^2$., (Phys. Lett. B, (463):339, 1999).

[26] X. Zheng et al., [Jefferson Lab Hall A Collaboration], *Precision measurement of the neutron spin asymmetries and spin-dependent structure functions in the valence quark region.*, (Phys. Rev. C, (70):065207, 2004).

[27] A. Airapetian et al., [HERMES Collaboration], *Measurement of the proton spin structure function g_1^p with a pure hydrogen target.*, (Phys. Lett. B, (442):484, 1998).

[28] B. Adeva et al., [Spin Muon Collaboration], *Next-to-leading order QCD analysis of the spin structure function g_1.*, (Phys. Rev. D, (58):112002, 1998).

[29] E. S. Ageev et al., [COMPASS Collaboration], *Measurement of the spin structure of the deuteron in the DIS region.*, (Phys. Lett. B, (612):154, 2005).

[30] P. L. Anthony et al., [E155 Collaboration], *Measurement of the Proton and Deuteron Spin Structure Functions g_2 and Asymmetry A_2.*, (Phys. Lett. B, (458):529, 1999).

[31] P. L. Anthony et al., [E155 Collaboration], *Precision Measurement of the Proton and Deuteron Spin Structure Functions g_2 and Asymmetries A_2.*, (Phys. Lett. B, (553):18, 1998).

[32] R. P. Feynman, *Very high-energy collisions of hadrons.*, (Phys. Rev. Lett., (23):1415, 1969).

[33] M. Gell-Mann, *A schematic model of baryons and mesons.*, (Phys. Lett., (8):214, 1964).

[34] C. Zweig, *An SU3 model for strong interaction symmetry and its breaking.*, (CERN Report, TH(401, 412), 1964).

[35] S. Y. Hsueh et al., *High-precision measurement of polarized-Σ^- beta decay.*, (Phys. Rev. D, (38):2056, 1988).

[36] R. Webb, *Erste Messungen transversaler Spinasymmetrien durch Einzelpionproduktion am COMPASS-Experiment.*, (Phd thesis, Friedrich-Alexander-Universität Erlangen-Nürnberg, 2004).

[37] V. N. Gribov and L. N. Lipatov, *Deep inelastic ep scattering in perturbation theory.*, (Sov. J. Nucl. Phys., (15):438, 1972).

[38] Y. L. Dokshitzer, *Calculation of the Structure Functions for Deep Inelastic Scattering and e^+e^- Annihilation by Perturbation Theory in Quantum Chromodynamics.*, (Sov. Phys. JETP, (46):641, 1977).

[39] G. Altarelli and G. Parisi, *Asymptotic freedom in parton language.*, (Nucl. Phys. B, (126):298, 1977).

[40] L. G. Greeniaus, *Deep inelastic scattering with spin.*, (Lectures presented for the Troisieme Cycle de la Physique en Suisse Romande, June 2000).

[41] F. Sozzi, *Measurement of transverse spin effects in COMPASS.*, (Phd thesis, Universitá degli Studi di Trieste, 2007).

[42] C. Berger, *Elementarteilchenphysik.*, (Springer Verlag, 2006).

[43] J. Soffer, *Positivity Constraints for Spin-Dependent Parton Distributions.*, (Phys. Rev. Lett., (74):1292, 1995).

[44] A. Bacchetta, U. D'Alesio, M. Diehl and C. A. Miller, *Single-spin asymmetries: the Trento conventions.*, (Phys. Rev. D, (70):117504, 2004).

[45] A. Bacchetta, M. Diehl, K. Goeke, A Metz, P. J. Mulders and M. Schlegel, *Semi-inclusive deep inelastic scattering at small transverse momentum.*, (JHEP, (0702):093, 2007).

[46] M. Diefenthaler et al., [HERMES Collaboration] *HERMES Measurements of Collins and Sivers Asymmetries from a transversely polarised Hydrogen Target.*, (Proceedings of DIS 2007: 579).

[47] A. Airapetian et al., [HERMES Collaboration] *Observation of the Naive-T-odd Sivers Effect in Deep-Inelastic Scattering.*, (arXiv:0906.3918v1 [hep-ex], 2009).

[48] V. Y. Alexakhin et al., [COMPASS Collaboration], *First measurement of the transverse spin asymmetries of the deuteron in semi-inclusive deep inelastic scattering.*, (Phys. Rev. Lett., (94):202002, 2005).

[49] E. S. Ageev et al., [COMPASS Collaboration], *A new measurement of the Collins and Sivers asymmetries on a transversely polarised target.*, (Nucl. Phys. B, (765):31, 2007).

[50] M. Alekseev et al., [COMPASS Collaboration], *Collins and Sivers asymmetries for pions and kaons in muonâdeuteron DIS.*, (Phys. Lett. B, (673):127, 2009).

[51] R. Seidl et al., [Belle Collaboration], *Measurement of azimuthal asymmetries in inclusive production of hadron pairs in* e^+e^- *annihilation at* $\sqrt{s} = 10.58$ GeV., (Phys. Rev. D, (78):032011, 2008).

[52] Yi Qiang, [JLab Hall A, E06-10 Collaborations], *The First Measurement of Neutron Transversity on a Transversely Polarized* $^3\mathrm{H}$e *Target.*, (Proceedings of CIPANP 2009 – to be published by AIP).

[53] P. Abbon et al., [COMPASS Collaboration], *The COMPASS Experiment at CERN.*, (NIMA, (577):455, 2007).

[54] C. Lefevre, *The CERN accelerator complex / Complexe des accélérateurs du CERN.*, (CERN Document Server, http://cdsweb.cern.ch/record/979035).

[55] L. Gatignon, *User Guide for the mM2 beam.*, (http://gatignon.home.cern.ch/gatignon/M2manual.html).

[56] G. Backenstoss, *Helicity of μ^- mesons from π-meson decay.*, (Phys. Rev. Lett., (6):415, 1961).

[57] R. L. Garwin, *Observations of the failure of conservation of parity and charge conjugation in meson decays: the magnetic moment of the free muon.*, (Phys. Rev. Lett., (105):1415, 1957).

[58] G. Abragam and M. Goldman, *Principles of dynamic nuclear polarisation.*, (Rep. Prog. Phys., (41):395, 1978).

[59] Kuraray Co. Ltd., Methacrylic Resin Division, Tokyo, Japan, (http://www.kuraray.co.jp).

[60] Hamamatsu Photonics K.K., 14-5 Shimokanzo, Toyooka village, Shizouka-ken, Japan, (http://www.hamamatsu.com).

[61] A. Teufel, *Entwicklung und Bau von Hodoskopen aus szintillierenden Fasern für das COMPASS-Experiment.*, (Phd thesis, Friedrich-Alexander-Universität Erlangen-Nürnberg, 2003).

[62] M. Frhr. v. Hodenberg., *A first reconstruction of COMPASS data.*, (Diploma thesis, Albert-Ludwigs-Universitä Freiburg, 2002).

[63] ***CO****MPASS* ***R****econstruction and* ***A****na****L****ysis.*, (http://coral.cern.ch).

[64] ***PH****ysics* ***A****nalysis* ***S****oftware and* ***T****ools.*, (http://ges.home.cern.ch/ges/phast/index.html).

[65] R. Brun, F. Rademakers et al., *ROOT – An objected-oriented Data Analysis Framework.*, (http://root.cern.ch).

[66] G. Venugopal, *Measurement of Transverse Momentum Dependent Asymmetries with COMPASS Experiment at CERN.*, (Phd thesis, Rheinische Friedrich-Wilhelms-Universität Bonn, 2008).

[67] A. Richter, *Zeitkalibration der Faserhodoskope und Qualitätsüberprüfung der Daten für das COMPASS-Experiment.*, (Diploma thesis, Friedrich-Alexander-Universität Erlangen-Nürnberg, 2006).

[68] X. Artru, *The Transverse Spin.*, (Proceedings of "Xeme Seminaire Rhodanien de Physique 'Le Spin en Physique' ", arXiv:0207309v2 [hep-ph], 2002).

[69] A. Bressan, *Origin and cure of the peak in y.*, (COMPASS Note 2006-13, 3 Apr 2007).

[70] A. Korzenev, Mail to the COMPASS collaboration, 9 Mar 2008.

[71] J. Podolanski and R. Armenteros, *Analysis of V-Events*, (Phil. Mag., (45):13, 1954).

[72] S. Levorato, *Measurement of transverse spin effects in COMPASS on a polarised proton target.*, (Phd thesis, Universitá degli Studi di Trieste, 2009).

[73] M. Stolarski, Mail to the COMPASS collaboration including cleaning method proposed by A. Korzenev, 9 May 2008.

[74] W. Vogelsang and F. Yuan, *Single-transverse spin asymmetries: From DIS to hadronic collisions.*, (Phys. Rev. D, (72):054028, 2005).

[75] A. Efremov, K. Goeke and P. Schweitzer, *Collins effect in semi-inclusive deeply inelastic scattering and in e^+e^- annihilation.*, (Phys. Rev. D, (73):094025, 2006).

[76] A. Efremov, K. Goeke and P. Schweitzer, *Collins Effect in SIDIS and in e^+e^- Annihilation.*, (AIP Conf. Proc., (915):579, 2007).

[77] M. Anselmino et al., *Transversity and Collins functions from SIDIS and e^+e^- data.*, (Phys. Rev. D, (75):054032, 2007).

[78] M. Anselmino, A. Prokudin et al., *Transversity and Collins Fragmentation Functions: Towards a New Global Analysis.*, (Proceedings of DIS 2008, arXiv:0807.0173v1 [hep-ph], 2008).

[79] M. Anselmino, M. Boglione, U. D'Alesio et al., *Update on transversity and Collins functions from SIDIS and e^+e^- data.*, (Submitted to Nucl. Phys. Proc. Suppl., arXiv:0812.4366v1 [hep-ph], 2008).

[80] J. C. Collins, A. Efremov et al., *Sivers effect in semiinclusive deeply inelastic scattering.*, (Phys. Rev. D, (73):014021, 2006).

[81] M. Anselmino et al., *Extracting the Sivers function from polarized SIDIS data and making predictions.*, (Phys. Rev. D, (72):094007, 2005).

[82] M. Anselmino et al., *Sivers Effect for Pion and Kaon Production in Semi-Inclusive Deep Inelastic Scattering.*, (Eur. Phys. J. A, (39):89, 2009).

[83] M. Diefenthaler et al., [HERMES Collaboration] *Transversity measurements at HERMES.*, (Proceedings of DIS 2005, AIP Conf. Proc., (792):933, 2005).

[84] S. Arnold et al., *Sivers effect at Hermes, Compass and Clas12.*, (JLAB Report, JLAB-THY-08-820, arXiv:0805.2137v1 [hep-ph], 2008).

[85] A. Martin, *COMPASS Results on Transverse Single-Spin Asymmetries.*, (Czech. J. Phys. (56):F33, 2006).

[86] M. Burkardt, *Impact Parameter Dependent Parton Distributions and Transverse Single Spin Asymmetries.*, (Phys. Rev. D, (66):114005, 2002).

[87] M. Burkardt, *Quark correlations and single-spin asymmetries.*, (Nucl. Phys. B Proc. Suppl., (141):86, 2005).

[88] S. J. Brodsky, D. S. Hwang and I. Schmidt, *Final-State Interactions and Single-Spin Asymmetries in Semi-Inclusive Deep Inelastic Scattering.*, (Phys. Lett. B, (530):99, 2002).

[89] S. J. Brodsky and S. Gardner, *Evidence for the Absence of Gluon Orbital Angular Momentum in the Nucleon.*, (Phys. Lett. B, (643):22, 2006).

Acknowledgements

Man hat den Eindruck, dass die moderne Physik auf Annahmen beruht, die irgendwie dem Lächeln einer Katze gleichen, die gar nicht da ist.

One has the impression that modern physics is based on assumptions, which somehow resemble the smile of a cat, which is not there.

A. Einstein (1879-1955),
German-american physicist,
Nobel Prize 1921

Bei allen, die zum Gelingen dieser Arbeit beigetragen haben und ohne deren Hilfe diese niemals möglich gewesen wäre, möchte ich mich gerne bedanken:

- Zunächst einmal bei meinem Doktorvater, Prof. Dr. Wolfgang Eyrich, dafür, dass er mir diese Doktorarbeit ermöglicht und mir dieses interessante Thema überlassen hat, sowie für seine Unterstützung und sein Interesse am Fortgang der Arbeit und die von ihm geprägte angenehme Atmosphäre in der Arbeitsgruppe.

- Bei PD Dr. Rainer Joosten von der Universität Bonn, mit der schon lange eine gute Zusammenarbeit mit unserer Arbeitsgruppe besteht, für die Mitbetreuung als erfahrener Wissenschaftler sowohl in der Analyse als auch bei der Betreuung der SciFis. Rainer war stets quasi rund um die Uhr mit Hilfe zur Stelle, ob bei einem Problem bei der Analyse, beim Schreiben eines Proceedings oder bei Problemen mit den SciFis.

- Bei allen Mitgliedern der Gruppe Eyrich (jetzige und ehemalige, die ich erlebt habe) für das angenehme Umfeld. Speziell erwähnen darf ich hier Dr. Andreas Teufel, den “SciFi-Meister”, der stets mit Rat und Tat bei allen Detektorfragen geholfen hat, meinen langjährigen Büro- und Wohnungsnachbarn Martin Krapp für so manchen Gefallen, ob am Institut bei Computerfragen oder anderem oder zu hause, Philipp Schrögel, den “master of LaTeX” für die Hilfe bei sehr speziellen LaTeX-Problemen, meinem ehemaligen Diplomanden Christopher Braun sowie Dr. Peter Schönmeier und Dr. Christian Vogel für manche Hilfe beim Programmieren. Allerdings auch bei allen anderen ehemaligen und jetzigen Gruppenmitgliedern: Christoph Adolph, Alexander Britting, Florian Hauenstein, Dominik Hertel, Julia Heimlich, Julian Jaus, Lukas Kober, PD Dr. Albert Lehmann, Luigi Pinna, Dr. Cecilia Pizzolotto, Sebastian Reinicke, Adrian Schmidt, Dr. Wolfgang Schroeder, Fred Uhlig und Dr. Richard Webb.

- Bei Prof. Dr. Jens Bisplinghoff und seiner Gruppe an der Universität Bonn für die gute Zusammenarbeit.

- Naturalmente anche vorrei ringraziare prof Bradamante e tutti del suo gruppo all' Istituto della Fisica Nucleare (INFN) di Trieste e dell'Università degli Studi di Trieste per la collaborazione (ed anche la possibilità di parlare l'italiano), particolarmente prof.ssa Anna Martin, prof Paolo Schiavon, dott. Andrea Bressan, dott. Stefano Levorato, Giulia Pesaro, Elena Rocco, Giulio Sbrizzai e dott.ssa Federica Sozzi, per chiamare solo quelli con cui ho lavorato di più.

- Bei Prof. Dr. Kay Königsmann und Prof. Dr. Horst Fischer und ihrer Gruppe an der Universität Freiburg, insbesondere Heiner Wollny, ebenfalls für die gute Zusammenarbeit.

- Of course I'd like to thank all members of the COMPASS collaboration at CERN for the pleasant working atmosphere.

- Bei Frau Jutta Dziwis, dem "guten Geist" unserer Arbeitsgruppe, die stets geduldig bei allen bürokratischen Hürden mit Rat und Tat zur Seite stand und ohne die unsere Gruppe wohl verloren wäre.

- Bei meinen Eltern, Christiane von Bernus und Dr. Franz Richter, dafür, dass sie mir mein Studium ermöglicht und mich immer unterstützt haben.

- Bei unserer Katze Otti für die Ablenkung und die lustigen Zeichen, die sie in den Laptop eingegeben hat. ;-)